Western Australian School of Mines: Minerals, Energy and Chemical Engineering

Department of Chemical Engineering

Synthesis of Nanomaterials and Their Integration in Wastewater Treatment Processes

Muhammad Rizwan Azhar

This thesis is presented for the Degree of
Doctor of Philosophy
of
Curtin University

March 2018

DECLRARATION

DECLARATION OF ACADEMIC INTEGRITY

To the best of my knowledge and belief this thesis contains no material previously published by any other person except where due acknowledgment has been made.

This thesis contains no material which has been accepted for the award of any other degree or diploma in any university.

Signature: 

Date: 5th of March 2018

DEDICATION

I would like to dedicate my thesis to

My parents, who have helped me achieving such a milestone in my life.

My wife, who accompanied me throughout this wonderful journey.

My brothers, who dreamed big for me and persuade me to continue my research.

My respected sisters, who prayed for me a lot every day.

All martyred children of Pakistan who would have been great asset to world.

ACKNOWLEDGMENT

In The Name of Allah, The Most Gracious, The Most Merciful.

Peace Be Upon Prophet Muhammad ﷺ.

I am humbly grateful to the Blessings of ALLAH Almighty and His Messenger, Prophet Muhammad ﷺ (Peace be upon him). I didn't get lost in the way of achieving this huge milestone. Moreover, I would like to express my utmost sincere appreciation to my supervisor, Professor Moses Tade. I am grateful for his continual guidance and knowledge, which have provided the energy for me to push through the difficulties during my PhD research. Technical support from Professor Shaobin Wang has been exceptional to produce excellent research outcomes in this PhD project. Dr. Vijay has been very friendly and helped me in continuing my ambitions to excel in the field of research.

To achieve big while working in research and academics can be very tiring at times, which require special energy and enthusiasm to overcome all difficulties associated with work environment. Throughout my life, my father has taught me integrity, truthfulness, hard work, and believe to accomplish tasks at hand and feel contended. Teachings of my mother, her unconditional love, affection and prayers made each and every tough step of PhD milestone as red roses for me. In addition, prayers from mother in law acted as an active catalyst to speed up my performance in exploring this wonderful world of research. The encouragement from my elder and younger brothers proved to be a spark to explore more and achieve big in my life. Due to their combined efforts, I could start my Bachelors in Chemical Engineering at University of the Punjab, Pakistan as a first step of my career, which has brought me to accomplish a doctorate degree. Without their efforts and sacrifices, nothing could have been possible.

All is that ends well is perfectly correct, however, a good start lays foundation of a success story at the end. So, my wonderful wife, proved to be the nicest addition to life, who had made my life so pleasant that I didn't feel dull in carrying out my research at any stage of PhD. Though, I explained and discussed ideas with her to get feedback as a first reviewer.

Friends and colleagues play an imperative part in making things easier in life. This can be more charming if they can contribute in your field. I am a lucky person for having wonderful friends from various disciplines, who have supported me in technical and social aspects throughout this journey of PhD. I would like thank Dr. Roshanak Dourusihi for her kindness and technical support in labs. Support and encouragement from my childhood friends are highly appreciated.

ABSTRACT

With the immense development of technology and fast development of urbanization, several water contaminants are being added to the list of chemicals of urgent concern. Therefore, treatment of wastewater is of prime importance throughout the world, particularly in developed and water scarce countries. Nanomaterials find extensive applications in various fields of science and technology in these days. Metal organic frameworks (MOFs) are a new class of functional nanomaterials which have exceptionally textural and functional properties, making them suitable for separation processes including wastewater treatment processes (WWTPs). However, MOFs are less explored in WWTPs, particularly in emerging water contaminants removal such as pharmaceuticals and personal care products (PPCPs). Moreover, there is a lack of literature on stability of MOFs in aqueous media particularly after using in WWTPs, advanced adsorption mechanism based on functionalities of MOFs and recycling/reuse of used MOFs in cascade applications. Furthermore, no studies are available on catalytic degradation of antibiotics using oxidizing agents with MOFs.

In this thesis, different water stable MOFs have been synthesized by either previously reported methods with modification or using novel techniques. All the synthesized MOFs were characterized using different techniques such PXRD, SEM, FTIR, N_2 adsorption-desorption, and TGA. Micro and mesoporous HKUST-1 was prepared using a solvothermal technique. Moreover, excellent performance of HKUST-1 was observed in adsorptive removal of sulfachloropyradazine (SCP), a sulfonamide antibiotic for the first time. Similarly, UiO-66 and ZIF-67 were synthesized using solvo/hydrothermal techniques. Performance of activated UiO-66 was superior compared to all other MOFs in adsorption of SCP in multiple adsorption cycles. In case of SCP adsorption, temperature has a positive effect on adsorption capacity of HKUST-1 and UiO-66. Moreover, new adsorption mechanism was proposed based on hydrophobic and pi-pi interaction between adsorbate-adsorbent. Owing to the successful application of these two MOFs in wastewater treatment processes, novel binary MOFs (HKUST-1 and UiO-66) were

then prepared to figure out their synergistic effects in adsorption process. It is interesting to report that the performance of binary MOFs is superior compared to their parent monometallic MOFs in adsorption of methylene blue (MB). Moreover, adsorption capacity of a composite MOF (95 % HKUST-1 & 5 % UiO-66) was almost double than commercial activated carbon. Initial pH and point of zero charge pH of materials (pH_{PZC}) are important factors in controlling adsorption process.

Furthermore, two Bio-MOF-11 were prepared by a facile synthesis method using cobalt and copper as metal nodes and adenine as organic linkers. Bio-MOF-11-Co showed high water stability in terms of structure intactness and textural properties. Mesoporous Bio-MOF-11-Co effectively activated peroxymonosulphate (PMS) to degrade p-HBA and SCP as representatives of personal care products and pharmaceuticals, respectively. Structural arrangement of adenine and cobalt in Bio-MOF-11 resulted in excellent performance in catalytic degradation of p-HBA and SCP. Performance of the catalyst was studied with various parameters such as catalyst/PMS loadings, temperature and recycle/reuse. A detailed degradation mechanism was proposed by testing adenine only in degradation reaction, justifying the role of Lewis basic sites in elimination of water contaminants by advanced oxidation processes. A systematic study was also performed on solvent modulated synthesis of MIL-96 for cascade applications ranging from CO_2 adsorption, p-HBA adsorption and dye degradation. The spent MIL-96 were heat treated in an inert environment to convert them into AlxOy/carbon composite which was further used in catalytic degradation of methyl orange. This study serves as a proof of concept for integrated application of MOFs in environmental remediation without generating any solid waste.

Carbon nanospheres were synthesized by a modified evaporation induced self-assembly at elevated temperatures to make the synthesis process more cost effective by reducing synthesis time. Moreover, cyclic applications of these mesoporous carbon with a high surface area were explored in adsorption-catalytic degradation-adsorption without losing efficiency. Such applications can play a significant role in integrated applications of these functional nanomaterials in wastewater treatment processes and beyond.

Overall, despite of large number of MOFs and their high surface area, application of MOFs is limited by their water stability. Therefore, new synthesis method such as electrochemical technique can be used to synthesize MOFs, which can help in preparing water stable MOFs in short time. Such synthesis processes are encouraged to explore for wastewater treatment processes and other applications such as energy storage, sensors and membrane technology. Moreover, fabrication of core-shell structures is another useful technique which can be useful in enhancing water stability and activity in exploring new applications of MOFs.

.

Publications of author in support of this thesis

M.R, Azhar, H.R, Abid, M.O., Tade V. Periasamy, H. Sun, S. Wang, "Cascade applications of robust MIL-96 metal organic frameworks in environmental remediation: Proof of concept", *Chemical Engineering Journal*, pp. 262-271, 2018, https://doi.org/10.1016/j.cej.2018.02.030.

M.R, Azhar, V. Periasamy, M.O., Tade, H. Sun, S. Wang, "Submicron sized highly water-stable metal organic framework (bio-MOF-11) for catalytic degradation of pharmaceuticals and personal care products", *Chemosphere,* pp. 105-114, 2018, https://doi.org/10.1016/j.chemosphere.2017.12.164 .

M.R, Azhar, H.R, Abid, H. Sun, V. Periasamy, M.O., Tade, S. Wang, "One-pot synthesis of binary metal organic frameworks (HKUST-1 and UiO-66) for enhanced adsorptive removal of water contaminants", *Journal of Colloidal and Interface Science*, pp. 685–694, 2017, https://doi.org/10.1016/j.jcis.2016.11.100 .

M.R, Azhar, H.R, Abid, V. Periasamy, H. Sun, M.O., Tade, S. Wang, "Adsorptive removal of antibiotic sulfonamide by UiO-66 and ZIF-67 for wastewater treatment", *Journal of Colloidal and Interface Science*, pp. 88-95, 2017, https://doi.org/10.1016/j.jcis.2017.04.001 .

M.R, Azhar, H.R, Abid, H. Sun, V. Periasamy, M.O., Tade, S. Wang, "Excellent performance of copper based metal organic framework in adsorptive removal of toxic sulfonamide antibiotics from wastewater", *Journal of Colloidal and Interface Science*, pp. 344-352, 2016, https://doi.org/10.1016/j.jcis.2016.06.032 .

Conference Presentations

M.R, Azhar, V. Periasamy, M.O., Tade, S. Wang, "Synthesis and characterization of metal organic frameworks for wastewater treatment process", One Curtin International Postgraduate Conference, Miri, Malaysia, December 10-12, 2017.

M.R, Azhar, V. Periasamy, M.O., Tade, S. Wang, "Insights into functional and textural properties of MIL-53 metal organic frameworks for adsorptive removal of toxic antibiotics", Chemeca, Melbourne, July 22-26, 2017.

Contents

List of Abbreviations

AC: Activated carbon

BDC: Benzene dicarboxylic acid

BTC: Benzene Tricarboxylic acid

BET: Brunauer–Emmett–Teller

BJH: Barrett-Joyner-Halenda

DMF: Dimethylformamide

GAC: Granulated activated carbon

HKUST: Hong Kong University of Science and Technology

MOFs: Metal organic frameworks

MWCNTs: Multiwall carbon nanotubes

MIL: Materials Institute of Lavoisier

WWTPs: Wastewater treatment Processes

MB: Methylene Blue

MO: Methyl Orange

p-HBA: para-hydroxybenzoic acid

PMS: Peroxymonosulfate

PAC: Powdered activated carbon

PSD: Pore size distribution

PZC: Point of zero charge

RhB: Rhodamine B

SCP: Sulfachlorpyradazine

UiO: University of Oslo

ZIF: Zeolitic imidazole framework

List of Tables

List of Figures

Chapter 1 Introduction

1.1 Background

Scarcity of clean water and environmental regulations made wastewater treatment a hot area of research throughout the world. There are different technologies and materials to treat the toxic chemicals in wastewater depending on the resources and extent of efficiency required to remove the wastes (Hasan & Jhung, 2014). Some pollutants such as pharmaceuticals and personal care products (PPCPs) (Bu, Wang, Huang, Deng, & Yu, 2013), herbicides/pesticides (Finizio, Azimonti, & Villa, 2011), dyes (Gupta & Suhas, 2009), spilled oil (Gong et al., 2014), and aromatics/organics (Ahmaruzzaman, 2008) have been detected in different natural surface water sources. These contaminants are required to be removed up to ppm and/or in ppb concentrations. There are several techniques utilized and/or under research to treat/remove waste from wastewater, which include advanced oxidation processes, adsorption, biological oxidation, chemical treatment, and incineration (Hartmann, Kullmann, & Keller, 2010; Khin, Nair, Babu, Murugan, & Ramakrishna, 2012). Every technique has some limitations associated with it. Advanced oxidation techniques produce secondary waste in terms of CO_2 which is a big environmental issue of the time. The addition of certain chemicals are harmful to the environment. Adsorption is a process in which waste can be removed without producing any further chemical and/or biological waste. It's a simple and efficient technique, generally requiring porous materials to be used as adsorbents in water treatment. The other advantage of the adsorption process is the regeneration of the materials used as adsorbents and adsorbate as well (Walcarius & Mercier, 2010). Since the last two decades a lot of research has been conducted on the synthesis of porous materials with high surface area, large pore volume, regular structure and pore size distribution. These materials include activated carbons, zeolites, mesoporous carbons and metal organic frameworks (MOFs) (Burtch, Jasuja, & Walton, 2014; Canivet, Fateeva, Guo, Coasne, & Farrusseng, 2014; Furukawa et al., 2014; Hernandez-Ramirez & Holmes, 2008; Titirici et al., 2015).

1.2 Background of Porous Nanomaterials

Zeolites and metal oxides have been largely used in separation processes in gas and liquid phases. However, zeolites face problems in terms of narrow pore size which usually lies in microporous range. On the other hand, metal oxides don't possess high surface, although transition metal oxides find their application largely in catalytic applications, both in synthesis of useful products and catalytic degradation of water contaminants (Saputra et al., 2013b; Shukla, Wang, Singh, Ang, & Tadé, 2010; Sun, Liu, Liu, & Wang, 2014a). However, leaching of toxic metals into water bodies is a drawback in using these materials at a large scale without properly studying their stability. Mesoporous silica is also included as one of the most studied materials in environmental applications. Availability of large surface area and large pore makes these materials suitable for adsorptive removal of unwanted chemicals (Hamoudi, Saad, & Belkacemi, 2007). Moreover, functionalization of tuneable pores and voids further enhance their capabilities in diversified applications. In the last two decades in comparison to MOFs, no other materials could compete in terms of functionalization and tuning of textural properties owing to their hybrid nature. Metal organic frameworks are high surface area materials for various applications including gas storage, gas purification, drug delivery, super capacitors and biological sensors (Erucar & Keskin, 2016; Lee & Jhung, 2010; Miller, Teplensky, Moghadam, & Fairen-Jimenez, 2016; Rada et al., 2015; Wang et al., 2016a). The diversity of metal precursors, ligands, and pre & post synthesis treatments make MOFs very useful materials in various fields mentioned earlier. The earlier applications of MOFs were limited to the gas adsorption and purification, so a lot of work has been done on increasing surface area, porosity and pore volume of the synthesized MOFs. The other competitor materials to the MOFs are zeolites and activated carbons (Hernandez-Ramirez & Holmes, 2008). However, zeolites and activated carbons have limitations namely, difficult to synthesize with less controllability of pore's tuning properties, mostly in case of activated carbons. Moreover, zeolites and activated carbons have been used for liquid phase and/or water related processes either, aqueous phase applications and/or water treatment owing to high surface area. One of the major areas of zeolites is water capture (Furukawa et al., 2014). On the other hand, a lot of research has been carried out to synthesise various MOFs with

tuneable pore geometry. The structure of MOFs primarily consists of two major components, metal centres and organic linkers; metal centres act as joints in the structure being nodes while organic linkers being the bridge to the neighbouring joints (Öhrström, 2015). In MOFs, organic and inorganic parts are linked together through coordination covalent bond. The tendency of organic materials being used as linkers is different i.e. di, tri, tetra dentate ligands e.g. carboxylates or other organic anions (phosphonate, sulfonate, and heterocyclic compounds).

1.3 Motivation and Objectives of this thesis

MOF synthesis without any external template (either organic or inorganic) makes it more studied material than zeolites. In MOF synthesis, solvent/s acts as templates. These solvents form weak interactions with the MOFs which in turn form intact neutral products and accessible pores at lower temperatures. Furthermore, various metal cations (di, tri, tetravalent cations) can take part in the formation of MOFs compared to zeolites where a few cations are involved in the formation of conventional zeolites (Al, Si, P) (Ferey, 2008). Moreover, the desired properties of MOFs can be achieved by in situ, and/or post synthetic treatment e.g., just changing the organic moieties in Zr-MOFs, increased surface areas can be achieved, e.g. UiO-66 (Zr-benzenedicarboxylate, Zr-BDC), UiO-67 (Zr-biphenyldicarboxylate, Zr-BPDC) and UiO-68(Zr-terphenyldicarboxylate, Zr-TPDC), having surface areas of 1187, 3000, and 4170 m^2/g, respectively. In case of post synthetic treatment, functionalities can be incorporated to enhance/control the physicochemical properties, e.g. by sulfonation, post-functionalization of amine groups with sulfones (Britt, Lee, Uribe-Romo, Furukawa, & Yaghi, 2010), modification with different acid anhydrides (Kandiah et al., 2010), and grafting of cysteamine or ethylenediamine. Similarly, different composites of MOFs can be prepared with various materials. Recently, various polyoxometalates (POMs) were successfully immobilized to the mesoporous coordination polymer MIL-101, resulting in a series of POM–MOF composite materials. These POMs are $K_4PW_{11}VO_{40}$, $H_3PW_{12}O_{40}$, and $K_4SiW_{12}O_{40}$ (Yan et al., 2014).

The objectives of this study are as follows.

1. Synthesis of various metal organic frameworks.

2. Removal of hazardous materials (antibiotics, dyes, personal care products etc.) from wastewater using MOFs as adsorbents.
3. Regeneration and recycling of the MOFs.
4. Synthesis of bio-MOFs for catalytic degradation of emerging water contaminants.
5. Synthesis of porous carbon materials using facile methods to reduce cost and chemical wastage.
6. Application of PCs in WWTPs.

1.4 Scope and Contribution of thesis

MOFs and porous carbons are important structured materials with tuneable surface properties with a very high surface area. The following are the beneficial contributions of the research carried out.

Synthesis of water stable MOFs for wastewater treatment.

1. Synthesis of high surface area materials by facile and cost-effective methods compared to conventional methods.
2. Kinetic study of wastewater treatment process; removal of hazardous materials from the wastewater.
3. Proposed adsorption mechanism of various adsorbates.
4. Water stability testing of bio-MOFs in advanced WWTPs.

1.4.1 Thesis outline

In order to achieve the objectives of this project, a thorough plan was followed in terms of synthesis, characterization and applications of MOFs in WWTPs. Chapter 1 includes introduction, chapter 2 contains literature review, while chapters 3 - 8 summarize synthesis, characterization and applications of MOFs and mesoporous carbons and finally chapter 9 concludes the thesis with future work and recommendations. It can be seen from the Figure that progress of the project was well defined.

Note: Chapters 3 – 8 are the author's journal publications, which this work reproduced as individual chapters, reader may like to read them separately, and the illustrations at some places in text may appear more than once. Publication 6 is under review. Appendix A contains the relevant copyright forms.

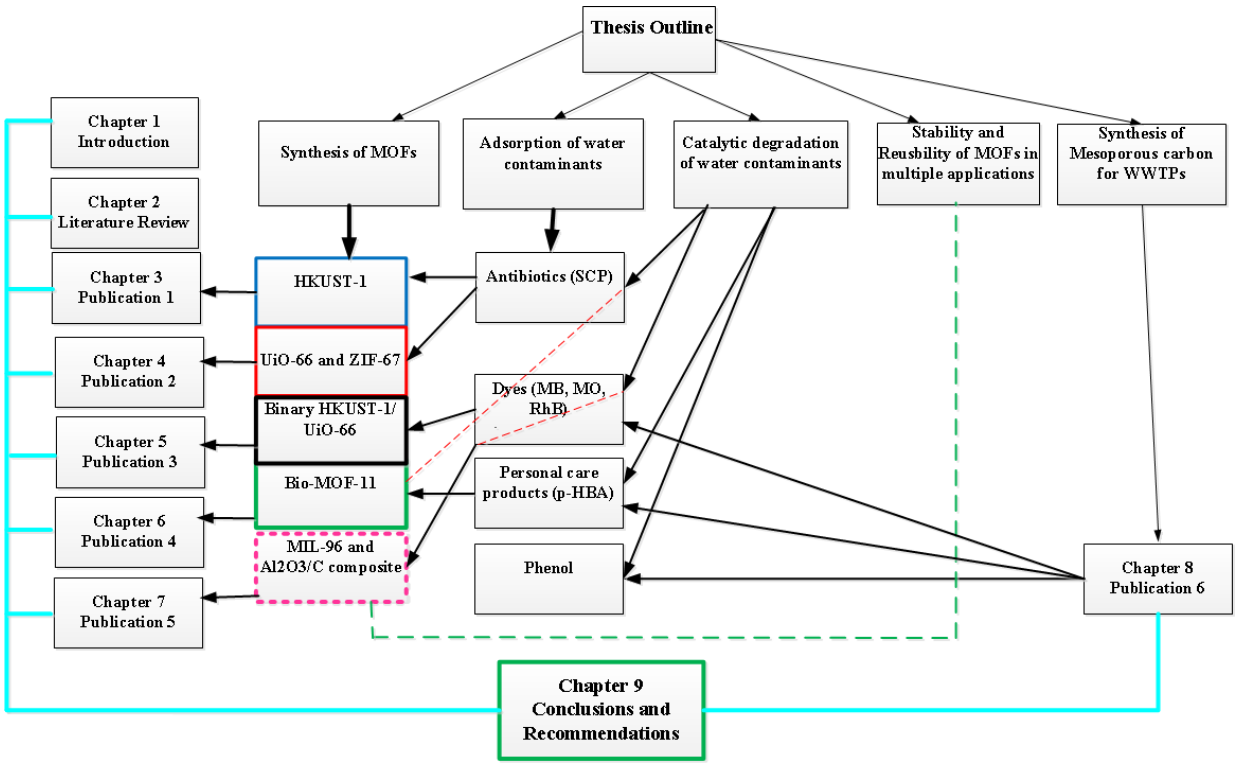

Figure 1-1 Thesis outline

Chapter 2 Literature Review

2.1 Introduction

The availability of drinking water is becoming more and more challenging as a rapid increase in population of the world along with immense industrialization has generated the increasing amount of wastewater. This increase is alarmingly high throughout the world (Chan, Chong, Law, & Hassell, 2009; Olsson, 2012; Ostace et al., 2013; Rossner, Snyder, & Knappe, 2009). A recent report shows that one billion people living in the arid regions will face absolute water scarcity in 2025 (Seckler, Barker, & Amarasinghe, 1999). The variety of industrial processes result in different types of waste materials in wastewater. Industrial processes like dying in textile industry (Belpaire, Reyns, Geeraerts, & Van Loco, 2015; Ning et al., 2015), pharmaceuticals, and personal care products (Ahmed, Zhou, Ngo, & Guo, 2015b; Blasioli et al., 2014a; Braschi et al., 2010b; Bu et al., 2013), oil refineries (Zhang, Wang, Tang, & DeLaune, 2015e), tanneries (El-Sherif, Tolani, Ofosu, Mohamed, & Wanekaya, 2013; Gomes, Piccin, & Gutterres, 2016; Lemos, Oliveira, & Lemos, 2011; Rahman & Singh, 2014) and petrochemical industry (Lakatos, Veres, Kundrát, & Mészáros, 2014; Li et al., 2015a) are main sources of water pollution.

The dyes used usually in textile, food processing, plastics and leather tanning have 700,000 tons annual production with 100,000 commercial dyes (Yagub, Sen, Afroze, & Ang, 2014). As most dyes are complex organic molecules and are required to be resistant towards many things such as the action of detergents. The textile industry alone consumes 10,000 tonnes ever year and approximately 100 tonnes of these dyes are discharged into water streams. However, it's one of the biggest challenges that environmental scientists face today since some of the dyes are carcinogenic.

A recent review on emerging contaminants i.e. pharmaceuticals and personal care products in aquatic life in China reported that annual production of pharmaceuticals and personal care products only in China is 25,000 tons per year with 112 products including 94 pharmaceuticals and 18 personal care products (Bu et al., 2013). Most of the pharmaceutical waste come from hospitals, agricultural and cattle farms and/or pharmaceutical industry (Lin & Tsai, 2009; Nielsen & Bandosz, 2016; Oliveira et al., 2015a; Rehman et al., 2015; Sim, Kim, Choi, Kwon, & Oh, 2013b; Tao et al., 2014b; Vyas, Turner, & Sewell, 2014). In most cases, pharmaceutical waste comes in the form of antibiotics which result in generation of sulphonamides, fluoroquinolones,

macrolides, tetracyclines, and ß-lactams (Ahmed et al., 2015b; Blasioli et al., 2014a; Braschi et al., 2010b; Carmona, Andreu, & Pico, 2014a; Dirany, Sires, Oturan, Ozcan, & Oturan, 2012a; Rehman et al., 2015). Among these PPCPs, six of PPCPs (erythromycin, roxithromycin, diclofenac, ibuprofen, salicylic acid and sulfamethoxazole) are identified with a serious risk by Environmental Protection Agency (EPA)'s screening level risk assessment (SLERA) (Richardson & Ternes, 2014).

However, in Australia, red meat industry is one of the major contributors in wastewater pollution (Ihsan Hamawand, 2015). The most of cleaning agents used in red meat industry are alkalis, acids (organic and inorganic), neutral, foaming agents and detergents. These cleansing agents result in water contamination with metals; another big threat is the discharge of heavy metals into wastewater and chlorine containing components. The heavy metals, e.g. Cu, Zn, Hg, Cr, Cd, Pb etc. are very toxic and some of them even cause various diseases including cancer (Al-Zoubi, Ibrahim, & Abu-Sbeih, 2015; Cherfi, Achour, Cherfi, Otmani, & Morsli, 2015; Jankovský et al., 2015; Pejman, Nabi Bidhendi, Ardestani, Saeedi, & Baghvand, 2015; Radi et al., 2015; Saidi, 2015; Sheet, Kabbani, & Holail, 2014; Tang et al., 2014). There are recent advancements in analytical techniques to determine the contaminants which were not detected with the simple ordinary analytical techniques. The EPA has listed 30 different contaminants to be monitored by drinking water utilities during 2013-2015. The list, which is called third unregulated contaminant monitoring rule (UCMR-3) of EPA, is getting bigger day by day and even includes heavy metals like Co along with other 14 contaminants listed in other drinking water priority list, contaminant candidate list 3 (CCL-3). The UCMR-3 mostly includes volatile organic compounds, dioxone, metals, chlorate, hormones, perfluorinated carbons (PFCs), and couple of virus as well (Richardson & Ternes, 2014).

There are various local and international governing bodies that are looking after these emerging threats and impose limitations of discharge of waste into water bodies depending on severity of the waste and its effects on living organisms. To keep pace with rapid advancements in different areas of science and technologies, researchers are exploring cutting edge technologies and processes in WWTPs using basic scientific techniques. However, treatment of wastewater is an ancient process

when people used sand, lime stone and other materials to treat wastewater, and clay minerals and activated carbons are studied today (Djukić et al., 2013; Du et al., 2015; Han et al., 2013; Vhahangwele & Mugera, 2015; Zhao, Qi, Chen, Ji, & Zhang, 2015b; Zhou et al., 2015). The modern wastewater treatment processes are adsorption (Ahmed et al., 2015b; Rossner et al., 2009; Zhao et al., 2015a), biological processes (Chan et al., 2009; e Silva, Sintra, Ventura, & Coutinho, 2014; Estrada, Kraakman, Lebrero, & Munoz, 2015; Nielsen & Bandosz, 2016; Pei et al., 2015), photodegradtion (Du et al., 2011; Sun et al., 2013; Wang, Li, Lv, Zhang, & Guo, 2014a; Xiao, Liu, Qin, & Cui, 2013b; Zhu et al., 2014), advanced oxidation and membrane technologies (Jiang, Zhang, & Yan, 2015; Stoller, Pulido, Di Palma, & Ferez, 2015; Yurtsever et al., 2015). With an increasing number of pollutants and/or potential pollutants, all of these mentioned processes are used separately and/or in combination in wastewater treatment processes. The ultimate goal is to establish a process by water recycle and reuse can be achieved (Chen et al., 2016c; Garcia & Pargament, 2015; Prieto, Prieto, Vazquez, & Ferreira, 2015).

Due to complexity of emerging contaminants, advanced materials and processes are necessary to develop for water cycle balance. However, most of treated wastewater is used in irrigation, landscaping, flushing, gardening etc. (Kajenthira, Siddiqi, & Anadon, 2012). The utilization of nanotechnology in wastewater treatment processes is getting popularity in recent years. The nanomaterials e.g. zeolites, activated carbons, polymeric membranes and metal organic frameworks (MOFs) are emerging materials in WWTPs (Adeyemo, Adeoye, & Bello, 2012; Blasioli et al., 2014a; Braschi, Paul, Gatti, Cossi, & Marchese, 2013; Dirany et al., 2012a; Estrada et al., 2015; Hasan & Jhung, 2014; Rossner et al., 2009; Saleh & Gupta, 2014; Sheet et al., 2014; Smith & Rodrigues, 2015; Tang et al., 2014). Among these materials, MOFs are getting more importance due to their robust nature.

MOFs are ultrahigh surface area materials, with tunable porosity and pore size distribution, with facile synthesis methods and high degree of freedom to achieve desired materials (Abid, Ang, & Wang, 2012a; Ahmad, Younus, Chughtai, & Verpoort, 2015; Ahmed, Khan, Hasan, & Jhung, 2013; Biswas & Van Der Voort, 2013; Colombo et al., 2011; Evans, Sumby, & Doonan, 2014; Gao et al., 2014; Horcajada et al., 2007; Janiak & Vieth, 2010; Jasuja, Jiao, Burtch, Huang, & Walton, 2014; Jasuja & Walton, 2013; Xu et al., 2014; Yang, Liu, & Sun, 2014). Moreover,

the use of MOFs in hydrogen storage, CO_2 capture, catalysis and supercapacitor is studied enormously in the last two decades (Banu, Friedrich, Brandani, & Düren, 2013; Basdogan & Keskin, 2015; Chen, Hoang, Rodrigue, & Kaliaguine, 2013; Choi, Park, & Kang, 2015; Chughtai, Ahmad, Younus, Laypkov, & Verpoort, 2015; Clough et al., 2014; Getman, Bae, Wilmer, & Snurr, 2012; Juan-Alcaniz et al., 2013; Kang, Sun, Kong, Lang, & Luo, 2014; Li et al., 2013b; Wang et al., 2015c; Wang et al., 2015d; Yilmaz & Keskin, 2014). However, the use of MOFs in WWTP is quite recent ranging from adsorption, photodegradation and oxidation processes (Ahmed & Jhung, 2014; Du et al., 2011; Hasan & Jhung, 2014; Sun et al., 2013; Xiao et al., 2013a; Xiao et al., 2013b; Zhu et al., 2014). The first reported MOF in WWTPs is dated back in 2010 by Haque et al (Haque et al., 2010b). The journey continues from that point and trend is getting importance in establishing new robust MOFs in WWTPs. Since the first reported study of MOF, the use of MOFs in WWTPs grows rapidly; either as pure MOFs and/or MOF composites. A detailed study on antibiotic removal by various MOFs has been reported recently (Azhar et al., 2016). Moreover, Azhar et al. also reported integrated approach to utilize MOFs in multiple applications (Azhar et al., 2018). Most of the studies on MOFs are focused on organic waste removal from wastewater. There are not much details on inorganic waste removal, e.g. heavy metals and inorganic anions.

2.2 Basics of metal organic frameworks

MOFs are composed of organic and inorganic species in special arrangements. Basically, MOFs can be constructed in various topologies depending on linkers, metal nodes, solvents and other operating parameters. However, main challenges include, careful structural arrangement, activation and characterization to justify textural and functional properties of MOFs. In its simplest form, metal or metal oxide nodes are attached to organic linkers, which can be carboxylic acids, nucleic bases, phosphonides, amides and combination of these organic species. Once basic building of MOFs i.e. secondary building units (SBUs) are formed, then repetition in one, two or three dimensions give rise to regular structures i.e. formation of network or framework.

2.3 Water stability of MOFs

MOFs are the most studied materials in the last decades since the first MOF was claimed by Yaghi et al. in 1995 (Yaghi, Li, & Li, 1995). However, the first used MIL-101-Cr and MIL-53-Cr for the adsorptive removal of methyl orange occurred in 2010. The reason is water instability of the MOFs and the recycle and reuse of them. Although, a limited number of MOFs have been used in WWTPs but the trend in using MOFs in WWTPs is growing fast. The journey of the MOFs started with the complex synthesis route of MOF production and continues with simple and robust synthesis methods and reuse of the materials in recent studies (Chen, Zhang, Guan, & Li, 2012; Haque et al., 2010b; Leng, Wang, Zhao, Hu, & Li, 2014). The use of different metals in MOFs for WWTPs application is getting popularity as this can play an important role in stability of the MOF and adsorption capacity. Though most of the studies till now are limited to dyes removal and organic waste by adsorption but utilization of MOFs in photo degradation is getting a popularity.

2.4 MOFs in Wastewater treatment

Recently MOFs have been applied in WWTPs in adsorption and catalytic and photocatalytic degradation of water contaminants. MOFs can be categorized according to their use and their types.

2.4.1 Adsorption of organic water contaminants

Haque et al. first used MIL-101-Cr and MIL-53-Cr for the adsorptive removal of methyl orange (Haque et al., 2010b). The functionalization of the MOFs proved to be a significant process in dyes removal. Pristine and functionalized MOFs were compared with activated carbon (AC) and the removal efficiency of MOFs was much better than AC. The MOFs used in this study possessed different surface properties and MIL-101-Cr showed superior results than MIL-53-Cr owing to its large pore size. Moreover, functionalization of MIL-101-Cr with ethylene diamine (ED) and protonated ED (PED) enhanced adsorption capacity. The performance order for the MOFs was as PED-MIL-101-Cr>ED-MIL-101-Cr>MIL-101-Cr. The

effect of pH on adsorptive removal is important in almost every adsorption study and faster adsorption was observed at lower pH on PED-MIL-101-Cr. The idea of hierarchically mesostructured MIL-101-Cr in the wastewater treatment has been implemented recently for the removal of MB and MO (Shen, Luo, Zhang, & Luo, 2015).

The adsorption of uranine over MIL-101-Cr was studied in comparison to AC and ZIF-8 (Leng et al., 2014). The extra-large surface area and large pores of MIL-101 make it more suitable for the adsorption of uranine compared to AC and ZIF-8. This high adsorption capacity can be explained by electrostatic interactions in the adsorption process. The adsorption capacity of MIL-101 is 7.25 times higher than AC. The synthesis of hierarchically mesostructured MIL-101 was studied using mineralizing agents and surfactants. Specifically, anhydrous sodium acetate or hydrofluoric acid used as mineralizing agents while well-known surfactant cetyltrimethylammoniumbromide (CTAB) were utilized for the synthesis of hierarchically mesostructured MIL-101. The addition of sodium acetate results in higher adsorption of dyes, however, CTAB resulted in large pore size and pore volume for enhanced cationic dye removal. Furthermore, kinetic studies showed that adsorption is fitted well with a pseudo second order kinetic model.

The roles of pH and temperature have been always important in the adsorption studies. In this case, the adsorption decreased with the increase in pH, showing electrostatic interaction is responsible for higher adsorption in MO removal. Moreover, thermodynamic study confirmed that adsorption was a spontaneous process. MIL-101-Cr was further tested for the removal of xylenol orange by Chen et al (Chen et al., 2012). The adsorption of xylenol orange was affected by pH strongly; lower pH favored the adsorption while higher pH deteriorated the adsorption and there was no adsorption at pH 12. However, the removal of xylenol orange was successful with adsorption capacity of 311 mg/g.

The removal of another toxic dye, malachite green (MG) was studied using MIL-100-Fe (Huo & Yan, 2012). The MOF possessed a high surface area of 1612 m^2/g with mesopores. The effect of pH was studied and an increase in adsorption capacity was observed with increase of pH form 1-4. However, a further increase in pH from 4-7 had no effect on adsorption while a decrease was observed in adsorption capacity

by increasing pH from 7-10. Moreover, electrostatic mechanism was proposed by supporting with the addition of NaCl and $CaCl_2$ to study the effect of univalent and divalent electrolyte on adsorption; initially, it had a negative effect with concentration of 0.01 mol/L, however, the effect became negligible at a concentration of 0.1 mol/L of these electrolytes. The adsorption capacity was increased by increasing temperature suggesting an endothermic process. Furthermore, it was concluded through the thermodynamic study that adsorption was controlled by entropy effect instead of enthalpy change. Moreover, adsorption isotherm of MG was also studied for MIL-101-Cr, MIL-53-Al and activated carbon for comparison. However, large surface, more active sites and negative charge makes MIL-100-Fe more suitable to remove the cationic dye MG than MIL-53-Al and MIL-101-Cr and AC. Furthermore, regeneration of the MOFs was possible by desorbing the dye using ethanol with 0.5% HCl. The higher regeneration and structural stability of MOFs proved the significance to be a potential wastewater treatment agent for MG.

The effect of pH and temperature on the adsorption highlighted another important parameter, i.e. influence of framework metals in the MOFs since it plays an important role in crafting useful properties in MOFs. The successful utilization of MOFs based on Cr and Fe as central metals proved to be successful in removing both cationic and anionic dyes. So, the significance of Cr and Fe was studied on adsorption behavior of MB and MO from wastewater for two high surface area MOFs i.e. MIL-100-Fe (1770 m^2/g) and MIL-100-Cr (1760 m^2/g) (Tong et al., 2013). The affinity of Cr with water tends to create competitive environment with MO molecules and water molecules to get into the cages of MIL-100-Cr than MO molecules. This adsorption of MO on MIL-100-Cr was almost 4.5 times less than MIL-100-Fe. However, in case of MB both MOFs showed higher adsorption (736.2 and 645.3 mg/g for MIL-100-Fe and MIL-100-Cr respectively) due to electrostatic interactions between cationic dye and anionic MOFs. Furthermore, MIL-100-Cr was used for mixture of dyes at a 1:1 ratio of MB and MO. In this case MIL-100-Cr selectively removed MB from the binary mixture due to electrostatic interactions with MB making it more suitable than MIL-100-Fe for mixture of dyes.

An Fe-MIL-100 has been prepared by selectively tuning valence of iron to tune surface area and pore size with and/or without HF and H_2SO_4 recently (Tan et al.,

2015). The MOFs were utilized in adsorptive removal of MB from aqueous solution and the highest adsorption of MB has been observed at i.e. 1105 mg/g. The kinetic study showed the pseudo second order kinetic model. The effect of pH revealed that adsorption increased with increasing pH from 2-8 and then became flat from pH 8-10 while zeta potential decreased with increasing pH. This behavior suggested that MOF surface becomes negative with increasing pH and enhances electrostatic interactions between MIL-100-Fe and cationic dye MB. The reusability of the MOF was studied for three cycles and a slight decrease in adsorption capacity was observed.

Enamul et al. reported amino functionalized MIL-101-Al for the removal of MB and MO. The adsorption capacity of the synthesized MOF has been reported as 762 mg/g. The kinetic study showed faster kinetics and high value of adsorption rate constant (Haque, Lo, Minett, Harris, & Church, 2014a). The mechanism proposed is electrostatic interaction and lower pH favored the higher adsorption. However, the structure of the MOF was not intact after utilization in MB adsorption but it retained in MO adsorption. In comparison to the amino functional MOF, there was very low adsorption of MB on MIL-101-Al suggesting that the role of amino group is very important in electrostatic interactions. Moreover, the thermodynamic study revealed the spontaneous adsorption process with endothermic nature.

The effect of pH on adsorption and role of electrostatic interactions between adsorbate and adsorbent is obvious, however, it's very important to explore significance of textural properties in adsorption. So, the application of three neutral MOFs were studied on different dyes, i.e. MO, MB and RB from DMF solution (Wang, Liu, Wang, Shao, & Su, 2013b). Through this study it's important to highlight the role of physical properties e.g. pore size and surface area in adsorption. In this study, stepwise synthetic strategy was adopted to construct three 12 connected MOF with fcu topology using metal organic polyhedron as precursor (Cu based). The prepared MOFs possessed microporous and mesoporous cages. MO and MB were successfully removed by using these MOFs but RB could not be removed due to its large size. The mechanism for the removal of MB in a mixture of MO and MB was explained that the induced anionic nature of MOF by the diffusion of Cl^{1-} ions resulted in removal of cationic MB dye. However, details about maximum adsorption capacity, effect of pH and temperature were not reported.

The application of copper based MOFs i.e. HKUST-1 (CuBTC) were studied for the removal of MB. HKUST-1 was synthesized with a surface area 279 m^2/g i.e. very low compared to usual HKUST-1 (1492 m^2/g) but the pores are changed to a mesoporous range with an average pore diameter as 2.95 nm (Lin et al., 2014). This was achieved by using ethanol/DMF as solvents, however, water was also used in this process. The adsorption was explained with the mechanism of electrostatic interaction and supported by effect of pH. As the pH values were increased from 2-7 the amount of dye adsorbed increased but further increase in pH after 7, the adsorption reduced and was almost zero at pH value 12. Moreover, lower pH i.e. 2-6 did not cause a significant change in equilibrium pH. However, the maximum adsorption was achieved at pH 7. Furthermore, surface charge behaviour of CuBTC was explained with the help of zeta potential. The surface charge of CuBTC becomes more positive at pH values <= 4 while it's more negative for pH >4. The adsorption data was more accurate with the second order kinetics and MOF could be regenerated using ethanol.

Another copper based MOF with a complex mixed linker synthesis approach was reported**.** In this study, terphenyltetra carboxylic acid (H_4TPTC) and terphenyl hexa carboxylic acids (H_6TPTC) were used as linkers in different ratios to synthesize MOF solvothermally using DMF as a solvent (Zhang et al., 2014d). The resultant MOFs with various ratios of linkers H_4TPTC/H_6TPTC were named as ZJU-24-0.25, ZJU-24-0.5, ZJU-24-0.75 and ZJU-24-0.89. The MOFs were isostructural to NOTT-101 but the surface area was lower than NOTT-101. The existence of COOH group on the pore surface was confirmed by single crystal structure determination for all ZJU MOFS. Furthermore, ZJU-24-0.89 was studied for adsorptive removal of MB due to its large pore channels and existence of COOH in the framework voids owing to high contents of H_6TPTC. The performance of ZJU-24-0.89 was compared with NOTT-101 for MB removal using different adsorption times i.e. 5 minutes to 12 h. ZJU-24-0.89 showed very fast kinetics in removing 50% of MB i.e. in just 5 minutes, however, it took 12 h to completely remove MB from the solution. NOTT-101 could only remove 5% of MB even after 12 h shown in Figure 2-1. Moreover, 902 mg/g of adsorption capacity was reported for ZJU-24-0.89 in 12 h operation, which is among the highest reported value for any porous material for MB. The existence of COOH groups in the pore surfaces of the framework gave rise to

interaction of MB molecules to form strong host-guest interaction into the pores of ZJU-24-0.89, which is further confirmed by molecular simulation. The crystal structure of the MOF is shown in Figure 2-2 before and after adsorption of MB. The summary of utilized MOFs for adsorption is given in Table 2-1.

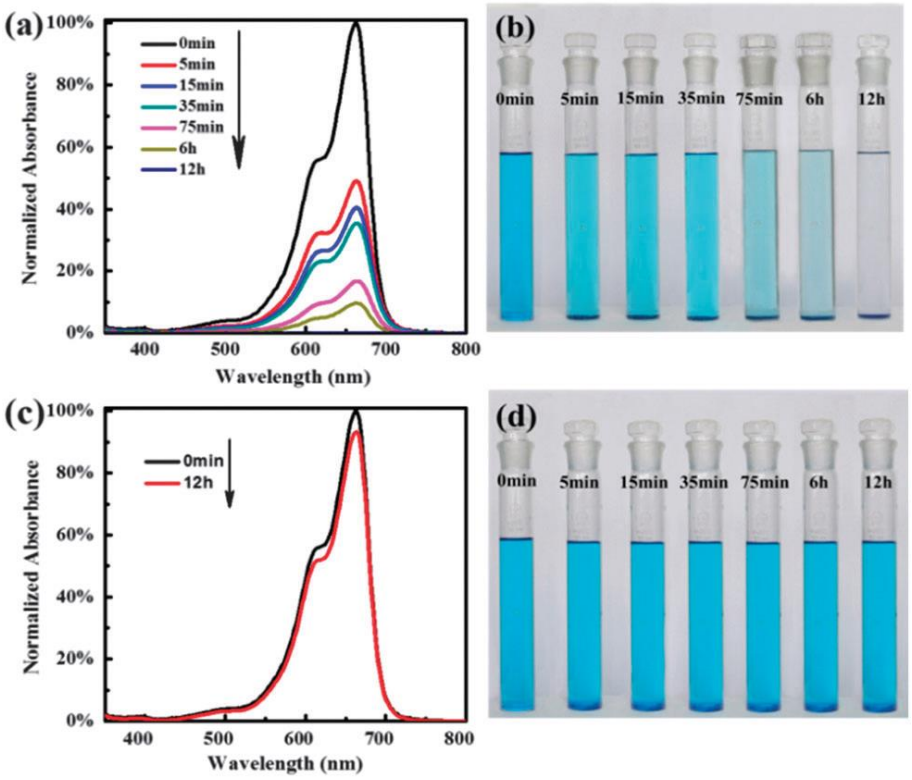

Figure 2-1 a) UV spectra of an aqueous MB solution during an adsorption test an adsorption test with ZJU-24-0.89; (b) photographs of the removal of MB in aqueous solution with ZJU-24-0.89 over time; (c) UV spectra of an aqueous MB solution during an adsorption test with NOTT-101; (d) photographs of the removal of MB in aqueous solution with NOTT-101 over time.

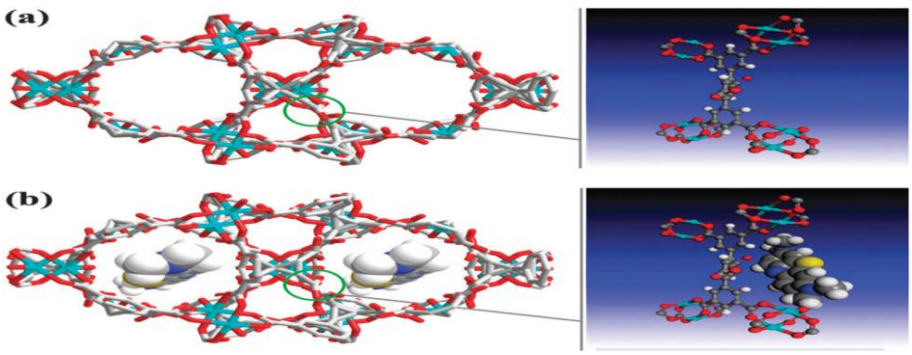

Figure 2-2 (a) Crystal structure of ZJU-24-0.89; (b) crystal structure of ZJU-24-0.89⊃MB with simulated MB molecules inside the pores.

The use of mixed ligand strategy for the synthesis of Zn based MOFs was studied recently. The conventional and highly studied ligand i.e. BDC was used in combination with (TIB) 1,3,5-triIJ1H-imidazol-1-yl)-benzene and 4,4'-biphenyl-dicarboxylic acid (H_2BDA). Three different MOFs were studied for the removal of Congo red (CR) dye. The MOFs showed excellent stability after several cycles of adsorption, which is a big achievement since previous Zn based MOFs are less water stable. Moreover, selective adsorption of CR in mixture of dyes i.e. CR+MB, CR+Rhodamine B (RhB), CR+MO makes the Zn based MOFs as a selective adsorbent material (Zhang, Gao, Liu, & Liu, 2015b)

A new copper based MOF has been synthesized hydrothermally using copper acetate and 4, 4′-bis(1,2,4-triazolyl-1-yl)-biphenyl (btb) ligand for extended synthesis time of 3 days. Single crystal X-ray diffraction study revealed a rare 3D trinodal (3, 4, 4)-connected network with 3, 4, 4T20 topology. The synthesized MOF showed good adsorption for a model dye i.e. Congo red**.** The resultant novel MOF showed high adsorption capacity (about 650 mg/g) of Congo red dye in its microspores. Moreover, the MOF exhibited fluorescence properties at room temperature, making it a potential in photocatalytic reactions (degradation) of dyes (Wang, Li, Yu, Van Hecke, & Cui, 2015f).

The presence of metal ions either cationic or anions/anionic complex is a one of major pollutants in wastewater. Inorganic anionic complexes include $Cr_2O_4^{2-}$ and $Cr_2O_7^{2-}$ ions, which can cause cancer by accumulating in living organisms. A new robust Cd based MOF using hexa[4-(carboxy-phenyl)oxamethyl]-3-oxapentaneacid (H_6L), 4,4’-di(1H-imidazol-1-yl)-1,1’-biphenyl (bib) and 1,3,5- tri(1H-imidazol-1-yl)benzene (tib) ligands has been synthesized and tested for $Cr_2O_4^{2-}$ and $Cr_2O_7^{2-}$ detection, dyes removal and sensitizing of Tb^{3+} recently. The MOFs exhibited varied topologies owing to the diff erent N-donor bridges and used for organic/inorganic waste removal/detection. Cationic and anionic dyes i.e. MB, RhB and MO were studied in adsorption. The synthesized MOF showed a high adsorption capacity in terms of cationic dye (MB) removal with adsorption capacity 317.19 mg/g. Moreover, successful encapsulation of Ln^{3+} was reported for Tb^{3+} after testing different $Ln(NO_3)_3$. This study highlights the robust nature of MOFs for various applications with tailored properties (Yi, Li, Wu, & Sun, 2015).

Table 2-1 MOFs for dyes removal with MIL's and other MOFs used in dyes removal.

MOF	Metal precursor	Linker	Surface area (m^2/g)	Dyes	Adsorption capacity Mg/g	Reference
MIL-101-Al	$AlCl_3.6H_2O$	NH_2BDC	1980	MB and MO	762, 188	(Haque et al., 2014a)
MIL-53-Cr	Cr	BDC	1438	MO	57.9	(Haque et al., 2010b)
MIL-100-Cr	Cr powder	BTC	1760	MO and MB	645 and 211	(Tong et al., 2013)
Mil-101-Cr	Cr Powder	BDC	3200	MO	194	(Haque et al., 2010b)
MIL-101-Cr	Cr	BDC	387	Xylenol orange	311	(Chen et al., 2012)
MIL-101-Cr	$Cr(NO_3)_2.9H_2O$	BDC	1500-3200	MB and MO	10 and 247	(Shen et al., 2015)
MIL-101-Cr	$Cr(NO_3)_2.9H_2O$	BDC	5900	Uranine	142.7 @ 45 °C	(Leng et al., 2014)
MIL-100-Fe	$Fe(SO_4)_2$	BTC	2776	MB	1105	(Tan et al., 2015)
MIL-100-Fe	Fe powder	BTC	1626	MG	485	(Huo & Yan, 2012)
Three	MOP Cu	Pyrazine,	N.A	MB, MO and	0.012 ,0.014	(Wang

neutral MOFs	based	bipyridine and bpe		RB	and 0	et al., 2013b)
HKUST-1	$Cu(NO_3)_2$. 3H2O	BTC	279	MB	4.4	(Lin et al., 2014)
ZJU	$Cu(NO_3)_2$. $3H_2O$	H4TPTC/ H_6TPTC	N.A	MB	902	(Zhang et al., 2014d)
$[Zn_3(BDC)_2(BDA)(TIB)_2]_n$	$Zn(NO_3)_2 \cdot 6H_2O$	BDC/BDA/TIB	N.A	Congo red, MB, RhB, MOI	60.2	(Zhang et al., 2015b)
Cu (II) H3ntba	$Cu(NO_3)_2$. 3H2O	Btb, H3ntba	N.A	Congo red	656	(Wang et al., 2015f)
$[Cd6 (L)_2 (bib)_2 (DMA)_4]$	$Cd(NO_3)_2 \cdot 4H_2O$	H_6L, bib	38-68	MB, MO and RhB	317.9, 102.4, 67.0	(Yi et al., 2015)

BDC: 1, 4-Benzene dicarboxylic acid, NH_2BDC: 2-Amino 1, 4-Benzene dicarboxylic acid, BTC: 1, 3, 5-Benzene tricarboxylic acid, btb= 4, 4′-bis(1,2,4-triazolyl-1-yl)-biphenyl, H3nbta = 5-nitro-1,2,3-benzenetricarboxylic acid), DMA= Dimethylacetamide, H_6L= hexa[4-(carboxy-phenyl)oxamethyl]-3-oxapentaneacid (H_6L), bib= 4,4'-di(1H-imidazol-1-yl)-1,1'-biphenyl, TIB= [1,3,5-tri(1H-imidazol-1-ly) benzene], BDA= 4,4'-biphenyl-dicarboxylic acid

The use of MIL's is quite successful in phenolic pollutants removal. In the field of phenolic organic removal, Sung et al. used several MIL's, e.g. MIL-53-Cr, MIL-101-Cr and MIL-100-Fe in removal of bisphenol A (BPA). MIL 101-Cr and MIL-100-Fe were compared with AC for BPA adsorption. Although all the MOFs showed significant adsorption of BPA, however, MIL-101-Cr showed faster kinetics compared to MIL-100-Fe due to large pore size. The adsorption capacity of MIL-101-Cr was 4.54 and 1.84 times higher than activated carbon and MIL-100-Fe. The π-π interaction and hydrogen bonding were suggested for the adsorption mechanism (Park, Hasan, Khan, & Jhung, 2013; Qin, Jia, Liu, Li, & Wu, 2014).

The removal of phenol and paranitrophenol (PNP) was studied using NH_2-MIL-101-Al, MIL-100-Cr and MIL-100-Fe (Liu, Yang, Zou, & Peng, 2014a). NH_2-MIL-Al showed very high adsorption of PNP as compared to MIL-100-Cr and MIL-100-Fe. Moreover, NH_2-MIL-101-Al showed exceptionally high selectivity of PNP over phenol than conventional AC due to hydrogen bonding between NH_2 and nitro group of PNP. The importance of the metal in MOFs is evident in various applications of catalysis, gas adsorption, drug delivery and in WWTPs. The efficient use of unsaturated metal sites have been explored recently by PNP removal using HKUST-1 (HKUST-1 is famous for its unsaturated metal sites) (Andrew Lin & Hsieh, 2015). In this study, HKUST-1 was synthesized with a facile method and tested for PNP removal and selective removal of PNP from its binary mixture of phenol. The MOF showed adsorption capacity of about 400 mg/g, almost 2.75 times higher than NH_2-MIL-Al due to affinity of nitro group and metal site of MOF. Furthermore, interaction of benzene ring with HKUST-1 due to π-π interactions resulted in a higher adsorption capacity. Moreover, kinetic study was presented with the pseudo second order kinetic model. Moreover, faster kinetics was observed at higher temperatures showing endothermic nature of the process.

Table 2-2 Summary of MOFs used for adsorptive removal of organic wastes.

MOF	Metal Precursor	Linker/s	Surface area (m^2/g)	Adsorbate	Adsorption capacity (mg/g)	Reference
CAU	$AlCl_3.6H_2O$	NH_2BDC	1281	NB	970±10	(Xie, Liu, Huang, Yang, & Zhong, 2014)
MIL-68-Al	$Al(NO_3)_3$	BDC	1417	NB	1130±10	(Xie et al., 2014)
MIL-101-Al	AlCl3	NH_2BDC	1942	PNP	122	(Liu et al.,

						2014a)
MIL-100-Fe	Fe	BTC	1754	Bisphenol A	55.6	(Qin et al., 2014)
MIL-100-Fe	Fe	BTC	1492	Naproxen Clofibric acid	115 N.A	(Hasan, Jeon, & Jhung, 2012)
MIL-53-Cr	$CrCl_3.6H_2O$	BDC	1438	2,4-dichlorophenoxyacetic acid	556	(Jung, Hasan, & Jhung, 2013)
MIL-101-Cr	$Cr(NO_3)_2.9H_2O$	BDC	3711	Bisphenol A	252.5	(Qin et al., 2014)
MIL-101-Cr	$Cr(NO_3)_2.9H_2O$	BDC	2555	Naproxen Clofibric acid	154 347	(Hasan, Choi, & Jhung, 2013)
MIL-101-Cr	$Cr(NO_3)_2.9H_2O$	BDC	3014	Naproxen Clofibric acid	132 312	(Hasan et al., 2012)
ZIF-8	$Zn(O_2CCH_3)_2$	2 methyl imidazole	1500	Phthalic acid	654	(Khan, Jung, Hasan, & Jhung, 2015)
UiO-66	$ZrCl_4$	BDC	710	Phthalic acid	187	(Khan et al., 2015)

NH_2-UiO-66	$ZrCl_4$	NH_2BDC	651	Phthalic acid	224	(Khan et al., 2015)
UiO-66	$ZrCl_4$	BDC	982	(MCPP)	370	(Seo, Khan, & Jhung, 2015)
UiO-66	$ZrCl_2$	BDC/NH_2 BDC	652	Pyridine	0.55 @ 70 °C	(Hasan et al., 2014)
HKUST-1	$Cu(NO_3)_2$.3H2O	BTC	1140	PNP	437 @ 60 °C	(Andrew Lin & Hsieh, 2015)

MCPP: Methylchlorophenoxypropionic acid

Recently, pharmaceuticals and personal care products (PPCPs) are found in wastewater, giving rise as emerging pollutants. Naproxen and clofibric acid are typical personal care products and pharmaceuticals. Zubair et al. used MIL-101 to remove naproxen and clofibric acid by adsorption (Hasan et al., 2012). MIL-101-Cr was compared with MIL-100-Fe and activated carbon for removal of naproxen and clofibric acid. The MIL-101 showed faster kinetics and higher adsorption compared to MIL-100-Fe and AC due to large surface area and pores. This study shows the pseudo 2^{nd} order kinetics with higher adsorption at lower pH, showing importance of electrostatic interaction in adsorption of naproxen and flobiric acid. Later, functionalization of MIL-101-Cr using aminomethanesulfonic acid (AMSA) and ethylene diamine (ED) to generate acidic (SO_3H) and basic (NH_2) groups respectively, was carried out to study the removal efficiency for naproxen and clofibric acid. This functionalization introduced acid base interactions between MOF and PPCPs resulting in high adsorption (Hasan et al., 2013). The schematic of introducing acid base sites in the synthesis of MOFs and removal of naproxen is shown in Figure 2-3.

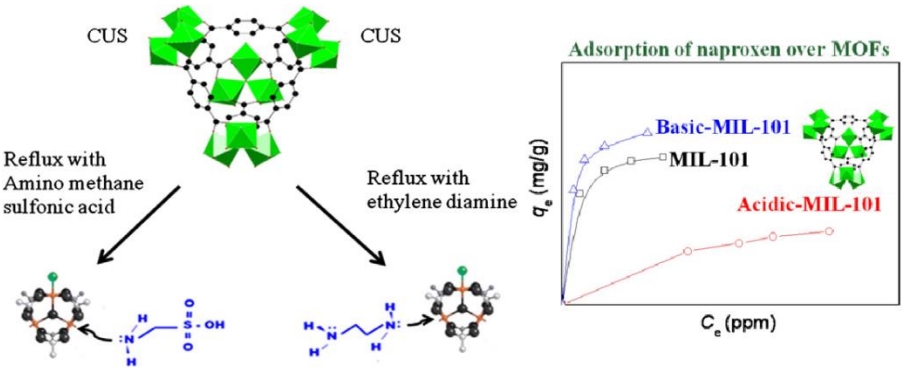

Figure 2-3 Modification of MOFs to introduce acidic and basic functional groups Modification of MOFs to introduce acidic and basic functional groups on CUS or open metal sites of MOFs and naproxen adsorption isotherms for MIL-101.

MIL-53-Cr was used in removal of herbicide 2,4-dichlorophenoxyacetic acid (2,4D) in comparison to conventional AC and USY zeolite (Jung et al., 2013). The MOF showed very high adsorption capacity due to strong electrostatic interactions between the negatively charged 2, 4D and positively charged surface of MIL-53-Cr. The adsorption was very fast on MIL-53-Cr and it removed most of the adsorbate in the first hour compared to AC, which showed gradual adsorption in 24 h. The adsorption was favored at lower pH and it had negative effect at pH values higher than 5 because of electrostatic repulsion. The isoelectric point for the MIL-53-Cr is 5 so adsorption is favorable at pH range of 3-5. However, slight adsorption at pH 6 signifies the π-π interaction between the benzene rings of adsorbent and adsorbate. Thermodynamic studies showed spontaneous exothermic adsorption with high reusability of the MIL-53-Cr.

The use of Al based MOF in removal of nitrobenzene (NB) has been reported (Xie et al., 2014). In this study CAU-1 and MIL-68-Al have been prepared by solvo/hydrothermal process and were selected among thirteen MOFs to treat NB. These MOFs showed high adsorption of NB and can be regenerated by using methanol. The adsorption data can be explained by Langmuir model with pseudo second order kinetics. The high adsorption capacities, i.e. 970±10 and 1130±10 mg/g, have been reported for CAU-1 and MIL-68-Al, respectively, which is higher than reported porous materials. The mechanism of adsorption process has been explained by Weber-Morris intra-particle diffusion model. It has been observed that both the intra-particle diffusion and film resistance play a role in rate determining

step i.e. adsorption controlling step. The adsorption is very high in first few minutes i.e. 5-20 and subsequently decreases due to film resistance and intra-particle diffusion resistance. The effects of temperature and pH were also reported in the study, however, increases in temperature resulted in decreased NB removal showing exothermic nature of the process. Moreover, an increase in pH from 2-4 results in higher adsorption while it had no significant effect in a range of 4-6 and then decreases from 6-10 on CAU-1. Almost similar effect of pH has been observed in case of MIL-68-Al for acidic and basic pH values. However, there is no significant change in the range of pH from 6-8.

A comparative study for the removal of phthalic acid (H2PA) and diethyl phthalate (DEP) has been reported (Khan et al., 2015) using activated carbon, ZIF-8, UiO-66, and NH_2-UiO-66. The adsorption capacities for ZIF-8, UiO-66 and UiO-66-NH_2 and AC were 654,187, 224 and 249 mg/g respectively. ZIF-8 showed a higher adsorption capacity than commercial AC, UiO-66 and NH_2-UiO-66 MOFs owing to electrostatic interaction between ZIF-8 and phthalic acid (H_2PA) while it was not effective to remove DEP due to its lesser charge in water solution. However, pH had a significant effect on adsorption due to acid base interactions in case of ZIF-8. The adsorption capacity increased by increasing pH up to 7 and then started decreasing gradually and becomes negative at pH value of 10. This can be explained by zeta potential measurements; the surface charge of ZIF-8 remains positive below pH 10 and then becomes negative, which is responsible for electrostatic repulsion between $ZIF\text{-}8^-$ and PA^{2-}. Moreover, H_2PA molecules dissociate into solution in two ways i.e. $H_2\text{-}PA/H\text{-}PA^-$ and $H\text{-}PA^-/PA^{2-}$ so the negative charge of adsorbate increases with increasing pH. The significance of acid base interactions is evident from NH_2-UiO-66 as there are more basic sites and higher adsorption is observed than pristine UiO-66. However, higher adsorption capacity and reusability of ZIF-8 makes a promising member for the adsorptive removal of H_2PA.

Some of the waste materials further decompose into ions creating sever environmental problems. The example of organoarsenic is one of the cases. Such organarsenic compounds can eventually converted into aresnates and arsenites which are very harmful according to EPA. The removal of organoarsenic material from wastewater has been reported recently using ZIF-8 in comparison to various porous materials e.g. MIL-53-Cr, MIL-101, AC and zeolite Y (Jung, Jun, Hasan, & Jhung,

2015). The adsorption study revealed a higher adsorption capacity of p-arsanlic acid could be achieved using ZIF-8 and even improvement in adsorption could be induced by tuning the pore size to the mesoporous range. Moreover, kinetic study suggested pseudo second order kinetic model for the adsorption study with the maximum adsorption capacity in the range of 730-790 mg/g for ZIF-8 and meso-ZIF-8. Due to large functionalities of ZIFs-8 possible mechanism of adsorption is a combination of electrostatic interactions, hydrogen bonding and π-π interactions. Moreover, the effect of central metal atom was studied for the adsorptive removal of p-arsanlic acid and roxarsone. Among various materials, i.e. MIL-53-Cr, MIL-100-Al, MIL-100-Cr, MIL-100-Cr, MIL-101-Cr, AC and zeolite Y, MIL-100-Fe proved to be the best adsorbent while MIL-100-Al and MIL-100-Cr had the same adsorption capacity range. In case of MIL-100-Fe organic materials i.e. p-arsanlic acid and roxarsone bound strongly compared to water molecules giving rise to a high adsorption capacity compared to MIL-100-Al and MIL-100-Cr. The proposed adsorption mechanism was electrostatic interactions (Jun et al., 2015).

The functionalization of UiO-66 with NH_2 groups showed significance removal of pyridine (Hasan et al., 2014). In this study, hydrogen bonding proved to be decisive in removal of pyridine by overcoming base-base repulsion of the NH_2 and N of the pyridine. However, it is required to carefully study the mechanism of the organic materials removal due to large number of functionalities of both adsorbate-adsorbent and, π-π interactions of the benzene rings of both them. Moreover, the increase in temperature resulted in an increased adsorption capacity of the MOF in case of vapor phase and liquid phase adsorption. This effect proved to be significant due to an enlarge window size of UiO-66-NH_2. The schematic of the hydrogen bonding in pyridine removal is shown in Figure 2-4. Therefore, it is vital to carefully choose the adsorbent possessing, specific textural properties and functionalities according to the adsorbate.

Figure 2-4 Schematic of pyridine removal through hydrogen bonding using NH2-UiO-66

The adsorptive removal of another herbicide, methylchlorophenoxypropionic acid (MCPP), from wastewater was studied using UiO-66, Cr MIL-53 and MIL-101 (Seo et al., 2015). The adsorption capacity of the UiO-66 is much higher than of AC and MIL-53 and MIL-101. The kinetic study showed a very high adsorption rate than that of AC with pseudo second order kinetic model. The mechanism of adsorption process has been revealed as electrostatic interaction and π-π interactions by studying pH effect on adsorption of MCPP. The adsorption is favored at a pH range of 2-4 and has a negligible effect from 4-6 with a slight decrease in adsorption. However, adsorption decreases sharply at higher pH values due to electrostatic repulsion. The recovery of MOF using benign solvents i.e. water/ethanol makes UiO-66 as a potential candidate to remove herbicides e.g. MCPP from wastewater.

2.4.2 Inorganic waste removal

The removal of heavy metals from wastewater has been a big challenge as most of them are very dangerous to health and even causing cancer. The utilization of MOFs in metal removal is less explored. However, some of the MOFs, e.g. HKUST-1, MOF-5 and FeBTC (Iron benzenetricarboxylate), have been studied for metal removal from wastewater. Specifically, the functionalization of Cu-MOF proved to be one of the successful processes in removing heavy metals e.g. Hg^{2+} from wastewater (Ke et al., 2011a). HKUST-1 was functionalized with thiol containing organic moiety to remove mercury. Though the functionalization resulted in decreased surface area and pore volume but the MOF proved to be very efficient in Hg^{2+} removal. The adsorption capacity of thio functionalized MOF was 714.29 mg/g

while no adsorption was observed on un-functionalized HKUST-1. The kinetics of the process showed that data can be explained with Langmuir model with 2nd order kinetics and correlation coefficient value of 0.9999. The concentration of Hg^{2+} in waste water ranges from few parts per billion (ppb) to parts per million (ppm). This study showed that functionalized HKUST-1 can be used in a wide range of initial concentration of Hg^{2+} ranging from 81 ppb to 1500 ppm. The schematic of the functionalization of HKUST-1 is shown in Figure 2-5.

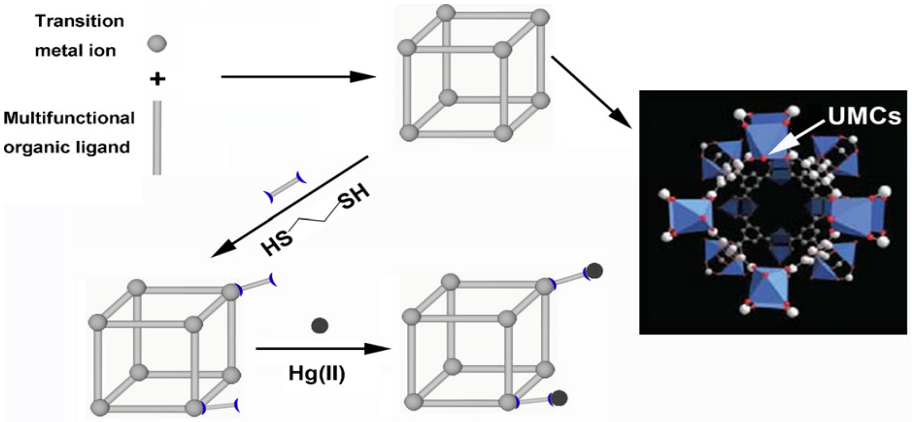

Figure 2-5 Schematic illustration of the thiol-functionalization of MOFs through coordination bonding between one thiol group of dithioglycol and coordinatively unsaturated.

The removal of As ion was studied by using Fe based MOF i.e. FeBTC (Zhu et al., 2012). In this study, FeBTC was compared with iron oxide nanoparticles (NPs). The adsorption capacity of FeBTC was 6 times faster than the conventional iron oxide nanoparticles of size 50 nm and 36 times higher than commercial iron oxide nanoparticles. Moreover, faster kinetics with spontaneous adsorption was observed compared to iron oxide NPs. However, adsorption of As ions was not onto the surface of MOF but into the cages of MOF, which is confirmed by FTIR and TEM. The successful implantation of MOFs in metal removal continued and new ZrBTC (MOF-808) with a facile synthesis method has been reported using microwave treatment in just 5 minutes. The synthesized MOF has been used in the removal of As ion from wastewater (Li, Yang, Sui, & Yin, 2015d). Another study on removal of Cu ions from wastewater has been reported using MOF-5 (Bakhtiari & Azizian, 2015). It has been observed that MOF-5 can be effectively used to remove Cu ions with an adsorption capacity of 290 mg/g. The kinetic studies showed that adsorption

data was fitted well with pseudo first order model. Moreover, adsorption was increased by increasing temperature showing that process is endothermic. Moreover, increase in pH from 3-5.2 resulted in increased adsorption and at pH value of 6 more copper ions precipitate as $Cu(OH)_2$ so as the selected pH range was 3-5.2. Furthermore, the highest removal efficiency is observed at pH value of 5.2.

The removal of phosphate from wastewater has been studied recently using UiO-66 (Lin, Chen, & Jochems, 2015). The functionalized MOF i.e. UiO-66-NH_2 was also tested. The functionalization slightly decreased the surface area and pore volume but adsorption capacity was increased than pristine UiO-66. The higher temperature resulted in higher adsorption which confirmed endothermic nature of adsorption in this case. Both pseudo 1st order and pseudo 2nd order kinetic models were used to analyze experimental data, but experimental data fits with 2nd order kinetics. Moreover, the isothermal adsorption data could be explained more accurately with Langmuir model. The possible mechanism of phosphate removal is electrostatic interaction between Zr-MOF (positive) and phosphate (negative). However, addition of NH_2 group in UiO-66 slightly increases adsorption due to additional adsorptive sites to phosphate.

The stability and regeneration of MOFs make them suitable to use in phosphate removal from wastewater and urine. The schematic of the phosphate removal by UiO-66 and UiO-66-NH_2 is shown in Figure 2-6.

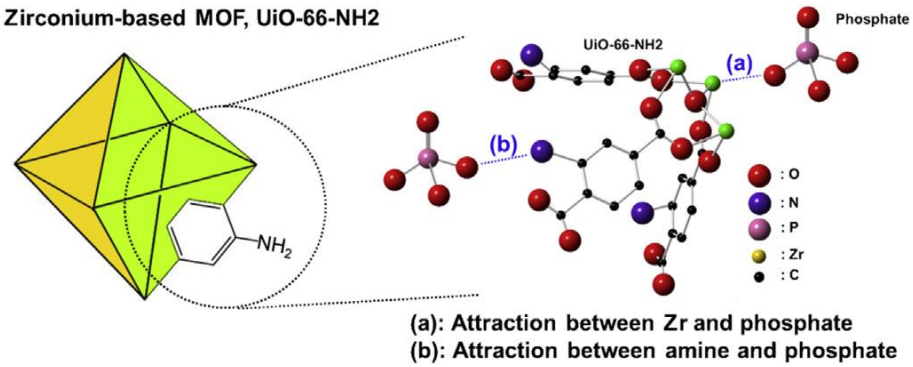

Figure 2-6 Schematic of removal of phosphate using UiO-66 and NH_2-UiO-66.

The removal of another anionic species i.e. perchlorate has been presented recently using Cu based MOFs (Li, Yang, Zhang, Zhu, & Niu, 2015b). The adsorption study showed that novel Cu based MOF efficiently removed perchlorate from wastewater. The adsorption capacity is 133.5 mg/g with favoured adsorption under acidic

conditions due to anionic nature of the adsorbate. The kinetic data fits more accurately with 1st order kinetic model and adsorption isotherms could be explained more accurately with Langmuir model. The combined effect of electrostatic interactions and ion exchange are the possible mechanism for the perchlorate removal.

Table 2-3 MOFs used for successful removal of heavy metal ions and inorganic anions

MOFs	Metal Source	Linker	Surface area	Adsorbates (metals)	Adsorption capacity (mg/g)	Reference
HKUST-1	$Cu(NO_3)_2$	BTC	1492	Hg^+	714.29	(Ke et al., 2011a)
MOF-5	$Zn(NO_3)_2$	BDC	888.5	Cu^+	290	(Bakhtiari & Azizian, 2015)
FeBTC	$FeCl_3 \cdot 6H_2O$	BTC	N.A	As^+	12.287	(Zhu et al., 2012)
UiO-66 NH_2-UiO-66	$ZrCl_4$	BDC NH_2BDC	990 815	Phosphate	237 165	(Lin et al., 2015)
CuBPD	CuAce	4, 4 - Bipyridine	N.A	perchlorate	133.5	(Li et al., 2015b)

2.5 Catalytic degradation of organic waste

MOFs are usually effective in photocatalytic degradation of dyes. Most of studies on MOFs in degradation of water contaminants focused on photocatalytic degradation due to their limitation of sustain harsh operating conditions of strong pH and reactive

sulphate species in case of persulfate (PS) and/or peroxymonosulphate (PMS). However, there are some studies on activation of PMS for catalytic degradation of conventional and emerging water contaminants. (Lin & Chang, 2015a) Lin et al. studied degradation of RhB using ZIF-67 with PMS as an oxidizing agent. Moreover, elimination of caffeine was also studied with other MOFs. Most of the studies on MOFs in catalytic degradation used either carbon or carbon/metal composite instead of pristine MOFs (Lin & Chen, 2016; Xia et al., 2014).

2.6 Factors affecting MOFs selection for WWTPs

The utilization of MOFs in wastewater treatment processes is mainly studied using adsorption. The reason behind is the simple process, less generation of further toxic and/or green-house gases. The other factors include surface and/or in situ modifications of functional groups in MOFs. The main factors usually considered in MOF selection for WWTPs are

- Synthesis process
- Water stability
- Structure and textural properties
- Importance of functionality of the MOFs i.e. functional linkers and/or multi linker MOFs
- Recycle and reuse
- Photocatalytic ability of the MOFs e.g. Fe and Co based MOFs.

There are numerous studies on synthesis and characterization of MOFs with tailored surface properties i.e. surface area, pore, PSD, pore volume etc. that use of MOFs in WWTPs is less explored to date. However, the success of MOFs in WWTP is encouraging/remarkable and a lot more will come in near future. Moreover, the MOFs tested till now are limited to few metals i.e. Cr, Al, Fe, Zr, and Zn in aqueous phase adsorption studies. The highest number of MOFs studied belong to Cr based MOFs and it is well known that Cr itself causes environmental problems in its Cr(VI) form. It is rarely mentioned in MOFs studies regarding secondary pollution by these framework metals e.g. Cr and Cd. However, structural stability is usually reported in most of studies using XRD technique. The utilization of other metals with less toxicity level in adsorption studies should be explored in future.

Furthermore, there are just a few studies on adsorptive removal of metal ions and inorganic pollutants using MOFs. There should be more studies in exploring MOFs utilization in metal and inorganic waste removals. Moreover, care should be taken in selecting specific range of initial waste concentration C_0 giving consideration to real time concentrations of typical waste materials in waste streams. This will give quite clear indication of MOFs application in WWTPs on commercial levels.

The waste stream discharged in water bodies usually contain more than one type waste materials in them e.g. dyes, metal ions, and PPCPs etc. The studies on individual type of waste materials has been reported so far using MOFs but there are less reports on combination of different types e.g. dyes + pharmaceutical waste, dyes + metal ions, pharmaceutical waste + metal ions of wastes in a single study. The combination of waste materials can be selected according to functionality, textural properties and post synthetic treatment of MOFs.

2.7 Summary

MOFs have been used in wastewater treatment owing to their excellent textural properties, abundance of functional groups and their tunability. Various MOFs have been explored for WWTPs, however, certain limitations such as less water stability, difficulty in regeneration and leaching of metal ions into water bodies are major hindrances for their wide spread applications. Aluminium, cadmium and chromium based MOFs have been studied extensively in WWTPs, however, leaching of metal ions are not reported in detail. Most of the MOFs are used in adsorptive removal of organic dyes while metal removal is least explored in WWTPs by MOFs. Adsorptive removal of phenolic compounds is getting popularity while more research is needed for application of MOFs in advanced oxidation processes.

Chapter 3 Excellent performance of copper based metal organic frameworks in adsorptive removal of sulfoneamide antibiotics from wastewater*

*Adopted with permission from (M.R, Azhar, H.R, Abid, H. Sun, V. Periasamy, M.O., Tade, S. Wang, "Excellent performance of copper based metal organic framework in adsorptive removal of toxic sulfonamide antibiotics from wastewater", *Journal of Colloidal and Interface Science*, pp. 344-352, 2016). Copyright Elsevier

3.1 Introduction

There are more than 250 antibiotics registered for human and veterinary medicine. The use of antibiotics is rapidly increasing throughout the world (Ahmed, Zhou, Ngo, & Guo, 2015a; Cruz et al., 2014; Tonucci, Gurgel, & Aquino, 2015). During the last decade the wide usage of antibiotics has caught public attention due to their presence in wastewater (Daughton & Ternes, 1999). The detection of antibiotics in the wastewater at various locations has made them highly studied pollutants nowadays (Michael et al., 2013). The accumulation of these antibiotics in the aquatic environment due to their persistent nature is a major concern to the scientists and environmentalists. Several studies showed that the exposure to the antibiotics with the concentrations in µg/L-mg/L are susceptible to inducing severe effects on survival, growth and body weight of microflora and microfauna (Chen & Zhou, 2014; Lai, Hou, Su, & Chen, 2009).

Sulfonamide antibiotics are usually used in human medicine as well as cattle farming. The residuals of sulfonamide antibiotics and metabolites discharged from agricultural runoff and wastewater treatment plants have high potential to enter surface and ground waters (Ji, Chen, Zheng, Xu, & Zhu, 2009; Michael et al., 2013; Tao et al., 2014a). The representative sulfonamides are sulfamethoxazole, sulfadiazine, sulfamerazine, and sulfchloropyridazine (SCP). Among these sulfonamide drugs, SCP is one of the most commonly used antibiotic in cattle farming either to treat bacterial infections and/or as a feed stock additives and husbandry because of its low cost and broad-spectrum antimicrobial activity. As a result, the discharge of SCP in water has been increased in recent years (García-Galán, Díaz-Cruz, & Barceló, 2012; Herrero, Borrull, Pocurull, & Marcé, 2014; Huerta et al., 2015; Rehman et al., 2015; Sim, Kim, Choi, Kwon, & Oh, 2013a; Tao et al., 2014a). Due to high consumption of SCP and discharge into wastewater, it is highly recommended to treat the wastewater to comply with local and international environmental regulations. The processes for the treatment of antibiotics, e.g. coagulation and advanced oxidation, are not very effective but high costing (C. Adams, 2002; Dirany, Sires, Oturan, Ozcan, & Oturan, 2012b; Kang et al., 2016; Rehman et al., 2015).

Adsorption has emerged as an effective and cost-effective method in waste removal without causing the problem of secondary pollutants. The efficiency of adsorption process is highly affected by the type of adsorbate, adsorbent, and operating conditions. Several adsorbents have been reported for the adsorption of antibiotics, e.g. multiwall carbon nanotubes, activated carbons, zeolites, clay, and metal organic frameworks (MOFs) (Braschi, Blasioli, Buscaroli, Montecchio, & Martucci, 2015; Carrales-Alvarado, Ocampo-Perez, Leyva-Ramos, & Rivera-Utrilla, 2014; Cychosz & Matzger, 2010; Fakhri & Behrouz, 2015; Liu et al., 2015c; Martucci et al., 2013; Nielsen & Bandosz, 2016; Smith & Rodrigues, 2015; Tonucci et al., 2015; Yang, Chen, Zhang, & Li, 2015).

MOFs are a new class of materials. The unique characteristics of MOFs such as high surface area, tuneable pore size, and functionalities make them promising materials in hydrogen storage, CO_2 capture, CH_4 storage catalysis and drug delivery (Abbasi, Rizvandi, Azadbakht, & Rostamnia, 2016; Abid et al., 2012c; Gandara, Furukawa, Lee, & Yaghi, 2014b; Grant Glover, Peterson, Schindler, Britt, & Yaghi, 2011; Rao, Lu, Xiao, Kan, & Deng, 2011; Rostamnia, Alamgholiloo, & Liu, 2016; Wang et al., 2015e; Zhang et al., 2015c). The use of MOFs in wastewater treatment processes (WWTPs) is relatively new dated back only to 2010. Since then, the research on MOFs in WWTPs is increasing rapidly, however, only few studies are available in pharmaceutical waste removal (Haque et al., 2010a).

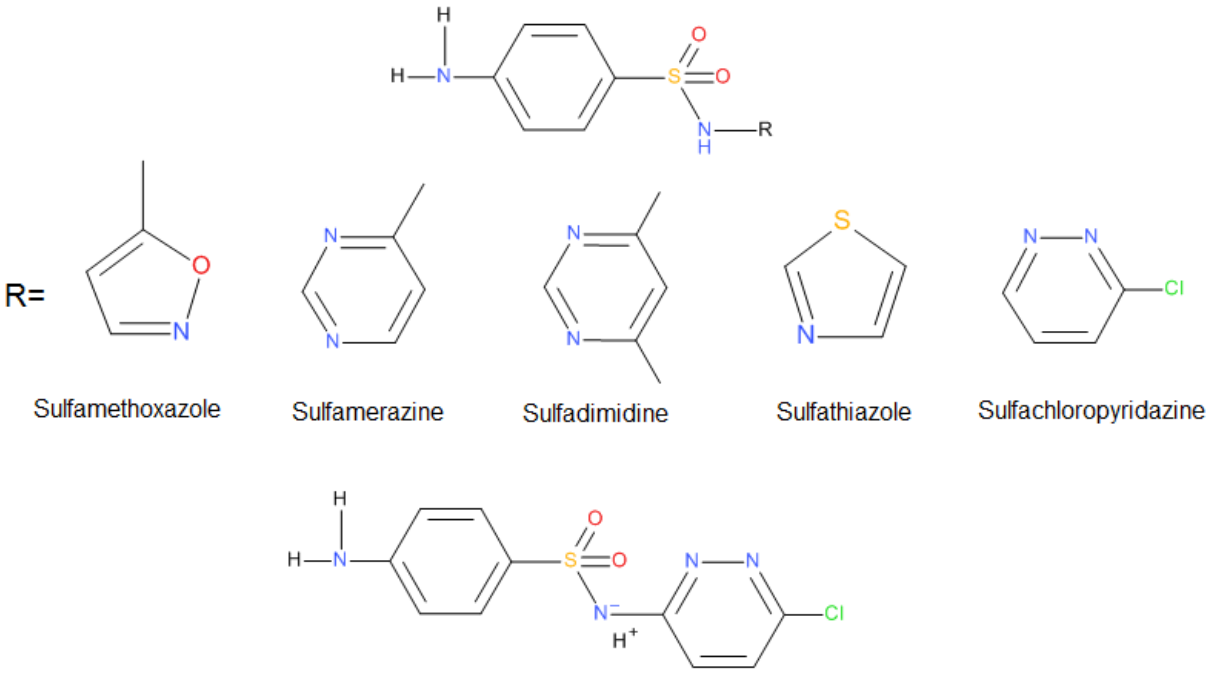

Scheme 3-1 General structures of sulofnamide antibiotics with some representative members including SCP.

HKUST-1, a copper based MOF, is considered as one of the thermodynamically stable MOFs. It has been the most studied MOF due to easy synthesis, high surface area, large pore volume and unsaturated metal sites. Recently, Lin et al. (Andrew Lin & Hsieh, 2015) studied HKUST-1 in phenol and paranitrophenol removal using adsorption technique. Other investigations include removal of methylene blue and Hg^{2+} (Ke et al., 2011b; Lin et al., 2014). There is no comprehensive study in antibiotic removal by such a promising MOF. Only one study in water stability of different MOFs toward adsorption of sulfasalazine was reported (Cychosz & Matzger, 2010). In this chapter, a detailed study on adsorptive removal of SCP, a representative sulfonamide antibiotic, is presented. The mechanism of adsorption, effect of pH, adsorption kinetics and isotherms are presented. A general structure of the sulfonamide antibiotics is shown in scheme 3-1.

3.2 Experimental

All the chemicals, i.e. $Cu(NO_3)_2 \bullet 3H_2O$, benzene tricarboxylic acids (BTC), ethanol, sulfachloropyradazine, and methanol were supplied by Sigma–Aldrich, Thermo Fisher Scientific, and Perth Scientific and used without further purification. In a

typical synthesis of HKUST-1, 1.087 g of $Cu(NO_3)_2 \bullet 3H_2O$ was dissolved in 15 mL absolute ethanol while 0.525 g of BTC was dissolved in another 15 mL absolute ethanol. Then, both the solutions were transferred into a Teflon autoclave and heated in an oven at 393 K for 12 h. The resultant blue crystals were filtered under vacuum and dried at 418 K overnight. The activation of the as-synthesized MOF was carried out using methanol for 2 d by immersing in methanol and subsequently dried at 418 K for later use in adsorption tests.

3.2.1 Synthesis of MOFs

All the chemicals, i.e. $Cu(NO_3)_2 \bullet 3H_2O$, benzene tricarboxylic acids (BTC), ethanol, sulfachloropyradazine, and methanol were supplied by Sigma–Aldrich, Thermo Fisher Scientific, and Perth Scientific and used without further purification. In a typical synthesis of HKUST-1, 1.087 g of $Cu(NO_3)_2 \bullet 3H_2O$ was dissolved in 15 mL absolute ethanol while 0.525 g of BTC was dissolved in another 15 mL absolute ethanol. Then, both the solutions were transferred into a Teflon autoclave and heated in an oven at 393 K for 12 h. The resultant blue crystals were filtered under vacuum and dried at 418 K overnight. The activation of the as-synthesized MOF was carried out using methanol for 2 d by immersing in methanol and subsequently dried at 418 K for later use in adsorption tests.

3.2.2 Characterization of MOFs

The linkage of metal clusters with organic ligands was studied using FTIR spectroscopy. The spectra were scanned from 650 to 4000 cm^{-1} with a resolution of 4 cm^{-1} using an attenuated total reflectance (ATR) technique on a Spectrum 100-FT-IR Spectrometer (Perkin Elmer). The morphology of HKUST-1 was studied using SEM analysis (Zeiss NEON 40 EsB CrossBeam). Thermal stability of MOFs was investigated by a thermogravimetric analysis (TGA) instrument, TGA/DSC1 STAR^e system-Mettler Toledo. The MOF sample was loaded into an alumina pan (150 µL) and heated to 973 K with an air flow rate of 10 mL/min. Powder X-ray diffraction (PXRD) patterns were obtained with an X-ray diffractometer (D8 Advance-Bruker aXS) using Cu Kα radiation (λ = 1.5406 Å), with accelerating voltage and current of 40 kV and 40 mA, respectively, for 2θ ranging from 5 to 60°. The surface area, pore

size, and pore volume were measured using N_2 adsorption/desorption isotherms on a Micromeritics Tristar II3020. The MOF sample was prepared for analysis at 453 K for 12 h under high vacuum prior to N_2 adsorption-desorption measurements.

3.2.3 Adsorption experiments

A 500 ppm aqueous stock solution of SCP was prepared by dissolving SCP powders in ultrapure water. Different concentrations of SCP (20–100 ppm) were prepared by further diluting the stock solution with water. In all the batch experiments, the MOFs were dried overnight under vacuum at 418 K and were kept in a desiccator or used directly after drying. A fixed amount (100 mg/L) of the MOFs was put in the aqueous SCP solutions (100 mL) having fixed concentrations from 20 to 100 ppm.
The concentration of SCP was analyzed on an ultra-high-performance liquid chromatography (UHPLC) system (Thermo-Fisher Scientific 3000) with a UV detector at the wavelength 270 nm. An Acclaim RSLC C-18 column was used and a mixed solution of 30% methanol and 70% acetic acid was applied as the mobile phase at a constant flow rate of 0.3 mL/min. A calibration curve was obtained for the SCP using different concentrations of SCP from 6.5 to 100 ppm.
The SCP solutions (pH 7.5) containing the adsorbents were mixed well using an orbital shaker and maintained for fixed time (10 min to 2 h) at 298 K. After adsorption for a pre-determined time, the solution was separated from the adsorbents by 45 µm syringe filters. The adsorption rate constant was calculated using pseudo-first or pseudo-second order reaction kinetics and the maximum adsorption capacity was studied using different initial concentrations of SCP for a period of 2 h. Moreover, thermodynamic parameters were calculated by studying the isotherms at 298, 308 and 318 K.

3.3 Results and discussion

3.3.1 Characteristics of MOFs

FTIR spectra (Figure 3-1) show the coordination of BTC and Cu ions. The bands at 1450 and 1649 cm^{-1} indicate -O–C-O- bonding and the bands at 1373 and 1548 cm^{-1}

indicate C=C stretching demonstrating the incorporation of BTC in the MOF (Ke et al., 2011b; Zhang et al., 2014c). The band at 750 cm^{-1} is inorganic finger print indicating bonding between Cu-O. The crystalline nature of the MOF is shown in Figure 3-2 (a-c) with PXRD and SEM.

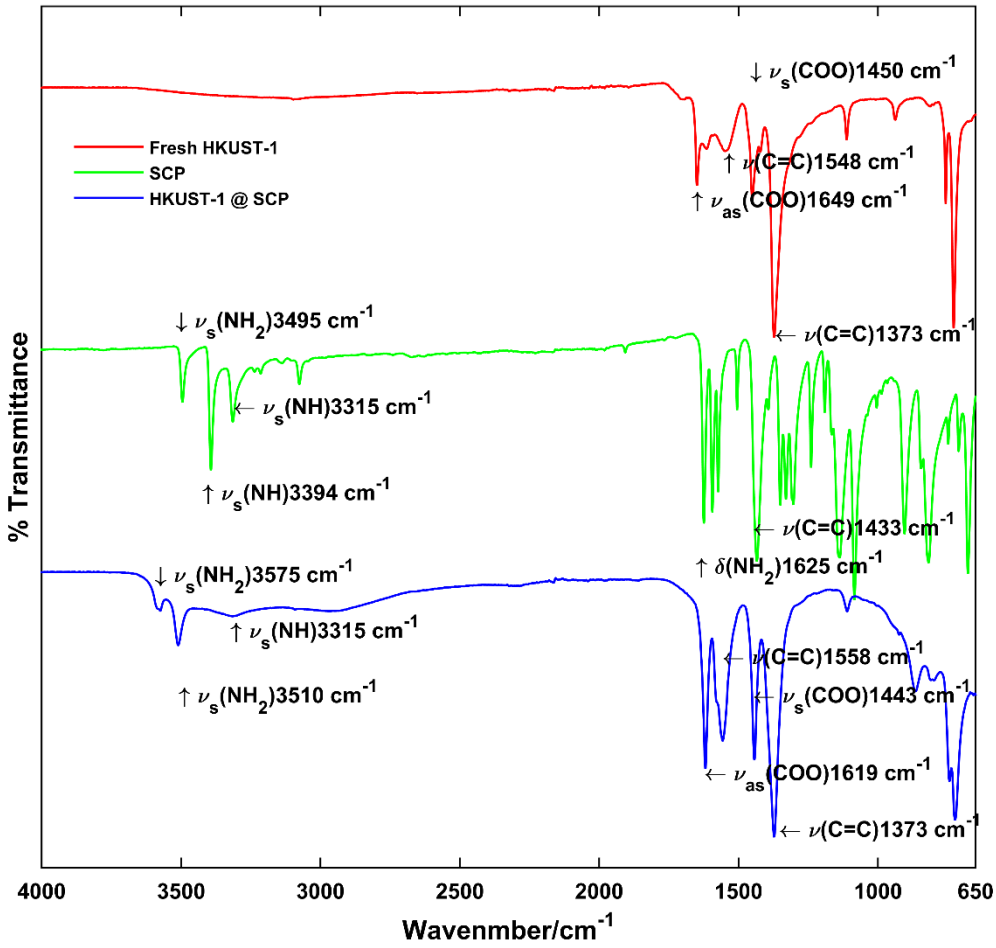

Figure 3-1 FTIR spectra of fresh, SCP adsorbed HKUST-1 and as-received SCP.

The sharp and distinct peaks show high crystallinity of HKUST-1, which is in a large crystal size as seen in SEM images (Figure 3-2 b and c). The normal size of the crystals is about 10 microns (Ke et al., 2011b; Lin et al., 2014; Yang et al., 2013). It is clear from SEM images that the crystals are in octahedral shapes with distinct edges (Figure 3-2c). Moreover, thermodynamic stability of the prepared MOF was tested at a temperature range of 313-973 K. There are mainly three regions in the decomposition pattern (Figure 3-2d). In the first step, the moisture is removed from

the MOF till 398 K, subsequently degradation of linkers starts in the second step from 548 K to 598 K. The structure of HKUST-1 is completely collapsed after degradation of organic linker at 598 K, where maximum weight loss occurs resulting in the formation of CuO. This shows that HKUST-1 is thermally stable till 573 K (Chui, Lo, Charmant, Orpen, & Williams, 1999b; Yang et al., 2013). Hence, TGA curve of HKUST-1 reinforces that removal of residual solvent molecules from the pores results in a high surface and large pore volume (Yang et al., 2013).

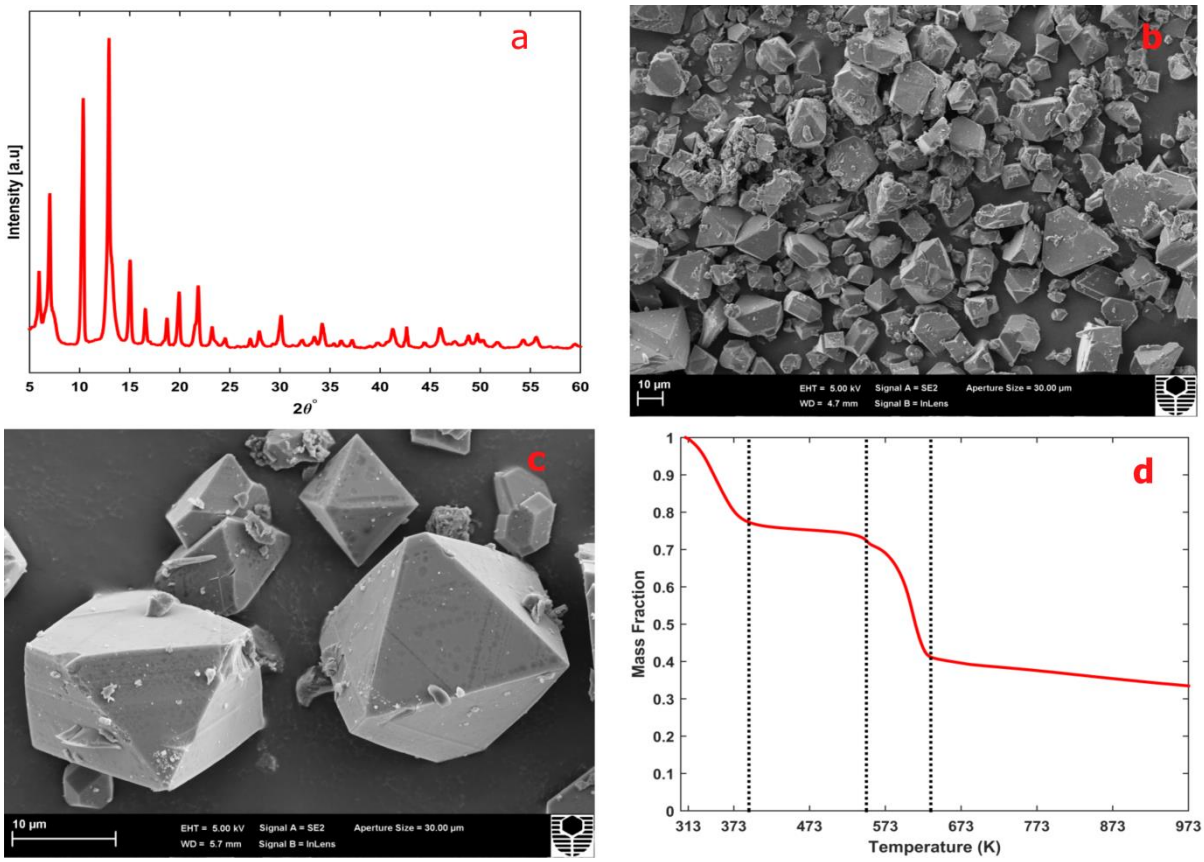

Figure 3-2 Characterization of synthesized HKUST-1: a) XRD, b and c) SEM, and d) TGA.

The N_2 adsorption-desorption isotherm indicates (Figure 3-3) HKUST-1 has a high surface area which is more attributed to microspores in combination with mesopores. The surface area was determined using the BET method and the pore size distribution (PSD) was studied using the Barret-Joyner-Halenda (BJH) method. The BET surface area of the methanol activated HKUST-1 is much high, mainly due to

micro-pores. However, the heat activated HKUST-1 presents a higher number of meso-pores compared to methanol activated HKUST-1. The activation with methanol removed unreacted BTC and solvent molecules resulting in a higher surface area by opening more micro-pores (Yang et al., 2013). The dipole moments of ethanol and methanol are very close to each other, i.e. 1.69 D and 1.70 D which results in efficient removal of ethanol molecules from MOF crystals. Moreover, miscibility of methanol is also high with water which plays its role in removing any water molecules present in HKUST-1 crystal (Yang et al., 2013). The removal of water molecules (adsorbed from environment) from crystal structure was also performed by heating at high temperature, e.g. 453 K before surface area analysis. It is interesting to note that the surface area is increased from 1100 m^2/g to 1700 m^2/g after methanol activation with average pore size of 1.7 nm. The single point (P/P_0 =0.995) total pore volume was also increased from 0.42 cm^3/g to 0.78 cm^3/g after activation with methanol. The size of micro-pores as well as meso-pores (1.7 and 4.5 nm) is larger than SCP molecules (0.81 × 0.87 × .65 nm) which is useful in adsorption of SCP on HKUST-1. Therefore, activated HKUST-1 was used in adsorption tests for SCP.

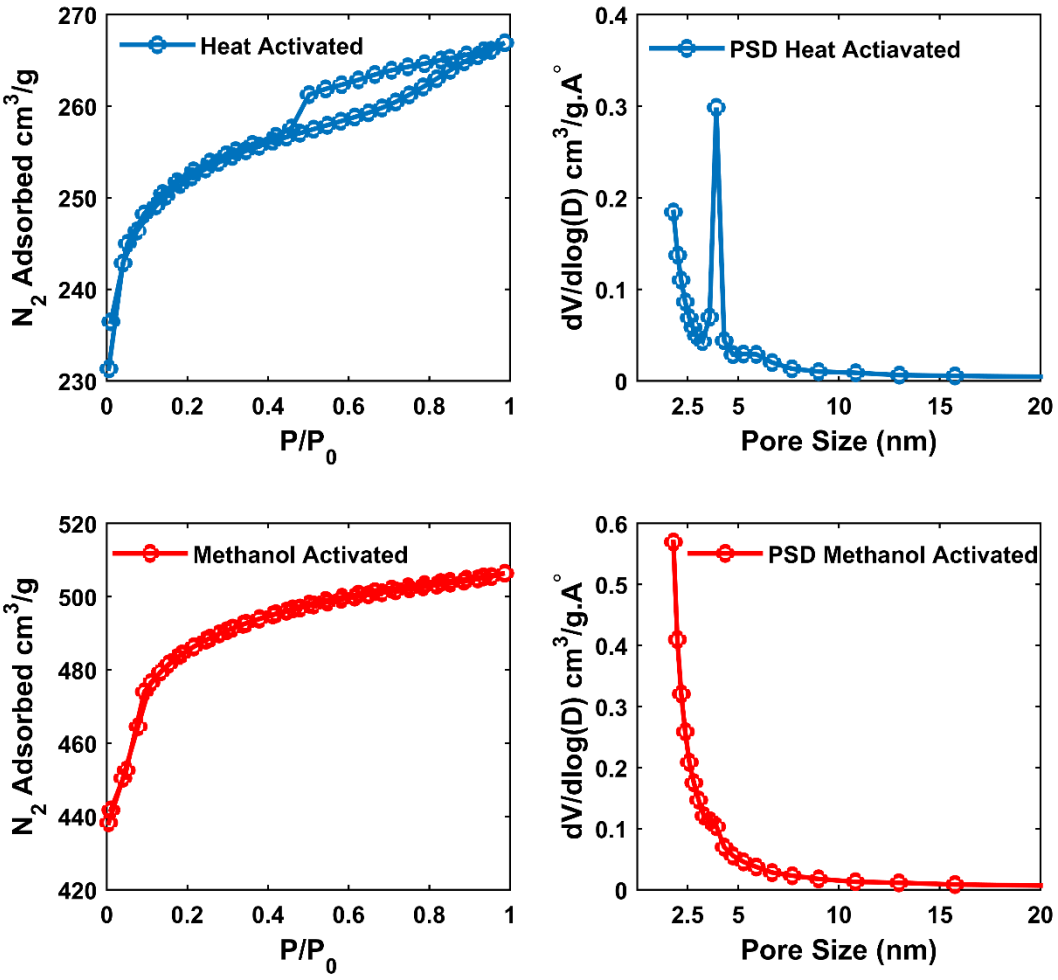

Figure 3-3 N2 adsorption-desorption isotherms and pore size distributions of heat

Effect of pH on adsorption

The pH of solution is one of the important parameters in adsorption study and it is essential to figure out the influence of any electrostatic interactions on adsorption from the test. In this study, adsorption of SCP was studied in a pH range of 3.5-11.5 using an initial concentration of SCP solutions at 40 ppm and 298 K (Figure 3-4). The adsorption of SCP on HKUST-1 showed the highest value at pH 3.5 while the lowest adsorption at pH 11.5. There is marginal decrease in adsorption from 5.5-9.5. The pH of point of zero charge for HKUST-1 is 4.0 (Lin et al., 2014) while pKa value of SCP is 5.5 (Ishihama, Nakamura, Miwa, Kajima, & Asakawa, 2002a). In solution SCP can exist in anionic, and/or neutral/cationic depending on pH of solution and function of its acidity. However, the larger amount of anionic and/or

neutral SCP is expected at pH ≥ 5.5 and protonation of SCP is less likely to occur (Braschi et al., 2010a).

At pH 3.5, the surface of adsorbent will be positively charged while negatively charged at pH > 4.0 (Lin et al., 2014). Taking the assumption of cationic SCP^{+}, there should be less adsorption at pH due to electrostatic repulsion between SCP^{+} and cationic surface of MOF. However, the adsorption of SCP is highest at pH 3.5 which signifies the existence of SCP^{-1} in abundance instead of SCP^{+} resulting in electrostatic attraction. Moreover, the adsorbent surface becomes more negative at pH > 4.0 till pH 11.5 and concentration of SCP^{-1} also increases resulting in electrostatic repulsion and decreased adsorption capacity.

Since, the adsorption capacity of MOF is significantly very high at all pH studied so the possibility of some other factors such as hydrogen bonding and π-π interactions cannot be ignored. The details on hydrogen bonding and π-π interactions are given in section 3.2.4.

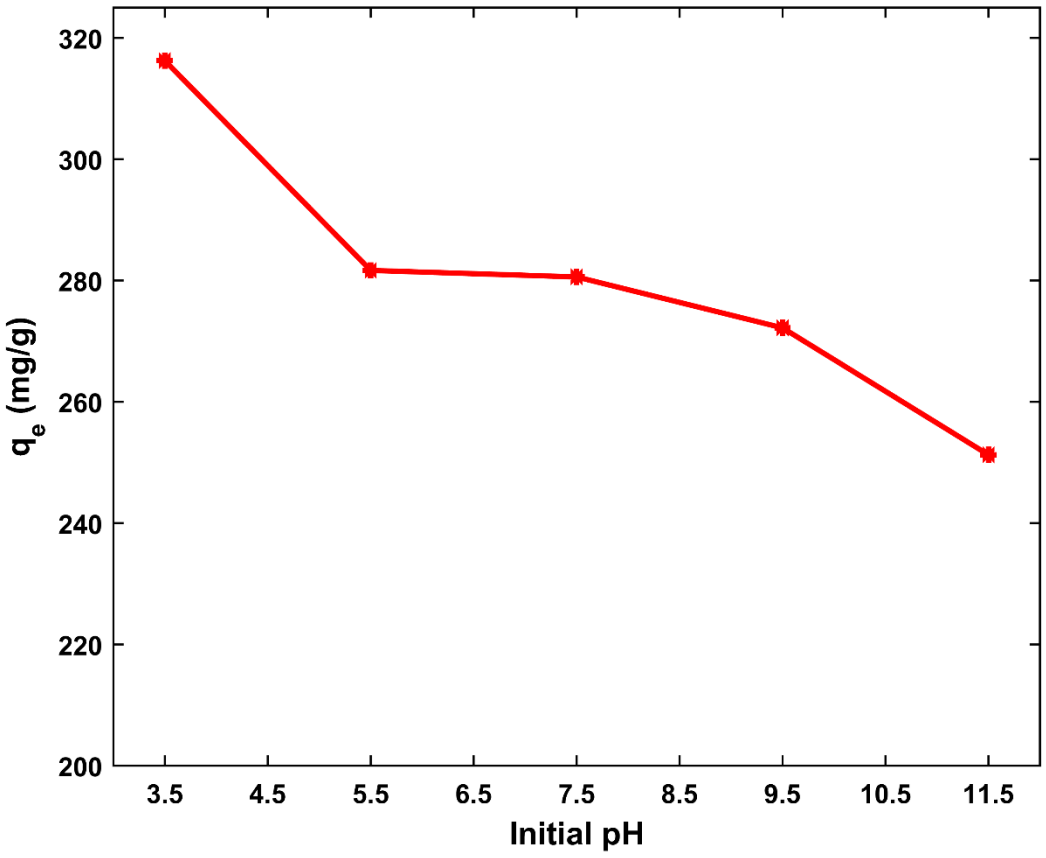

Figure 3-4 Effect of pH on SCP adsorption over HKUST-1 C0 =40 ppm at 298 K for 2 h.

.

3.3.2 Adsorption kinetics

The kinetic study is important in adsorption process for implementation at a larger scale. There are two kinetic models usually employed for adsorption, i.e. pseudo 1st order and pseudo 2nd order (Ho & McKay, 1999a, b). The mathematical expressions of the both cases are given as follows.

$$\ln(q_e - q_t) = \ln q_e - k_1 t \quad (3\text{-}1)$$

$$\frac{t}{q_t} = \frac{1}{k_2 q^2{}_e} + \frac{1}{q_e} t \quad (3\text{-}2)$$

Where q_e is the amount of SCP adsorbed at equilibrium (mg/g); q_t is the amount adsorbed at time t (mg/g); t is the adsorption time in minutes; k_1 and k_2 are the first-order and second-order rate constants, respectively. The experimental data were best fit with the pseudo 2nd order with R^2 values of 0.999. The dynamic adsorption plots for the pseudo 2nd order model for parametric calculations are given in Figure 3-5.

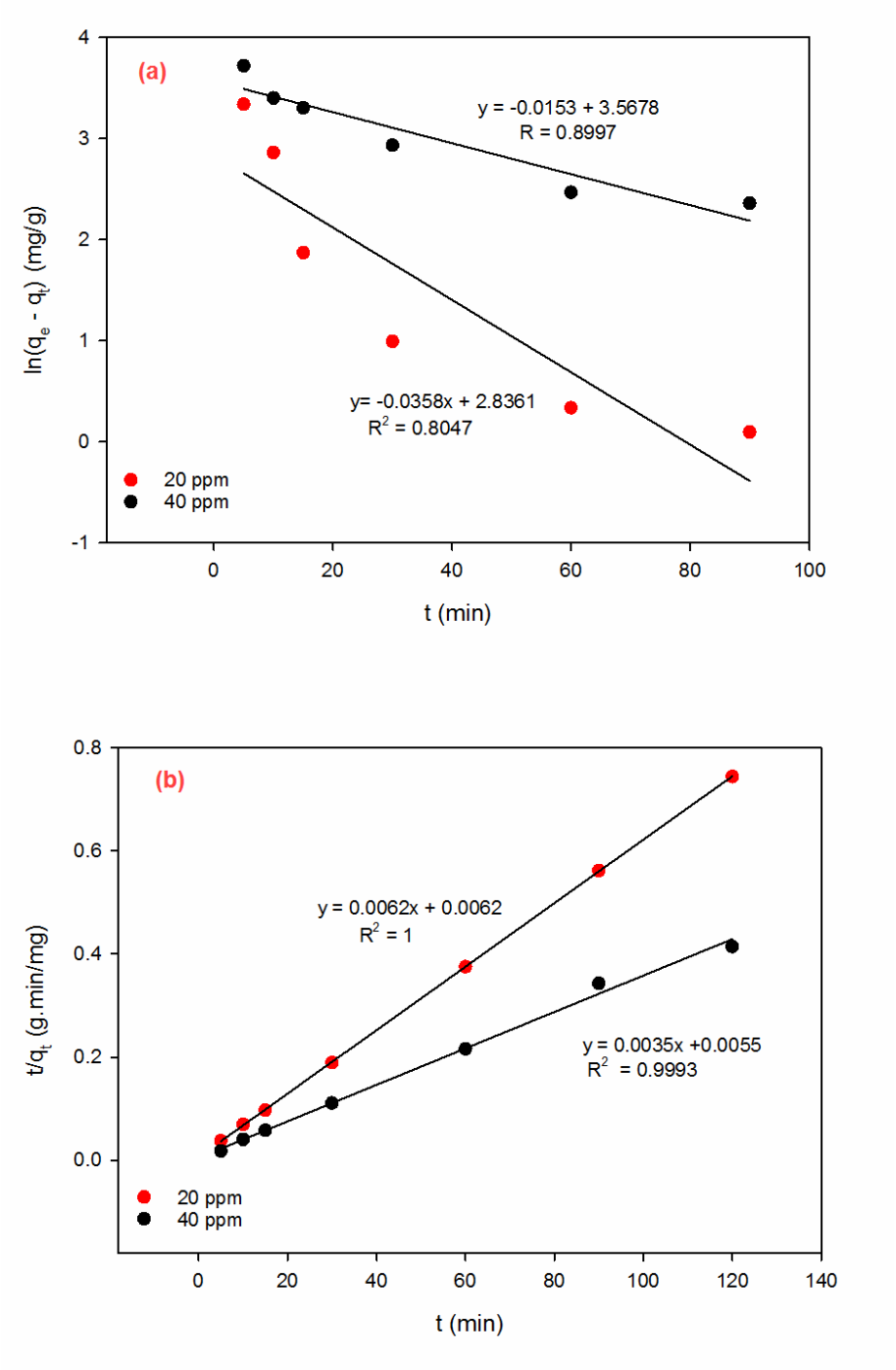

Figure 3-5 Pseudo 1st (a) and 2nd order (b) plots for SCP adsorption kinetics on HKUST-1.

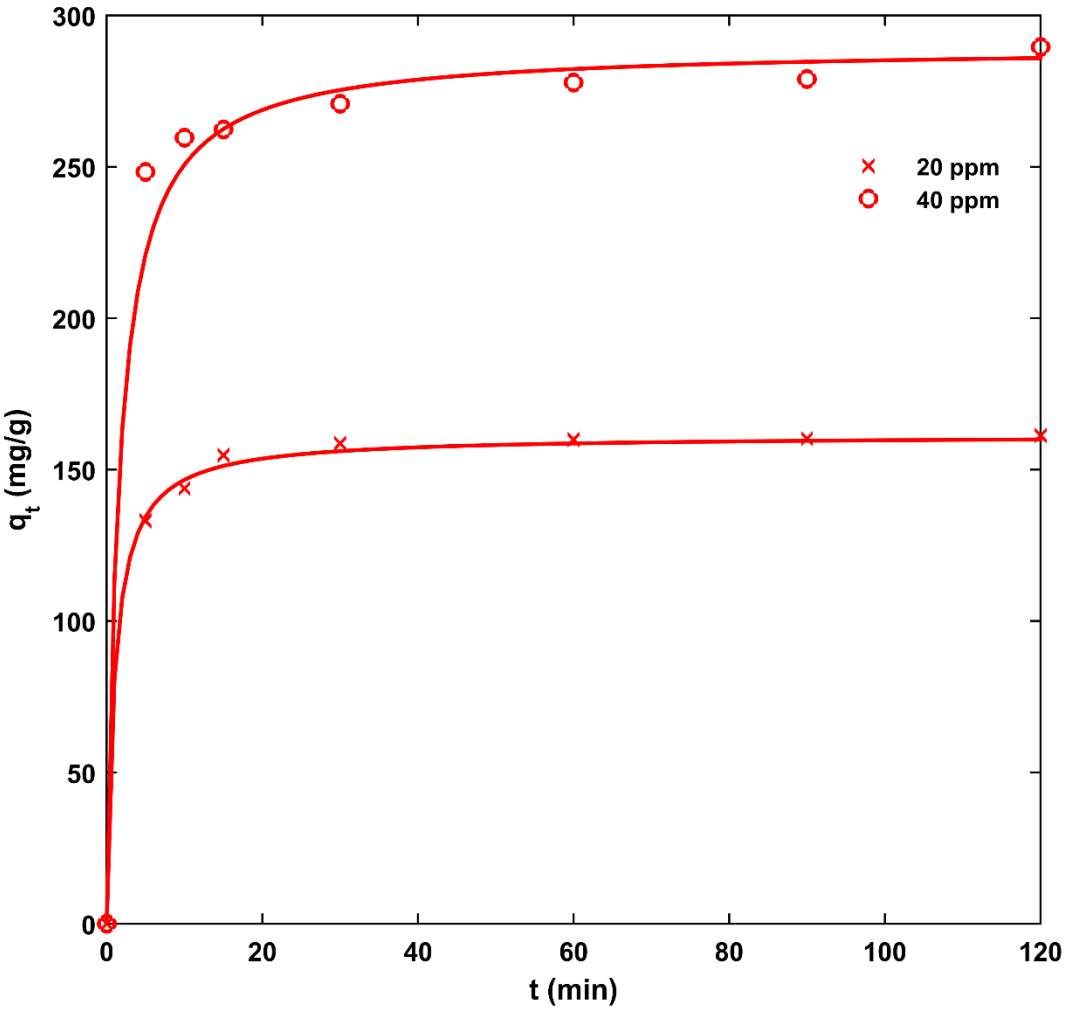

Figure 3-6 Kinetic adsorption of SCP over HKSUT-1 with different initial concentrations of SCP at 298 K: solid lines show pseudo 2nd order kinetic model.

It is also evident from Figure 3-6 that adsorption is very fast and most of the SCP uptake is completed in 10 min. The fast adsorption suggests instantaneous adsorption due to the presence of large number of pores for adsorption. The values of kinetic constants k_2, were decreased with increasing initial concentration from 20 ppm to 40 ppm. This may occur due to larger number of SCP molecules competing to occupy active adsorption sites. However, it is clear from Figure 3-6 that the equilibrium was reached in almost 30 minutes. The faster kinetics is attributed to high surface area and large pore volume and open metal sites of the HKUST-1 (Koh, Rana, Wong-Foy, & Siegel, 2015; Münch & Mertens, 2012).

The faster kinetics has been reported in adsorptive removal of SCP using zeolite Y and the adsorption was completed in almost one minute. However, slower adsorption of SCP was also reported using a different zeolite and equilibrium was reached in 4 h (Braschi et al., 2010a; Martucci et al., 2013). In a specific adsorption process, kinetic parameters depend on the nature of adsorbate-adsorbent interactions.

In the present study, availability of large number of pores and unsaturated metal sites (created by removing ethanol/H_2O molecules) by methanol activation and heating at 418 K resulted in fast kinetics. The removal of water molecules created cationic sites in HKUST-1 which behaved as active sites for anionic SCP giving rise to very fast kinetics. The kinetic parameters for SCP removal for 2nd order kinetic model are given in Table 3-1.

Table 3-1 Pseudo 2nd order kinetic parameters of SCP on HKUST-1 at 298 K.

Initial Concentration (ppm)	$q_{e,exp}$ (mg/g)	Pseudo 2nd order		
		k_2 (g. min/mg)	$q_{e\ cal}$ (mg/g)	R^2
20	161	6.2×10^{-3}	160	1.00
40	289	2.2×10^{-3}	286	0.999

3.3.3 Isothermal adsorption tests

The isothermal data were analyzed using two famous adsorption models, i.e. Langmuir and Freundlich isotherms (Freundlich, 1906a; Hameed, 2009; Langmuir, 1918). The mathematical expressions for both the models can be written as follows.

Langmuir model: $$\frac{C_e}{q_e} = \frac{1}{K_L q_m} + \frac{C_e}{q_m} \quad (3\text{-}3)$$

Freundlich model: $$\ln q_e = \ln K_F + \frac{1}{n} \ln C_e \quad (3\text{-}4)$$

where q_e represents equilibrium SCP concentration on an adsorbent (mg/g), C_e represents SCP equilibrium concentration in solution (mg/L), q_m is the monolayer capacity of SCP adsorption (mg/g), K_L represents the Langmuir adsorption constant

(L/mg). K_F and n are characteristic constants of Freundlich model, representing adsorption capacity and intensity.

The favorability of an adsorption system can also be expressed in terms of a dimensionless separation factor (R_L) shown below, where C_m is the maximum initial concentration of adsorbate. The adsorption process is favorable at the $0 < R_L < 1$. The values of R_L for adsorption of SCP on HKUST-1 are well below (Table 3-2), suggesting favorable adsorption of SCP (Lin et al., 2014).

$$R_L = \frac{1}{1 + C_m K_L} \tag{3-5}$$

The plots for parametric calculations of Langmuir isotherms are given in Figure 3-7. The values of Langmuir parameters at different temperatures are presented in Table 3-2.

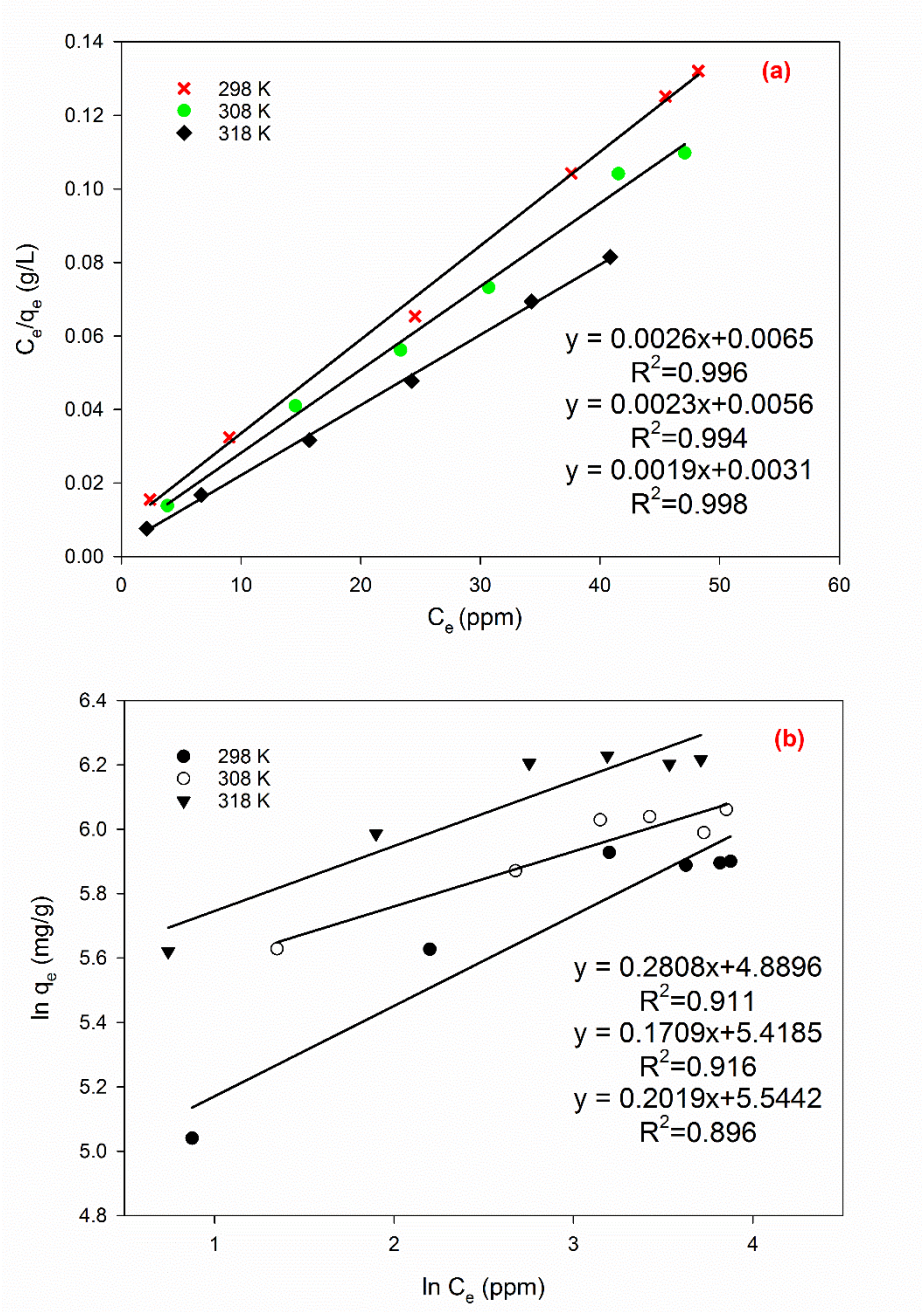

Figure 3-7 Langmuir and Freundlich isotherm plots for SCP adsorption on HKUST-1.

Table 3-2 Langmuir isothermal parameters of SCP on HKUST-1 at different temperatures.

Temperature K	$q_{m,exp}$ (mg/g)	Langmuir model			
		$q_{m,c}$ (mg/g)	K_L (L/mg)	R_L	R^2
298	365	384	0.40	0.027	0.996

308	429	413	0.41	0.026	0.994
318	501	526	0.61	0.017	0.998

The isothermal data at varying temperatures fit more accurately with Langmuir model as shown in Figure 3-8. The maximum adsorption capacity can be obtained from Figure 3-7a using 1/slope of plots between C_e vs C_e/q_e and are presented in Table 3-2. As it can be seen that the maximum adsorption capacity and adsorption constant are increasing with temperature. At 298 K, the adsorption capacity is 384 mg/g and can be as high as 526 mg/g at 318 K.

Several studies have been reported on adsorption of different sulfonamide antibiotics including SCP using granulated activated carbon (GAC), multiwall carbon nanotubes (MWCNTs), and zeolites. Adams et al. (C. Adams, 2002) studied the removal of SCP using various wastewater treatment techniques including adsorption on powdered activated carbon (PAC). It was reported that more than 90% of the SCP was removed at a very low concentration of SCP, e.g. 50 parts per billion (ppb) in 4 h. Moreover, Ilaria et al. reported the removal of SCP by high loading of silica zeolites (HSZ-Y and mordenite) (Braschi et al., 2010a; Braschi et al., 2010c; Martucci et al., 2013). The structural modifications after adsorption of SCP suggested that one molecule of SCP adsorbed on one cage of the zeolites. The adsorption capacity of the zeolites was high and guest-host interactions were discussed based on FTIR study. However, no details were provided about the effect of pH and/or temperature on adsorption.

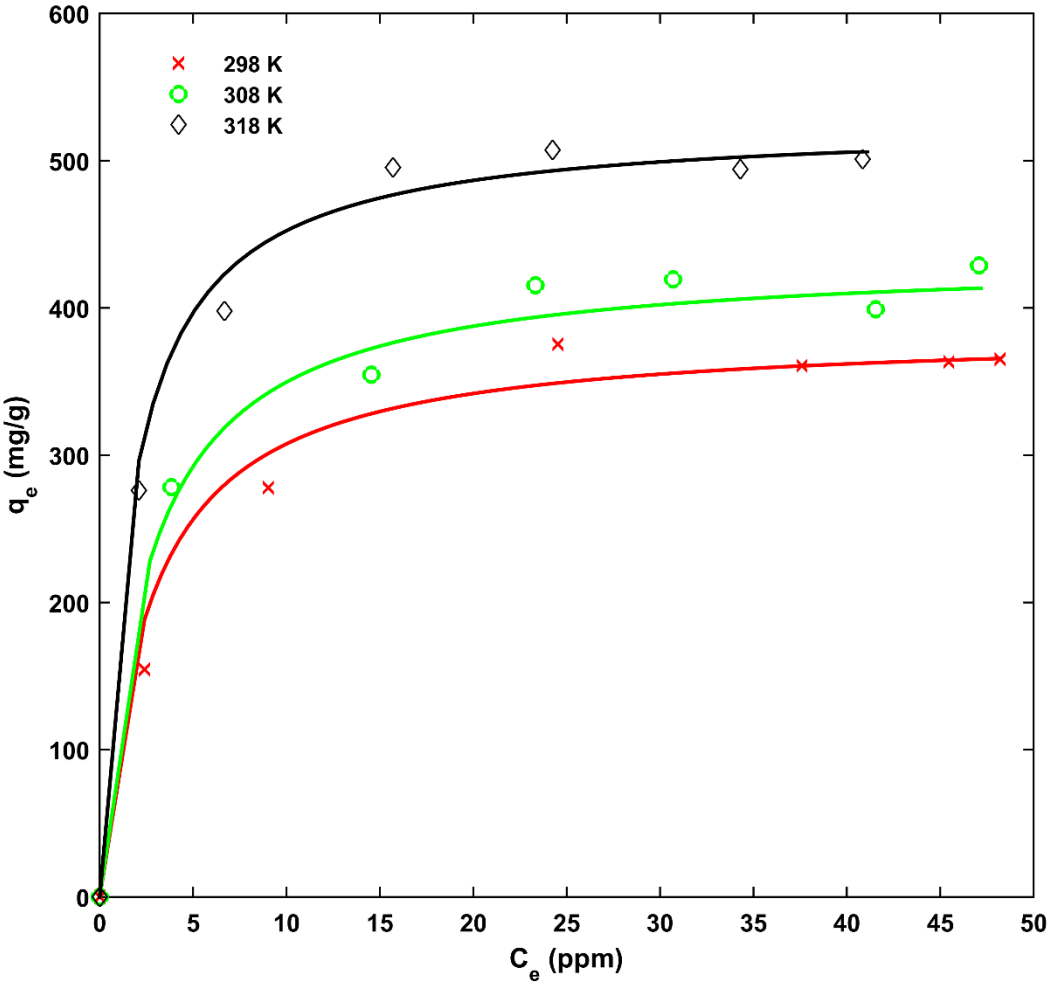

Figure 3-8 Adsorption isotherms of SCP on HKUST-1 at different temperatures; solid lines show Langmuir isothermal model.

A comparison of adsorption capacity of SCP is given in Table 3-3. It is clear from Table 3-3 that the adsorption capacity of HKUST-1 is the highest for the SCP.

In this study, adsorption investigation revealed a high adsorption capacity of HKUST-1 MOF with very fast kinetics. The high adsorption capacity is attributed to high surface area, large pore volume, unsaturated metal sites and functionalities of HKUST-1.

Table 3-3 Comparison of adsorption capacity of SCP over different adsorbents.

Adsorbent	Maximum adsorption capacity, q_m (mg/g)	Reference
PAC	4.5	(C. Adams, 2002)
Faujasite zeolite Y	280	(Braschi et al., 2010a)
HSZ-690HOA zeolite	151	(Martucci et al., 2013)
HKUST-1	384	Present study

3.3.4 Plausible adsorption mechanism

The pH of solution is important in adsorption to study a plausible adsorption mechanism. Fukahori et al. (Fukahori, Fujiwara, Ito, & Funamizu, 2011) studied pH dependent adsorption of five sulfonamide antibiotics using a zeolite HSZ-385. It was reported that adsorption capacity decreased severely by increasing pH higher than pKa values of the antibiotics and the maximum adsorption was achieved at their pKa values. Moreover, Thomas et al. (Thomas, Gebbink, & Tolls, 2006) studied the sorption behaviour of SCP in comparison with tylosin and oxytetracycline in agricultural soils (Thomas et al., 2006). The relationship between sorption coefficients and pH was studied comprehensively using the agricultural soils. It was observed that adsorption of SCP decreased to almost zero at a pH range 6.5-7.5.

SCP mainly exists neutral and/or in anionic form in the pH range of 5.5-6.0 owing to pKa value of 5.5 and comparatively high concentration is expected at pH above 6 (Ishihama et al., 2002a). The pH of point of zero charge for HKUST-1 was found to be 4.0, which shows HKUST-1 exits in cationic form below 4.0, neutral at 4.0 and anionic at pH higher than 4.0 (Lin et al., 2014). In order to figure out plausible mechanism, batch adsorption experiments were conducted in pH range corresponding to cationic, anionic and neutral nature of the adsorbent and adsorbate. The adsorption capacity of the MOF decreases with increasing pH from 3.5-11.5. The pKa value of SCP is 5.5 signifying that SCP exits in anionic form at pH $\geq$ 5.5 while HKUST-1 also in anionic form. There are two possibilities for SCP to mainly

exist in cationic or anionic/neutral forms at pH 3.5. However, the chances of SCP in its cationic form by protonation of heterocyclic nitrogen (strongest basic in the SCP molecule as SCP^{+}) compared to nitrogen of NH and/or NH_2 is less, due too low Kb value of SCP (pKb>12) (Braschi et al., 2010a; http://www.medicinescomplete.com/mc/clarke/current/index.htm). Moreover, it is also clear from higher adsorption capacity of SCP at pH 3.5 due to electrostatic attractions at the top of hydrogen bonding and π-π interactions. The decrease is sharp in 3.5-5.5 as the HKUST-1 mainly exists with negatively charged surface, which results in electrostatic repulsion between anionic MOF and SCP^{-1}. However, the decrease in adsorption capacity from acidic to strongly basic range is 25% less than the acidic range suggesting some other factors contributing to the high adsorption of SCP despite of electrostatic repulsion between anionic adsorbate and adsorbent.

Since, significant adsorption was observed in a whole pH range 3.5-11.5, some other important factors for the adsorption such as hydrogen bonding and π-π interactions are proposed based on FTIR results. The bands at 1430-1450 cm^{-1} and 1625-1650 are assigned to $\nu_{(COO)}$ and $\nu_{as\text{-}(COO)}$ of HKUST-1 while the strong band at 1373 cm^{-1} and 1545-1560 cm^{-1} are assigned to $\nu_{(C=C)}$ of benzene ring of the HKUST-1 MOF. The appearance of bands at 3574, 3510, and 3315 cm^{-1} suggest incorporation of SCP into the MOF. It is also clear (Figure 3-1) that the stretching frequency for NH_2 and NH are at 3495, 3392 and 3314 cm^{-1} for SCP. Moreover, the characteristic bands at 1624 cm^{-1} in SCP due to NH_2 bending shifted to lower frequency of 1618 cm^{-1} after adsorption on the MOF overlapping with 1625 cm^{-1} band of $\nu_{as\text{-}(COO)}$ in fresh HKUST-1.

The shifting of bands from 1433 cm^{-1} to 1443 cm^{-1} suggests stretching due to attraction of H-bond formed with H of NH_2 from SCP and oxygen of HKUST-1 cluster. The existence of hydrogen bonding is reinforced from bands 3574 and 3510 cm^{-1} in SCP adsorbed HKUST-1 (Figure 3-1). The possibility of H-bond between Cu-O-Cu and H of amide group is indicating the removal of SCP in its neutral form indicated by the band at 3315 cm^{-1} (Scheme 3-2b).

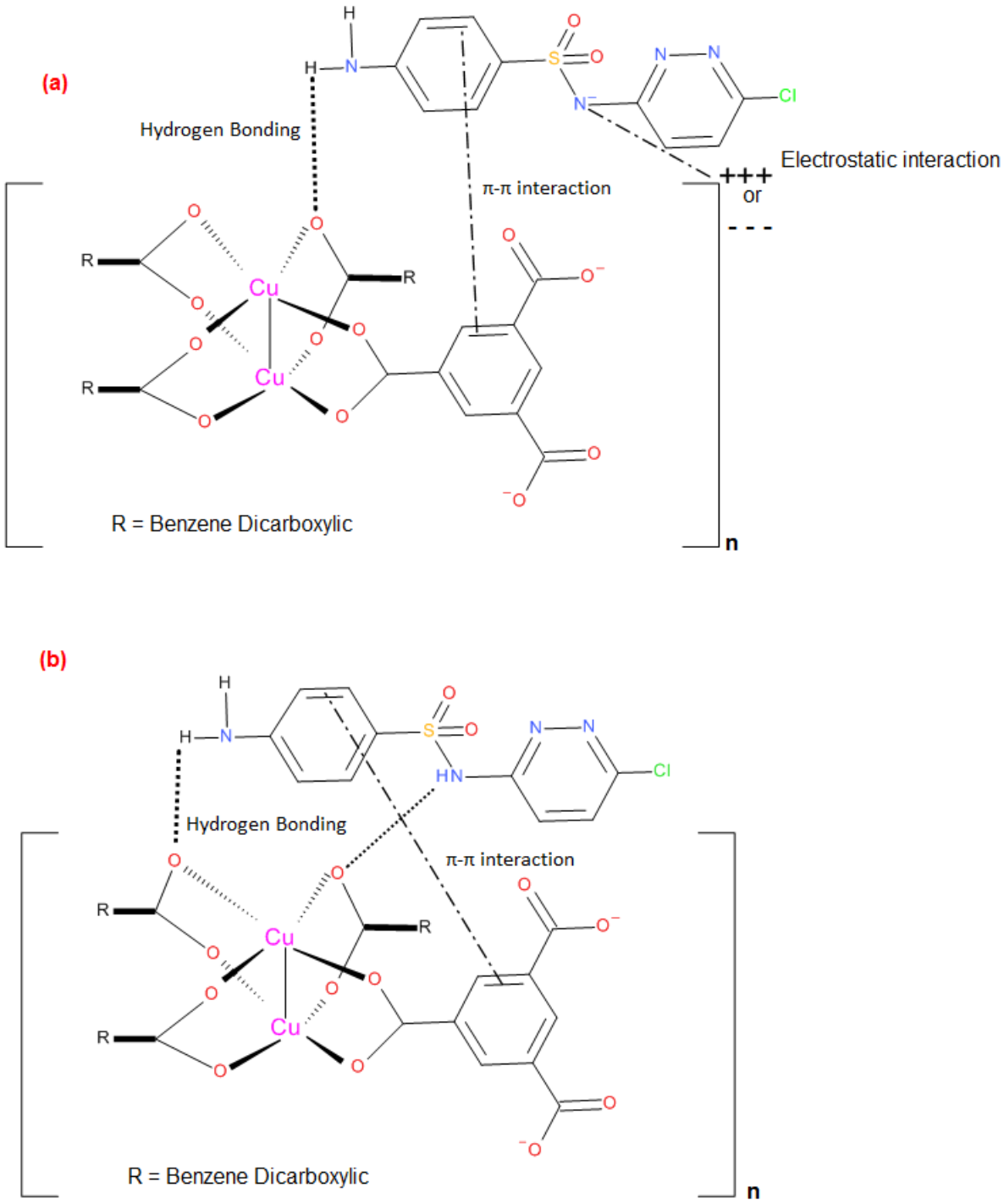

Scheme 3-2 The possible adsorption mechanism of SCP on HKUST-1.

There are also some other contributions to the adsorption due to π-π interaction between the benzene ring of the MOF and SCP which is evident from the shifting of band from 1548 before adsorption to 1557 cm^{-1} after adsorption. However, there is not a significant shifting, suggesting a weak π-π interaction.

Therefore, it can be concluded from the pH and FTIR studies that high adsorption of SCP on HKUST-1 is attributed to electrostatic interaction, hydrogen bonding, and π-π interactions.

3.3.5 Adsorption thermodynamics

The thermodynamic parameters were obtained from the adsorption tests at three different temperatures, i.e. 298, 308 and 318 K for 2 h. The equation for the Gibbs free energy (Haque et al., 2010a; Haque, Lo, Minett, Harris, & Church, 2014b) is given below.

$$\Delta G = -RT \ln K_L \quad (3\text{-}6)$$

Where, ΔG represents Gibbs free energy, K_L (L/mol) the Langmuir constant, T is temperature in K and R is universal gas constant. The negative value of ΔG shows spontaneous nature of adsorption process (Haque et al., 2010a).

Entropy (ΔS) and enthalpy (ΔH) can be obtained from the van't Hoff's equation (Haque et al., 2010a; Haque et al., 2014b).

$$\ln K_L = \frac{\Delta S}{R} - \frac{\Delta H}{RT} \quad (3\text{-}7)$$

A linear plot of ln K_L and 1/T was obtained for the enthalpy and entropy calculations (Figure 3-9). The values of thermodynamic parameters are given in Table 3-4. The positive enthalpy change suggests that the adsorption is an endothermic process. However, the positive entropy suggests increased randomness with adsorption of SCP. The values of ΔH (4 kJ/mol) and ΔS (110.3 J/mol K) suggests very little desorption of pre-adsorbed water molecules (Haque et al., 2010a). This observation also reinforces the presence of unsaturated metal sites in HKUST-1 by the removal of water molecules (Andrew Lin & Hsieh, 2015; Chui et al., 1999b; Ke et al., 2011b). Therefore, the isothermal data at different temperatures revealed that adsorption of SCP on HKUST-1 is a spontaneous and endothermic process.

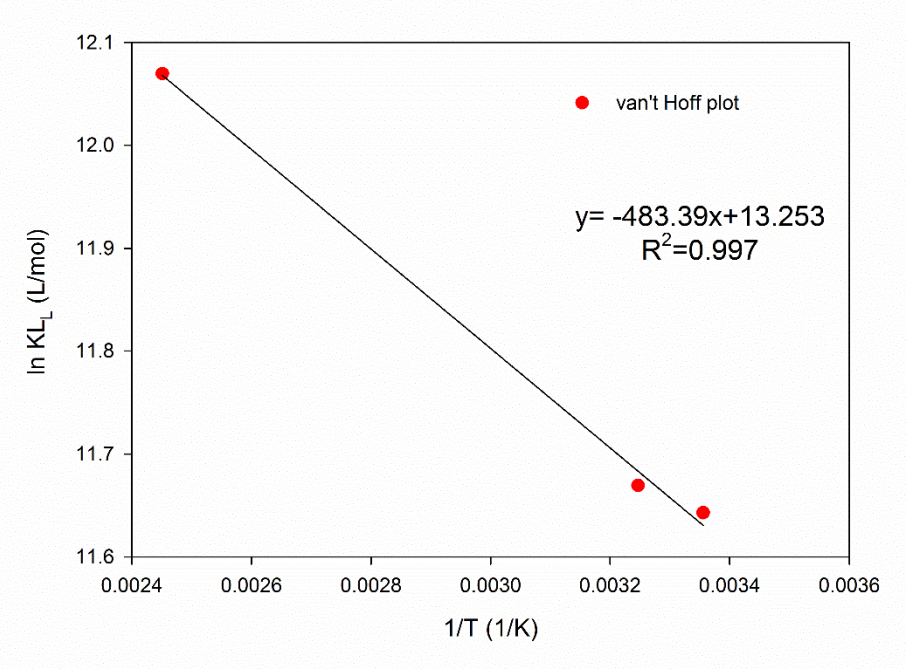

Figure 3-9 van't Hoff's plot for estimating ΔH and ΔS of SCP adsorption on HKUST-1.

Table 3-4 Thermodynamic parameters of SCP adsorption over HKUST-1.

Temperature	ΔG (kJ/mol)	ΔH (kJ/mol)	ΔS (J/mol K)
298	-28.8	4.0	110.3
308	-29.8		
318	-40.9		

3.4 Conclusions

The removal of a model sulfonamide antibiotic was studied using a high surface area MOF. The methanol activation of HKUST-1 MOF resulted in high surface area, large pore volume and unsaturated metal sites. These unsaturated metal sites played an important role in faster kinetics of SCP removal. Moreover, the adsorption isothermal tests showed that experimental data fit more accurately with Langmuir model. The Langmuir adsorption capacity of HKUST-1 was calculated to be 384 mg/g at 298 K, the highest among the studied adsorbents. Furthermore, thermodynamic study showed that adsorption of SCP on HKUST-1 is an

endothermic process. A plausible adsorption mechanism was proposed using pH and FTIR studies. It was concluded that electrostatic interactions, hydrogen bonding, and π-π interactions are the main factors in SCP removal from wastewater using HKUST-1. In future studies, it will be more interesting to focus on effect of hydrogen bonding, π-π interactions and hydrophobicity of some other water stable MOFs in adsorption.

Chapter 4 Adsorptive removal of antibiotic sulfonamide by UiO-66 and ZIF-67 for wastewater treatment*

* Adopted with permission from (M.R, Azhar, H.R, Abid, V. Periasamy, H. Sun, M.O., Tade, S. Wang, "Adsorptive removal of antibiotic sulfonamide by UiO-66 and ZIF-67 for wastewater treatment", *Journal of Colloidal and Interface Science*, pp. 88-95, 2017).

4.1 Introduction

The increasing use of pharmaceuticals in many areas is resulting in high discharge of pharmaceutical wastes into the environment. Particularly, the use of sulfonamide antibiotics is increasing largely due to their high demand in cattle farming, agriculture and other pharmaceutical uses (Bu et al., 2013; Carmona, Andreu, & Pico, 2014b; Chen & Zhou, 2014; Daughton & Ternes, 1999). The amphoteric behavior of sulfonamide antibiotics helps them migrate to the environment in acidic and basic media (Burkhardt, Stamm, Waul, Singer, & Muller, 2005). Moreover, it is not possible to treat them in conventional wastewater plants because of their anionic and antibacterial nature (Michael et al., 2013). The prolonged exposure to the sulfonamide antibiotics even in very small amount may cause harmful effects on humans and aquatic life, such as green algae, Daphnia magna, and lemna minor (Brain, Ramirez, Fulton, Chambliss, & Brooks, 2008; Fabianska, Bialk-Bielinska, Stepnowski, Stolte, & Siedlecka, 2014). The detection of sulfonamide antibiotics is occurring in sewage treatment plants, wastewaters from hospitals, agricultural and cattle farms (Michael et al., 2013; Oliveira et al., 2015b; Sim et al., 2013a).

It is crucial to develop efficient processes to mitigate sulfonamide antibiotics from wastewater streams. The removal of sulfonamide antibiotics has been tested using various processes such as adsorption, membrane filtration, chemical remediation, catalytic and photocatalytic degradations (Ahmed et al., 2015a; Braschi et al., 2010c; Fabianska et al., 2014; Koyuncu, Arikan, Wiesner, & Rice, 2008; Yang et al., 2015; Zessel, Mohring, Hamscher, Kietzmann, & Stahl, 2014). However, membrane filtration induces high operating cost and generates membrane fouling (Chang, Clech, Jefferson, & Judd, 2002). Catalytic and photocatalytic degradations of antibiotics convert them completely to small molecules but high cost of catalysts and promotors limit the use of such processes at a large scale (Mehrjouei, Müller, & Möller, 2014).

Adsorption is a feasible and economical process for the removal of sulfonamide antibiotics. However, there are still various challenges in adsorption process such as less effectiveness to remove very low concentration of adsorbate, limited operating

pH range and regeneration of adsorbents (Fukahori et al., 2011; Thomas et al., 2006). Some common adsorbents have been studied in adsorptive removal of sulfonamide antibiotics, e.g. zeolites, powder activated carbon (PAC), and multiwall carbon nanotubes (MWCNTs). The adsorption capacity of PAC or MWCNTs is very low compared to zeolites (Braschi et al., 2010c; C. Adams, 2002; Yang et al., 2015) and the effect of operating conditions e.g. pH and temperature effect on adsorption was not well resolved (Blasioli et al., 2014b; Braschi et al., 2010a; Braschi et al., 2010c).

Metal organic frameworks (MOFs) are new functional materials with tuneable textural properties. The high surface area, large pore volume, and synergic effects of both organic and inorganic moieties make them unique materials. However, most of MOFs have been used in gas-phase applications such as hydrogen storage, CH_4, CO_2 capture and other gas adsorptions. Other applications of MOFs include drug delivery, lithium ion batteries, catalysis and aqueous phase adsorption to remove toxic chemicals (Abid et al., 2012a; Deleu, Stassen, Jonckheere, Ameloot, & De Vos, 2016; Horcajada et al., 2012; Jeremias, Lozan, Henninger, & Janiak, 2013; Koh et al., 2015; Odoh, Cramer, Truhlar, & Gagliardi, 2015; Yang et al., 2013; Zhao et al., 2016). The limited use of MOFs in wastewater treatment processes is due to instability of MOF structure after exposure to water and the structure of MOFs is partially and fully destroyed in humid and/or aqueous conditions (Burtch et al., 2014; Haque et al., 2014b).

The family of cobalt (ZIF-67) and zirconium based MOFs (UiO-66) are water stable (Lin & Chen, 2016; Qian, Sun, & Qin, 2012). UiO-66 is one of the most stable MOFs and has been used in different wastewater treatment processes (WWTPs) (Cavka et al., 2008; Chen et al., 2015b; Lin et al., 2015; Seo et al., 2015). The robustness of UiO-66 is evident from its use in adsorption of cationic and anionic wastes. The main focus in the above-mentioned studies is on widely known adsorption mechanism such as electrostatic interaction, hydrogen bonding and π-π interactions. There is less focus on the structural defects of UiO-66 affecting its hydrophobicity (Ghosh, Colon, & Snurr, 2014; Ling & Slater, 2016; Shearer et al., 2014; Valenzano et al., 2011). The proper selection of synthesis conditions and activation processes results in defect free UiO-66 in terms of absence of unreacted benzene dicarboxylic acid linkers into its structure. In the present study, details on adsorptive removal of a toxic sulfonamide antibiotic, sulfachloropyradazine (SCP) is

reported mainly focusing on effects of activation and purity of UiO-66. It was found that UiO-66 is superior to other MOFs and the previously studied adsorbents.

4.2 Experimental

4.2.1 Materials

All the chemicals, i.e. $ZrCl_4$, benzene dicarboxylic acids (BDC), N,N-dimethylforramide (DMF), $Co(NO_3)_2 \bullet 6H_2O$, 2-methyl imidazole (2-MIM), sulfachloropyradazine (SCP), HCl, NaOH and methanol were supplied commercially from Thermo Fisher Scientific, Perth Scientific and Sigma–Aldrich.

4.2.2 Synthesis of MOFs

In a typical synthesis of UiO-66, 0.529 g of $ZrCl_4$ and 0.37 g of BDC were dissolved in each 30 mL DMF. Then, both solutions were transferred into a Teflon autoclave and heated in an oven at 120 °C for 24 h. The resultant crystals were filtered under vacuum and immersed in chloroform for activation of the as-synthesized MOF for 5 days and subsequently dried at 180 °C for later use in adsorption tests.

The synthesis of ZIF-67-H_2O was carried out using $Co(NO_3)_2.6H_2O$ and 2-methyl imidazole (2-MIM). In a typical synthesis, 1.24 g $Co(NO_3)_2.6H_2O$ and 1.50 g 2-MIM was dissolved in 100 ml water separately. Later on, $Co(NO_3)_2.6H_2O$ solution was added slowly to 2-MIM solution while stirring vigorously. The mixture was stirred for another 6 h then the crystals were separated by centrifugation, washed 2 times with methanol and subsequently dried at 120 °C.

The synthesis of ZIF-67-CH_3OH was carried out in the same way mentioned above for ZIF-67-H_2O, however, the solvent methanol was used instead of water.

4.2.3 Characterization of MOFs

An X-ray diffractometer (D8 Advance-Bruker aXS) was used for powder X-ray diffraction (PXRD) patterns employing Cu Kα radiation (λ = 1.5406 Å) at accelerating voltage of 40 kV and current of 40 mA for 2θ ranging from 5 to 60°.

The crystal morphology of MOFs was studied using Zeiss NEON 40 EsB CrossBeam for SEM analysis. A thermogravimetric analysis (TGA) instrument (TGA/DSC1 STAR^e system, Mettler Toledo) was used for investigation of thermal stability of MOFs, using an alumina pan (150 µL) and heated to 700 °C in air with a flow rate of 10 mL/min. The linkage of metal clusters with organic ligands was studied using FTIR spectroscopy, scanning from 650 to 4000 cm^{-1} with a resolution of 4 cm^{-1} on a Spectrum 100-FT-IR Spectrometer (Perkin Elmer) by an attenuated total reflectance (ATR) technique. A Micromeritics Tristar II3020 was employed to measure N_2 adsorption/desorption isotherms to obtain the surface area, pore size, and pore volume. Prior to N_2 adsorption-desorption measurements, MOF samples were prepared at 180 °C for 12 h under high vacuum.

4.2.4 Adsorption study

An aqueous stock solution of SCP (500 mg/L) was first prepared in ultrapure water (414R-HP-520, Hydro-check system, INC keeping set point of 15 MegaOhm-cm). Different SCP solutions (5–100 mg/L) were then prepared by further diluting the stock solution with ultrapure water. In all the batch experiments, the MOF samples were dried at 150 °C under vacuum for overnight and used directly or kept in a desiccator. A fixed amount (100 mg/L) of the MOFs was put in the SCP solutions (100 mL) in an orbital shaker at 250 revolutions per minute (rpm).

An ultra-high-performance liquid chromatograph (UHPLC, Thermo-Fisher Scientific 3000) was used for SCP analysis with a UV detector at the wavelength 270 nm using an Acclaim RSLC C-18 column and a mixed solution of 30% methanol and 70% acetic acid at a constant flow rate of 0.3 mL/min. A calibration curve was obtained for the SCP using different concentrations of SCP from 6.5 to 100 mg/L. In all adsorption experiments, the amount of SCP adsorbed was calculated by the following equation.

$$q_e = \frac{(C_0 - C_e)V}{m_{ads}} \qquad (4\text{-}1)$$

Where, q_e is amount of SCP adsorbed at equilibrium (mg/g), C_0 and C_e are initial and equilibrium SCP concentrations (mg/L), respectively, V is the volume of SCP solution used and m_{ads}, is the mass of adsorbent (g).

The SCP solutions (pH 5.5) were mixed well with the adsorbents using an orbital shaker and maintained for 5 min to 2 h at 25 °C. After the fixed-time adsorption, the solution was separated by 0.45 µm syringe filters. The pseudo-first or pseudo-second order reaction kinetic models were used for calculating the adsorption rate constant. The maximum adsorption capacity was studied using different initial concentrations of SCP for a period of 2 h. Moreover, thermodynamic parameters were obtained by studying the isotherms at 25, 35 and 45 °C.

4.3 Results and discussion

4.3.1 Characterization of MOFs

The strong crystalline nature of the synthesized MOFs (UiO-66 and ZIF-67) is clearly demonstrated from XRD patterns (Figure 4-1) in accordance with the earlier reported results (Cavka et al., 2008; Guo, Xing, Lou, & Chen, 2016; Qian et al., 2012).

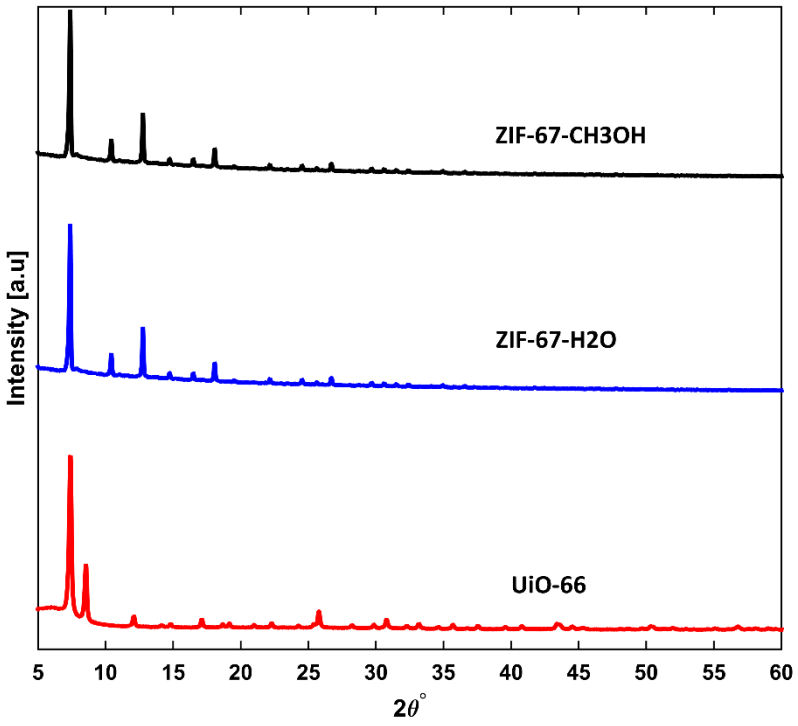

Figure 4-1 XRD pattern of ZIF-67 and UiO-66.

The XRD patterns show that all the synthesized MOFs are highly crystalline and morphology can also be seen in SEM images (Figure 4-2). ZIF-67-H_2O and ZIF-67-CH_3OH present in chamfered cubic crystals while UiO-66 MOFs are in cubic crystals (Abid et al., 2012c; Lin & Chang, 2015b; Qian et al., 2012). The scale bar for ZIF-67 MOFs is 1 micron and 100 nm for UiO-66.

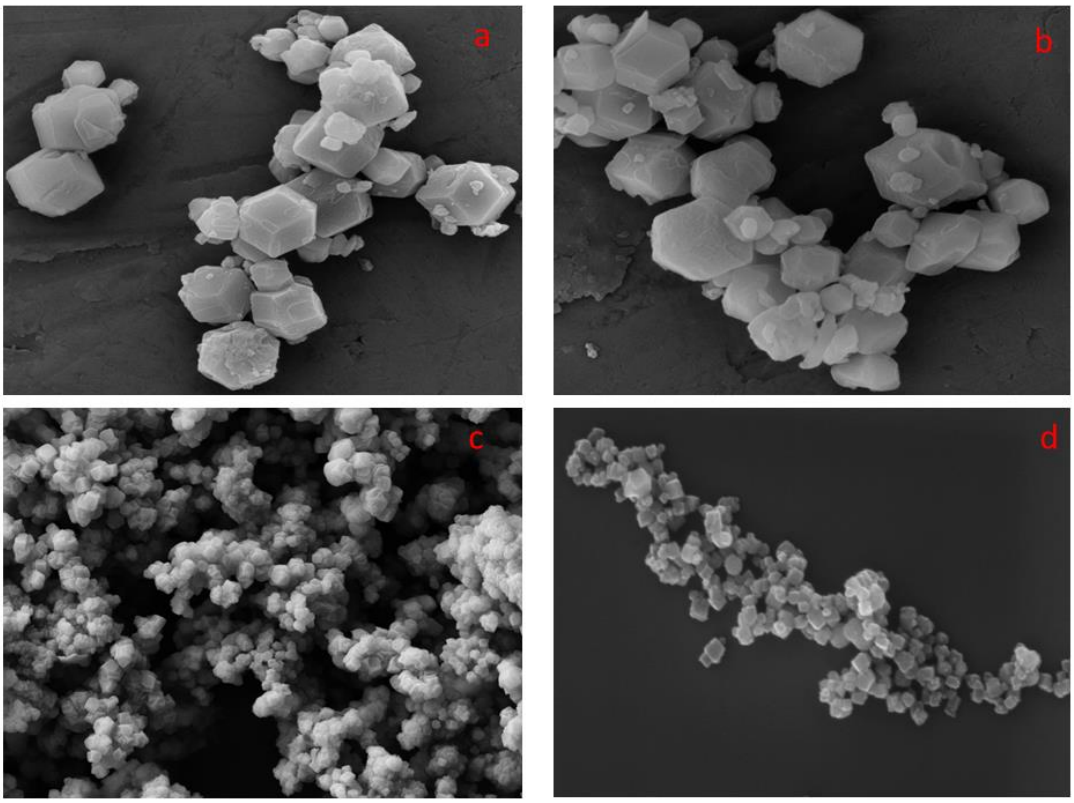

Figure 4-2 SEM images of UiO-66 and ZIF-67. (a) ZIF-67-H2O, (b) ZIF-67-CH3OH and (c, d) UiO-66

FTIR spectra (Figure 4-3) shows the coordination of organic linkers and metal-secondary building units (SBUs). The coordination of 2-MIM with Co ions in ZIF-67-H_2O and ZIF-67-CH_3OH is confirmed by the peak at 1141 cm^{-1} is attributed to C≡N of 2-MIM while the peak at 1576 cm^{-1} belongs to C-C of the linkers. Moreover, the broad peak in the range of 3000-3500 cm^{-1} belongs to OH of the solvent in ZIF-67-H_2O and peaks at 2927 and 3135 cm^{-1} represent C-H stretching in ZIF-67-CH_3OH (Andrew Lin & Lee, 2016; Lin & Chang, 2015b).

In case of UiO-66, the peaks at 3675 cm^{-1} show the presence of OH group at the external surface. The most distinct peak at 1408 cm^{-1} shows symmetric stretching of O-C-O of deprotonated BDC in UiO-66 structure. Moreover, asymmetric stretching of O-C-O is shown at 1595 cm^{-1}. The presence of peak at 1526 cm^{-1} represents C-C ring of benzene in MOF structure. The peak at 816 cm^{-1} signifies OH in UiO-66 while the peaks at 677 and 748 cm^{-1} are attributed to μ_3 –O stretching with Zr-(OC) (Valenzano et al., 2011).

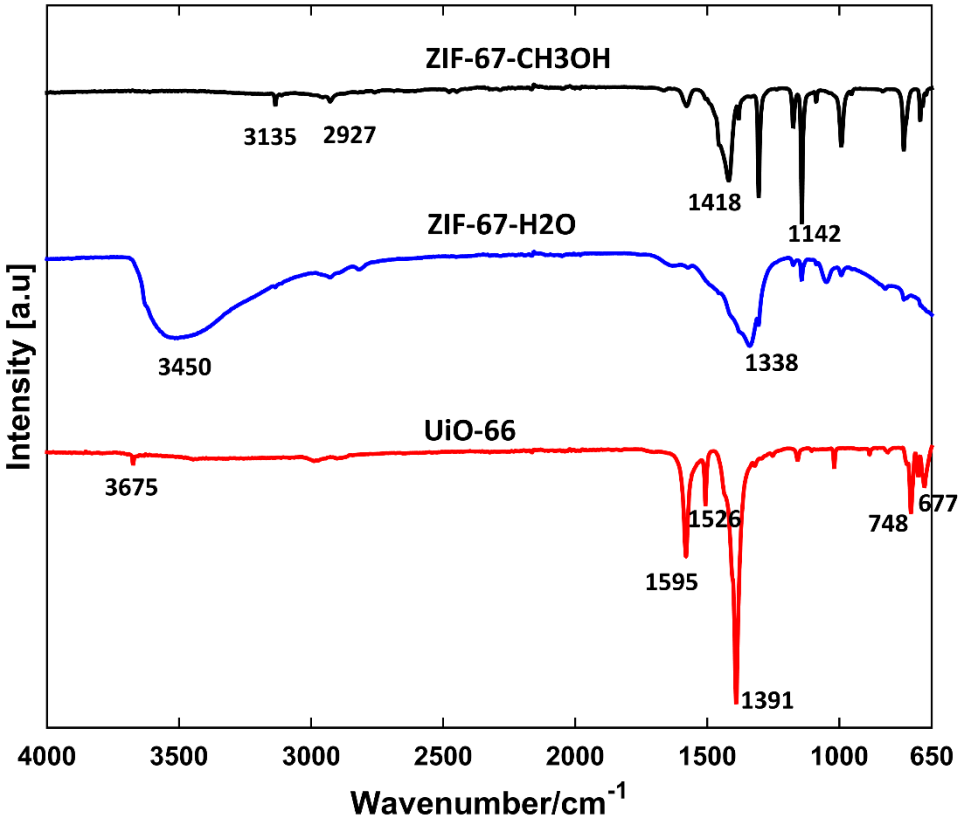

Figure 4-3 FTIR spectra of ZIF-67 and UiO-66 MOFs.

N_2 adsorption-desorption isotherm (Figure 4-4) was used to study surface area of prepared MOFs using the multipoint BET method while external surface area was calculated with t-plot method. The total pore volume was calculated at P/P_0 = 0.99. Furthermore, the pore size distribution was carried out using a micro porous (MP) method for the average pore size. The details of textural properties are given in Table 4-1. It can be seen from Figure 4-4 that synthesized MOFs exhibited type I isotherm in case of ZIF-67-CH_3OH and non-activated UiO-66 without any hysteresis between adsorption-desorption of nitrogen showing microporous nature of these two samples. In case of ZIF-67-H_2O (type IV with H3 hysteresis), a characteristic of mesoporous materials and for chloroform activated UiO-66, N_2 isotherm is of type I and there is hysteresis between adsorption-desorption curves which shows microporous nature in combination with some meso and macroporous. Moreover, all the synthesized MOFs possess high surface areas at 684-1809 m^2/g (Table 4-1). The surface areas of ZIF-67-H_2O and ZIF-67-CH_3OH are 684 and 1809 m^2/g, respectively. The surface area of ZIF-67 is similar to earlier reported results (Lin & Chen, 2016; Qian et al., 2012).

Moreover, the surface area of non-activated UiO-66 sample is 703 m^2/g which is similar to some of the earlier reported results (Chen et al., 2015b; Seo et al., 2015; Wang, Liu, Chen, & Li, 2015a). However, after activation with chloroform, the BET surface area was found to be 1155 m^2/g. This surface area is very similar to the theoretically calculated surface area (1125 m^2/g) of perfectly structured UiO-66 showing the absence of any unreacted BDC in synthesized MOF (Shearer et al., 2014; Valenzano et al., 2011).

Therefore, the XRD, SEM, FTIR and BET surface area analyses showed that all the MOFs are well synthesized, demonstrating the good crystalline structure and porosity. The adsorption tests were carried out using non-activated and chloroform activated UiO-66 and ZIF-67 samples. There is no significant adsorption of SCP on ZIF-67 samples despite of their high surface area (Shao et al., 2014a). The adsorption does not solely depend upon surface area of adsorbents which is obvious in present study. In case of ZIF-67-CH_3OH, surface area is almost 2.6 times higher than ZIF-67-H_2O but there is slight difference between adsorption of SCP on each of them. Moreover, although, the average pore diameter of ZIF-67-CH3OH (0.86 nm) is comparable to the size of SCP molecules (0.81 × 0.87 × 0.65 nm) but still there is not very high adsorption of SCP suggesting weak interactions between ZIF-67-CH_3OH and SCP. Moreover, ZIF-67-H_2O is mesoporous material with pore size 3.95 nm, still there is not high adsorption of SCP on it, justifying lack of strong interactions between SCP and ZIF-67 MOFs (Seo et al., 2015). However, non-activated and chloroform activated UiO-66 samples showed significant SCP adsorption and chloroform activated UiO-66 presented the highest adsorption capacity (Figure 4-5). The adsorption was high on UiO-66 samples showing specific interactions between SCP and UiO-66 MOFs (Seo et al., 2015). Since, surface area of activated UiO-66 is about 1.5 times higher of non-activated UiO-66 and adsorption of SCP is more than double compared to non-activated UiO-66. Generally, there is no direct link between textural properties and adsorption of SCP on UiO-66 MOFs. Thus, more adsorption tests were carried out using chloroform activated UiO-66 sample to study the effects of various adsorption parameters and a plausible mechanism is proposed for adsorption of SCP on UiO-66.

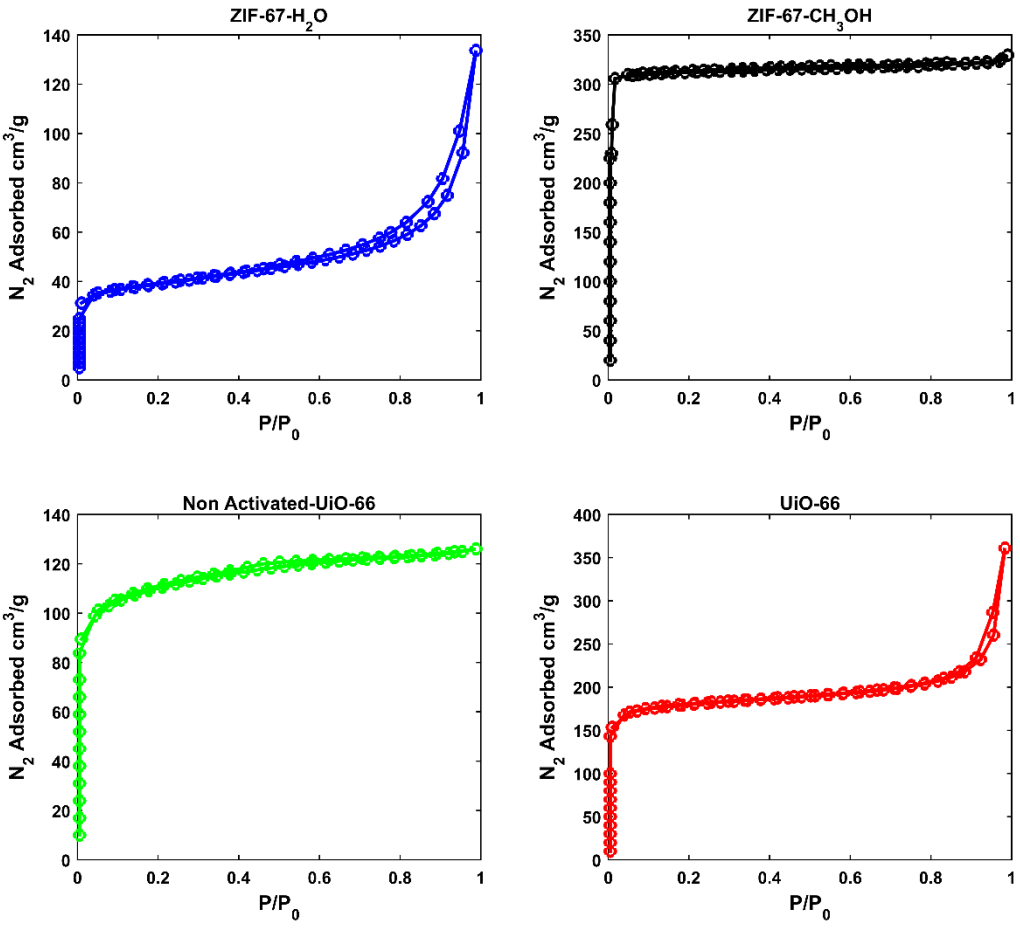

Figure 4-4 Nitrogen adsorption-desorption isotherms for ZIF-67 and UiO-66 MOFs.

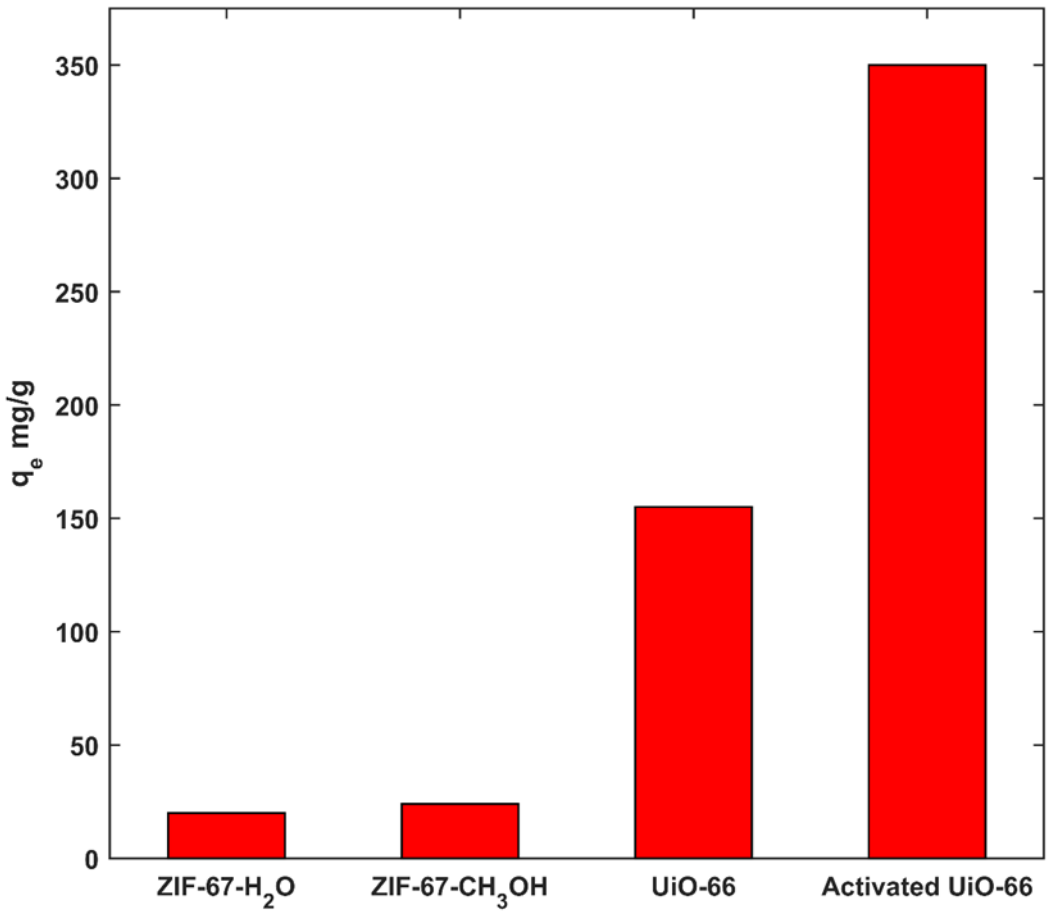

Figure 4-5 SCP adsorption on MOFs ZIF-67 and UiO-66 at 25 °C.

Table 4-1 Textural properties of ZIF-67 and UiO-66 MOFs

MOFs	BET Surface area (m^2/g)	t-plot external surface area (m^2/g)	Total Pore volume (cm^3/g)	Average pore diameter (nm)
ZIF-67-H_2O	684	46	0.17	3.95[a]
ZIF-67-CH_3OH	1809	110	0.49	0.86
Non activated UiO-66	703	97	0.55	0.72
UiO-66	1155	140	0.65	0.82

4.3.2 pH effect on performance of MOFs

It is important to study the effects of solution pH and zeta potential of UiO-66 on adsorption to probe adsorption mechanism. This can be used to figure out the influence of the electrostatic interactions on adsorption. In this study, the pH range was selected in such a way to cover charge/s on adsorbate and adsorbent in solution/suspension, i.e. 3.5-11.5, an initial concentration of SCP solutions at 40 mg/L and 25 °C (Figure 4-6). The pH was adjusted using 0.1 M HCl and 0.1 M NaOH and measured by a WP-81 Cond TDS sal pH meter. It is clear from Figure 4-6 that adsorption capacity decreases with increasing solution pH from 3.5-11.5, indicating the role of electrostatic repulsion between negatively charged adsorbent and anionic adsorbate at pH $\geq$ 5.5.

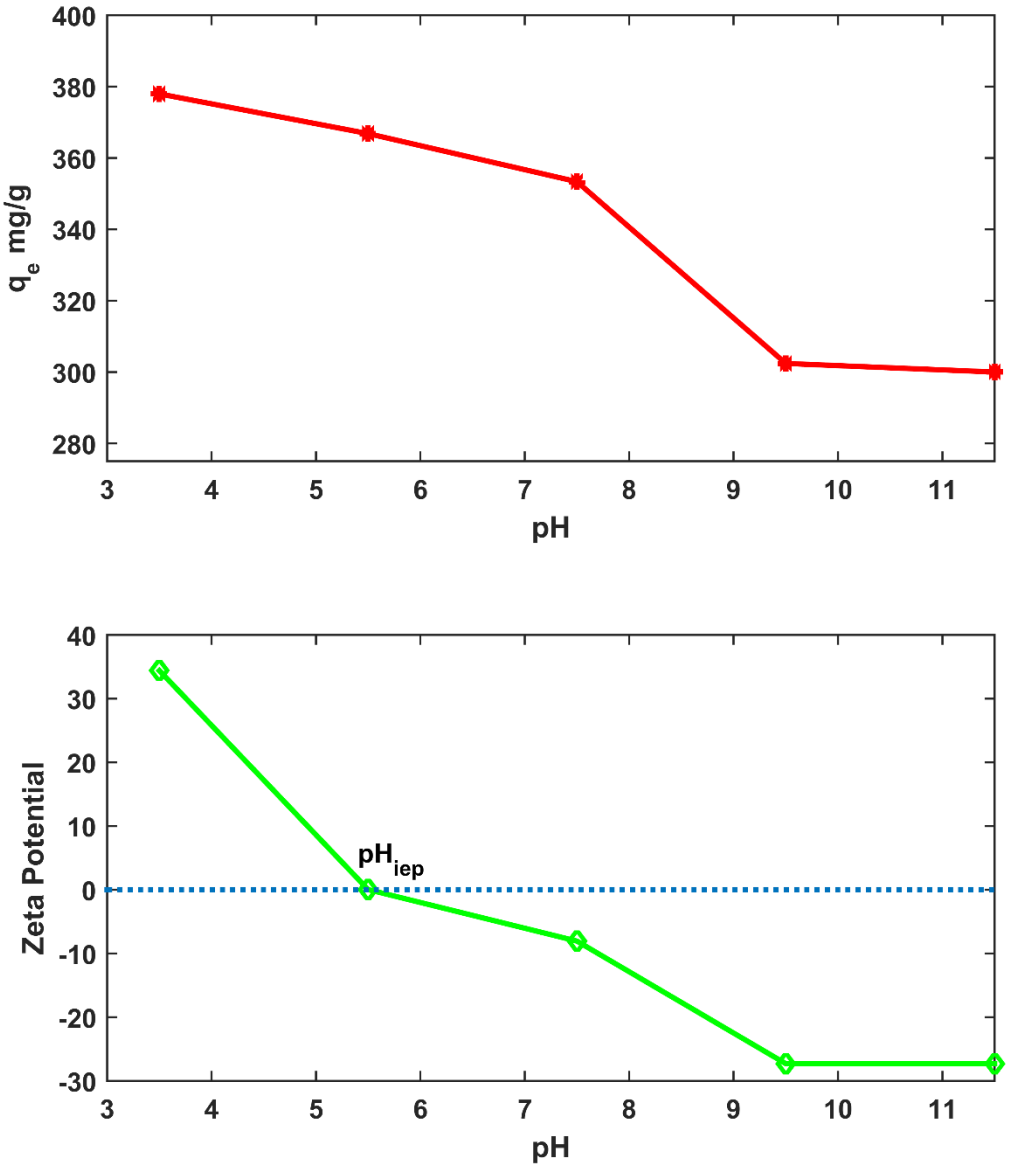

Figure 4-6 Effect of solution pH and zeta potential of UiO-66 on adsorption of SCP over UiO-66.

It is interesting to mention that pH of isoelectric point (pH_{iep}) for UiO-66 is 5.5, the same as pKa value of SCP. At this pH, adsorbent and adsorbate in suspension have no charge but adsorption is very high, suggesting some other factors plays roles in adsorptive removal of SCP.

The adsorption capacity of UiO-66 for SCP at pH 11.5 (strongly basic) is 20% less than that at neutral pH, i.e. 5.5. Thus, the rest adsorption experiments were carried out at pH 5.5 to elaborate the adsorption mechanism for neutral suspensions.

Moreover, pH results show that UiO-66 can be used over a wide range of pH for SCP removal on a large scale.

4.3.3 Kinetics of adsorption process

The effect of time on adsorption of SCP on UiO-66 was studied using different initial concentrations of SCP at 25 °C. Moreover, the adsorption data were best fitted with the pseudo 2nd order kinetic model with R^2 values of 0.999 (Table 4-2). The mathematical expression of the pseudo 2nd order kinetic model is listed as follows (Ho & McKay, 1999a).

$$\frac{t}{q_t} = \frac{1}{k_2 q^2_e} + \frac{1}{q_e} t \qquad (4\text{-}2)$$

Where q_e is the amount of SCP adsorbed at equilibrium (mg/g); q_t is the amount adsorbed at time t (mg/g); t is the adsorption time in minutes and k_2 is the second-order rate constant. The dynamic adsorption plots for the pseudo 2nd order model for parametric calculations are given in Figure 4-7.

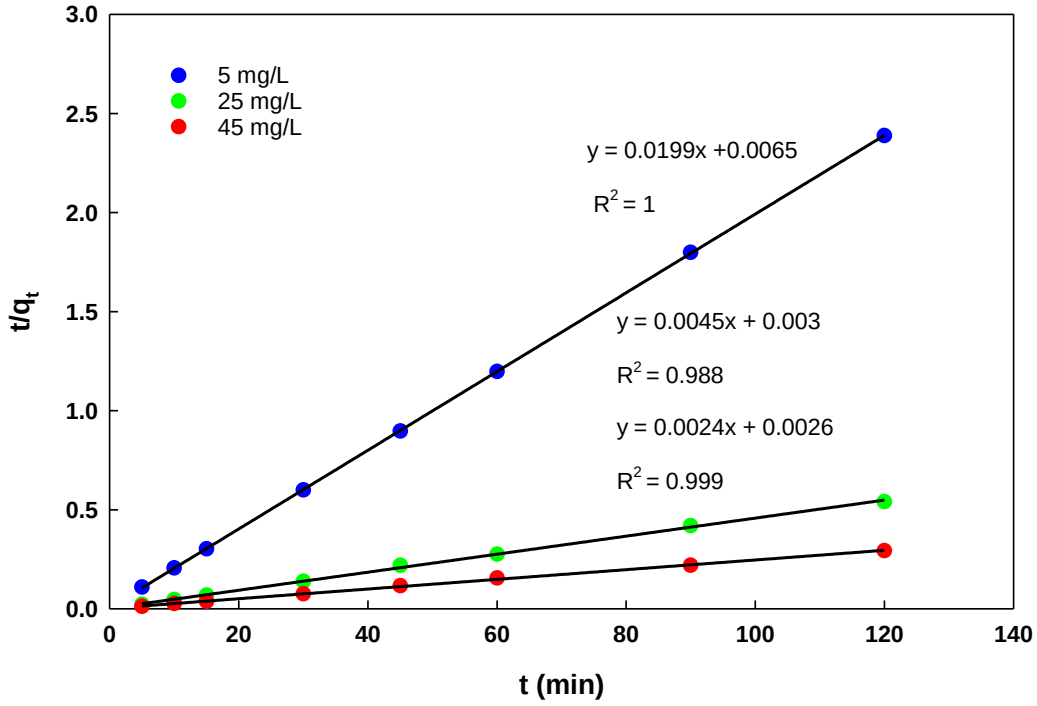

Figure 4-7 Kinetic plots for adsorption of SCP over UiO-66 at different initial concentrations.

Table 4-2 Pseudo 2nd order kinetic parameters for SCP adsorption on UiO-66 at 25 °C with different initial concentrations.

Initial Concentration (mg/L)	$q_{e,exp}$ (mg/g)	Pseudo 2nd order		
		k_2 (g. min/mg)	$q_{e\ cal}$ (mg/g)	R^2
5	50	8.8×10^{-2}	50	1.00
25	221	6.1×10^{-3}	220	0.998
45	408	2.2×10^{-3}	404	0.999

It is evident from Figure 4-8 that adsorption is very fast and most of SCP uptake is completed in 10 min, faster than previously studied HKUST-1 (Azhar et al., 2016). The values of kinetic rate constants, k_2, were decreased with increasing SCP initial concentrations for 5, 25 and 45 mg/L. This may occur due to larger number of SCP

molecules competing to occupy active adsorption sites. The faster kinetics is attributed to specific interaction between UiO-66 and SCP. It is also interesting to note that UiO-66 removes almost all the SCP in 10 minutes even at very low concentrations i.e. 5 mg/L, making it suitable material for adsorption of SCP on a larger scale.

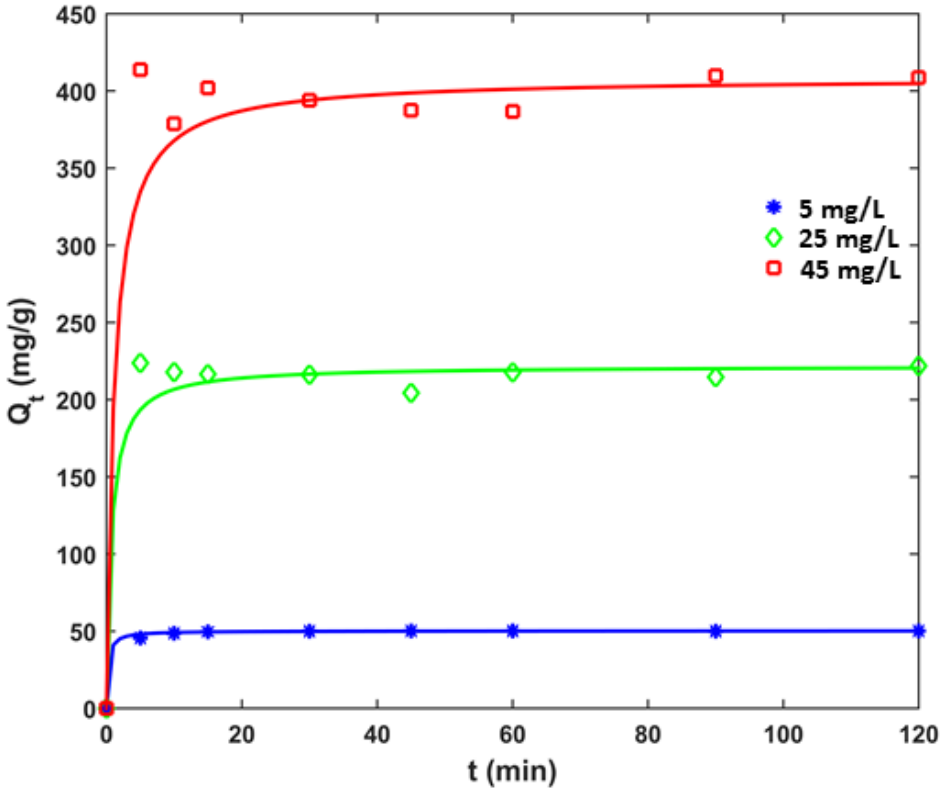

Figure 4-8 Effect of time on adsorption of SCP over UiO-66 with different initial concentrations at 25 °C.

It is observed from N_2 adsorption-desorption isotherms of fresh and SCP adsorbed UiO-66 samples that the surface area remained intact (Figure 4-9) which shows that adsorption takes place on the surface instead of inside the pores. Moreover, the external surface area of UiO-66 decreased significantly after SCP adsorption reinforcing the surface adsorption while micropores remained intact in SCP used sample. The size of SCP molecules (0.81 × 0.87 × 0.65 nm) is comparable to the average pore size of UiO-66 (0.82 nm). However, SCP molecules adsorb on the

external surface of UiO-66 and do not experience any intra-pore resistance resulting in the very fast kinetics.

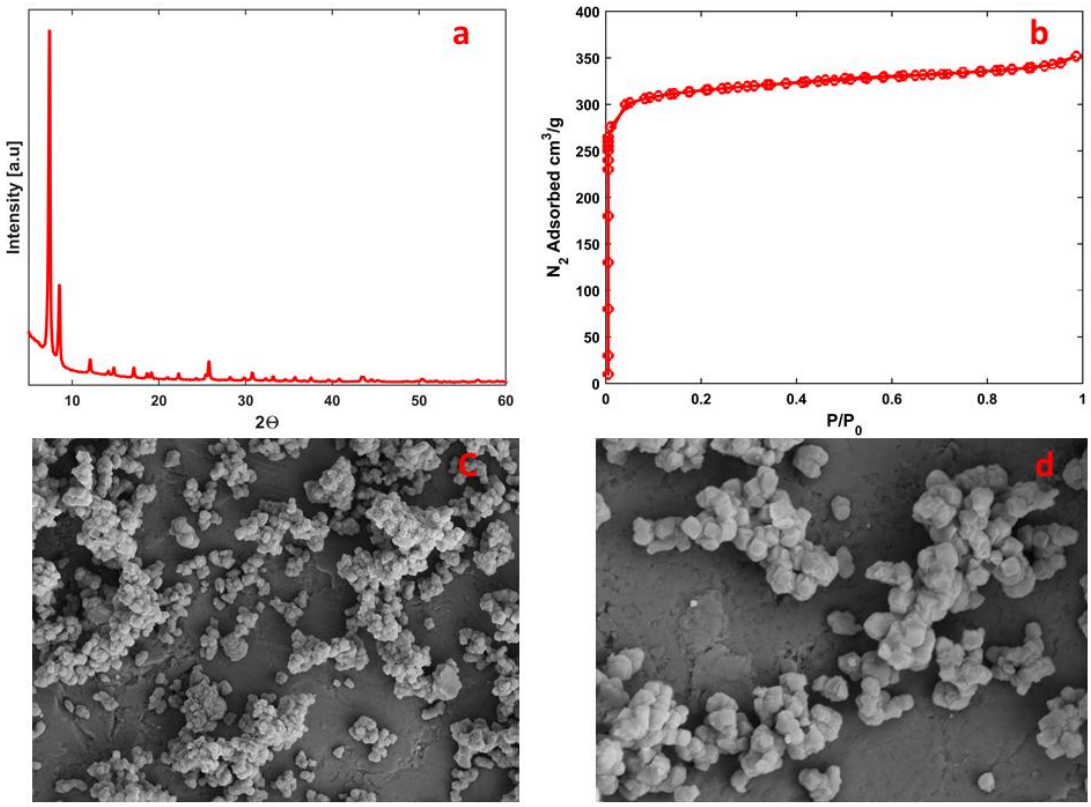

Figure 4-9 Stability of UiO-66 after SCP adsorption; (a) XRD, (b) N2 adsorption-desorption isotherm for BET surface area and (c, d) SEM

4.3.4 Adsorption and adsorption mechanism

The adsorption isotherms were studied at different temperatures for SCP adsorption on UiO-66 and the maximum adsorption capacity was calculated using Langmuir isothermal model (Langmuir, 1918). The linear mathematical expression of Langmuir isotherm can be written as follows.

Langmuir model: $$\frac{C_e}{q_e} = \frac{1}{K_L q_m} + \frac{C_e}{q_m} \qquad (4\text{-}3)$$

where q_e represents equilibrium SCP concentration on an adsorbent (mg/g), C_e represents SCP equilibrium concentration in solution (mg/L), q_m is the monolayer capacity of SCP adsorption (mg/g), and K_L represents the Langmuir adsorption constant (L/mg).

The isothermal data at different temperatures fit with Langmuir model as shown in Figure 4-10 and the maximum adsorption capacity and K_L are given in Table 4-3. The plots for parametric calculations of Langmuir isotherms are given in Figure 4-11. It can be seen that the maximum adsorption capacity and adsorption constant are decrease with increasing temperature and the highest adsorption capacity of 417 mg/g is achieved at 25 °C. Another way of expressing adsorption capacity is number of molecules of adsorbate per nm^2 of the adsorbent surface (Thomas & Kelley, 2010). The external surface area of UiO-66 is 140 m^2/g which gives maximum of 6.27 SCP molecules/nm^2 of adsorbent surface.

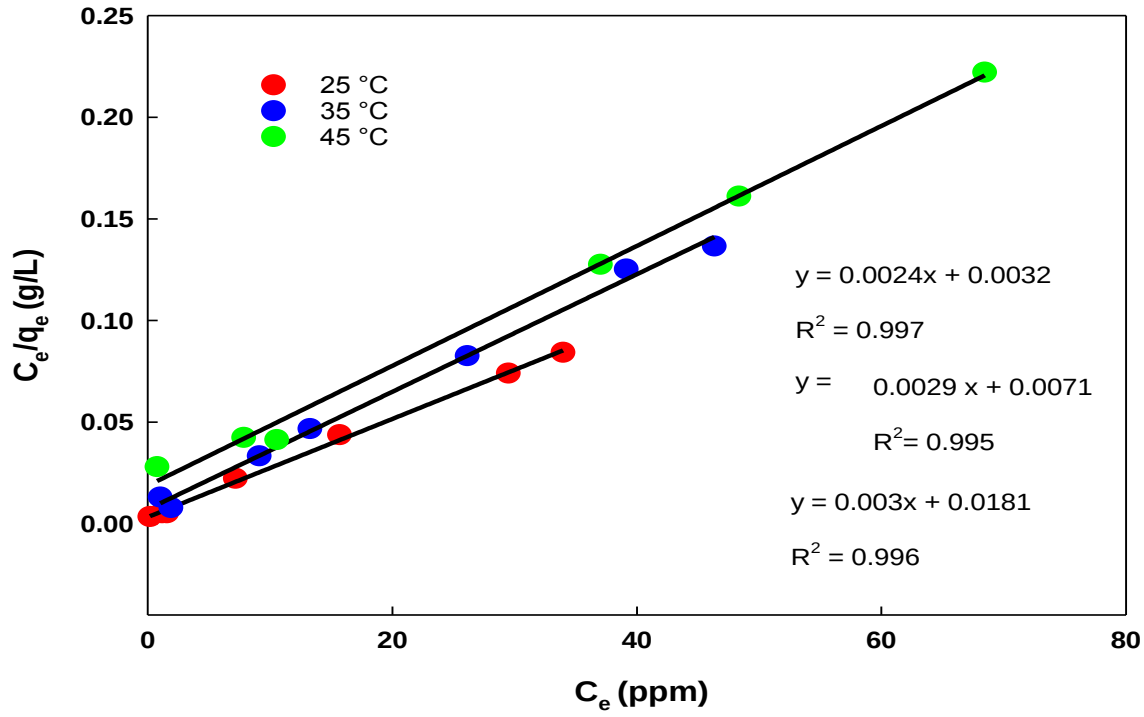

Figure 4-10 Isothermal plots of SCP adsorption over UiO-66 for Langmuir parameters.

Table 4-3 Langmuir adsorption parameters of SCP adsorption over UiO-66 at different temperatures.

		Langmuir model			
Temperature (°C)	$q_{m,exp}$ (mg/g)	$q_{m,c}$ (mg/g)	K_L (L/mg)	R_L	R^2
25	403	417	0.75	0.017	0.997

35	339	357	0.41	0.029	0.995
45	312	330	0.16	0.059	0.996

The adsorption favorability factor (R_L) can be obtained from Eq.4 and the values are in the range $0 < R_L < 1$ at all three temperatures for UiO-66 (Table 4-3), suggesting the favorable adsorption of SCP (Lin et al., 2014).

$$R_L = \frac{1}{1 + C_m K_L} \quad (4\text{-}4)$$

C_m represents the highest initial concentration of SCP in adsorption experiments.

Most of previous studies in SCP adsorption are limited to conventional adsorbents such as granulated activated carbon (GAC) and zeolites. Only HKUST-1 was reported in adsorptive removal of SCP. A comparison of adsorption capacity of SCP is given in Table 4-3, showing the adsorption capacity of UiO-66 is the highest among all adsorbents at 25 °C.

Contrary to HKUST-1 (Azhar et al., 2016), the high adsorption capacity of UiO-66 is not affected by high surface area and porosity rather it depends on specific interaction between SCP and UiO-66. The contributions in such a high adsorption capacity are electrostatic interaction, π-π and hydrophobic interactions. The details on adsorption mechanism are provided in following section.

Table 4-4 Comparison of adsorption capacity of SCP on different adsorbents.

Adsorbents	Maximum adsorption capacity, q_m (mg/g)	Reference
PAC	4.5	(C. Adams, 2002)
Faujasite zeolite Y	280	(Braschi et al., 2010a)
HSZ-690HOA zeolite	151	(Martucci et al., 2013)
HKUST-1	384	(Azhar et al., 2016)
UiO-66	417	Present study

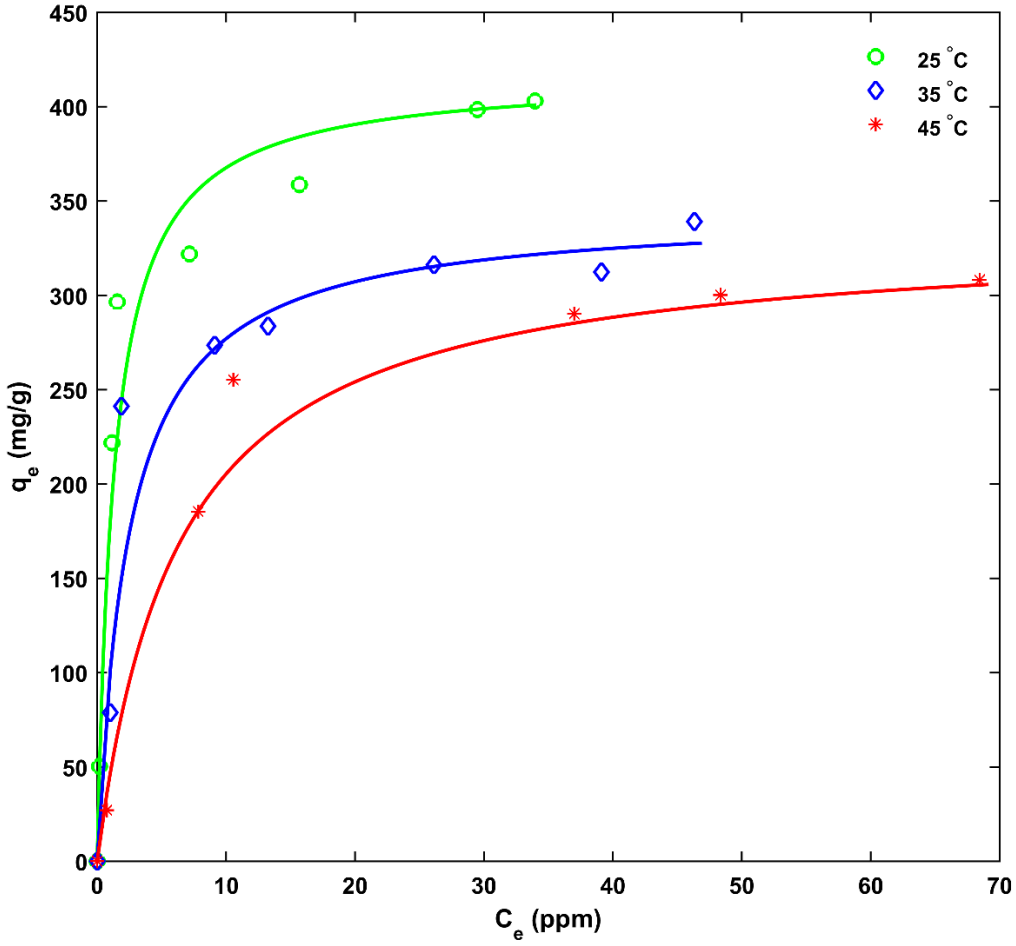

Figure 4-11 Adsorption isotherms of SCP adsorption on UiO-66 at different temperatures.

The surface charge of an adsorbent and cationic/anionic nature of an adsorbate are main factors in adsorption process. In the present study, SCP is an amphoteric adsorbate which may exist as $SCP^{\pm}$ or SCP^{0} depending on the solution pH. The pKa value of SCP is 5.5, which suggests SCP mainly exists in an anionic form at pH > 5.5 and neutral at pH 5.5 (Ishihama et al., 2002a). Interestingly, the pH_{iep} for UiO-66 is 5.5. This gives rise to electrically neutral suspension of UiO-66 in SCP adsorption at pH 5.5 (Seo et al., 2015). It is clear from Figure 2 that adsorption capacity decreases with increasing pH from 3.5-11.5, suggesting the effect of electrostatic interaction on adsorption of SCP on UiO-66. However, it is important to mention that adsorption capacity of UiO-66 is very high at pH 5.5, which is the pH of neutral suspension owing to pKa value of SCP and pH_{iep} of UiO-66. At pH 5.5, the main factor in adsorption mechanism would be hydrophobic interaction due to low solubility of SCP compared to its enhanced solubility at higher pH and inherent

nature of UiO-66 in structurally defect-free form and zero surface charge (Ghosh et al., 2014; Thomas et al., 2006). At pH 3.5, the surface charge of UiO-66 is positive (Figure 4-6), while SCP can be a mixture of cationic or neutral/anionic species. The chances of cationic SCP^{+} are less due to a low K_b value of SCP ($pK_b > 12$) which assures the availability of neutral and/or anionic form of SCP (Azhar et al., 2016; http://www.medicinescomplete.com/mc/clarke/current/index.htm). Therefore, adsorption capacity is the highest at this pH due to electrostatic attraction in addition to hydrophobic and π-π interaction which is also confirmed by fractional decrease in adsorption capacity at pH 3.5-5.5.

The adsorption capacity of UiO-66 in strongly basic conditions (11.5) is 80% of that at the neutral conditions (pH=5.5) while there is a marginal decrease in adsorption capacity from pH 5.5-7.5 and 7.5-9.5, which can be explained by electrostatic repulsion between negatively charged UiO-66 (zeta potential) and anionic SCP^{-1}. Moreover, the solubility of SCP increases at higher pHs, which results in enhanced hydrophilicity of SCP and decreased adsorption (Thomas et al., 2006). In order to deduce plausible adsorption mechanism, the less explored hydrophobic interactions are taken into account along with π-π interaction.

The defect-free UiO-66 is hydrophobic compared to missing linker counterpart. A study has suggested defects and missing linkers of UiO-66 making them hydrophilic (Ghosh et al., 2014). This hydrophilicity promotes the interaction of UiO-66 with water molecules instead of adsorbate, thus resulting in a decreased adsorption capacity. This can be found on non-activated UiO-66 (Figure 4-5) which possesses missing linkers and unreacted BDC^{-} for enhanced hydrophilicity and repulsion between anionic SCP and BDC^{-} (Ghosh et al., 2014). However, chloroform activated UiO-66 produced an almost perfect structure of UiO-66, resulting in high adsorption of SCP due to hydrophobicity and π-π interaction. The plausible mechanism of SCP adsorption on UiO-66 is shown in Figure 4-12 at different pH values. Moreover, the adsorption of SCP with no charge at pH_{iep} (5.5) of UiO-66 and pKa value of SCP is also shown confirming very significant roles of hydrophobicity and π-π interactions.

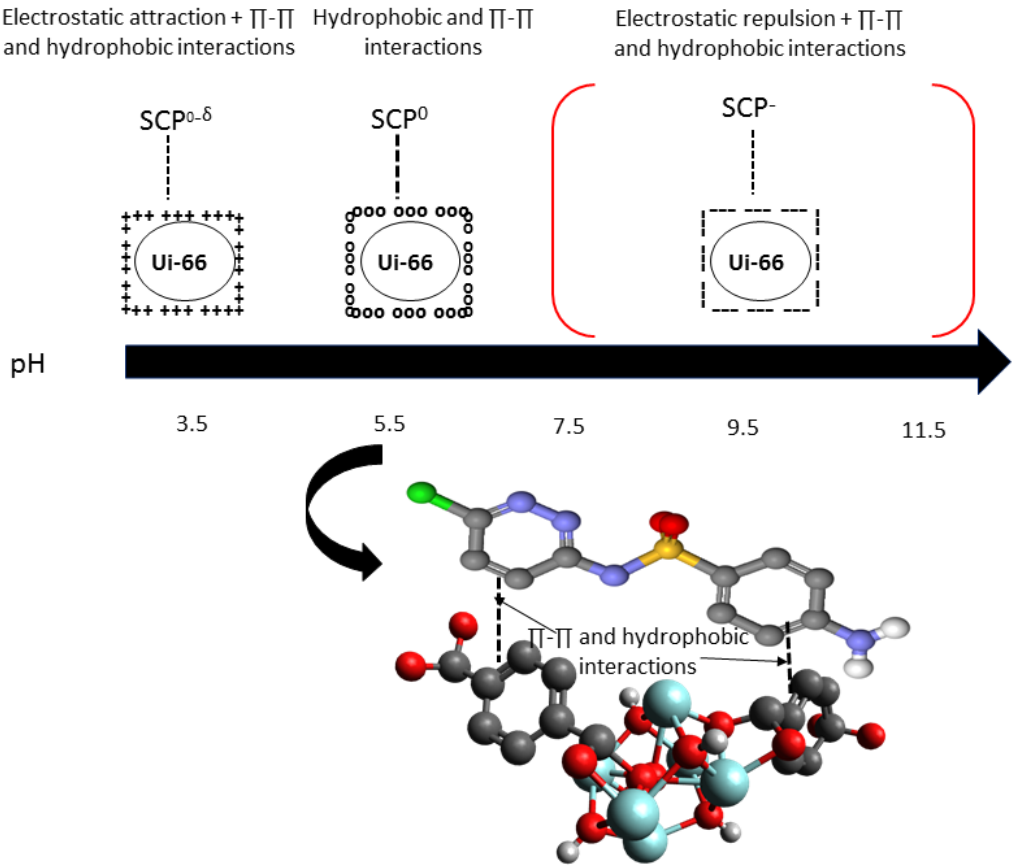

Figure 4-12 Plausible adsorption mechanism of SCP on UiO-66; colour scheme, cyan: Zr, red: oxygen, Grey: carbon, white: hydrogen, purple: nitrogen, yellow: sulphur, green: chlorine. The oxygen atoms on BDC are omitted for clarity.

4.3.5 Regeneration and reuse of UiO-66

It is important for the practical application of an adsorbent for its regeneration and reuse. In this study, a dilute solution of NaOH (0.01 M) was used for the regeneration of MOF due to high solubility of SCP in a basic medium (Thomas et al., 2006). The used adsorbent was shaken in NaOH solutions for 0.5 h and subsequently filtered and washed with water. Moreover, the adsorbent was dried at 150 °C for reuse. The regeneration procedure was adopted for consecutive three runs. It is interesting to mention that UiO-66 retains more than 80% adsorption capacity after four runs (Figure 4-13). The XRD pattern of the used UiO-66 (fourth run) and SEM (Figure 4-9) show there is no difference between the fresh and fourth regenerated UiO-66, indicating structural stability of this versatile MOF. Moreover, the N_2 adsorption-desorption isotherm is not affected by the adsorption of SCP

(Figure 4-9), indicating textural structure stability of UiO-66 after SCP adsorption. The microporous surface remains the same after SCP adsorption as the size of SCP molecules is comparable to the average size of micropores in UiO-66. However, the macropores of UiO-66 are disappeared in the used UiO-66 sample which is clearly shown from the absence of hysteresis at 0.99 and slight reduction in BET surface area in the used sample (Figure 4-9). The BET surface area of the used UiO-66 is 1055 m^2/g. The high adsorption capacity, fast kinetics, wide range of operating pH and easy regeneration and reuse of UiO-66 makes it a suitable candidate for large scale wastewater treatment processes.

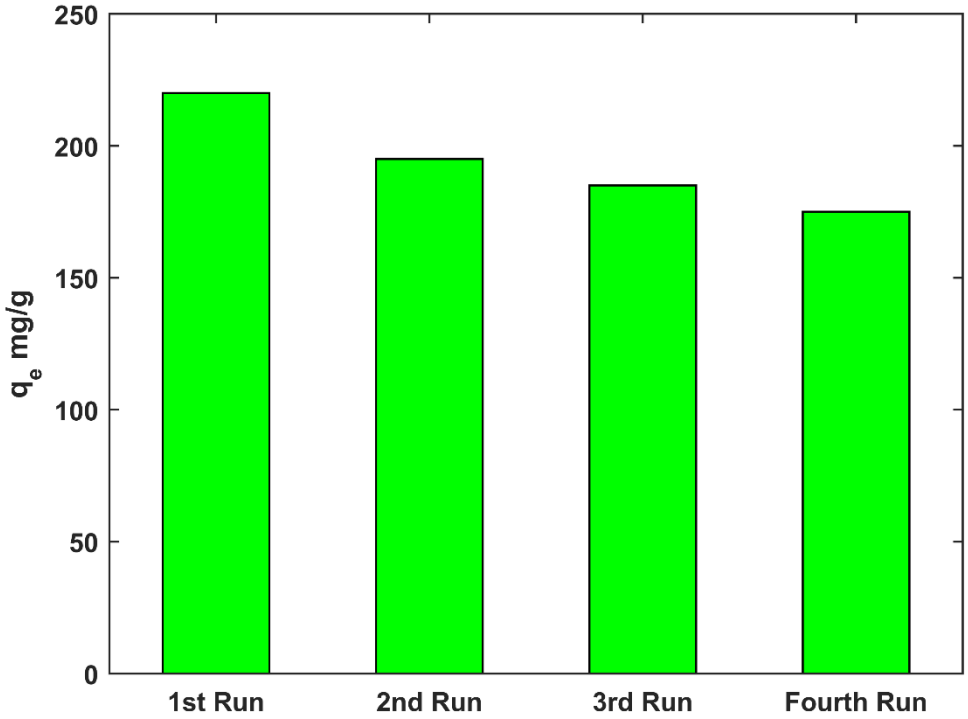

Figure 4-13 Recyclability of UiO-66 MOF for four adsorption runs, C0 = 25 mg/L at 25 ℃.

4.3.6 Thermodynamics of adsorption

The solubility of SCP depends on temperature (Martucci et al., 2013; Perlovich et al., 2011), so the adsorption data were collected at three different temperatures, i.e. 25, 35 and 45 ℃, to study the effect of temperature on adsorption. Moreover, thermodynamic parameters such as enthalpy (ΔH) and entropy (ΔS) were

calculated using the van't Hoff plots (Haque et al., 2010a; Haque et al., 2014b). The mathematical expression for the van't Hoff equation can be written as follows.

$$\ln K_L = \frac{\Delta S}{R} - \frac{\Delta H}{RT} \quad (4\text{-}5)$$

The Gibbs free energy (ΔG) can be calculated by the following equation to indicate spontaneity of the adsorption process.

$$\Delta G = -RT \ln K_L \quad (4\text{-}6)$$

Where, ΔG represents Gibbs free energy, K_L (L/mol) is the Langmuir constant, T is temperature in K and R is universal gas constant. The negative value of ΔG shows spontaneous nature of adsorption process (Haque et al., 2010a).

A linear plot of ln K_L and 1/T was obtained for the enthalpy and entropy calculations (Figure 4-14). The values of thermodynamic parameters are given in Table 4-5. The negative enthalpy change suggests that the adsorption is an exothermic process. Moreover, the adsorption is controlled by enthalpy instead of negative entropy for SCP adsorption on UiO-66 (Jia et al., 2015). The small negative value of ΔS (-100.9 J/mol K) suggests very little desorption of pre-adsorbed water molecules signifying the effect of activation (Haque et al., 2010a). Therefore, the isothermal data at different temperatures revealed that adsorption of SCP on UiO-66 is a spontaneous and exothermic process.

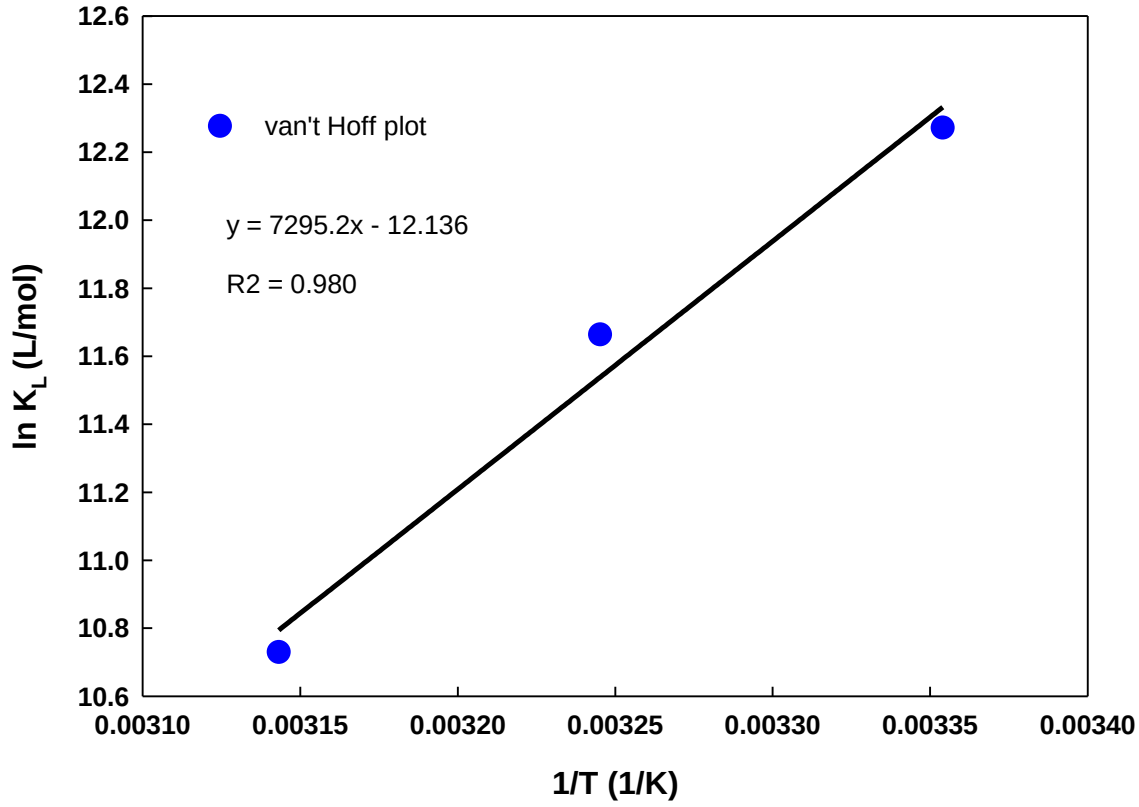

Figure 4-14 The van't Hoff plot for thermodynamic parameters of SCP adsorption over UiO-66

Table 4-5 Thermodynamic parameters of SCP adsorption on UiO-66.

Temperature (°C)	ΔG (kJ/mol)	ΔH (kJ/mol)	ΔS (J/mol K)
25	-30.4	-60.6	-100.9
35	-29.8		
45	-28.3		

4.4 Conclusions

UiO-66 and ZIF-67 MOFs have been synthesized and characterized for wastewater treatment processes. ZIF-67 MOFs showed limited affinity in adsorption of SCP while UiO-66 exhibited strong affinity for SCP. Chloroform activated UiO-66 was in

detail studied for adsorptive removal of SCP, a model sulfonamide antibiotic. The UiO-66 has a high surface area and defect-free structure for its enhancing hydrophobicity, fast kinetics and high adsorption capacity of SCP. The Langmuir adsorption capacity of the UiO-66 is 417 mg/g at 25 °C, the highest among the studied adsorbents. Moreover, thermodynamic study showed that adsorption of SCP on the UiO-66 is an exothermic process. The pH effect on adsorption showed that the contribution from electrostatic interactions is accounting for just 20% while the adsorption mainly takes place due to hydrophobicity and π-π interactions. The UiO-66 adsorbent was regenerated by a facile method and reused in four runs without a significant loss in adsorption capacity. The present study highlights the importance of finely tuned structure of MOFs in adsorption process.

Chapter 5 One pot synthesis of binary (HKUST-1 and UiO-66) metal organic frameworks for methylene blue [*]

[*] Adopted with permission from (M.R, Azhar, H.R, Abid, H. Sun, V. Periasamy, M.O., Tade, S. Wang, "One-pot synthesis of binary metal organic frameworks (HKUST-1 and UiO-66) for enhanced adsorptive removal of water contaminants", *Journal of Colloidal and Interface Science*, pp. 685–694, 2017). Copyright Elsevier.

5.1 Introduction

Metal organic frameworks (MOFs) have emerged as a promising class of porous materials in the last two decades (Wang et al., 2015d). There is an increasing literature on the synthesis and application of new and existing MOFs with tailored properties. The beauty of MOFs lies in their tuneable textural and chemical properties (Abid et al., 2012a; Jiang et al., 2014; Zhang et al., 2015d; Zhou et al., 2015). The high surface area, tuneable pore size, incorporation of various functionalities by in situ and/or post-synthesis treatment make them highly demanding materials in gas adsorption, gas separation, catalysis, energy storage, supercapacitors, biomedical and wastewater treatment processes (Gandara, Furukawa, Lee, & Yaghi, 2014a; Lin et al., 2014; Phan, Czaja, Gandara, Knobler, & Yaghi, 2011; Xiao et al., 2013a; Yee et al., 2013). Recently, MOFs-based composites with various materials have gained attention (Ahmed & Jhung, 2014; Ahmed et al., 2013; Peterson et al., 2013; Yan et al., 2014; Yang et al., 2014; Yilmaz & Keskin, 2014).

In recent years, with the immense industrialization and urbanization, the amount of wastewater has increased sharply while fresh and potable water is continuously decreasing. The wastes discharged from various industries include heavy metals, personal care products, pharmaceuticals, herbicides and dyes. The amount of dyes produced every year is approximately 9 million tons with 100,000 varieties (Shao et al., 2014; Yagub et al., 2014) and are usually used in textile, food and colouring industries. These dyes are causing harmful effects on aquatic life. Removal of the dyes is vital as some of them are even carcinogenic (Belpaire et al., 2015). Methylene blue has been widely studied in wastewater treatment processes, being one of the common dyes discharged into water bodies (Asfaram, Ghaedi, Azqhandi, Goudarzi, & Dastkhoon, 2016a; Asfaram, Ghaedi, Goudarzi, & Rajabi, 2015; Asfaram, Ghaedi, Hajati, & Goudarzi, 2015; Belpaire et al., 2015; Haque, Jun, & Jhung, 2011). There are various methods of dye removal namely, catalytic oxidation, biological degradation and adsorption (Du et al., 2011; Hayat, Mahmood, Pervez, Bhatti, & Baig, 2015; Tan et al., 2015).

Adsorption is one of the promising methods for dye removal from water. However, there are various challenges in the removal of dyes including MB from wastewater, e.g. low adsorption capacity of adsorbents, limited operative pH range and regeneration of the materials (Haque et al., 2014b; Lin et al., 2014; Shen et al., 2015). Pristine as well as composite adsorbents, e.g. activated carbons, graphene, graphene oxide, mesoporous carbons, clays, zeolites, activated carbon-metal oxide composites and MOFs have been reported for the adsorptive removal of MB from wastewater (Asfaram, Ghaedi, Hajati, Goudarzi, & Dil, 2017; Asfaram, Ghaedi, Yousefi, & Dastkhoon, 2016b; Dil et al., 2016; Shao et al., 2014; Wang, Ng, Wang, Li, & Hao, 2012; Wu et al., 2014; Xiao et al., 2013a; Zhou et al., 2015). However, wastewater treatment processes (WWTPs) using MOFs are very limited due to instability of the MOFs in aqueous media, low adsorption capacity, limited operating range in terms of pH. Enamul et al. (Haque et al., 2010b) reported the first ever MOF application in WWTPs for the removal of methyl orange using Cr based MOF. It was observed that functionalization of the MOF with NH_2 group resulted in adsorption capacity of 194 mg/g for methyl orange. Ever since, some other MOFs have been employed in the removal of dyes but limited to a group of MILs, i.e. MIL-53, MIL-100, and MIL-101 (Dawood & Sen, 2012; Haque et al., 2011; Huo & Yan, 2012; Leng et al., 2014; Tong et al., 2013). The use of Cu based MOFs (HKUST-1) has gained attention for last couple of years when a CuBTC was used in the adsorptive removal of MB. However, very limited MB was removed [7]. Moreover, electrostatic interaction was reported as the main factor in removal of MB confirmed by the pH effect. In another study, terphenyl tetracarboxylic acid (H_4TPTC) was used in combination with terphenyl hexa carboxylic acid (H_6TPTC) for MOF synthesis resulting in a higher adsorption capacity of MB (Zhang et al., 2014d). However, the cost of the linkers for preparation is very high to implement at a larger scale.

There are some studies on adsorptive removal of MB using Cu based MOFs and UiO-66 (Chen et al., 2015b; Lin et al., 2014; Zhang et al., 2014c). UiO-66 and HKUST-1 are stable MOFs in aqueous media and have been used in various organic waste removal processes (Hasan & Jhung, 2014; Hasan et al., 2014; Seo et al., 2015). Composites of HKUST-1 with graphite oxide have been reported in ammonia adsorption and MB removal (Li et al., 2013a; Petit & Bandosz, 2010). The synergic

effect of zirconium hydroxide composited with HKUST-1 in toxic chemicals (ammonia, cyanogen chloride, and sulfur dioxide) removal by physically mixing with zirconium hydroxide was also tested (Peterson et al., 2013). However, there are no studies on bimetallic Cu and Zr MOFs in WWTPs. In the present study, binary MOFs were synthesized in situ to make a comparison of their capacity for adsorptive removal of MB. Specifically, carboxylic acid based linkers were selected to reinforce functionalities in composite MOFs with a bi-metallic configuration (Cu and Zr). Interestingly, the adsorption of MB on composite MOFs is much higher than the pristine MOFs. This study opens new horizons in terms of in situ synthesis of composite MOFs with synergic effects in WWTPs.

5.2 Experimental

5.2.1 Materials

Dimethylformamide (DMF, 99%), benzene-1, 4-dicarboxylic acid (BDC, 98.9%), $ZrCl_4$ (99.9 %), $Cu(NO_3)_2 \bullet 3H_2O$ (99 %), benzene tricarboxylic acid (BTC, 95 %), hydrochloric acid (HCl, 36.5 %), sodium hydroxide (NaOH, 97 %), methylene blue (MB, 82 %), and methanol (99.9 %) were supplied by Sigma–Aldrich (Australia). An activated carbon (AC, 98 % C) was purchased from Perth Scientific Pty Ltd (Australia) and used without further purification. The ultrapure water (IBIS Alpha, 15.5 mΩ cm, IBIS technology) was obtained from our laboratory.

5.2.2 Synthesis of pristine and composite MOFs

A pristine HKUST-1 was prepared with modification from a reported method (Chui, Lo, Charmant, Orpen, & Williams, 1999a). In a typical synthesis, 1.087 g of $Cu(NO_3)_2 \bullet 3H_2O$ was dissolved in 15 mL absolute ethanol while 0.525 g of BTC was dissolved in another 15 mL absolute ethanol. Then, both solutions were transferred into a Teflon autoclave and heated in an oven at 125 ℃ for 24 h. The resultant MOF was filtered under vacuum and dried at 155 ℃ overnight. The sample was labelled as C.

A pristine Zr-UiO-66 was synthesized by a reported procedure with slight modification (Cavka et al., 2008). In a typical synthesis, 1.087 g $ZrCl_4$ and 0.525 g benzene dicarboxylic acid (BDC) were separately dissolved in a solvent (DMF) of 15 mL. Both solutions were stirred for 15 min, mixed together and then stirred for 20 min. Finally, the solution was transferred to an autoclave and heated in an oven at 125 °C for 24 h. The sample was designated as Z.

In the synthesis of binary metal organic frameworks, Zr-UiO-66/Cu-HKUST-1(C1), 1.087 g of $Cu(NO_3)_2 \bullet 3H_2O$ and 0.525 g of BTC were separately dissolved in 15 mL absolute ethanol, mixed and stirred at 300 rpm and 60 °C for 4 h. Then 0.0544 g $ZrCl_4$ and 0.0263 g BDC were dissolved in DMF and stirred at 300 rpm and 60 °C for 4 h. Subsequently, the above two solutions were poured into a Teflon autoclave and heated in an oven at 125 °C for 24 h.

For the synthesis of Cu-HKUST-1/Zr-UiO-66 (Z1), 1.087 g $ZrCl_4$ and 0.525 g BDC were dissolved in 15 mL DMF each and mixed together. Then 0.0544 g $Cu(NO_3)_2 \bullet 3H_2O$ was dissolved in 0.75 mL H_2O and 0.0263 g BTC was dissolved in 0.75 mL absolute ethanol, mixed and stirred at 60 °C. Finally, two solutions were poured into a Teflon autoclave and put in an oven at 125 °C for 24 h.

All the MOFs were filtered under vacuum and dried at 155 °C overnight. Moreover, all the MOFs were activated using methanol for 48 h. In the activation process, fixed quantity of MOF was soaked in 50 mL methanol and replenished with fresh methanol after 24 h.

5.2.3 Characterization of MOFs

FTIR spectra were used to check the functional groups on the organic ligands and coordinated metal atoms. The spectra were scanned with a resolution of 4 cm^{-1} using an attenuated total reflectance (ATR) technique on a Spectrum 100 FT-IR Spectrometer (Perkin Elmer). SEM analysis (Zeiss NEON 40 EsB CrossBeam) was conducted to study the morphologies of the pristine and composite MOFs. Thermal stability of MOFs was investigated by a thermogravimetric analysis (TGA) instrument, TGA/DSC1 STAR^e system-METTLER TOLEDO. All the MOF samples were loaded into an alumina pan and heated to 800 °C at a rate of 5 °C/min. An air

flow rate was maintained at 10 mL/min. X-ray powder diffraction patterns were obtained with X-ray diffractometer (D8 Advance-Bruker aXS) using Cu Kα radiation (λ = 1.5406 Å), at accelerating voltage and current of 40 kV and 40 mA, respectively, for 2θ ranging between 5-40°. The surface area, pore size and pore volume were measured using N_2 adsorption/desorption isotherms on a Micromeritics Tristar II3020. The samples were evacuated at 180 °C for 4-12 h prior to the adsorption measurements under high vacuum. The multi-point BET surface area was calculated by N_2 adsorption in P/P_0 =0.05-0.15, single point pore volume was calculated at P/P_0 = 0.99 and pore size distribution was determined using the Barrett-Joyner-Halenda (BJH) method. The point of zero charge (pH_{PZC}) was determined using an immersion technique (Fiol & Villaescusa, 2008). Suspensions of 10 g/L of MOF were put into contact with 0.03 M KNO_3 solutions adjusted at different pH values of 3-10. The suspensions were aged for 24 h until an equilibrium pH value was reached. The change in pH (|ΔpH|) during equilibration was calculated and the pH for PZC was identified as the initial pH with zero or minimum |ΔpH|.

5.2.4 Adsorption study

The MB concentrations were determined using the maximum absorbance (at 664 nm) of the solutions through UV spectra of the solutions obtained by a spectrophotometer (Thermo Spectronic Genesys 20, Thermo Scientific™).

First, the calibration curve was obtained from the spectra of the standard solutions which were prepared in various concentrations (1–10 ppm) at a specific pH of 7.5 measured by WP-81 pH-Cond-Salinity meter. The initial pH of MB solution was adjusted using 0.1 M HCl and 0.1 M NaOH.

Second, 1000 ppm aqueous stock solution of MB was prepared by dissolving MB in ultrapure water. Different concentrations of MB (5–100 ppm) were prepared by further diluting the stock solution with water to study adsorption isotherms.

In all the batch experiments, the MOFs were dried overnight under vacuum at 140 °C and were kept in a desiccator. A fixed amount of the MOFs was put in the aqueous dye solutions (100 mL) having fixed dye concentrations from 5 to 100 ppm. The MB solutions (pH 7.5) containing the adsorbents were mixed well with magnetic stirring and maintained for fixed time (10 min to 12 h) at 25 °C. After

adsorption, the solution was separated from the adsorbents by a high-speed centrifuge for 5 min, and the dye concentration was determined by the UV-Vis spectrophotometer and then the amount of dye adsorbed was calculated by the following equation.

$$Q_e = \frac{(C_0 - C_e)V}{m_{ads}} \quad (5\text{-}1)$$

Where Q_e is amount of dye adsorbed at equilibrium (mg/g), C_0, initial dye concentration (ppm), C_e equilibrium dye concentration (ppm), volume of dye solution used (l) and m_{ads}, is the mass of adsorbent (g).

5.3 Results and discussion

5.3.1 Characterization of MOFs

All the samples were characterized for the binding between metal atoms and linkers (BDC and BTC) (Figure 5-1). The characteristic peak of HKUST-1 (C) and its composite MOF (C1) at 728 cm^{-1} are attributed to Cu-O bond confirming metal-linker coordination (Lin et al., 2014). Moreover, the peak at 745 cm^{-1} represents Zr-O bond in UiO-66 (Z) and its composite MOF (Z1) (Valenzano et al., 2011). The bands at 1550-1630 cm^{-1} indicate C=O, while region of 1450-1580 cm^{-1} belongs to C=C of aromatic ring. Moreover, the strong band at around 1370 cm^{-1} also represents C=C of benzene (Abid et al., 2012c; Lin et al., 2014; Rodger, 1997; Zhang et al., 2014d). Furthermore, the peaks shifting was observed in case of MB adsorption on MOFs, suggesting host-guest interaction of organic moieties of the MOFs and organic dye (MB). Generally, the peaks were shifted marginally in case of Z and Z1 compared to significant peaks shifting of C and C1 after MB adsorption (Figure 5-1). The shifting of peaks in the range of 1368-1391 cm^{-1} and 1562-1582 cm^{-1}, in particular reinforces the π-π interaction of benzene rings of host-guest. The details on adsorption mechanism are given in section 5.4.

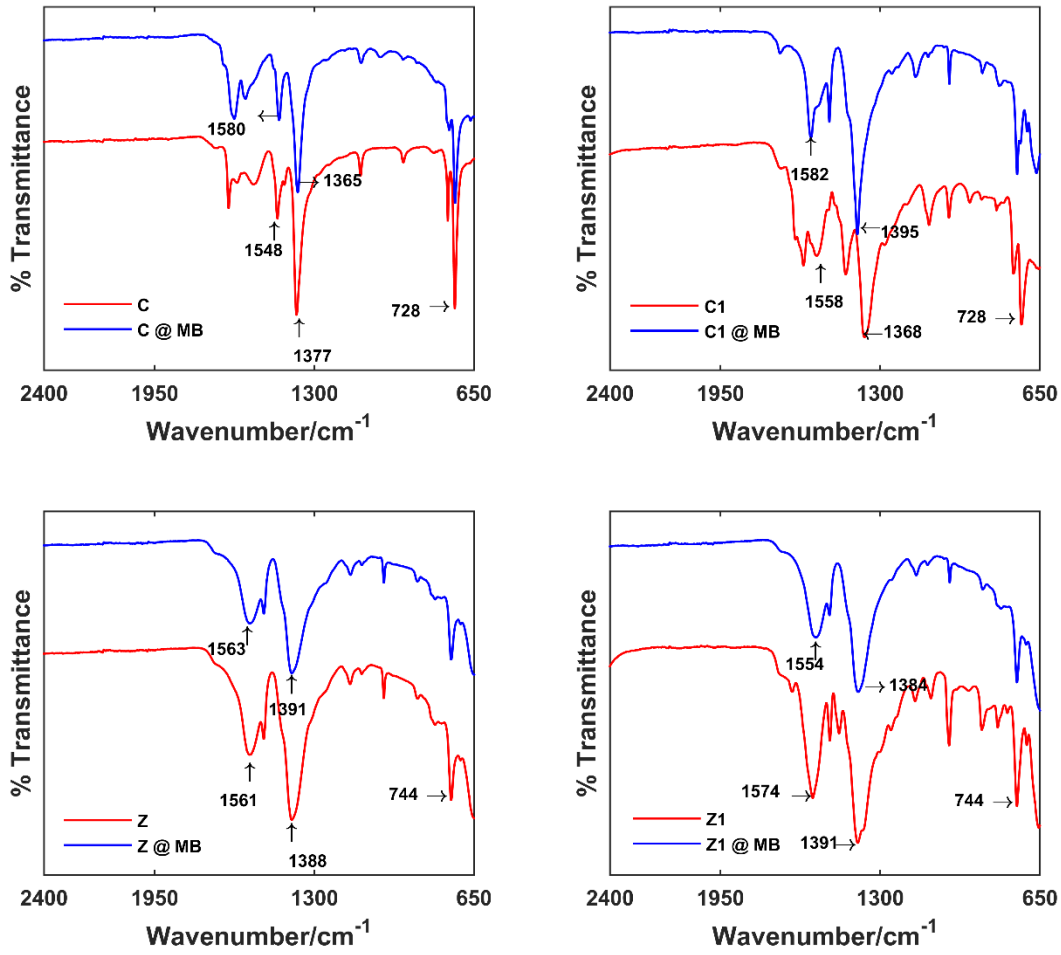

Figure 5-1 FTIR spectra of fresh and MB adsorbed pristine and composite binary MOFs.

The structure of the synthesized single and binary MOFs was studied using XRD (Figure 5-2). It is clear that the structure of composite MOFs is similar to the structure of pristine HKUST-1 and UiO-66. The XRD patterns also show the high crystallinity of pure HKUST-1 and UiO-66 MOFs, which have been studied extensively in literature (Andrew Lin & Hsieh, 2015; Seo et al., 2015; Valenzano et al., 2011). Moreover, bimetallic MOFs, C1 and Z1, exhibited similar degree of crystallinity in XRD pattern to their parent MOFs (HKUST-1 and UiO-66) as previously reported (Ke et al., 2011a). Furthermore, distinct octahedral shape crystals can be seen from SEM analysis (Figure 5-3). Similarly, the crystals of bimetallic HKSUT-1 (C1) are also in octahedral shape. Moreover, distinct macro-

pores can be seen in C1 (Figure 5-3 inset). In the case of Z, the particles are almost in cubic shape in 200 nm range, whereas Z1 is similar to parent UiO-66 (Abid et al., 2012c; Cavka et al., 2008).

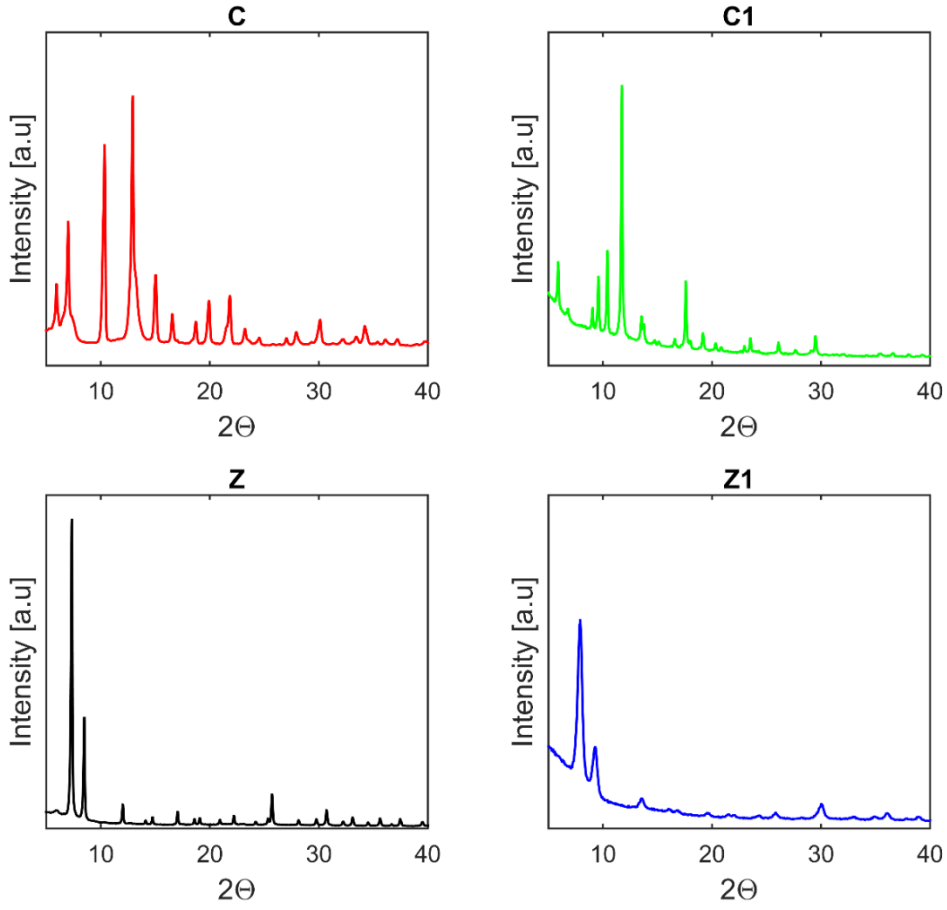

Figure 5-2 XRD patterns of pristine and composite binary MOFs.

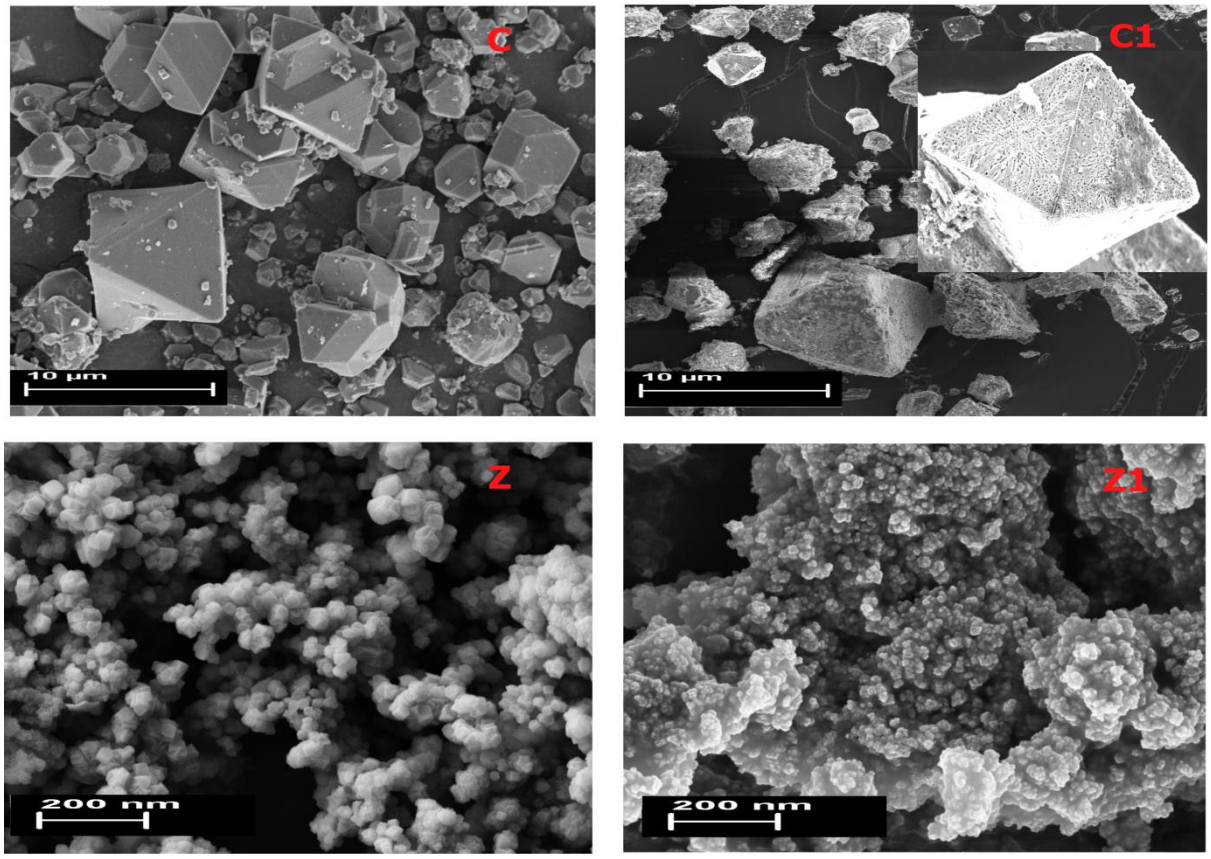

Figure 5-3 SEM images of pristine and composite binary MOFs.

Thermal stability of pristine and composite MOFs was studied by TGA. In Figure 5-4, it can be seen clearly that pristine and composite UiO-66 MOFs are more stable than pristine and composite HKUST-1 MOFs. The degradation starts with the removal of H_2O at around 100-120 °C and the major weight loss occurs between 300 and 350 °C for C and C1, which is due to the structural decomposition of organic linkers. However, in case of C1 the thermal stability increases to some extent due to a synergetic effect of UiO-66 and a major weight loss occurs at 370 °C (Song, Oh, & Lah, 2013). For Z1, the degradation of the MOF occurs with the removal of H_2O and then with the degradation of the structure, but the stability of Z1 is less than that of Z due to incorporation of less stable HKUST-1 (C) into the composite. It is evident from Figure 5-4 that Z and Z1 are stable up to a temperature of 450 °C while C and C1 are stable up to 325-370 °C. Moreover, the higher residual weight in the composite MOFs is due to the larger amount of two metallic species (Yan et al., 2014).

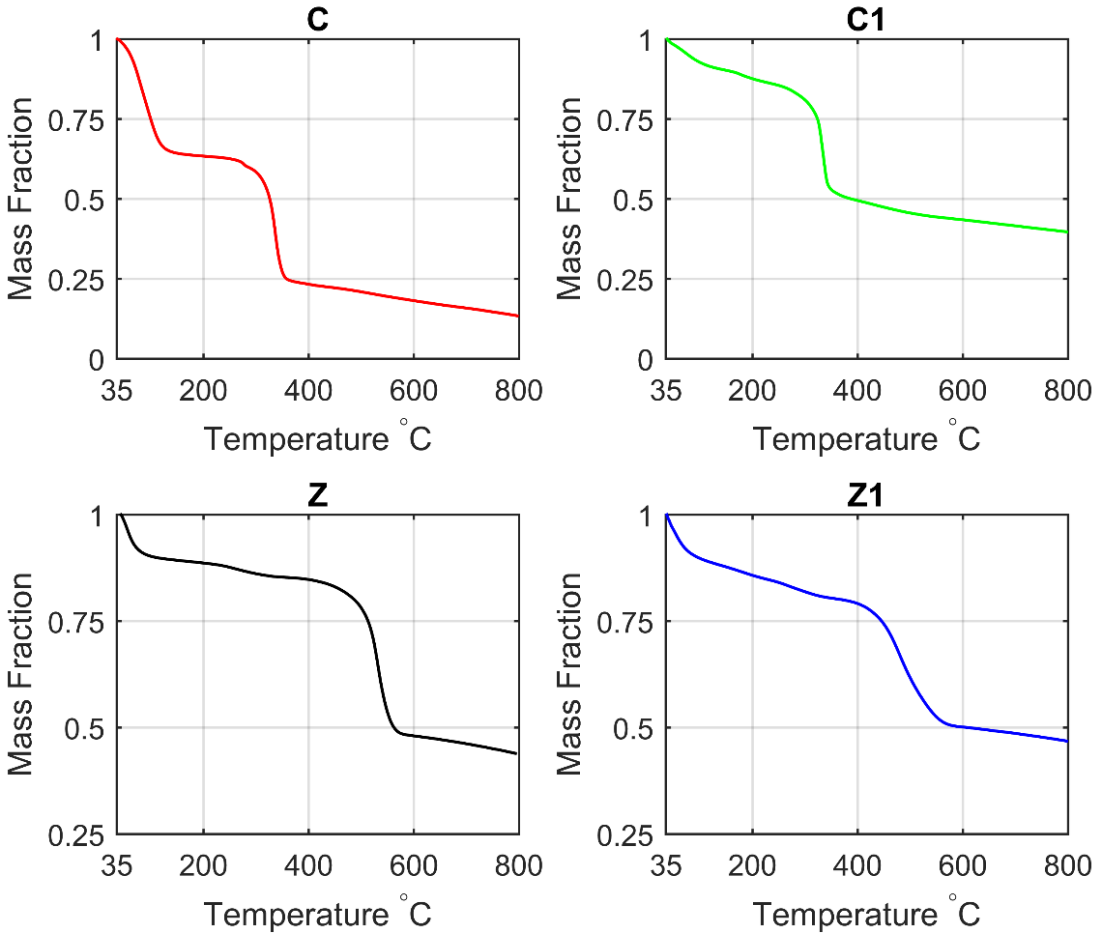

Figure 5-4 TGA analysis of pristine and composite binary MOFs.

Table 5-1 Composition and textural properties of synthesized MOFs and commercial activated carbon.

Sample	Composition	F Surface area (m^2/g)	Total Pore volume (cm^3/g)	Average pore diameter (nm)
C	HKUST-1	1726	0.78	1.8
C1	HKUST-1 with 5% UiO-66	719	0.33	4.6
Z	UiO-66	1125	0.56	1.7
Z1	UiO-66 with 5% HKUST-1	625	0.33	2.3
AC	AC (98%)	2010	1.85	2.1

The pore size and surface area are important properties for adsorption applications. The synthesized MOFs exhibited high surface area and large pore volume. Pristine HKSUT-1 (C) and UiO-66 (Z) showed type I isotherm and higher surface area than the composite MOFs (Figure 5-5). The main contribution in such a high surface area is due to microspores which become more prominent by activating with methanol resulting in opening the microspores by removing unreacted BDC/BTC and solvent guest molecules (Abid et al., 2012c). The composite MOFs, C1 and Z1, exhibited type IV isotherm with H4 and H2 hysteresis, respectively, which may be attributed to majority of mesoporous structure. However, the surface area and total pore volume decreased in the bimetallic MOFs, which is similar to the earlier reports (Gotthardt, Schoch, Wolf, Bauer, & Kleist, 2015; Gul-E-Noor et al., 2012). It has been already mentioned that the mixed metal MOFs are accompanied with reduction of surface area and pore volume as in bimetallic HKUST-1/Ru and HKUST-1/Zn (Gotthardt et al., 2015; Gul-E-Noor et al., 2012). Gul-E-Noor et al. [50] reported the BET surface area of bimetallic HKUST-1/Zn-MOF compared to pristine HKUST-1 was reduced by 27%. While it was significantly reduced by 63% in Cu-Ru-BTC MOF. In the present study, bimetallic MOF with addition of 5% UiO-66 resulted in almost 58% decrease in surface area but the pores are enlarged to mesoporous in C1 while 5% addition of UiO-66 in HKUST-1 resulted in 44% decrease in surface area (Z1). However, the reduction of surface area and pore volume didn't disturb adsorptive performance of bimetallic MOF. The average pore diameter was calculated using the BJH method from desorption data and is given in Table 5-1. The pore diameter of bimetallic MOFs increased and micropores are transformed to mesoporous. The hysteresis between adsorption-desorption isotherm of N_2 at higher relative pressures depicts mesoporous nature of the materials (Abid et al., 2012c). The pore volume as a function of pore diameter is shown in Figure 5-6 to determine pore size distribution. The maxima for binary MOFs clearly lie in mesoporous range compared to pristine MOFs (Figure 5-6).

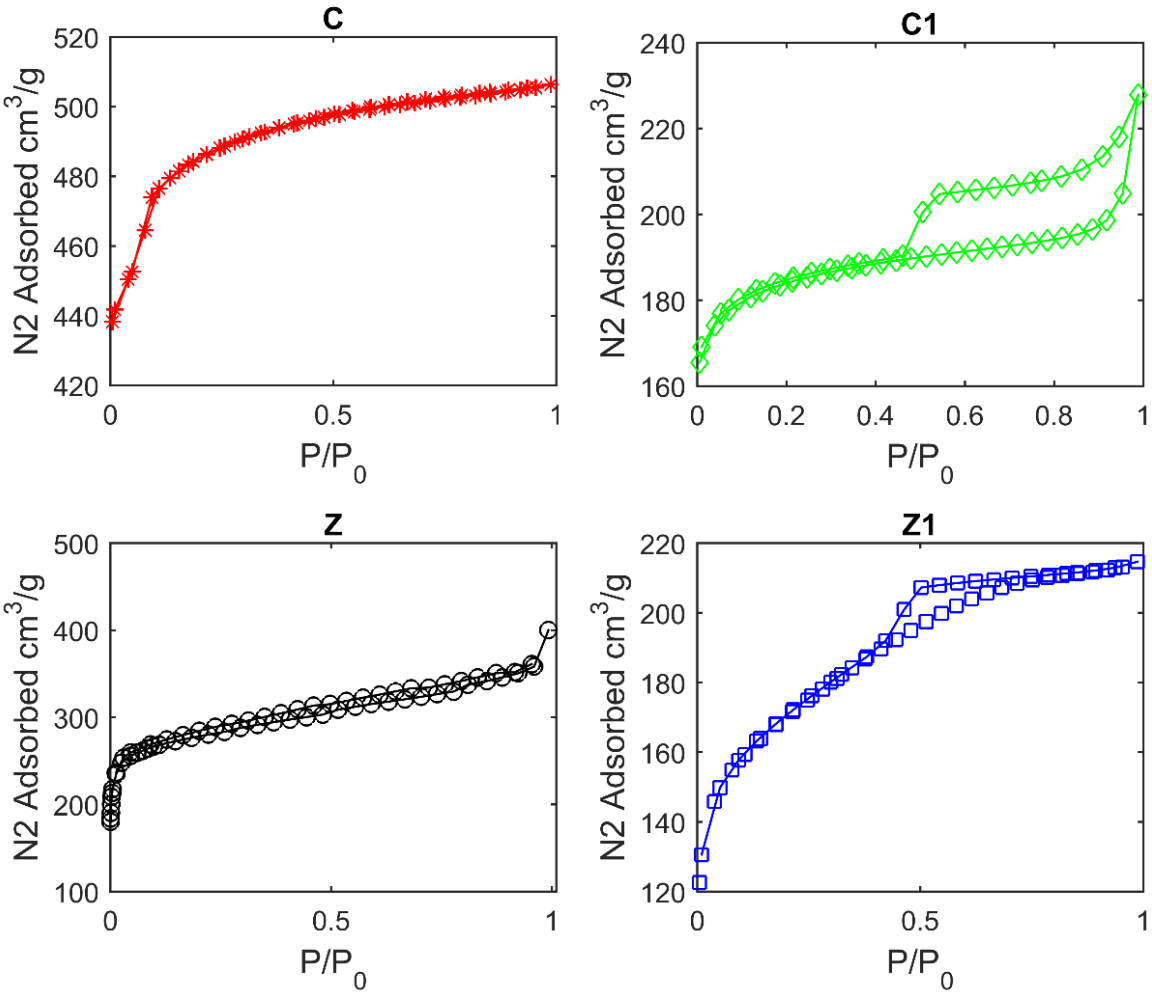

Figure 5-5 Nitrogen Adsorption-Desorption isotherms for BET analysis of pristine and composite binary MOFs.

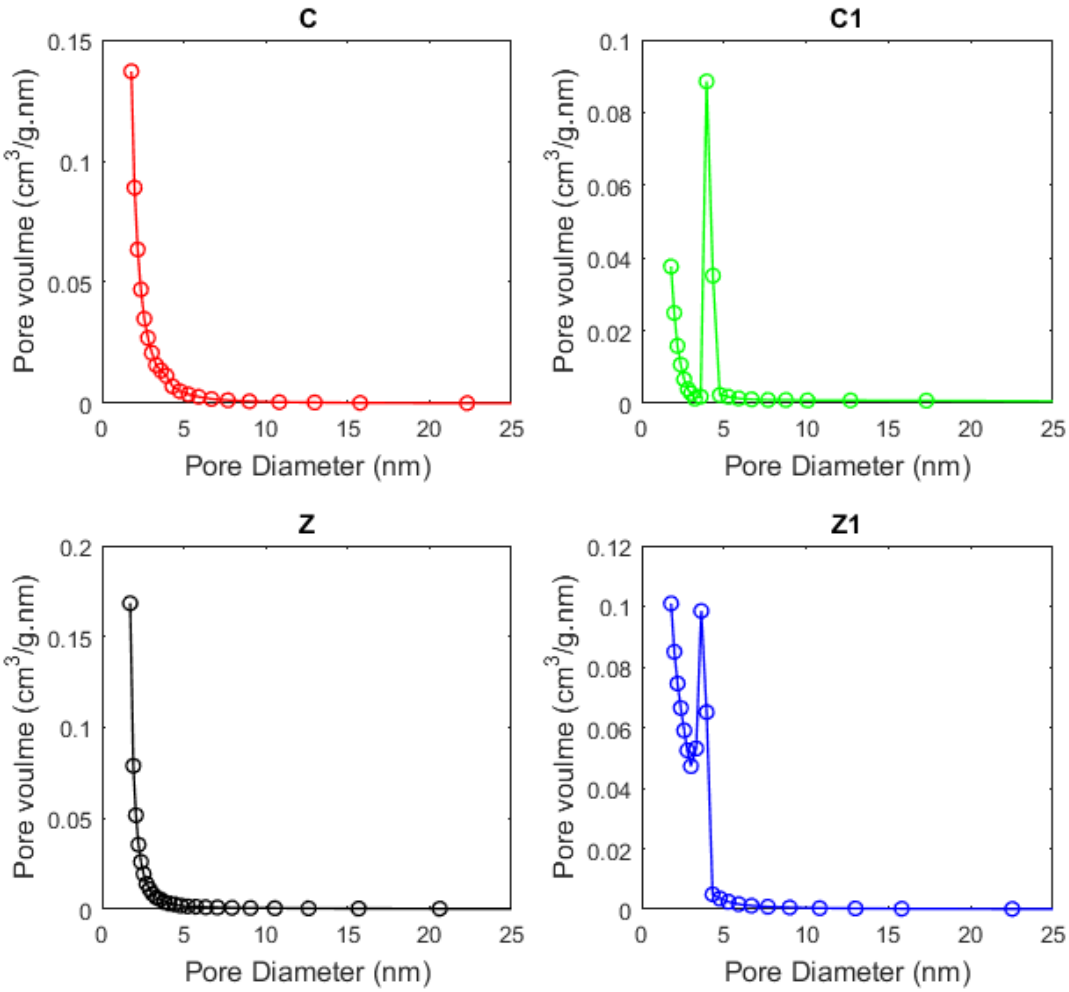

Figure 5-6 Pore size distribution of pristine and composite binary MOFs using BJH method.

5.3.2 pH effect on performance of MOFs

It is very important to study the effect of initial pH as it has a strong effect on adsorption capacity. In this study, the pH range was selected in 3-12 at 25 °C with initial concentration of MB at 5 ppm (Figure 5-7). Generally, the adsorption of MB increases with the pH increase, showing the significance of electrostatic interaction in the adsorptive removal of MB. However, in industrial processes, the pH of wastewater varies widely. For the studied MOFs, significant removal of MB has been observed in all pH values between 3 and 12. The point of zero charge (pH_{PZC})

was determined using the immersion technique (Fiol & Villaescusa, 2008). The pH_{PZC} for C, Z, C1, and Z1 are 4.2±0.2, 5.5±0.2 (Lin et al., 2014; Seo et al., 2015), 5.0±0.2 and 4.0±0.2, respectively (Figure 5-8). The surface of MOFs becomes positively charged below their pH_{PZC}, while negatively charged above pH_{PZC}. The adsorption of MB is less at pH 3 while it starts increasing with higher pH. Since the pH_{PZC} of MOFs is less than 6 so the surface of MOFs becomes negatively charged at pH higher than 6. Moreover, MB is a cationic dye which is adsorbed in higher quantity due to electrostatic interactions. As seen, the maximum adsorption for all MOFs occurs at pH 7-9. The initial pH for all further experiments was selected as 7.5 in this study.

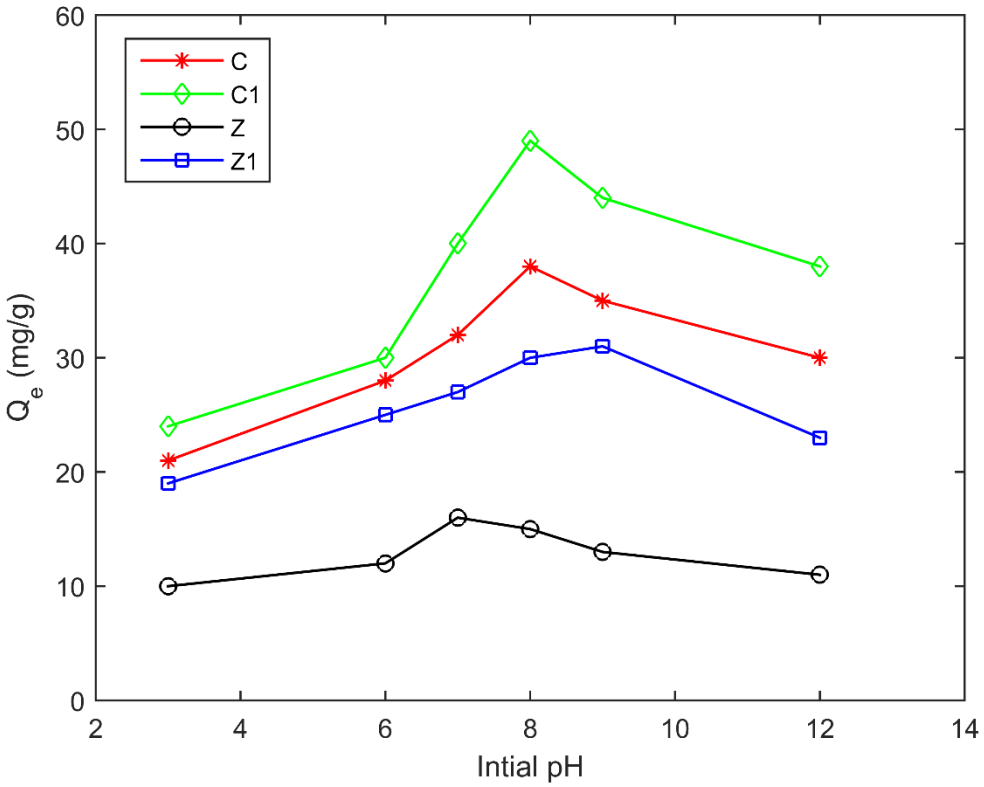

Figure 5-7 Effect of Initial pH on adsorption of MB, C0=5 ppm at 25 °C.

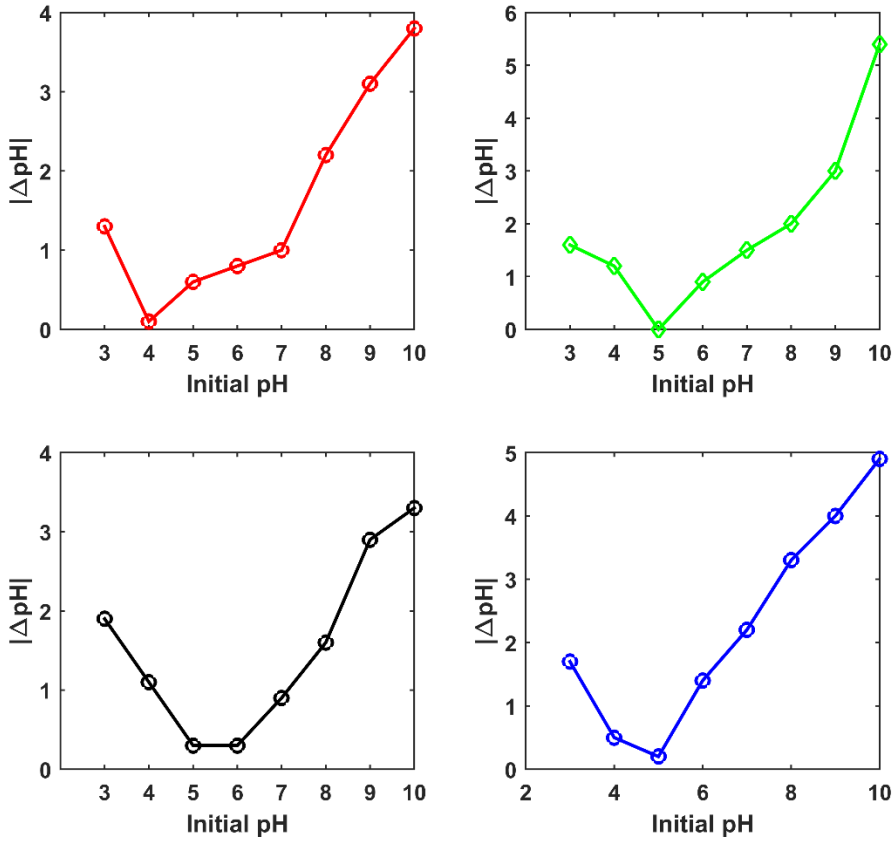

Figure 5-8 Point of zero charge measurement of MOFs using immersion technique.

5.3.3 Kinetics of adsorption process

All the samples were tested for the adsorption kinetics using a fixed amount of adsorbent and adsorbate concentrations for 12 h at 25 °C. The adsorption data were analysed using pseudo first-order and second-order kinetic models (Figure 5-9 and 5-10) (Ho & McKay, 1999a, b).

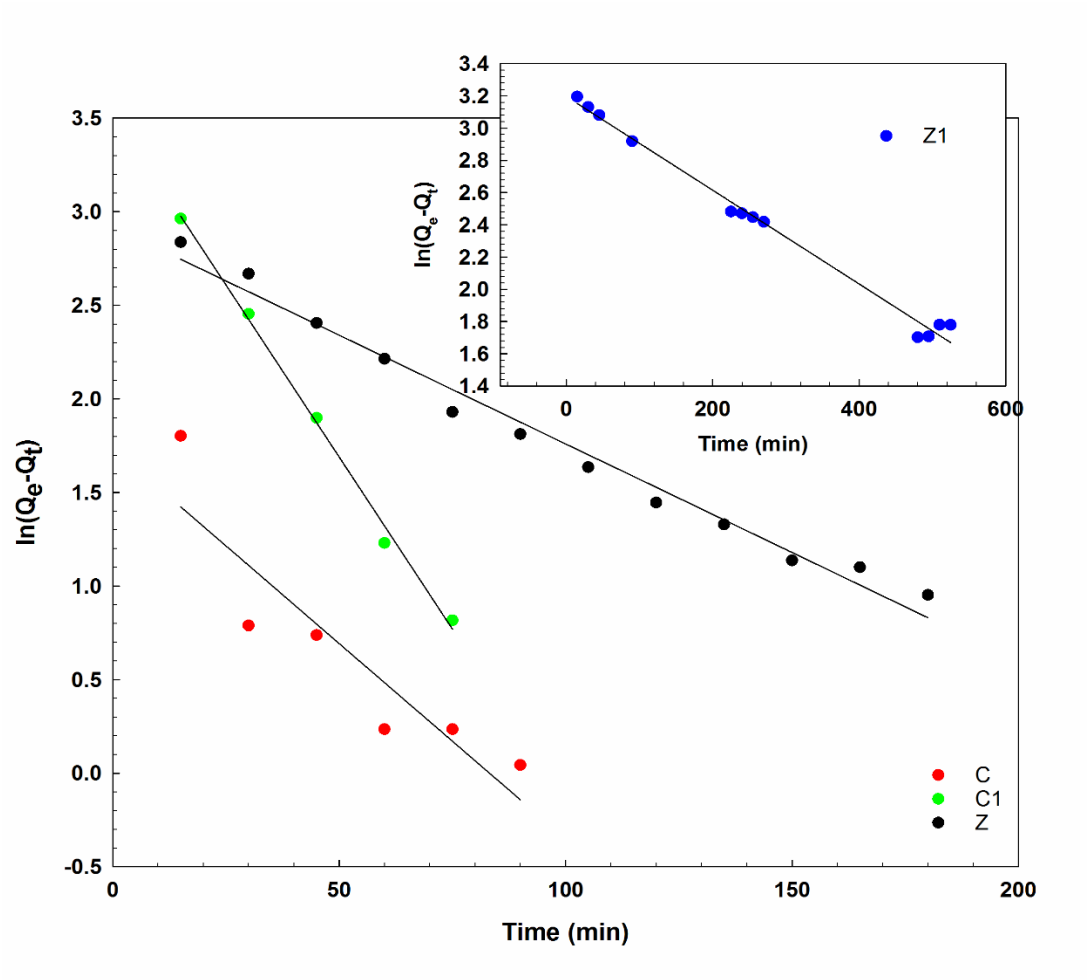

Figure 5-9 Pseudo 1st order fitting of adsorption data on MOFs.

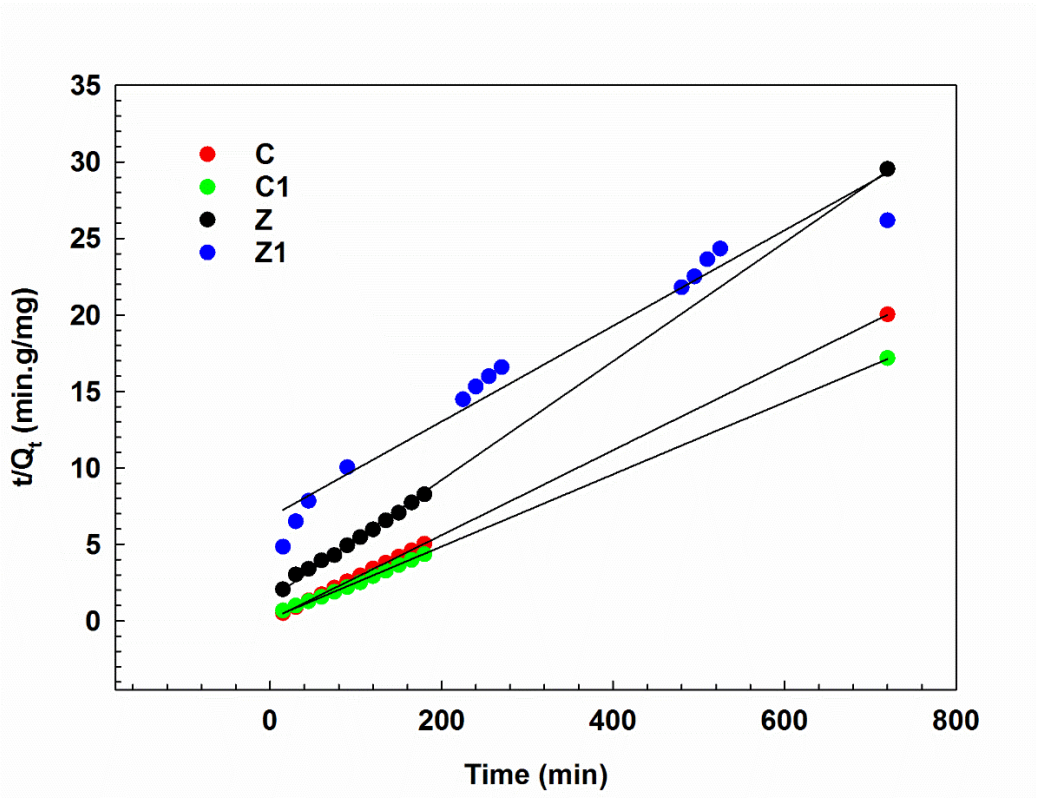

Figure 5-10 Pseudo 2nd order model fitting of adsorption data.

There is not a big difference between experimental and calculated values of Q_e using pseudo 1st order kinetic model and pseudo 2nd order models. The values of R^2 are higher in both cases. The pseudo 1st order and pseudo 2nd order kinetic models can be written as follows.

$$\ln(Q_e - Q_t) = \ln Q_e - k_1 t \qquad (5\text{-}2)$$

$$\frac{t}{Q_t} = \frac{1}{k_2 Q^2{}_e} + \frac{1}{Q_e} t \qquad (5\text{-}3)$$

Where, Q_e is the amount of MB adsorbed at equilibrium (mg/g); Q_t is the amount adsorbed at time t (mg/g); t is the adsorption time in minutes. The calculated values of k_1, k_2, $Q_{e,\exp}$ and $Q_{e,cal}$ are given in Table 5-2. In case of AC, all MB is removed in just first 5 min so it's not shown here.

Table 5-2 Kinetic parameters for MB removal using Co=5 ppm for pristine and composite binary MOFs.

MOFs	Pseudo 1st order kinetics				Pseudo 2nd order kinetics		
	$Q_{e,exp}$ mg/g	k_1 min^{-1}	$Q_{e,cal}$ mg/g	R^2	k_2 g.min/mg	$Q_{e,cal}$ mg/g	R^2
C	35.9	$2.1x10^{-2}$	35.9	0.831	$1.2x10^{-2}$	35.8	1.000
C1	41.9	$3.9x10^{-2}$	41.6	0.994	$3.9x10^{-3}$	41.6	0.999
Z	12.2	$1.1x10^{-2}$	12.2	0.983	$2.0x10^{-3}$	11.6	0.999
Z1	27.5	$2.9x10^{-3}$	24.1	0.990	$1.5x10^{-4}$	20.4	0.961

In general, as the surface of the adsorbent is covered with the adsorbate molecules, the tendency of adsorbate molecules to get into and/or on the surface becomes low due to less number of available sites for the adsorption (Dawood & Sen, 2012). The kinetic behaviours of all the MOFs are given in Figure 5-11. The adsorption is faster on C compared to all other MOFs. The adsorption kinetics of C1 is also faster than Z and Z1 owing to both large pore size and surface area (Haque et al., 2010b). Generally, smaller pore sizes of adsorbents than MB molecules result in slow diffusion of MB molecules into the pores. However, the pore size of all studied MOFs is larger than the size of MB molecules facilitating higher adsorption of MB on C due to its larger pore compared to C1, Z and Z1. Most of the adsorption is achieved in 150 min. However, most of the adsorption is achieved on C in the first 90 min. It can also be noted that the adsorption on Z1 is a gradual process and adsorption quantity gradually increases during all 12 h of operation. In case of Z1, the data was obtained in regular intervals for all the 12 h and it was fitted more accurately with pseudo 1st order kinetic model.

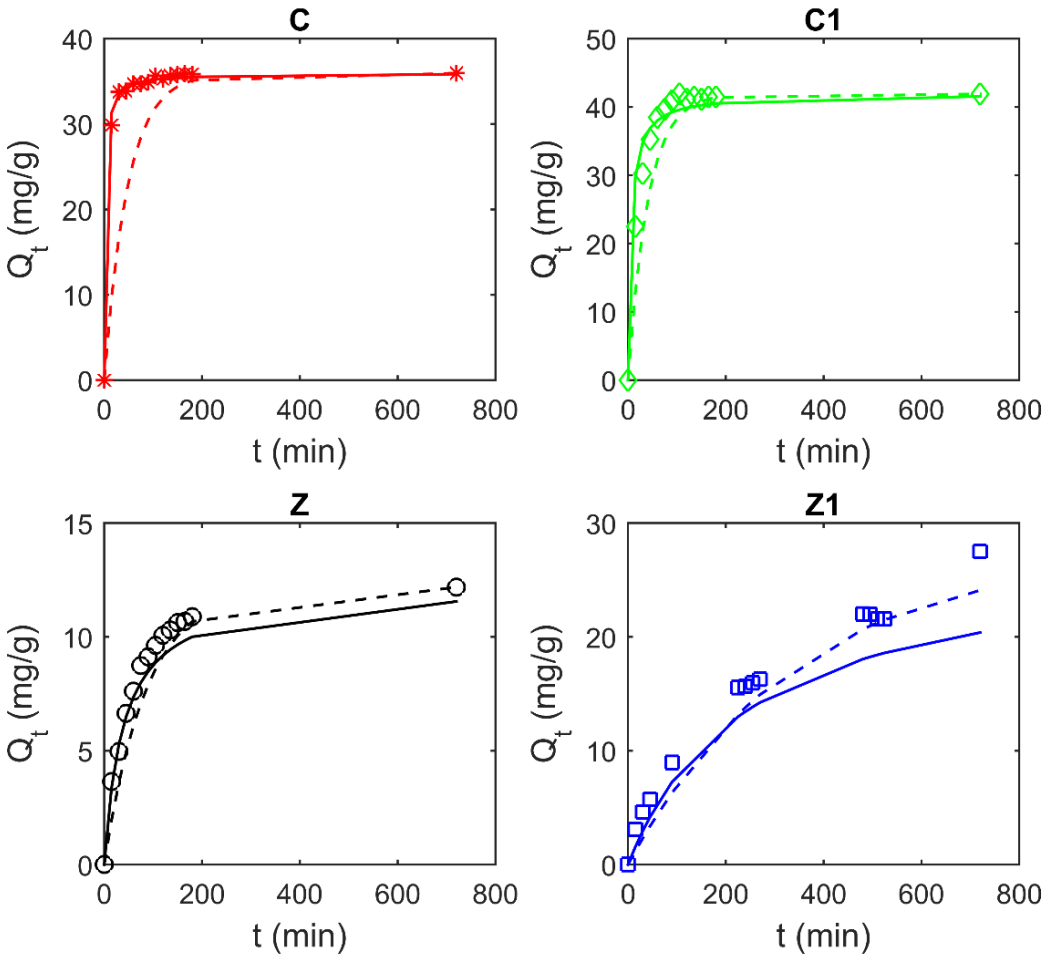

Figure 5-11 Kinetics of MB adsorption on pristine and composite binary MOFs, C0=5 ppm at 25 °C, dashed lines: pseudo 1st order model, sloid line pseudo 2nd order model.

5.3.4 Adsorption and adsorption mechanism

The adsorption isotherms of MB are shown in Figure 5-9. The adsorption data was fitted with two well-known models, i.e. Langmuir and Freundlich isotherms (Figure 5-12 and 5-13) (Hameed, 2009; Langmuir, 1918).

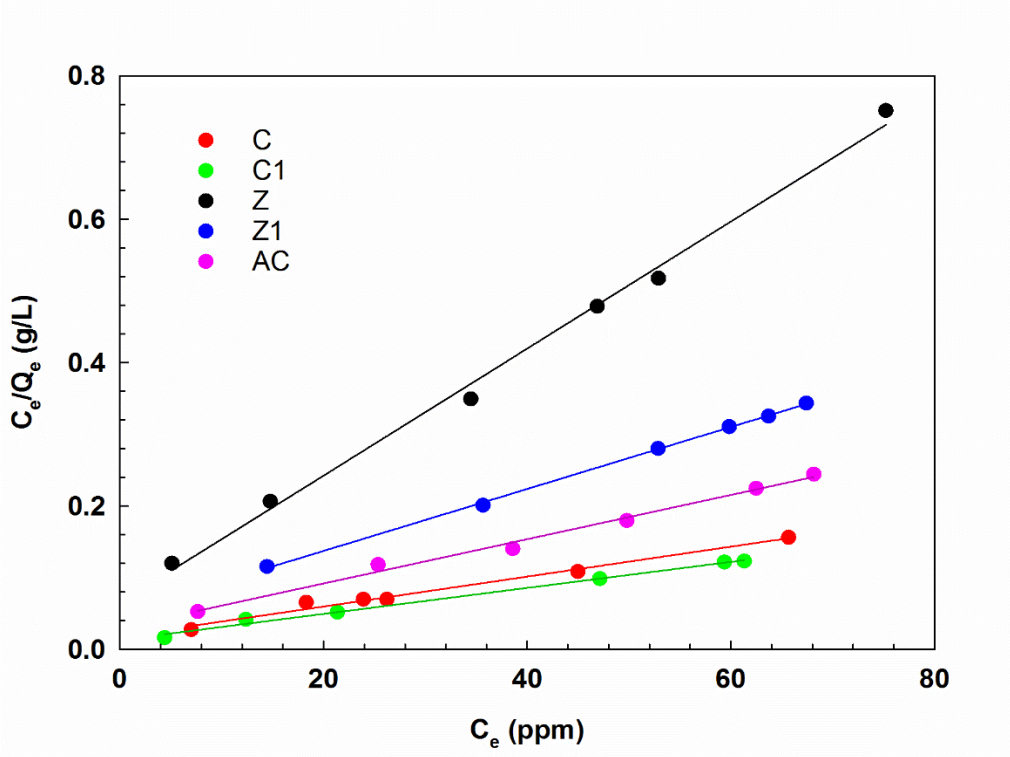

Figure 5-12 Fitting of adsorption data with Langmuir isotherm.

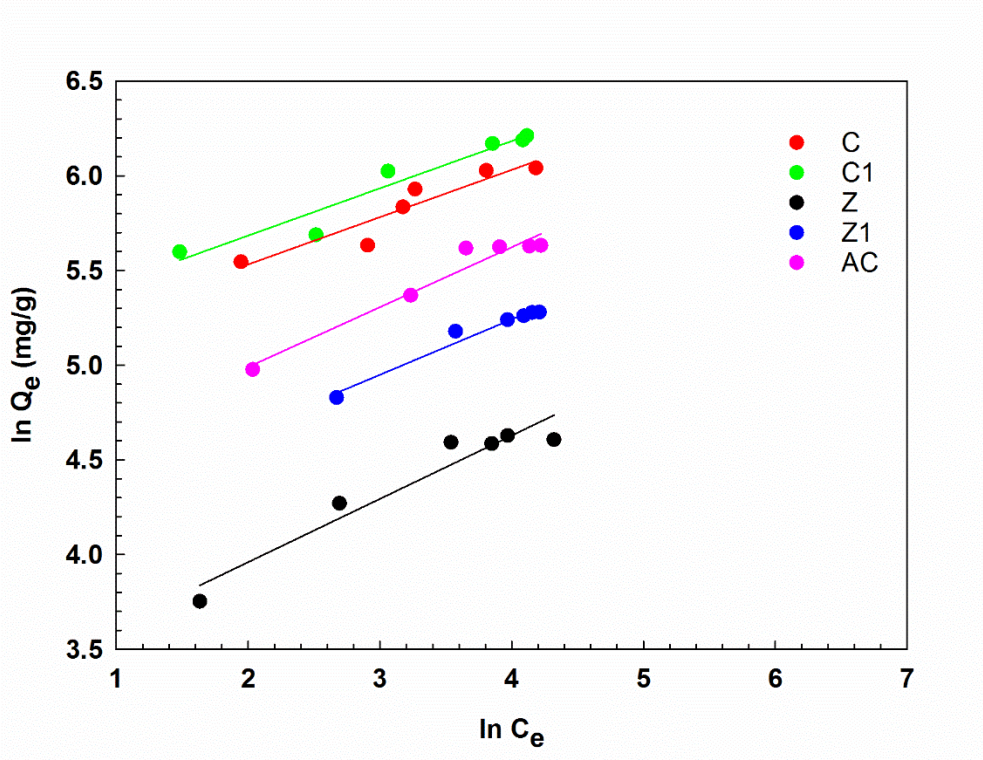

Figure 5-13 Freundlich adsorption isotherm fitting of adsorption data on MOFs.

The mathematical forms of both the models are given below.

Langmuir model: $$\frac{C_e}{Q_e} = \frac{1}{K_L Q_m} + \frac{C_e}{Q_e} \quad (5\text{-}4)$$

where Q_e represents equilibrium dye concentration on an adsorbent (mg/g), C_e represents dye concentration in solution (mg/L) at equilibrium, Q_m is the monolayer capacity of dye adsorption (mg/g), K_L represents the Langmuir adsorption constant (L/mg). The favourability of an adsorption system can also be expressed in terms of a dimensionless separation factor (R_L) defined as follows.

$$R_L = \frac{1}{1 + C_m K_L} \quad (5\text{-}5)$$

Where, C_m is the maximum initial concentration of adsorbate. The adsorption process is favourable in the $0 < R_L < 1$.

Freundlich model: $$\ln Q_e = \ln K_F + \frac{1}{n} \ln C_e \quad (5\text{-}6)$$

where Q_e represents equilibrium dye concentration on an adsorbent (mg/g), C_e represents dye concentration in solution (mg/L) at equilibrium, K_F and n are the Freundlich constants, characteristics of the system.

The adsorption data was fitted more accurately with the Langmuir model compared to the Freundlich model based on high R^2 values and the difference between the experimental and calculated values of maximum adsorption capacity. The values of Langmuir and Freundlich parameters are given in Table 5-3. The adsorption capacities of composite MOFs were higher than pristine HKUST-1 and UiO-66. The adsorption capacity is the highest on C1 compared to all other MOFs. The adsorption capacity is increased due to the synergic effects of UiO-66 and larger pore size of C1. The pristine UiO-66 i.e., Z, presents the adsorption of MB less than all other MOFs and AC with a capacity of 107 mg/g. For the composite UiO-66 (Z1), the adsorption capacity is increased to 208 mg/g, almost double of adsorption capacity of Z. The increased adsorption capacity may result from the synergic effects of

HKUST-1, which has a higher adsorption capacity in both pristine and composite forms. It is clear that the textural properties don't have a large effect on adsorption for the studied MOFs. Previously, an effect of metal ions on the adsorption of MB, MO and MB/MO mixture has been reported elsewhere [32] on two identical surface area MOFs, MIL-100-Fe and MIL-101-Cr. MIL-100-Fe was more efficient for dye adsorption compared to MIL-100-Cr.

Table 5-3 Adsorption isotherms for the MOFs and AC.

		Langmuir model				Freundlich model		
MOFs/AC	$Q_{m,exp}$ (mg/g)	$Q_{m,c}$ (mg/g)	K_L (L/mg)	R_L	R^2	K_F (mg/g)	n	R^2
C	420	454	0.195	0.045	0.978	153.	4.01	0.876
C1	498	526	0.221	0.039	0.988	170.	4.01	0.935
Z	100	107	0.229	0.049	0.990	26.9	2.99	0.927
Z1	196	208	0.219	0.049	0.988	58.7	3.42	0.967
AC	279	303	0.200	0.049	0.985	78.1	3.16	0.949

The adsorption capacity of different adsorbents is presented in Table 5-4 for a comparison with the MOFs and AC studied in this study. The adsorption capacities of the HKUST-1 and its composite MOFs are higher than MWCNTs, MIL-100-Cr, HKUST-1, HKUST/GO and Fe_2O_3/carbon. However, adsorption capacities of MIL-101-Al and ZJU-24 are higher than both copper and zirconium MOFs presented in this study.

The adsorption of dyes is usually dependent on the electrostatic interactions, π-π interactions, hydrogen bonding and hydrophobic interactions among adsorbents and the dyes. In a typical adsorption process, one or combination of all these mechanisms can occur (Lin et al., 2014; Park et al., 2013; Qin et al., 2014; Wang et al., 2012; Zhang et al., 2014d). In the present study, the adsorption of MB at pH range 3-12 is significantly high, which shows that some other factors play important roles in the MB removal from water, for example, π-π interaction. The pH_{PZC}s for all the MOFs are less than pH 6 (Figure 5-8), which shows that the surface of the MOFs may be positively charged at pH less than 6 and negatively charged at pH higher than 6. MB

is a cationic dye, so there should be minimum adsorption in pH range 3-6 due to electrostatic repulsion and maximum at pH of 10.

The adsorption on C is slightly decreased with increasing pH values greater than 8, which might result in the formation of NaCl from Na^+ ions (NaOH used for pH adjustment) and Cl^- ions from MB [7]. Furthermore, a marginal increase in the adsorption on Z with increasing pH higher than 8 is observed. However, it is not possible to conclude that electrostatic interaction is the only mechanism for MB removal from pH study. The significance of other factors such as π-π interactions can be revealed by FTIR (Figure 5-1). The bands at ≈1370 cm^{-1} and ≈1580 cm^{-1} belong to $(C=C)_v$ of benzene ring (Zhang et al., 2014d). The FTIR bands are drifted after the adsorption of MB on MOFs, signifying the π-π interactions of the benzene rings of MOFs and MB. In case of C, the bands from 1377 cm^{-1} is shifted to 1365 cm^{-1} and the one at 1548 cm^{-1} is shifted to 1580 cm^{-1}. Similarly, in case of C1, the bands at 1558 cm^{-1} shifted to 1582 cm^{-1} and band at 1368 cm^{-1} shifted to 1395 cm^{-1}. However, in case of Z a small drift from 1388 cm^{-1} to 1391 and 1561 cm^{-1} to 1563 cm^{-1} shows a minor effect of π-π interactions. The bands at 1391 cm^{-1} and 1574 cm^{-1} shifted to 1384 cm^{-1} and 1554 cm^{-1}, respectively on Z1. The presence of BTC and BDC into framework provides extra benzene rings which help in forming stronger π-π interactions. Moreover, the availability of high electron density owing to the COO- group provides active sites to cationic MB molecules, resulting in a higher adsorption capacity (Zhang et al., 2014d). These observations attest to the complex adsorption mechanism of MB on the MOFs.

Table 5-4 Comparisons of adsorption capacities of MB removal on different materials.

Material	Maximum adsorption capacity, Q_m (mg/g)	Reference
MIL-100-Cr	211	(Tong et al., 2013)
MOF-235	187	(Haque et al., 2011)
MIL-101-Cr	10	(Shen et al., 2015)
HKUT-1/GO	183	(Li et al., 2013a)
HKUST-1	5	(Lin et al., 2014)
HKUST-1	454	This study

UiO-66	107	This study
HKUST-1@5% UiO-66	526	This study
UiO-66@5% HKUST-1	208	This study
AC	303	This study
MIL-101-Al	762	(Haque et al., 2014b)
MWCNT	59	(Wang et al., 2012)
ZJU-24	962	(Zhang et al., 2014d)
UiO-66	143	(Chen et al., 2015b)
Fe_2O_3/carbon	303	(Xiao et al., 2013a)
ZnS/AC	244	(Asfaram et al., 2016a)

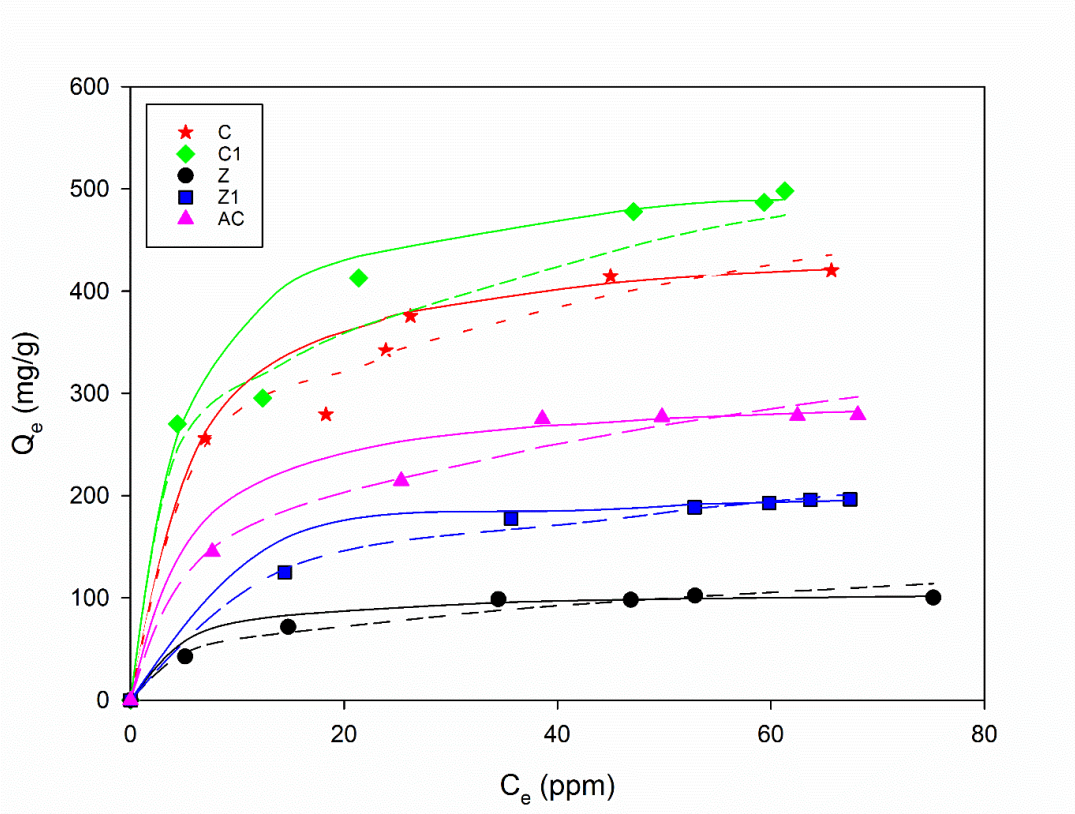

Figure 5-14 Data fitting with Langmuir and Freundlich adsorption isotherms of MB on pristine and composite binary MOFs and AC; solid lines: Langmuir model, dashed lines: Freundlich model.

5.4 Conclusions

In this study, pristine and composites of HKUST-1 and UiO-66 MOFs have been synthesized and tested for the adsorption of MB from wastewater. The binary MOFs have reduced surface area, larger pore size and high thermal stability compared to pristine MOFs verified by various characterization techniques. Generally, all the MOFs showed high adsorption capacity and in some cases higher than the commercial activated carbons. However, binary MOFs in particular, showed high adsorption capacity of MB despite of reduced surface area compared to pristine MOFs. The kinetic study showed that fast kinetics was observed on MOFs and can be fitted with pseudo 1^{st} and pseudo 2^{nd} order models. The enhanced adsorption capacity of composite MOFs, highlights the synergetic effects of multi-MOF systems. The maximum adsorption capacities of composite MOFs, C1 and Z1, are 526 and 208 mg/g, respectively. The effect of pH showed that electrostatic interactions play a key role in the adsorption process. However, other controlling factors are π-π interactions. The robustness of synthesized MOFs over a wide range of pH makes them suitable for the adsorptive removal of MB and other contaminants.

Chapter 6 Facile synthesis of submicron sized Bio-MOFs for catalytic degradation of antibiotics and personal care products *

* Adopted with permission from (M.R, Azhar, V. Periasamy, M.O., Tade, H. Sun, S. Wang, "Submicron sized highly water-stable metal organic framework (bio-MOF-11) for catalytic degradation of pharmaceuticals and personal care products", *Chemosphere*, pp. 105-114, 2018). Copyright Elsevier.

6.1 Introduction

Parabens are the esters of para-hydroxybenzoic acid (p-HBA), which are widely used in food preservation, cosmetics, pharmaceuticals and personal care products (PPCPs). Also, on an industrial level, they are used in cigarettes, varnishes, glues and animal feeds (Dodge et al., 2015; Soni, Carabin, & Burdock, 2005). However, parabens are biodegradable into their derivatives mainly p-HBA, which is more persistent to further biodegradation than parabens and can be often found in wastewater treatment plants (Evans, Davies, & McRae, 2016; Wang & Kannan, 2016). Various studies on parabens and p-HBA have shown that their estrogenic nature produces various adverse effects on living organisms including impotency in male and breast cancer in females (Pugazhendhi, Pope, & Darbre, 2005; Tavares, Martins, Oliveira, Ramalho-Santos, & Peixoto, 2009).

Moreover, the rapid growth in population increases a widespread use of antibiotics. The persistent nature of antibiotics, particularly sulfoneamide antibiotics, is a major concern due to their strong toxic effects on aquatic life (Brain et al., 2008; Bu et al., 2013; Cruz et al., 2014). One of the sulfomeamide antibiotics is sulfachloropyradazine (SCP), which is widely used in animal husbandry. The detection of PCCPs in sewage wastewater is alarming and has attracted researchers to develop the processes for efficient elimination of the hazardous chemicals from wastewater including p-HBA and SCP (Kang et al., 2016; Wang & Kannan, 2016; Wu & Fang, 2003).

In recent years, various materials have been used in removal of parabens, their derivatives and SCP, e.g. activated carbons, carbon nanotubes, heteroatom doped carbons, zeolites, and metal oxides. The usual methods for such toxic chemical removals include adsorption, catalytic and photocatalytic degradation (Arshadi, Mousavinia, Amiri, & Faraji, 2016; Bai, Yang, & Wang, 2015; Duan et al., 2015b; Huang et al., 2015; Kebir, Boudjemaa, & Bachari, 2015; Nichela et al., 2015; Pouya et al., 2015). Adsorption performs well in phase separation without completely destroying the contaminants. However, low adsorption capacities, difficulty in recycle and reuse of adsorbents are the drawbacks (Ahmed et al., 2015a). On the other hand, advanced oxidation processes (AOPs) can transform the contaminants

into small non-toxic fragments and subsequently to CO_2 and H_2O. However, selection of a suitable material to activate available oxidants is one of main challenges in AOPs (Chen et al., 2016a; Wang et al., 2015g).

In the past decade, a lot of research has been conducted in synthesizing hybrid organic-inorganic materials namely, metal organic frameworks (MOFs). High surface area, tuneable porosity, and availability of various functional groups make these materials highly interested (Liu, Li, Oh, Fang, & Xi, 2016; Marques et al., 2015; Marshall et al., 2016; Martin & Haranczyk, 2013). However, most of the MOFs have been used in gas-phase processes, e.g. CO_2 and H_2 adsorption and storage (Almáši, Zeleňák, Kuchár, Bourrelly, & Llewellyn, 2016; Chen et al., 2015a; Li et al., 2013b). Although, other uses in catalysis, drug delivery, lithium ion batteries, and cooling are increasing, still few attempts have been made in catalytic degradation of water contaminants using MOFs (Erucar & Keskin, 2016; Jonckheere et al., 2016; Kim, Kim, Kim, Cho, & Ahn, 2013; Kozlova et al., 2016; Li et al., 2014; Ning et al., 2016). A major problem associated with the use of MOFs in water treatment is their instability to sustain in aqueous media (Qadir, Said, & Bahaidarah, 2015).

Some water-stable MOFs have been studied in adsorptive removal of toxic organic wastes in the last few years. However, the investigations are limited to Al, Cr and Zr based MOFs with carboxylic acid linkers (Haque et al., 2014b; Kim et al., 2013; Wang et al., 2015a). Similar to adsorption studies on MOFs in wastewater treatment processes (WWTPs), only limited MOFs have been investigated in catalytic degradation to date and most of such studies focus on degradation of dyes. In some cases, H_2O_2 has been used for degradation by generating $^{\bullet}OH$ (Du et al., 2011; Sun et al., 2013; Zhu et al., 2014). However, activation of other oxidizing agents in AOPs such as peroxydisulfate (PDS) and peroxymonosulfate (PMS) is a more interest to effectively use MOFs in AOPs. PMS is a promising oxidizing agent, proved to be effective in various catalytic degradation processes (Ghanbari & Moradi, 2017). Although various studies are available to activate PMS using metal based or metal free catalysts (Duan et al., 2016; Lin & Chang, 2015a; Saputra et al., 2013b, c; Shukla, Wang, Sun, Ang, & Tadé, 2010), MOFs offer simultaneous availability of organic-inorganic moieties for diverse applications.

Recently, adenine based MOFs, typically known as bio-MOFs, have been studied in drug delivery and CO_2 adsorption. However, the synthesis of bio-MOFs is complicated and requires cryogenic steps along with solvent exchange activation by chloroform or methanol (An et al., 2012; Li et al., 2013b). In the present study, a facile method for the preparation of bio-MOFs has been proposed. Moreover, a cobalt based bio-MOF, namely bio-MOF-11-Co, possesses a high water stability and was used in catalytic degradation of p-HBA and SCP via effective activation of PMS.

6.2 Materials and methods

6.2.1 Synthesis procedure

$Co(CH_3COO)_2$, adenine, N,N-dimethylformamide (DMF), and $Cu(CH_3COO)_2$, H_2O_2, PDS and PMS (Oxone®) were purchased from Sigma-Aldrich, Australia and used without further purification. Ultrapure water (15 Ω) was produced by an Agilent water purification system in our laboratory.

The bio-MOFs were synthesized by a facile method without any cryogenic step (An, Geib, & Rosi, 2010). Specifically, 0.90 mmol cobalt acetate was dissolved in 18 mL DMF. Meanwhile, 2.70 mmol adenine was added to 54 mL DMF and stirred vigorously for 1 h to achieve complete dissolution. Subsequently, the two solutions were added to a 120 mL autoclave and 0.25 mL of ultrapure water was also added in. The autoclave was heated in a programmable oven at a heating rate of 1 °C/min to 120 °C and maintained at 120 °C for 24 h. A purple crystal product was filtered, washed three times with 54 ml DMF in each washing cycle and dried at 130 °C overnight to obtain bio-MOF-11-Co.

Similarly, bio-MOF-11-Cu was synthesized as stated above using copper acetate instead of cobalt acetate. Moreover, another MOF, copper benzene tricarboxylate (CuBTC), was prepared using previously reported method and details of the synthesis and characterization are given in previous studies (Azhar et al., 2016; Chui et al., 1999b).

6.2.2 Characterization

The synthesized bio-MOFs were characterized using Fourier transform infrared spectroscopy (Perkin Elmer's Spectrum 100-FT-IR), X-ray diffraction (Bruker D8, Co Kα irradiation), scanning electron microscopy (Neon Zeiss), thermal gravimetric-differential scanning calorimetry (TG-DSC, TGA/DSC1 STAR^e system from Mettler-Toledo), N_2 adsorption-desorption isotherms (Micromeritics Tristar 3000II) and elemental analysis (2400 Series II CHNS/O analyser by Perkin-Elmer for carbon, nitrogen and hydrogen). Particle size distribution was carried out on a Malvern Zetasizer nano ZS instrument by dispersing small amount of MOF (25 mg/L) particles in ultrapure water. Electron paramagnetic resonance (EPR) spectra were obtained on a Bruker EMS-plus to detect free radicals generated during activation of PMS. Total organic carbon was measured on a Shimadzu TOC-vcph analyzer.

6.2.3 Catalytic degradation of p-HBA and SCP

All the degradation experiments were conducted using a batch reactor. In each experiment, 100 mL of p-HBA (pKa, 4.5) or SCP (pKa 5.5) solution at a concentration range of 15-45 mg/L was prepared from their stock solution at 1000 mg/L (Ishihama, Nakamura, Miwa, Kajima, & Asakawa, 2002b; Schroder, Budesinsky, & Roithova, 2012). The amounts of catalyst and oxidant were fixed at 0.05 g/L and PMS at 0.5 g/L, respectively, unless specified elsewhere. The temperature of the reactor was controlled at 25 °C using a water bath and stirring of the solutions was induced using mechanical stirrers at 300 rpm. The initial pH of p-HBA solutions was at 4.2 while it was at 5.5 for SCP.

In all experiments, a catalyst was added in p-HBA or SCP solutions and stirred for 30 min to establish adsorption-desorption equilibrium prior to introducing PMS. At certain time intervals (5-120 min), water samples were withdrawn and filtered with 45 µm PTFE syringe filters, and subsequently 0.5 mL methanol was added as a quenching agent to stop further reaction. The concentrations of p-HBA samples were analyzed by a high-pressure liquid chromatography (HPLC, Thermo-Fisher Scientific Ultimate 3000) with an OA column (150 × 4 mm, 5 µm) and a UV detector was set at 270 nm. The mobile phase was made of 60% acetic acid solution (0.3 mM pH 4.2) and 40% absolute methanol with 1.0 mL/min flow rate. A different

column (Acclaim RSLC C-18 column) was used to analyze the concentration of SCP using a different ratio of acetic acid to methanol, i.e. 70% and 30%, respectively, with a flow rate of 0.3 mL/min. After each run, the catalyst was vacuum filtered, washed with de-ionized water and dried at 130 °C overnight for reuse tests. All the experiments were conducted at least twice to check the reproducibility of the results.

6.3 Results and Discussion

6.3.1 Characterization of bio-MOF-11

FTIR spectra was collected using powder samples from 650 – 4000 cm^{-1} to confirm linkage of Co and adenine and the presence of functional groups in the MOFs. The linkage of metal nodes and adenine linkers are clearly observed from Figure 6-1a. The low intensity peaks in the range of 600-700 cm^{-1} are the fingerprint profiles representing Co-O stretching vibrations (Jonckheere et al., 2016; Li, Sullivan, & Rosi, 2013c; Li et al., 2016b; Lin & Chen, 2016). The characteristic peaks at 3334 and 3189 cm^{-1} represent N-H stretching of amine in adenine. The bands in 1500-1600 cm^{-1} show stretching and bending modes of imidazole ring of adenine, particularly, the strong peak at 1595 cm^{-1} shows the presence of C-N bending. The bands at 1300-1450 cm^{-1} indicates C-H stretching in the adenine structure.

The crystallinity of bio-MOF-11-Co was studied by XRD at 2θ from 5-30°. The XRD patterns (Figure 6-1b) are identical to earlier reported studies showing successful synthesis of bio-MOF-11-Co (An et al., 2010; Li et al., 2013b). Bio-MOF-11-Co was also studied by TG-DSC at 35-800 °C in air environment at a flow rate of 70 mL/min to figure out the thermal stability of MOF structure with temperature. It can be seen from Figure 6-1c that loosely attached surface solvent/moisture removal took place up to 100 °C and then removal of bonded solvent molecules of DMF in the structure proceeded till 270 °C. After that, progressive degradation of the organic linkers started, and complete collapse of structure occurred from 300-400 °C. Meanwhile, a broad DSC peak can be seen in Figure 6-1c, indicating the oxidation of adenine at 350 °C (Duan, Sun, Tade, & Wang, 2017a). After 550 °C, cobalt oxides subsequently started converting from CoO to Co_3O_4 and Co_2O_3 in air (Azhar et al., 2017b; Saputra et al., 2013a). Moreover, SEM shows nanosized crystals of bio-MOF-11-Co (Figure 6-1d). In the

previous studies, the size of crystals was reported in few microns (2-10 µm) (Li et al., 2013c), however, in the present study, the nanosized crystals are obtained, probably due to autoclaving and progressive heating and cooling. Crystals can be seen as small discs which grew in a cauliflower pattern in few hundred nanometer sizes. Dynamic light scattering technique was used to obtain a particle size distribution, which show the particle sizes from 200 to 600 nm (inset of Figure 6-1d). Different synthesis conditions can result in varying morphologies and particle sizes, which have been reported previously for other MOFs such as HKSUT-1, ZIF-67 and MIL-96 (Guo et al., 2016; Sindoro, Jee, & Granick, 2013; Wang, Guo, Chai, Li, & Liu, 2013a).

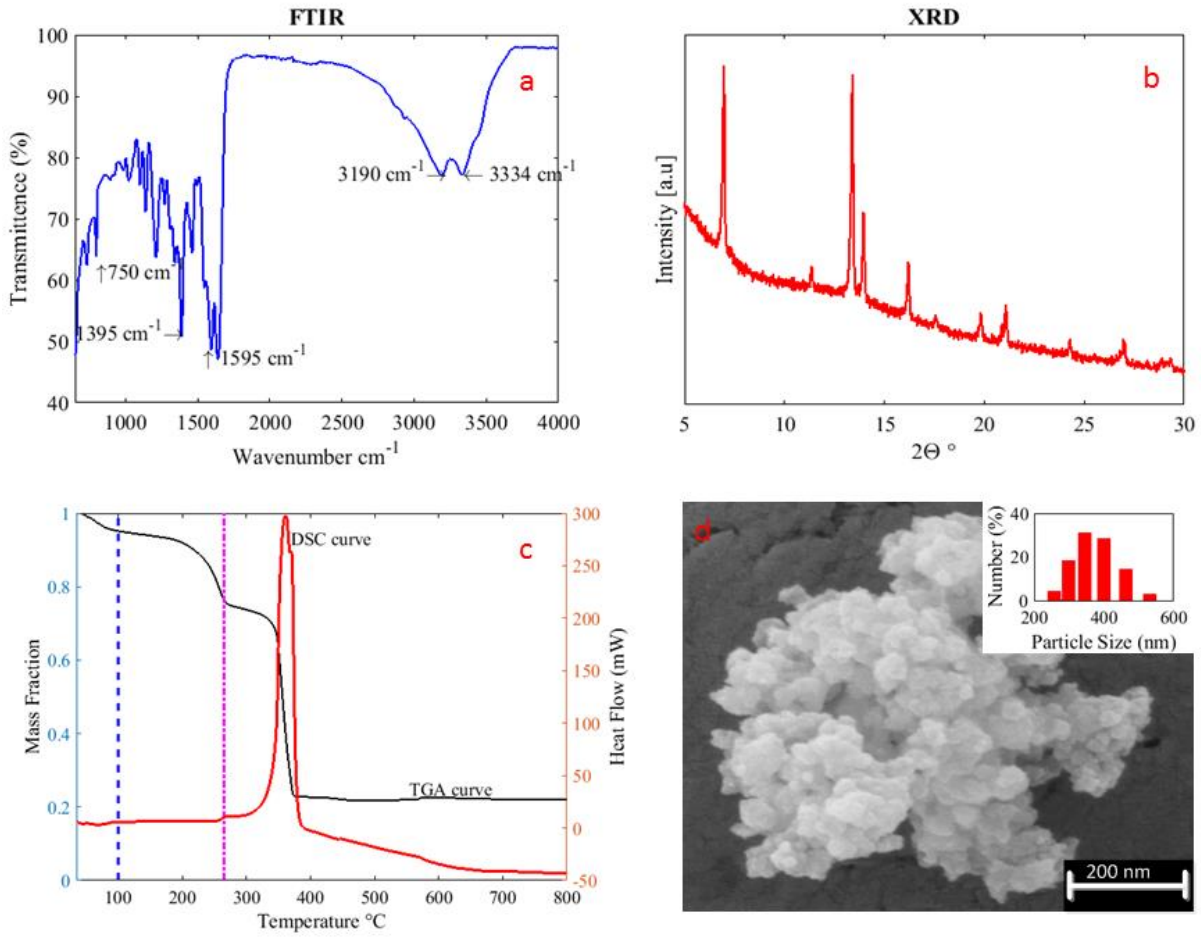

Figure 6-1 Characterizations of bio-MOF-11-Co; a) FTIR pattern, b) XRD, c) TGA/DSC and d) SEM (inset particle size distribution).

In order to check the textural properties of the synthesized materials, nitrogen adsorption-desorption measurements were studied at -196 °C (Figure 6-2). The surface area was calculated using the multi-point BET method at P/P_0 = 0.005-0.24. The surface area of bio-MOF-11-Co is 370 m^2/g. The adsorption-desorption isotherm is of type IV with a hysteresis loop in desorption of P/P_0= 0.45-0.95, which indicates mesoporosity of the synthesized bio-MOF-11-Co. Total pore volume was calculated at P/P_0=0.99 and found to be 0.61 cm^3/g. The surface area of bio-MOF-11-Co is less than the value reported previously. Various factors control the surface area and pore size in MOFs. Previously, a wide range of area was reported for ZIF-67 and HKUST-1 ranging from 700-1400 m^2/g by changing the solvent and/or other synthesis parameters (Guo et al., 2016; Lin et al., 2014).

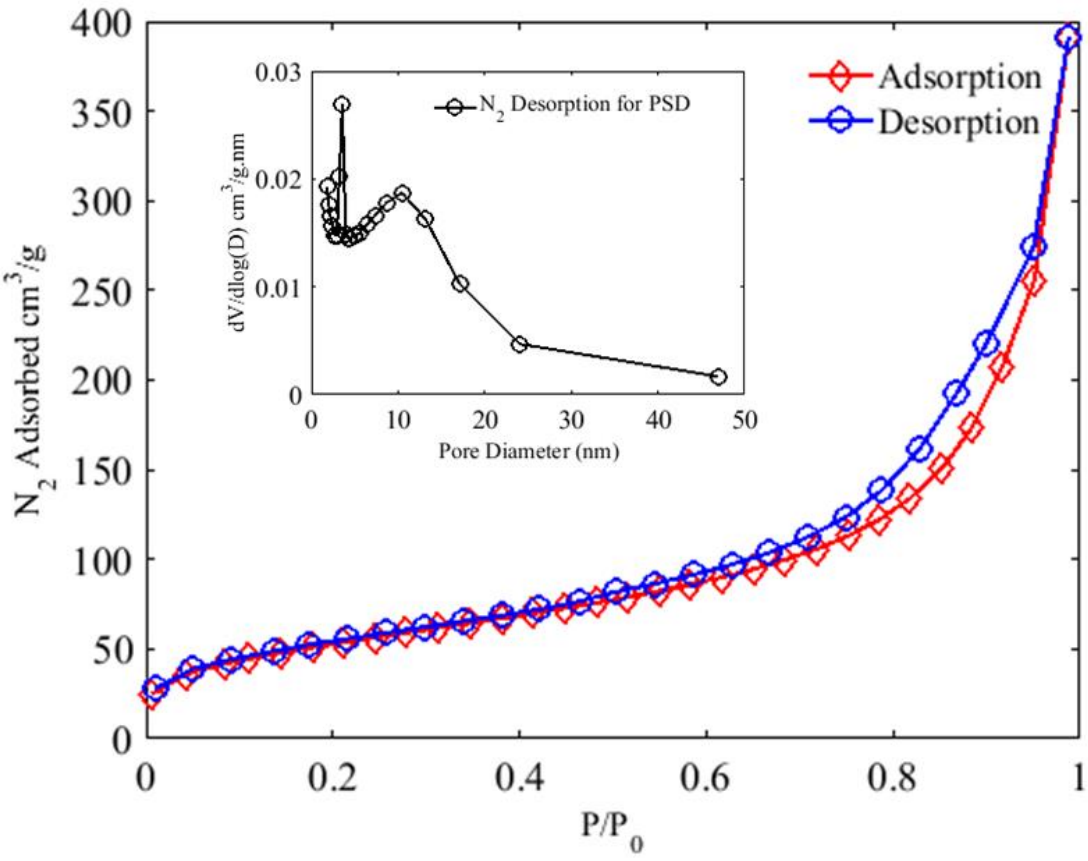

Figure 6-2 N_2 adsorption-desorption isotherms of bio-MOF-11-Co for surface area and pore size distribution using the BJH method.

Pore size distribution (PSD) was determined by the Barrett-Joyner-Halenda (BJH) method using N_2 desorption branch. Two main peaks are indicating a high

concentration of mesopores in the range of 3-5 nm and 10-15 nm, respectively (Figure 6-2 inset). Generally, mesoporous materials show better performance than microporous materials due to less resistance for penetration of guest molecules in adsorption and/or catalytic degradation. So, sacrificial practice of reduced surface area can be adopted to tailor materials for a specific application with required textural properties (Kim & Huh, 2016; Liu et al., 2016).

6.3.2 Oxidant screen test with bio-MOF-11

It has been reported that copper is active in catalytic reactions in WWTPs, thus a CuBTC was tested for PMS activation. However, CuBTC could not sustain in PMS-containing water solution. Similarly, bio-MOF-11-Cu was also degraded in water and these two MOFs were neither tested further nor their characterizations are included in this chapter. But bio-MOF-11-Co not only sustained in water but also effectively activated PMS for catalytic degradation of organics. Furthermore, conventional oxidizing agents, i.e. H_2O_2 and PDS, were also used to check their effectiveness in degradation of p-HBA and SCP (Figure 6-3).

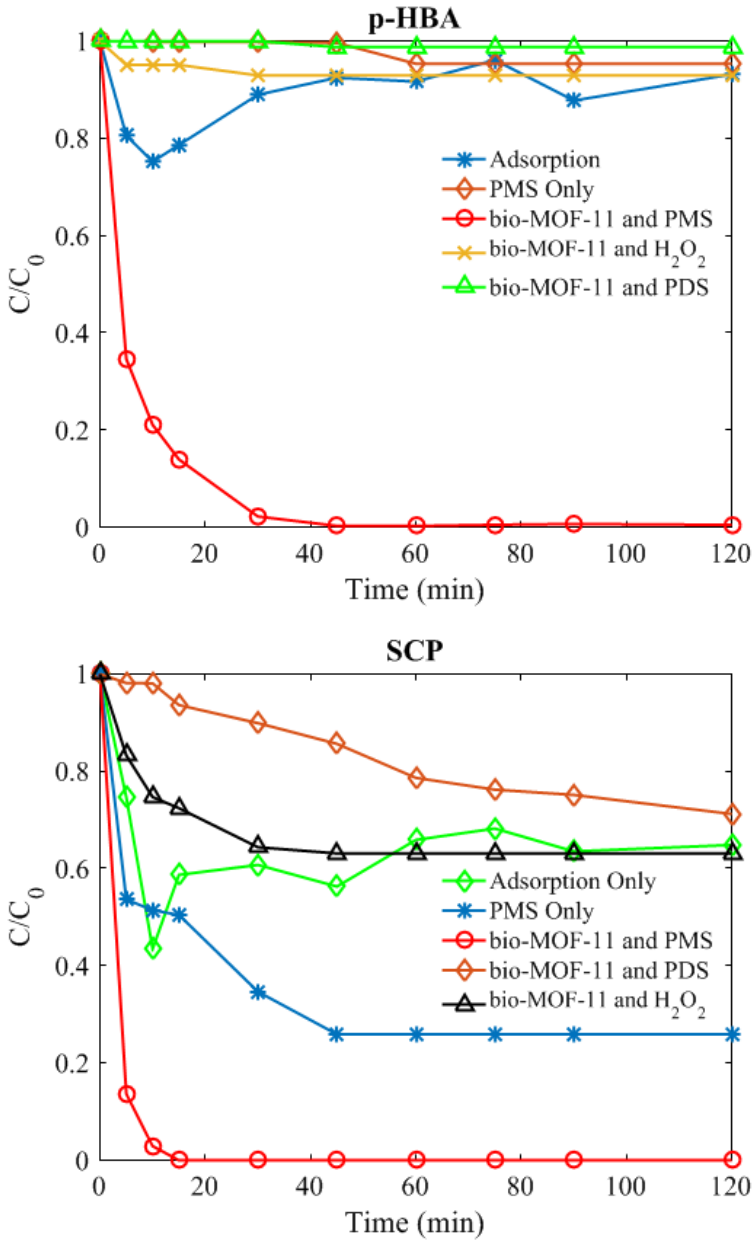

Figure 6-3 Adsorption and catalytic degradation of p-HBA and SCP (C0= 45 mg/L, bio-MOF-11=50 mg/L, PMS=500 mg/L, PDS=500 mg/L and H2O2= 0.3 mL at 25 °C).

It is shown that adsorption of p-HBA and SCP on bio-MOF-11-Co occurred initially in 15 min and then desorption happened in the next 15-20 min for p-HBA and SCP to reach equilibrium, which may be attributed to mesopores of bio-MOF-11-Co (Liu et al., 2016). The adsorption of p-HBA is only 10% while it is higher for SCP at about 40% after 2 h (Figure 6-3). For oxidation by using H_2O_2 and PDS with bio-MOF-11-Co, a marginal decrease in the concentration of p-HBA, suggests much less effectiveness of these two conventional oxidizing agents for catalytic degradation.

However, SCP degradation can be up to 40% with H_2O_2 and 25% with PDS within 120 min. For PMS, SCP and p-HBA degradations are significantly different from H_2O_2 and PDS. SCP decomposition by PMS alone could occur at a slower rate and reached 70% in 40 min while it took only 20-30 min for 100% removal of SCP and p-HBA with the presence of PMS and bio-MOF-11-Co. In generally, SCP degradation is fast than p-HBA, which could be attributed to their different chemical structure and stability. The chemical bonding with C-S-N in SCP will be easy to be broken. Previously, different behaviors of these three oxidants for organic degradation were observed showing activity in PMS > PDS > H_2O_2 (Sun et al., 2014a). H_2O_2 could not be effectively activated by Co-based catalysts for generation of hydroxyl radicals. Moreover, H_2O_2 is only effective to react with various metal ions in a narrow pH range around 3. In this work, solution pH was at 4.2 or 5.5, which is not favorable to H_2O_2 activation. Similarly, PDS as a symmetric oxidant can not be activated by Co species to be dissociated into reactive sulfate and hydroxyl radicals. However, it has been well known that Co species are the most efficient catalysts for PMS activation. Therefore, bio-MOF-11-Co is much effective in activation of PMS for SCP and p-HBA degradation, better than H_2O_2 and PDS. Rate constants were calculated using pseudo 1^{st} order kinetics (Figure 6-4). The value of rate constant for p-HBA degradation with PMS/bio-MOF-11-Co is 0.214 min^{-1} while the rate constants are 0.353 and 0.025 min^{-1} for SCP degradation in PMS/bio-MOF-11-Co and PMS, respectively.

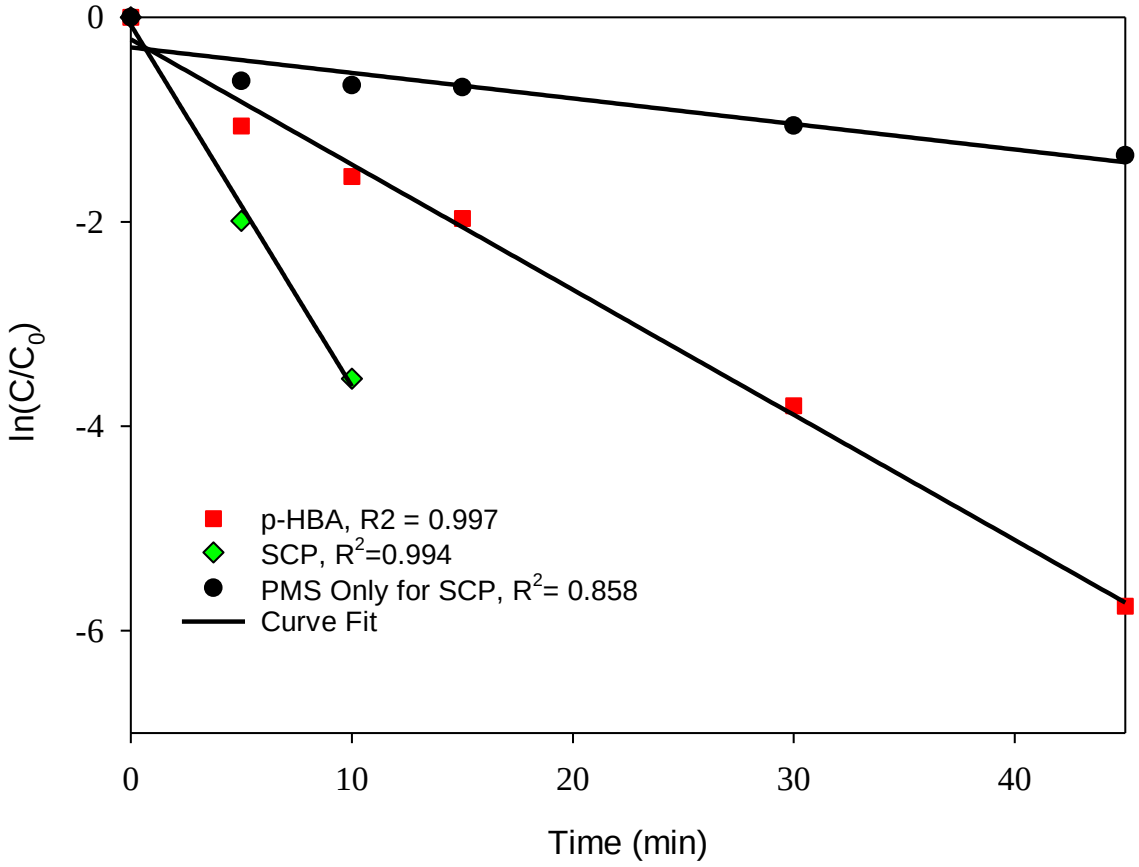

Figure 6-4 Kinetic fitting for degradation of p-HBA and SCP with BioMOF-11 and PMS ; bio-MOF-11 = 50 mg/L, PMS= 500 mg/L at 25 °C

TOC measurements were also carried out to check mineralization of p-HBA and SCP. It was observed that 75 and 85% mineralization took place for p-HBA and SCP, respectively, in bio-MOF-11-Co/PMS after 2 h (Figure 6-5). However, TOC removal in SCP degradation with PMS alone showed only 15% mineralization in 2 h, which is not as good as SCP decomposition. This observation suggests that SCP might transform into intermediate species instead of complete mineralization (Dirany et al., 2012a). Further investigations were then carried out in the PMS/bio-MOF-11-Co system owing to its efficient performance.

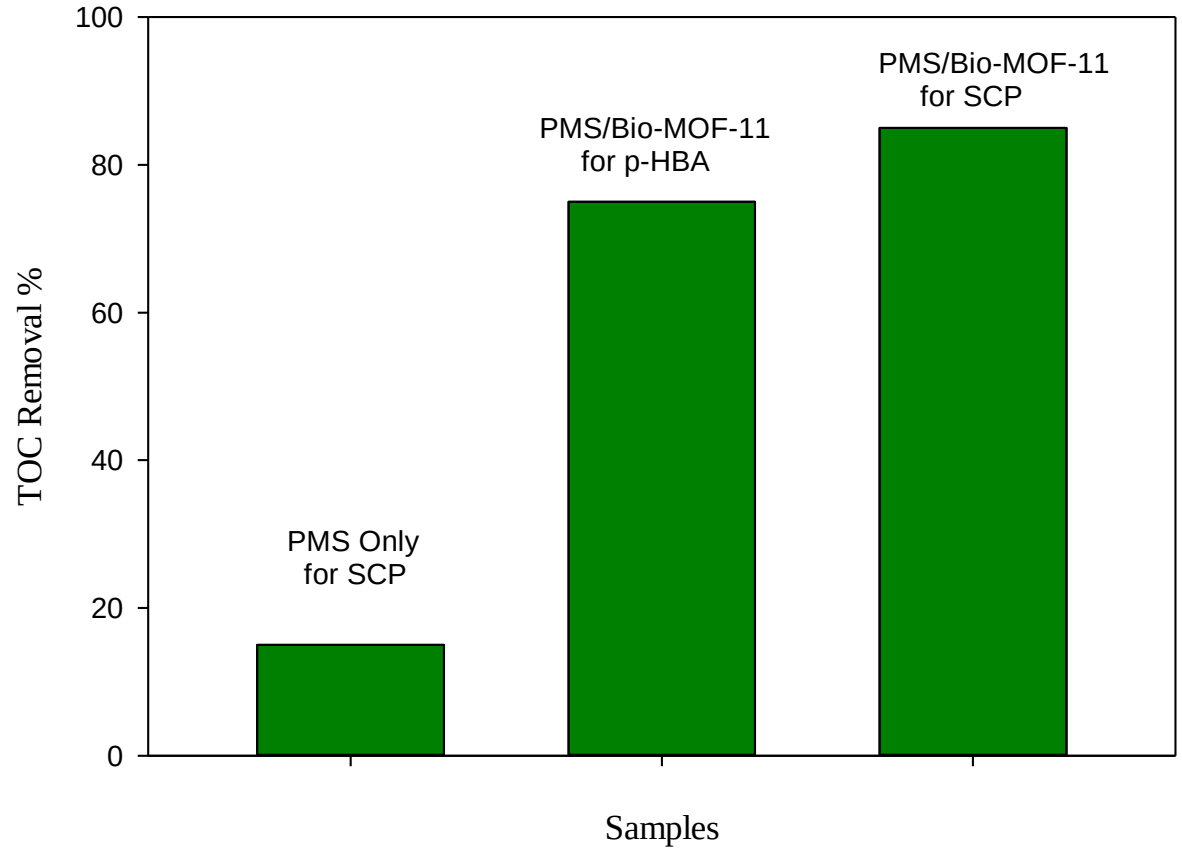

Figure 6-5 TOC removal for p-HBA and SCP in PMS/Bio-MOF-11-Co system bio-MOF-11 = 50 mg/L, PMS= 500 mg/L at 25 °C

6.3.3 Catalytic degradation of p-HBA and SCP in PMS/bio-MOF-11-Co

The amount of organic wastes presented in water streams is one of the important parameters in WWTPs, since degradation efficiency and time required to completely mineralize the contaminants are essential to make the degradation process cost effective. The usual concentration of tested toxins in simulated WWTPs experiments is 20 mg/L. In the present study, various concentrations (15-60 mg/L) of p-HBA and SCP were studied in order to decipher the effectiveness of bio-MOF-11-Co in WWTPs (Figure 6-6).

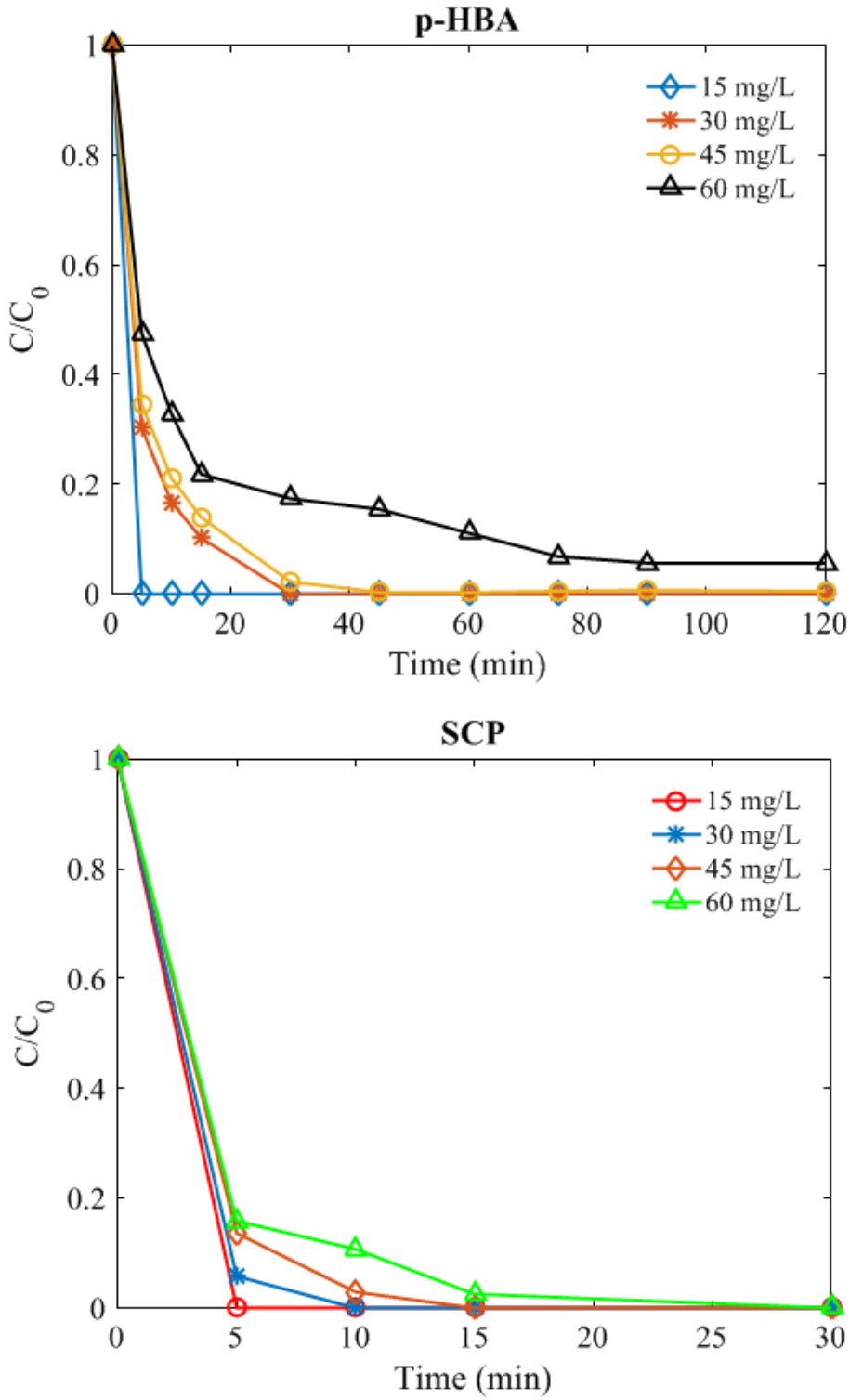

Figure 6-6 Effect of initial concentration of p-HBA and SCP; bio-MOF-11 = 50 mg/L, PMS= 500 mg/L at 25 °C

Generally, the catalyst at 50 mg/L was effective in complete removal of p-HBA up to 50 mg/L in 45 min while 15 min was sufficient for SCP removal at 25 °C. It took

more than 15 min to entirely mitigate 60 mg/L of SCP, however, 90% removal of p-HBA was possible in 120 min. It has been previously observed that SCP degraded rapidly by PDS activation using carbon based catalysts (Tian et al., 2016). Moreover, degradation reactions at higher temperatures of 35 and 45 °C were further tested (Figure 6-7). Interestingly, degradation of both p-HBA and SCP into various components was achieved in just 5 min at 45 °C while it took 10 min at 35 °C in case SCP but p-HBA degraded in 5 min. However, it might take longer time for mineralization of resultant side products even at higher temperatures.

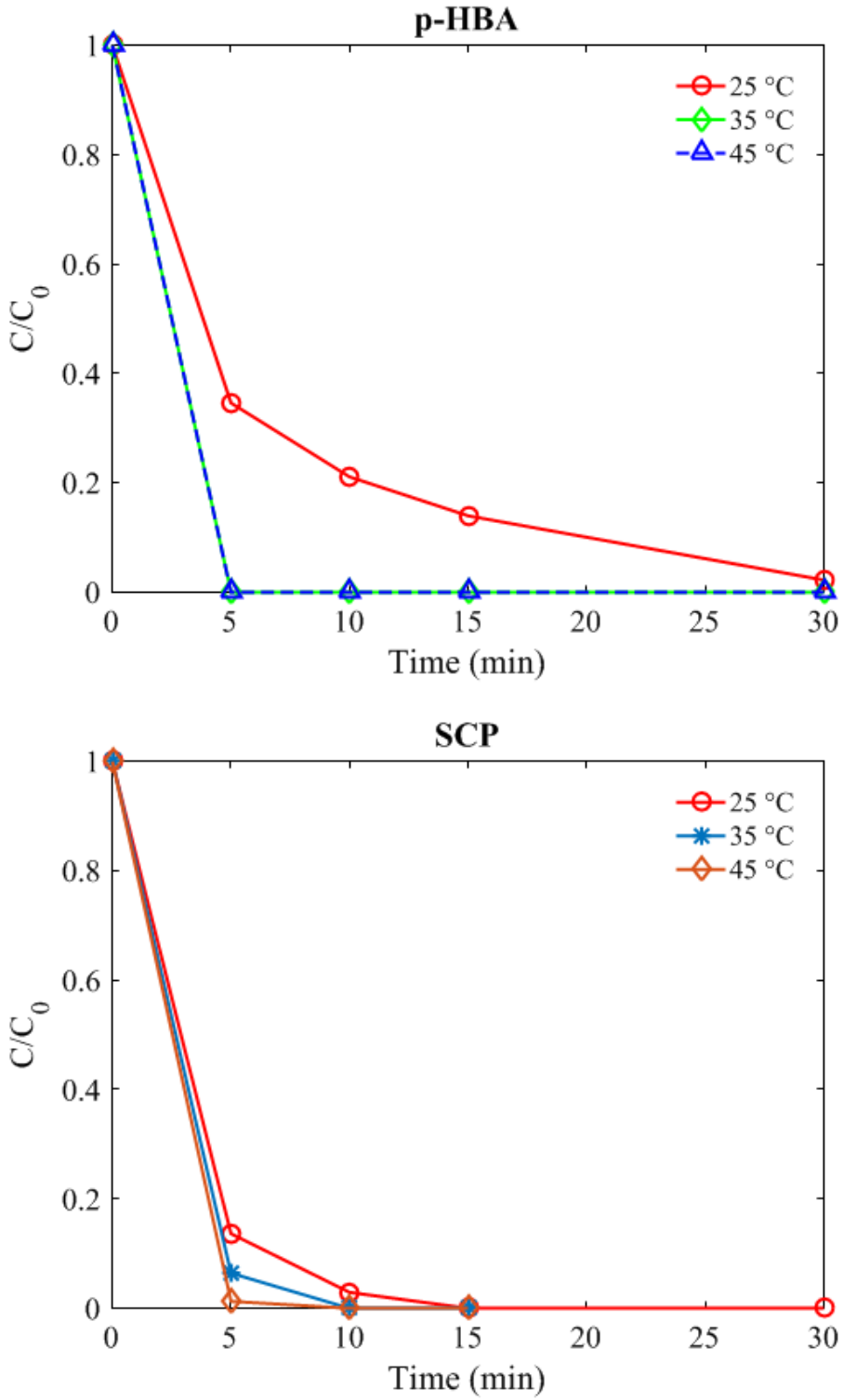

Figure 6-7 Effect of reaction temperature on kinetics of p-HBA and SCP degradation; C0 = 45 mg/L, bio-MOF-11 = 50 mg/L and PMS = 500 mg/L.

The loading of PMS is a crucial factor in oxidation of water contaminants. Degradation efficiency was affected significantly with a low loading of PMS (Figure

6-8). Specifically, at PMS loading of 250 mg/L, only 85% of p-HBA was degraded after 2 h compared to that of 0.5 h by doubling the amount of PMS. There was marginal difference in catalytic efficiency at PMS concentration of 750 mg/L. However, the degradation of p-HBA was very fast at 1000 mg/L of PMS. In comparison to p-HBA, complete degradation of SCP was achieved at 250 mg/L in 30 min. In further experiments, the amount of PMS was selected at 500 mg/L. In previous studies, much high quantities of PMS were required with Co_3O_4 catalyst systems (Saputra et al., 2013b).

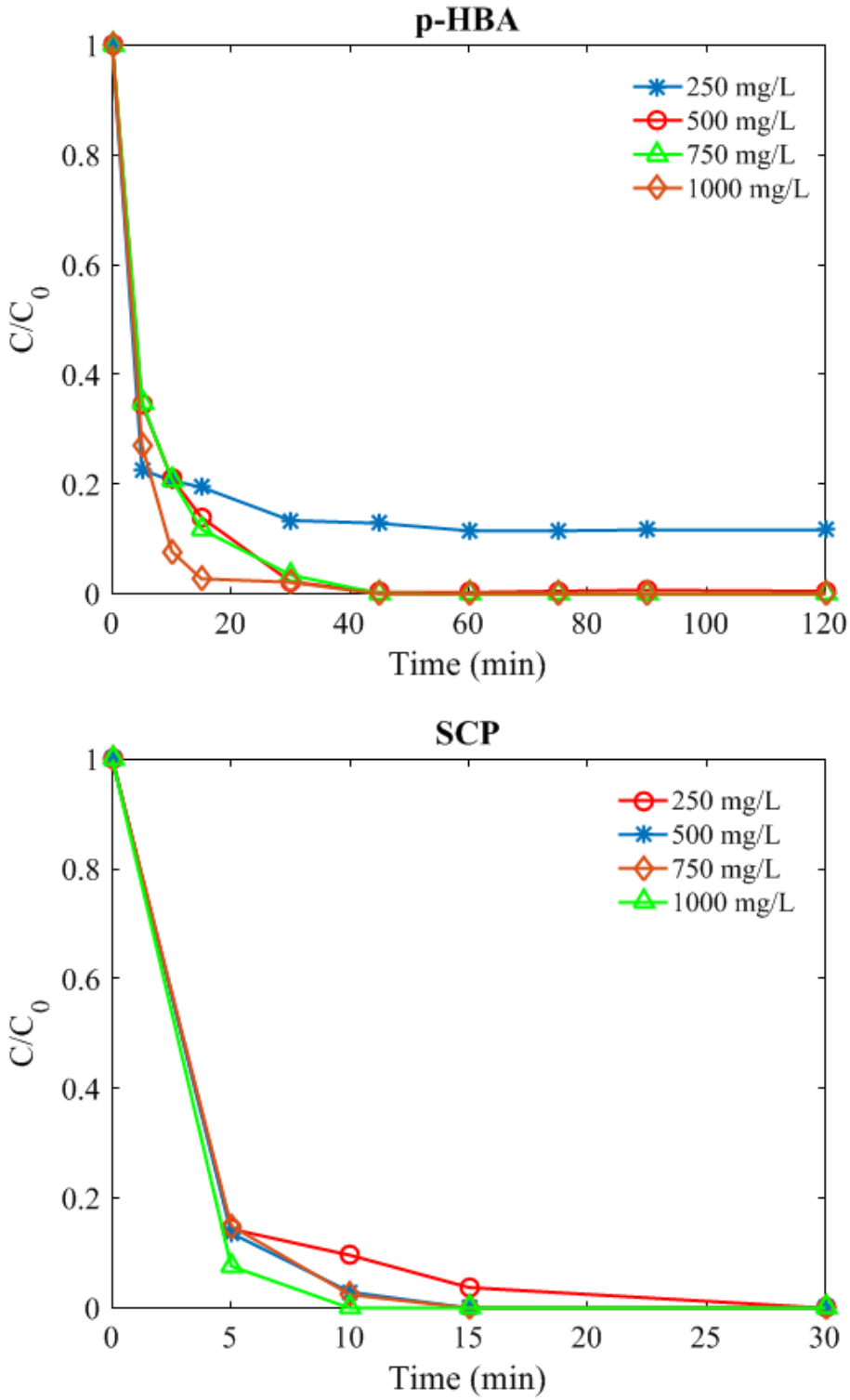

Figure 6-8 Effect of PMS loading on degradation of p-HBA and SCP (C0= 45 mg/L, bio-MOF-11=50 mg/L at 25 °C).

The effect of active sites in terms of catalyst loading was studied to comprehend its effect on efficiency of the degradation process. The amount of catalyst was varied

from 25-150 mg/L as shown in Figure 6-9. Generally, low loadings of bio-MOF-11-Co were sufficient to completely remove both the toxins from water. It was noticed that the bio-MOF-11-Co at even 25 mg/L was sufficient in complete degradation of both p-HBA and SCP, however, the reaction completion time was shorter for SCP at all loadings of the catalyst compared to p-HBA. It was very interesting to note that it just took 5 min for the residual concentration of p-HBA and SCP dropped to zero at 150 mg/L of bio-MOF-11-Co. In consideration of loadings of catalyst and PMS as well as reaction time, bio-MO-11-Co is a superior catalyst compared to previously studied catalysts for p-HBA and SCP degradation (Bai et al., 2015; Rivas, Beltrán, Frades, & Buxeda, 2001; Subramanian, Pangarkar, & Beenackers, 2000; Wang et al., 2016c).

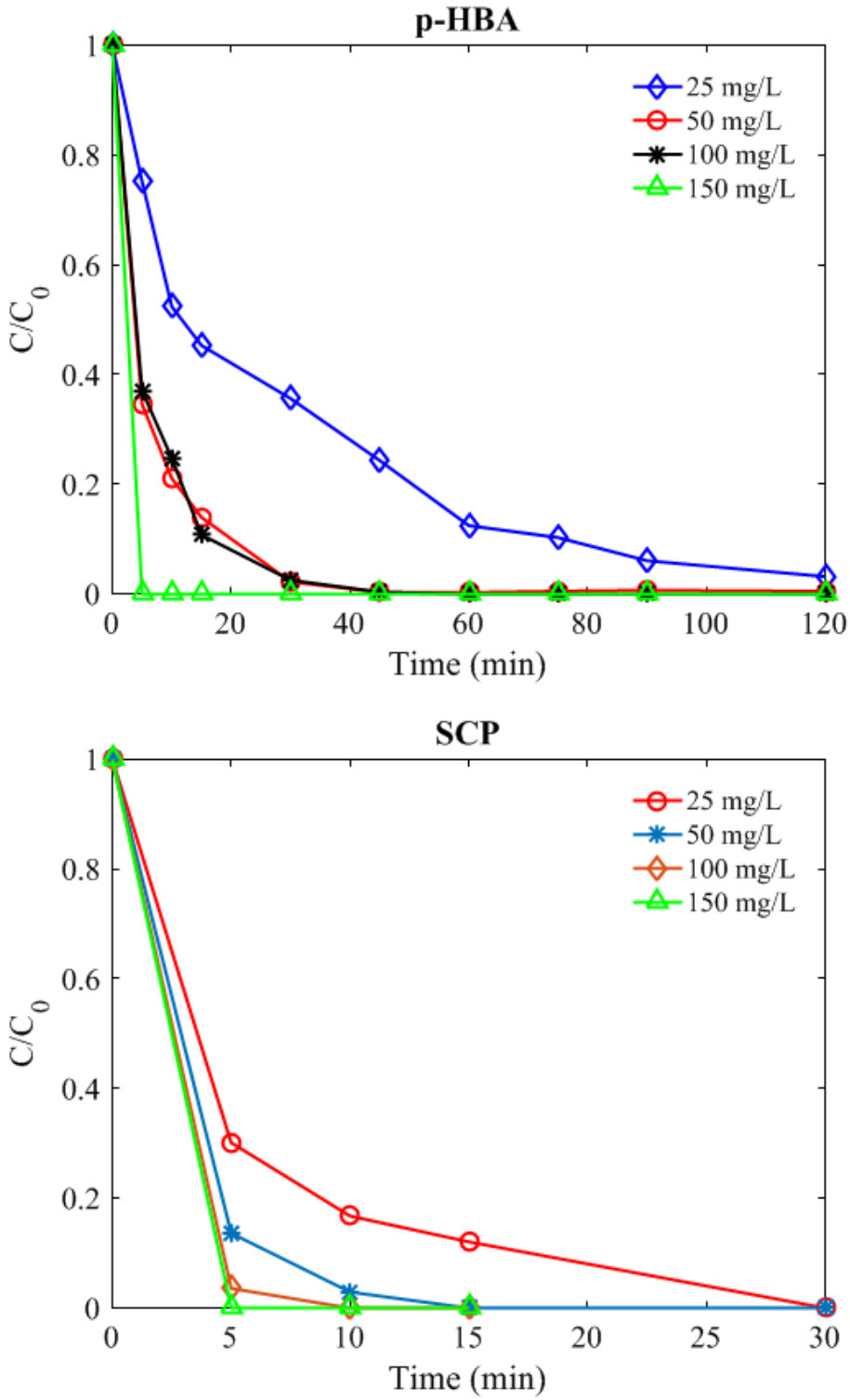

Figure 6-9 Effect of catalyst loading on degradation of p-HBA and SCP (C0 = 45 mg/L, PMS = 500 mg/L at 25 °C).

Since, bio-MOF-11-Co is an efficient catalyst for both p-HBA and SCP, therefore, simultaneous removal of these water contaminants was also tested (Cho, Lee, & Oh,

2008). Although, it was not convenient to analyse both analytes with single HPLC column due to different mobile phase, however, detection of p-HBA and SCP was carried out using dedicated HPLC columns. It can be seen from Figure 6.10 that complete degradation of SCP was achieved in 30 mins while more than 70 % p-HBA was also removed in combined degradation test. It can be noted that all the conditions were same in combined degradation test in terms of catalyst loading, PMS amount, and reaction temperature.

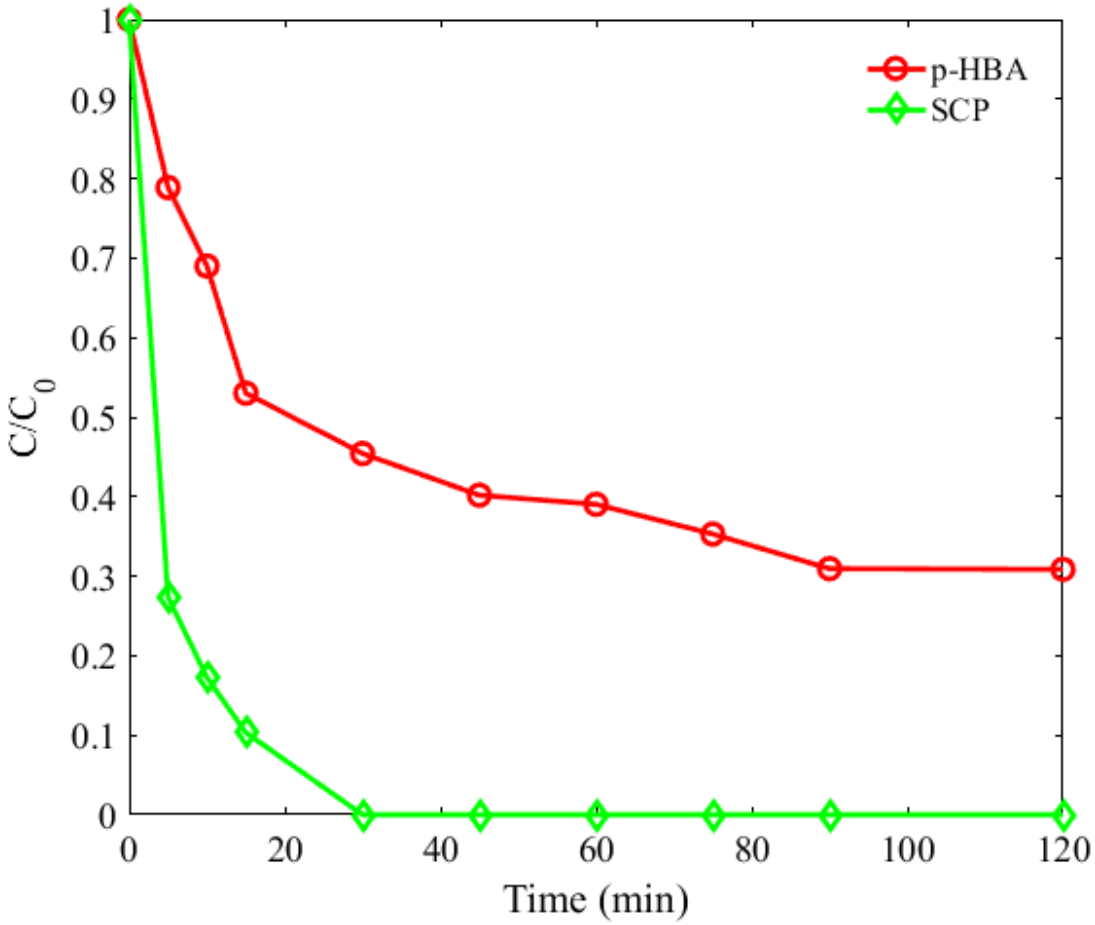

Figure 6-10 Simultaneous degradation of p-HBA and SCP; C0 = 45 mg/L, bio-MOF-11 = 50 mg/L and PMS = 500 mg/L

6.4 Degradation mechanism of p-HBA and SCP

In activation of PMS, generation of reactive radicals is an imperative step in effective degradation of organic wastes. So, the generation of the radicals, i.e. sulfate and hydroxyl radicals, were studied with 5,5, dimethyl-pyrroline-oxide (DMPO) as a

spin trapping agent in EPR analysis (Oh, Dong, & Lim, 2016). In a reaction, 0.08 M DMPO was used in the EPR tests to confirm the generation of free radicals.

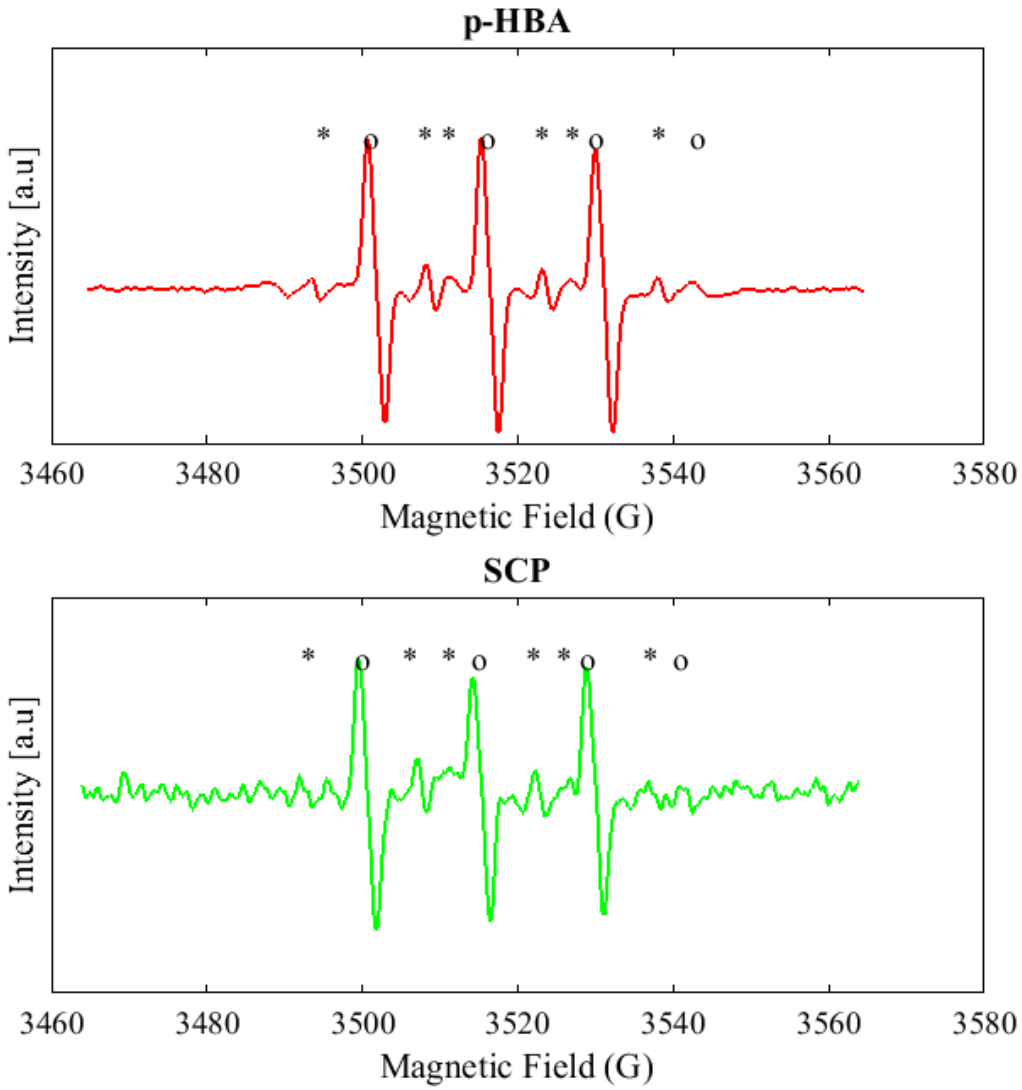

Figure 6-11 EPR spectra of PMS activation using bio-MOF-11 as a catalyst, bio-MOF-11=50 mg/L, PMS=500 mg/L, C0=45 mg/L, DMPO=0.08 M after 20 min of reaction at 25 °C; ‘o’ indicates DMPO- and ‘*’ shows DMPO- .

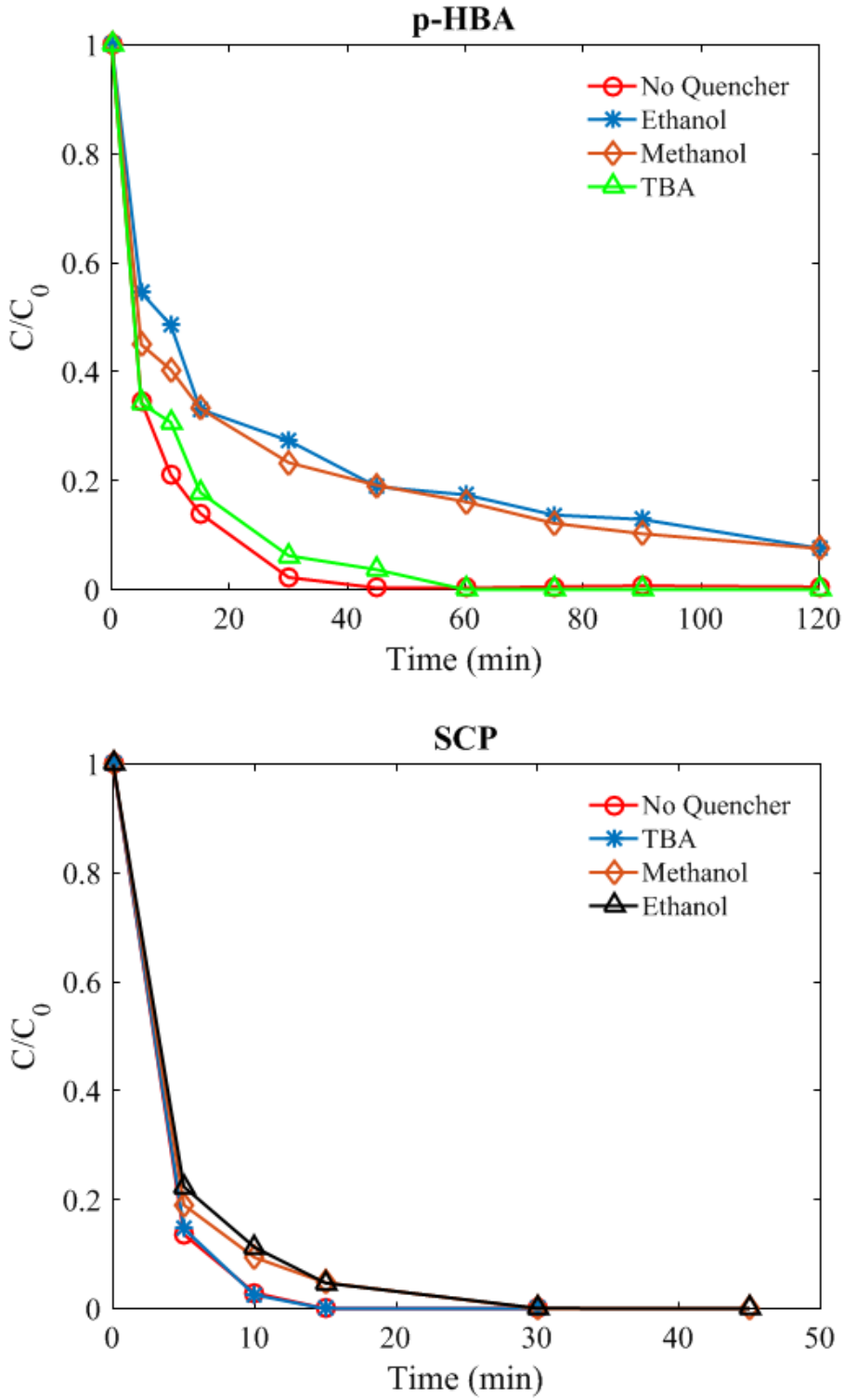

Figure 6-12 Effect of different quenching agents (10 mM) on degradation process. (C0 = 45 mg/L, bio-MOF-11=50 mg/L and PMS = 500 mg/L at 25 °C).

It can be seen from Figure 6 that both $SO_4^{-\bullet}$ and $HO^{\bullet}$ radicals, which are responsible for degradation of p-HBA and SCP (Wang et al., 2015g), can be

identified through the signals of DMPO-$HO^{\bullet}$ and DMPO-$SO_4^{-\bullet}$. The spectra were scanned after 20 min of reaction while complete degradation of both contaminants have been completed in 30 min of reaction time. Overall, both $SO_4^{-\bullet}$ and $HO^{\bullet}$ radicals play their roles in degradation of p-HBA and SCP.

Furthermore, the effectiveness of free radicals in catalytic degradation reactions can be verified by using different free radical quenchers. Generally, tert-butyl alcohol (TBA) is used to capture free hydroxyl radicals, and methanol for sulfate radicals, while ethanol can capture both of these radicals (Indrawirawan, Sun, Duan, & Wang, 2015a). To check the influences of hydroxyl and sulfate radicals, 10 mM of TBA, ethanol and methanol were introduced into the reaction mixture individually prior to introducing PMS (Figure 6.12). For p-HBA reaction system, ethanol and methanol hindered the reaction rates and complete degradation was not possible, which suggests a higher contribution of sulfate radicals in degradation reactions. In comparison, there was not a big difference by introducing the quenchers in the reaction for SCP degradation. This shows that oxidation of SCP is easier compared to p-HBA which is more persistent. Moreover, only a small amount of free radicals can result in complete elimination of SCP, which is also evident from the investigations of PMS and catalyst loadings (Figs. 6-8 and 6-9). From EPR spectra and quenching tests, it can be concluded that both $SO_4^{-\bullet}$ and $HO^{\bullet}$ radicals play their roles in degradation of p-HBA and SCP.

Due to the hybrid nature of MOFs, it is interesting to study the detailed mechanism of the catalytic degradation of p-HBA and SCP on bio-MOF-11-Co. The heterogeneous catalytic degradation can be explained by basic sites in the framework in terms of cyclic nitrogen and variable oxidation states of cobalt in bio-MOF-11-Co. The sulfate radicals can be generated by variation of cobalt oxygen states, i.e. Co^{2+} and Co^{3+}. By continuous transition of cobalt states, high concentrations of both $SO_4^{-\bullet}$ and $HO^{\bullet}$ radicals resulted in fast degradation of pollutants. In addition, the pores in bio-MOF-11-Co are large enough to accommodate persulfate ions and subsequently converting them into sulfate radicals which attack p-HBA and SCP (Figure 6-13A).

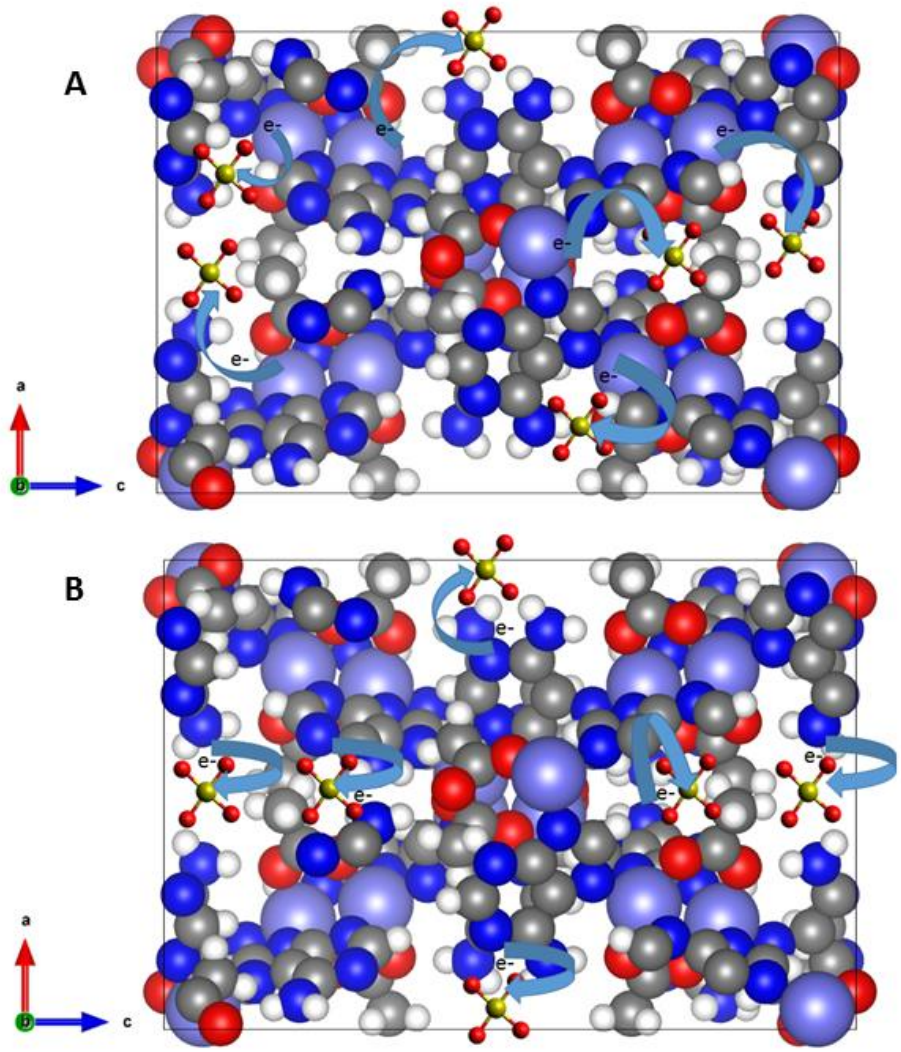

Figure 6-13 Schematic representation of activation of PMS by bio-MOF-11; cobalt = purple, carbon= grey, oxygen= red, hydrogen= white and nitrogen= blue.

The effectiveness of the transition in oxidation states of cobalt has been reported previously for degradation of rhodamine B by ZIF-67 (Lin & Chang, 2015a). Moreover, it is also an important factor in other transition metal compounds such as Mn_xO_y and Fe_xO_y for advanced oxidation processes. A detailed study on variable oxidation states of manganese oxides has been reported in activation of PMS for degradation of phenol (Saputra et al., 2013a; Saputra et al., 2013b, c).

Metal leaching was tested to check the stability of the catalyst and Co ion concentrations after water soaking of as-synthesized and used materials were determined using ICP-OES. It was observed that there was small amount of leached

Co^{2+} in water (Table 6-1). Specifically, water soaking metal leaching was negligible, i.e. less than 1 ppm while it was 1.24 ppm in SCP test and 1.75 ppm for p-HBA degradation. It is interesting to note that a higher concentration of free cobalt ions (> 5 mg/L) in SCP solution results in precipitation of Co oxides (Figure 6-14). This suggests that homogeneous Co ions could not make a significant contribution to organic degradation.

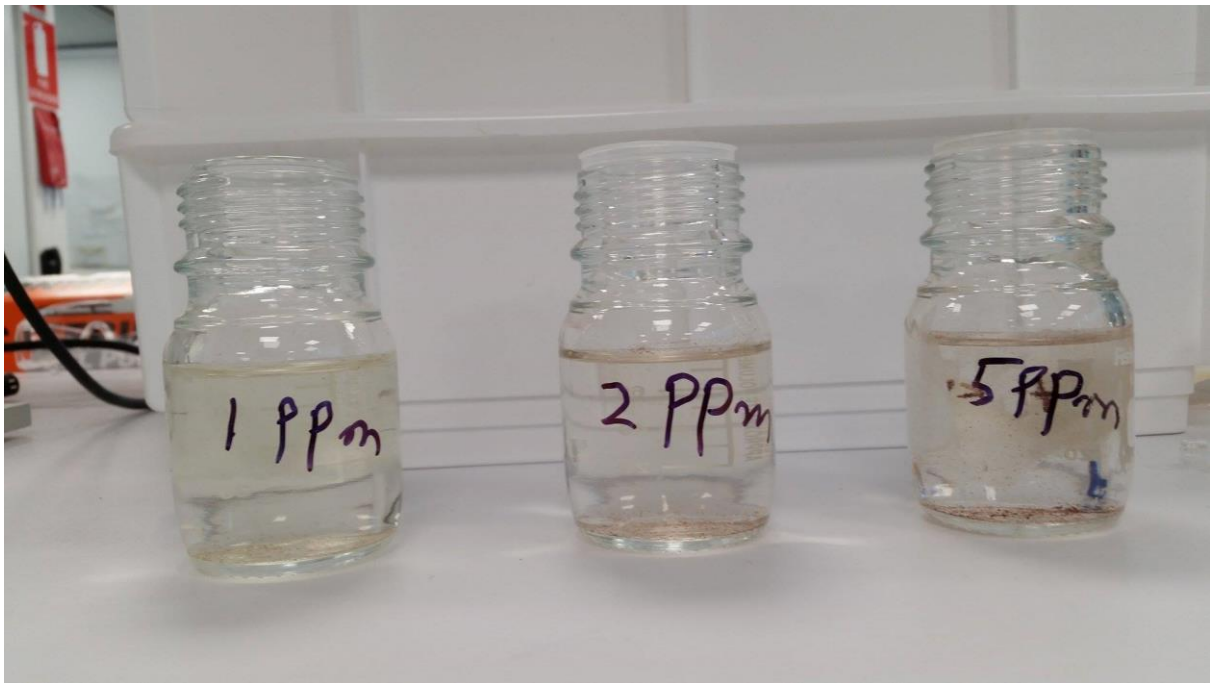

Figure 6-14 Precipitation of SCP with cobalt ions; C0 = 45 mg/L, Co2+ = 1-5 mg/L and PMS = 500 mg/L.

Table 6-1 Water stability of bio-MOF-11-Co under various conditions.

MOFs	Metal leaching (Co^{2+}) mg/L
70 days water soaked bio-MOF-11	0.98
used bio-MOF-11 in p-HBA degradation	1.75
used bio-MOF-11 in SCP degradation	1.24
p-HBA 1st reused bio-MOF-11	0.92
SCP 1st reused bio-MOF-11	0.83

Another important factor for degradation is generation of free radicals through electron transfer from organic moieties of bio-MOF-11. Large abundance of electron rich nitrogen atoms in adenine and bio-MOF-11 facilitates electron transfer to generate $SO_4^{-\bullet}$ and/or $HO^{\bullet}$ radicals very rapidly. It has been reported that doping of heterogeneous atoms such as nitrogen and sulfur assists the generation of radicals and ultimately high degradation efficiency (Indrawirawan et al., 2015a). In bio-MOF-11-Co, two Co^{2+} ions are bridged by adeninates through positions 3 and 9 and two acetates. This results in a square secondary building unit (SBU) of cobalt adeninate clusters, which subsequently are coordinated to N7 atoms of adeninates to Co^{2+} ions of neighbouring clusters, generating a three-dimensional framework structure with augmented Ivt network topology (Figure 6-13A). This topology produces periodic cavities throughout the structure and each cavity is defined by 16 interconnected square building units. In every cavity, four NH_2 groups and four pyrimidine groups are directly exposed, which facilitate electron transfer phenomenon at a large extent, resulting in efficient degradation of p-HBA and SCP (Figure 6-13B) (An et al., 2010). However, it is of interest to verify intactness of crystallinity, surface area and pore structure of bio-MOF-11 in order to verify its water stability. Powder XRD pattern of water soaked samples for different times and recovered catalyst samples from degradation reaction showed high crystallinity of bio-MOF-11-Co (Figure 6-15).

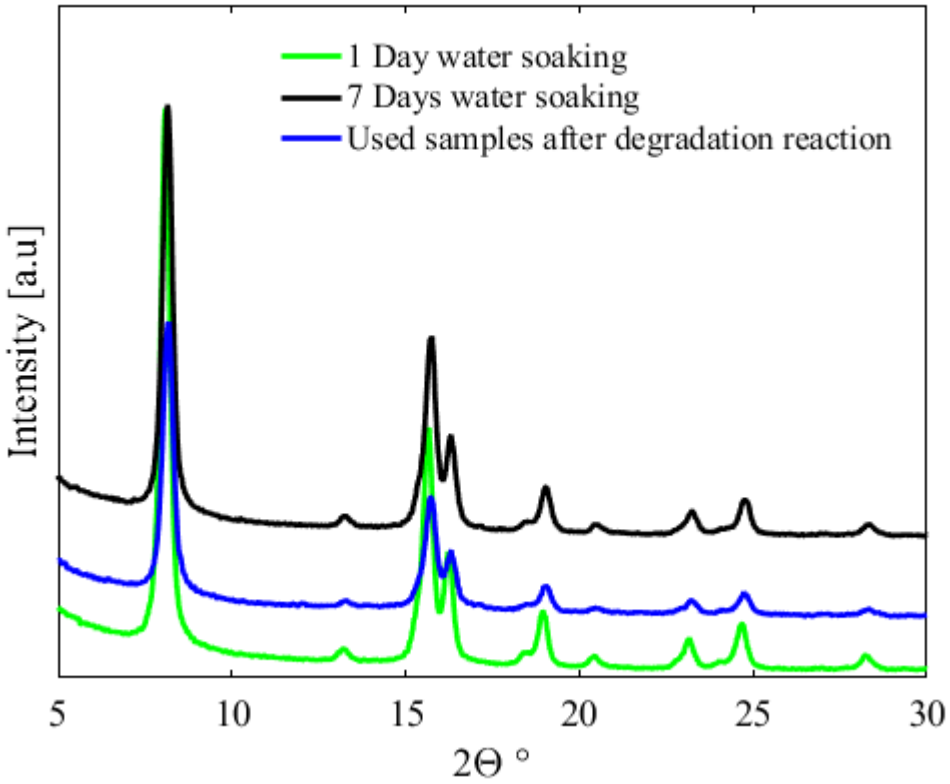

Figure 6-15 Powder XRD pattern of water soaked and recovered bio-MOF-11-Co from degradation reactions of p-HBA and SCP bio-MOF-11.

Moreover, nitrogen adsorption-desorption isotherm of used catalyst showed that there is no change in pore structure with marginal decrease in surface which might be due to adsorption of small amount of water molecules through hydrogen with structural adenine of bio-MOF-11-Co. Furthermore, BET surface of used bio-MOF-11-Co was 350 m^2/g while total pore volume decreased to 0.50 cm^3/g and PSD remained similar to as synthesized MOF (Figure 6-16).

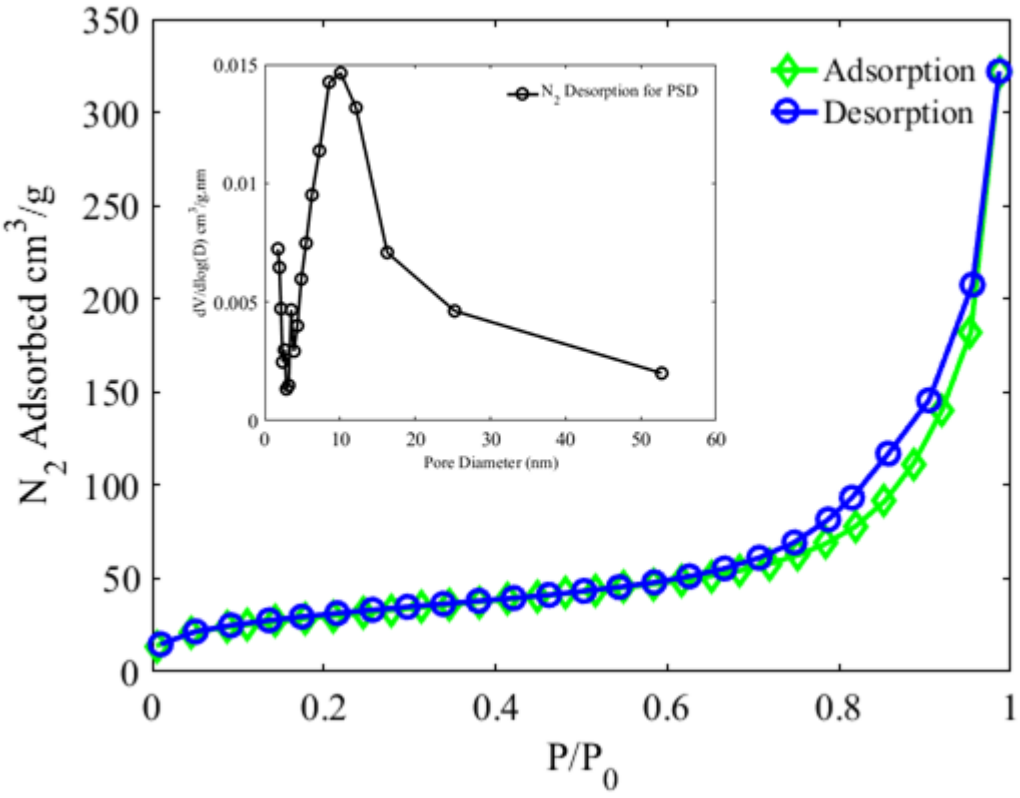

Figure 6-16 N_2 adsorption-desorption isotherms of recovered bio-MOF-11-Co from degradation reactions of p-HBA and SCP for surface area and pore size distribution.

The Lewis basic sites i.e. NH_2 and pyrimidine inside the pores can attribute to fast and efficient activation of PMS to degrade water contaminants. Previously, significance of NH_2 functionalization of MOFs has been reported in adsorption and even oxidation of pollutants from wastewater (Haque et al., 2014b; Wang et al., 2015b). Moreover, it has been reported that strong basicity of heterocyclic and/or amidic nitrogen in doped carbons play a significant role in catalytic processes. Specifically, increasing nitrogen contents in graphene resulted in faster degradation of SCP and phenol with doping level of nitrogen at 7.2 atomic% in graphene (Indrawirawan et al., 2015a). For bio-MOF-11-Co, nitrogen contents including those of coordinated to cobalt and freely exposed in cavities as Lewis bases are at 26 wt% by elemental analysis.

In order to verify the significance of the Lewis basic sites of adenine, adenine was then used to activate PMS for degradation of SCP and p-HBA. It was observed that adenine could activate PMS to degrade both SCP and p-HBA up to 60% with a

slower rate compared to bio-MOF-11-Co while SCP was almost completely removed with adenine only (Figure 6-17).

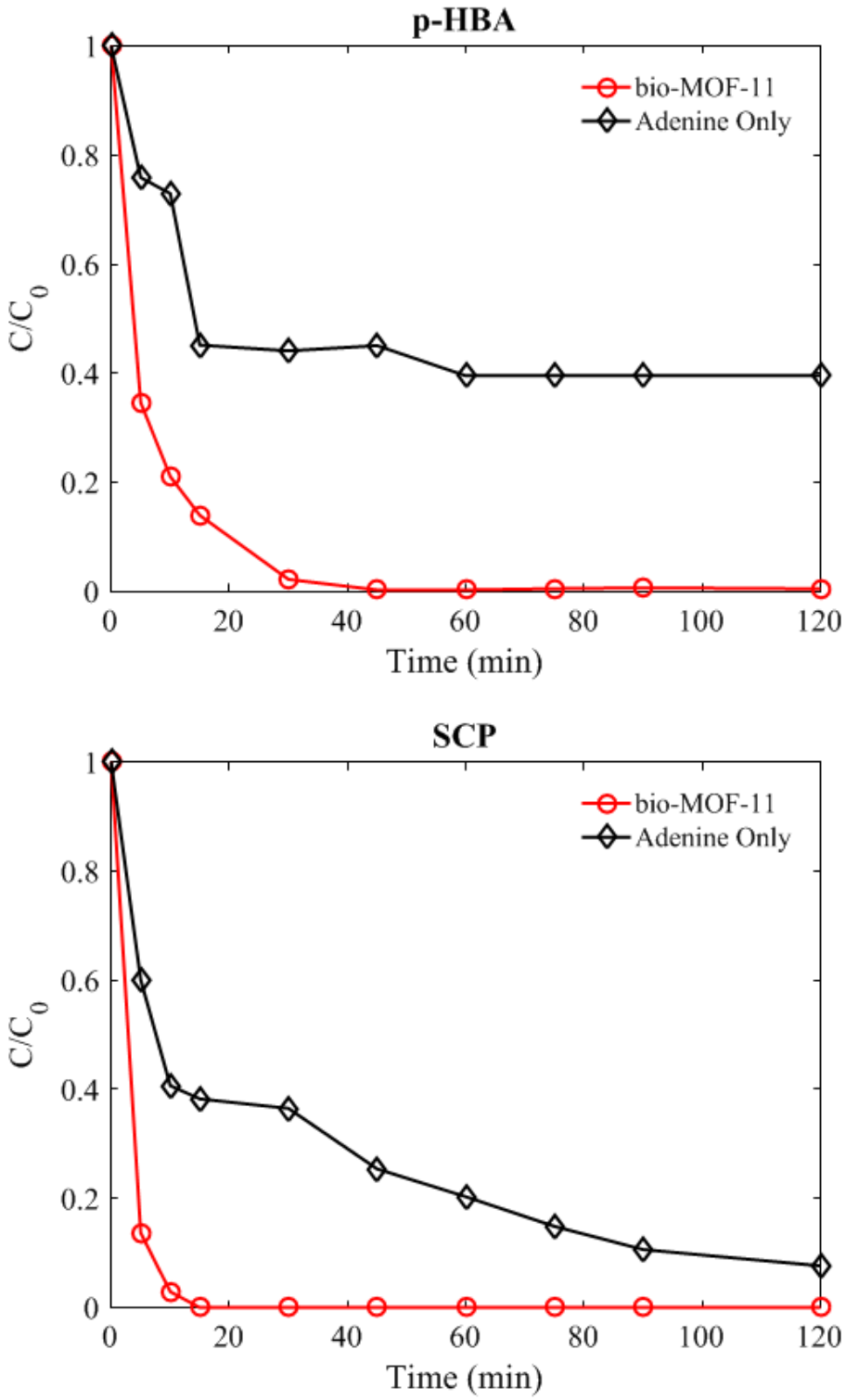

Figure 6-17 Verification of electron transfer behaviour for PMS activation with adeninates. C0 = 45 mg/L, Adenine = 50 mg/L and PMS = 500 mg/L.

This gives rise to exploring more ways to utilize adenine and other nitrogen rich species to be used in advanced oxidation processes owing to its high functionality and lower solubility in water. Generation of sulfate and hydroxyl radicals by the Lewis bases of adenine can be explained by electron transfer. Thus, a complete degradation mechanism with a combined effect of organic and inorganic moieties of bio-MOF-11-Co can be explained by the following steps (Equations 1-10).

$$HSO_5^- + bio-MOF-11@Co^{2+} \rightarrow SO_4^{-\bullet} + OH^- + bio-MOF-11@Co^{3+} \quad (1)$$

$$HSO_5^- + bio-MOF-11@Co^{3+} \rightarrow SO_5^{-\bullet} + H^+ + bio-MOF-11@Co^{2+} \quad (2)$$

$$HSO_5^- + e^- \rightarrow HO^\bullet + SO_4^{2-} \quad (3)$$

$$HSO_5^- + e^- \rightarrow SO_4^{-\bullet} + OH^- \quad (4)$$

$$HSO_5^- + e^- \rightarrow SO_5^{-\bullet} + H^+ \quad (5)$$

$$HO^\bullet + SO_4^{2-} \rightarrow SO_4^{-\bullet} + OH^- \quad (6)$$

$$SO_4^{-\bullet} + OH^- \rightarrow SO_4^{2-} + HO^\bullet \quad (7)$$

$$p-HBA/SCP + SO_4^{-\bullet} \rightarrow several steps \rightarrow CO_2 + H_2O + SO_4^{2-} \quad (8)$$

$$p-HBA/SCP + HSO_5^{-\bullet} \rightarrow several steps \rightarrow CO_2 + H_2O + SO_4^{2-} \quad (9)$$

$$p-HBA/SCP + HO^\bullet \rightarrow several steps \rightarrow CO_2 + H_2O + SO_4^{2-} \quad (10)$$

6.5 Regeneration and reuse of bio-MOF-11-Co

The effectiveness of any catalyst depends on its reusability to make a process cost effective. Since, bioMOF-11 showed high water stability not only in pure water but also in the presence of PMS for catalytic degradation reactions (Figure 6-8 & 6-9). In this study, bio-MOF-11-Co was reused in three times without any post treatment except washing and drying at 130 °C (Figure 6-18). Even after the third reuse, the catalyst could degrade SCP in 30 min. However, it was not the same for p-HBA

which took two hours for complete degradation in the 1st and 2nd reused cycles and only 80% degradation was possible in the 3rd reuse cycle. The degradation of p-HBA is comparatively difficult than SCP under the similar conditions. Interestingly, there was marginal difference for SCP in degradation rate in first 15 min in the 2nd and 3rd recycles which increased progressively with time. On the contrary, the degradation kinetics of SCP were similar in all three recycle runs, suggesting robust nature of bio-MOF-11-Co in catalytic degradation.

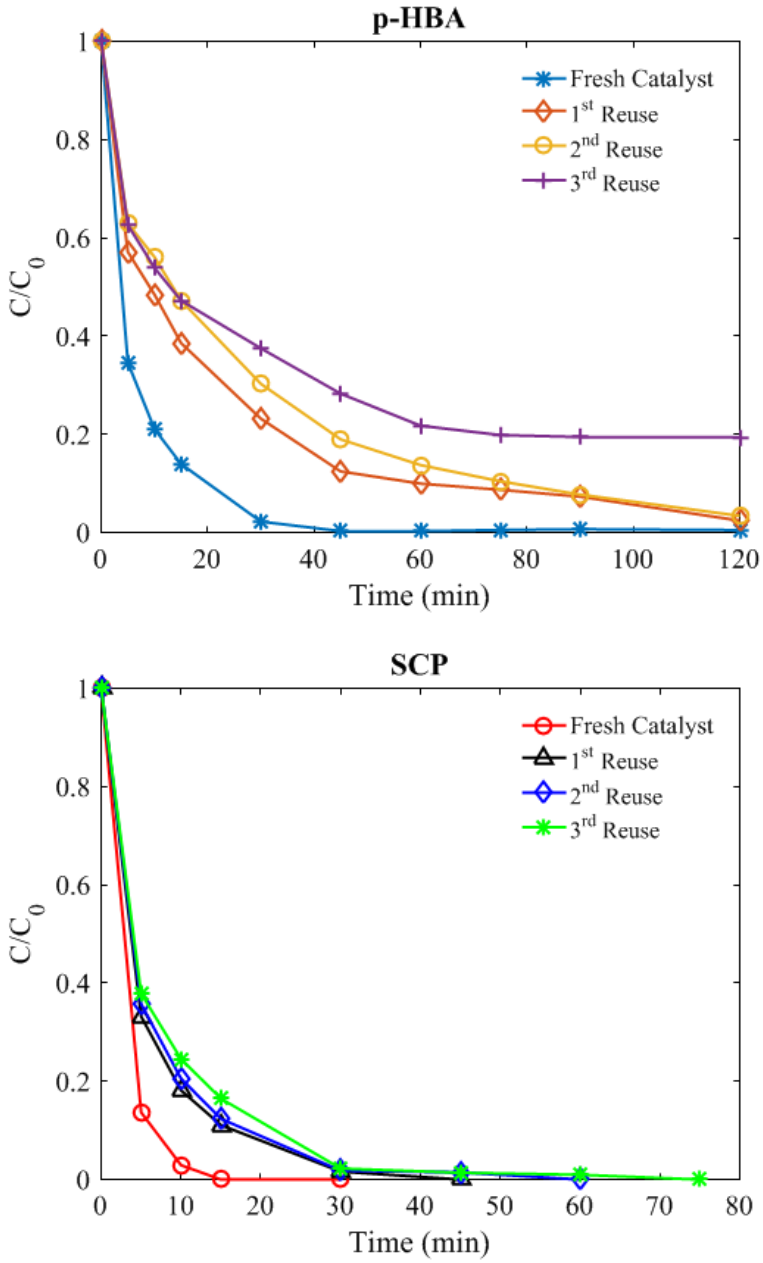

Figure 6-18 Catalytic stability in reuse for three runs (C0 = 45 mg/L, bio-MOF-11=50 mg/L and PMS = 500 mg/L at 25 °C).

Metal leaching was also determined in the recycled catalyst tests (Table 6-1). Compared to the fresh samples, the leaching of metal was significantly reduced in reuse for both SCP and p-HBA, probably due to the chemical stability of heterogeneous inner structure of bio-MOF-11-Co and slow kinetics of SCP and p-HBA degradation (Shukla, Sun, Wang, Ang, & Tadé, 2011a, b).

6.6 Conclusions

In this study, highly water-stable bio-MOF-11-Co was synthesized and tested for catalytic degradation of p-HBA and SCP. The synthesized MOF showed high crystallinity, water stability and mesoporosity. The catalysts are highly active, kinetically fast and stable for PMS activation for organic degradation. The removal of both contaminants, p-HBA and SCP, was possible in less than 30 min with initial concentrations of 45 mg/L at 25 °C. Moreover, complete elimination was possible in just 5 min for p-HBA and SCP at 45 °C. A plausible mechanism was proposed from the structure of bio-MOF-11-Co in activation of PMS. The results showed that availability of Lewis bases in the structure of bio-MOF-11 promotes electron transfer behavior of bio-MOF-11-Co in activation of PMS, which subsequently degrade water contaminants. This study showed that the bio-MOF-11-Co can be effectively used as catalysts in water remediation.

Chapter 7 Cascade applications of robust MIL-96 metal organic frameworks in environmental remediation: Proof of concept*

* Adopted with permission from (M.R, Azhar, H.R, Abid, M.O., Tade V. Periasamy, H. Sun, S. Wang, "Cascade applications of robust MIL-96 metal organic frameworks in environmental remediation: Proof of concept", *Chemical Engineering Journal*, pp. 262-271, 2018) Copyright Elsevier.

7.1 Introduction

Environmental problems are on a constant rise in today's human life around the world. Because of the fast economic developments, energy consumption has rapidly augmented producing huge amount of pollutants to the environment.(Haines, 2003; Kurokawa et al., 2013) Meanwhile, high production and consumption of personal care products for a better life are also creating more threats to marine life as a result of their discharge into water bodies.(Evans et al., 2016) Many methods are used to control the emission of environmental toxics and enhance their removal efficiency and robust materials are immensely needed for environmental remediation including various gas- and liquid-phase processes. Hybrid porous materials are hopeful to capture greenhouse gases such as CO_2 and CH_4 (Abid, Pham, Ang, Tade, & Wang, 2012b; Lässig et al., 2011; Yuan et al., 2013) and metal organic frameworks (MOFs) are much promising in adsorption and storage of greenhouse gases. However, liquid phase adsorption using MOFs has not much explored and more attention of research is focused on robust MOFs for their applications.(Bao et al., 2016; Jian et al., 2016; Li, Xu, Feng, Hu, & Bu, 2016a; Millward & Yaghi, 2005)

Since MOFs are a relatively new class of porous hybrid materials to be synthesized by hydrothermal/solvothermal processes.(Qi, Luo, Che, & Zheng, 2008; Yaghi & Li, 1995; Yang, Zhao, Ding, Wang, & Zhao, 2007) Yet, slight changes in synthesis conditions can result in improved textural properties, different morphologies and better thermal stabilities. Modulation has been used in the synthesis processes of MOFs to improve the surface modifications and their applications in gas adsorption, drug delivery, catalysis, and other fields.(McGuire & Forgan, 2015) It was found that temperature and solvents have great impacts on the engineering of crystalline structure of MOFs.(Zhang et al., 2014a) Addition of co-solvent can alter the properties of the hybrid materials due to their different coordination behaviors.(McGuire & Forgan, 2015) Previously, porous ZIF-8 membranes were prepared via an interfacial formation method by using methanol as co-solvent.(Li, Wee, Volodin, Martens, & Vankelecom, 2015c) Depending on solution pH and co-solvent used, diverse topologies were obtained in MIL-96, MIL-100 and MIL-

110.(Seoane et al., 2015). MIL-96 is a less explored MOF in environmental applications despite of its high hydrothermal stability. Moreover, MIL-96 does not create secondary pollution due to its water stability and nontoxic nature of aluminium. Therefore, MIL-96 needs more attention of research community for wide and effective utilizations. The solvent capability to remove water from the MOF cluster can be ranked as acetonitrile < DMF ~ methanol < isopropyl alcohol.(Yang & Clark, 2014) MIL-96 has been synthesized under mild hydrothermal conditions with controlled crystal size and morphology by using mixed reactants.(Abid, 2012) The fractional addition of precursors, $C_9H_{21}O_3Al$ and Me3btc as an aluminium source and a ligand resulted in modified textural properties, morphology, particle size and CO_2 adsorption of MIL-96.(Liu et al., 2015b)

Hybrid materials are usually expensive and suffers from fast deactivation to become solid wastes. Recycling use of the expensive synthetic materials or transformation of the used solids to other materials will reduce the solid waste disposal to the environment meanwhile generate new application. In this chapter, we will demonstrate a strategy for recycling use and transformation of MOFs for different applications, showing a cascade process in environmental applications.

In this study, we prepared MIL-96 by a co-solvent method to investigate the effects of ethanol and methanol on different morphology and crystal size of MIL-96. Since alcohols are benign solvents compared to acetonitrile, DMF and other toxic solvents, therefore, two commonly used ethanol and methanol were employed for the investigation. The synthesized MIL-96 was firstly used for CO_2 adsorption. Then, the used MIL-96 was treated by a temperature swing process and subsequently tested for liquid-phase adsorption for water treatment in removal of para-hydroxybenzoic acid (p-HBA), a representative of parabens used in personal care products. Finally, the exhausted samples were pyrolysis-treated to obtain a metal/carbon catalyst and further utilized in catalytic degradation of an organic dye, methyl orange (MO), with peroxymonosulfate (PMS).(Yagub et al., 2014) In this way, we demonstrate a strategy for proof-of-concept in cascade application of materials for their recycle and new use.

7.2 Experimental procedures

7.2.1 Materials

$Al(NO_3)_3 \bullet 9H_2O$ and 1,3,5-benzenetricarboxylic acid (H_3btc, BTC), methanol (CH_4O), and ethanol (C_2H_6O) were supplied from Sigma Aldrich. Deionized water was supplied from an ultra-purity system in the laboratory. MIL-96 was synthesized by a hydrothermal process at 220 °C for 48 h (Abid, 2012; Abid, Rada, Shang, & Wang, 2016). MIL-96-methanol (MIL-96-Me) was synthesized similarly as MIL-96. In detail, $Al(NO_3)_3 \bullet 9H_2O$ (19.833 mmol, 7.44 g) was firstly dissolved in 26.8 mL of H_2O, and 4.18 mmol (0.88 g) of BTC was added into the mixture, and then 0.1 mL of methanol was added to the solution. After mixing 30 min, the solution was transferred to a 125 mL Teflon lined stainless-steel autoclave and placed in a preheating oven at 220 °C for 2 days. MIL-96-ethanol (MIL-96-Et) was also synthesized by the same procedure as described above using ethanol instead of methanol under the same conditions.

For activation, the prepared samples (MIL-96, MIL-96-Me and MIL-96-Et) were immersed in methanol for 5 days, filtered and dried at 120 ºC for 2 h. Finally, they were heated at 200 °C under vacuum for 12 h.

7.2.2 Synthesis of MIL-96 and Al2O3/carbon composite

Carbonization of used sample after liquid-phase adsorption test was carried out under N_2 flow (70 mL/min) in a tube furnace. A used MIL-96 sample was heated at a rate of 1 °C/min up to 350 °C and soaked at that temperature for 1 h and further heated at a ramp of 2 °C/min to 750 °C for 2 h.

7.2.2.1 Characterization of Materials

Powdered X-ray diffraction (PXRD) profiles were recorded in a range of 2θ = 5-70° with a diffractometer of D8 Advance (Model Bruker aXS) using Cu Kα radiation (λ= 1.5418 nm). Thermal stability and weight loss profiles were accomplished on a

METTLER-TOLEDO thermo-gravimetric analyzer (TGA, Model TGA/DSC1 STAR^e). About 10-20 mg of samples was placed in an alumina crucible and heated from 35 to 900 °C at 10 °C/min in air. N_2 adsorption/desorption isotherms and textural properties were measured and calculated by an Autosorb-1 from Quantachrome instruments. Samples were poured in a quartz sample tube and evacuated under 5-10 torr at 200 °C for 72 h. Infrared spectra were obtained by a Fourier transform infrared (FTIR) spectrometer (Model 100-FT-IR) from Perkin Elmer) for functional groups on the structure. Scanning electron microscopy (SEM) was performed on a Zeiss NEON 40 EsB CrossBeam for morphological analysis. Zeta potential measurements were carried out on Malvern zeta sizer nano ZS at different pH values (2.5 – 10.5). Dilute suspensions were prepared and pH was adjusted with 0.1 M HCl and 0.1 M NaOH before zeta potential measurements. X-ray photoelectron spectroscopy (XPS) was performed on a Kratos AXIS Ultra DLD system under an ultrahigh vacuum atmosphere (1×10^{-9} mBar). All elements were calibrated by setting the dominant C1s peak at 284.5 eV. The measurements were carried out under charge neutralizer to overcome charging of sample. Moreover, the peaks were fitted with the Shirley background and quantified by the CasaXPS software.

CO_2 adsorption was determined by a Gemini I-2360 instrument from Micrometrics. An activated MOFs sample of 120 mg was evacuated with Vacprep 061 at 120 °C under vacuum for one day for removing the moisture till the pressure is going down 50 mm Hg. Then the sample tubes were connected to the analysis port in Gemini-I-2360 for CO_2 adsorption at 25 °C. N_2 measurements were also carried out using ultra high purity N_2 (99.999%) on Gemini I-2360 at 25 °C.

After CO_2 and N_2 adsorption tests, used samples were heated at 160 °C for 4 h, inducing heat/temperature swing desorption of adsorbed gases from the pores.(Li & Hill, 2017) A stock solution with a concentration of 1000 mg/L of p-HBA was prepared by dissolving 1000 mg of p-HBA in ultrapure water. Dilution of the stock solution was performed to obtain p-HBA solutions at varying concentrations for liquid-phase adsorption on MIL-96. All the tests were carried out at 25 °C unless otherwise specified.

Degradation of methyl orange (MO) was tested on carbonized MIL-96 samples. In a particular run, 2.5 mg of catalyst was put into 50 mL of MO solution and allowed to achieve adsorption/desorption in 30 min and then 50 mg of PMS was added to initiate catalytic reaction at 25 °C. After regular intervals, 3 mL solution was withdrawn and centrifuged to separate solids and clear solution for UV-vis measurements on a UV-vis spectrophotometer (Thermo Spectronic Genesys 20, USA).

7.3 Results and discussion

7.3.1 Characteristics of MIL-96 samples

Figure 7-1(A) shows XRD patterns of MIL-96, MIL-96-Me and MIL-96-Et. Most of peaks are the same as those of MIL-96 reported. However, the intensities of peaks in modified samples are reduced, which may attribute to the change in the crystal size of MIL-96-Me and MIL-96-Et.

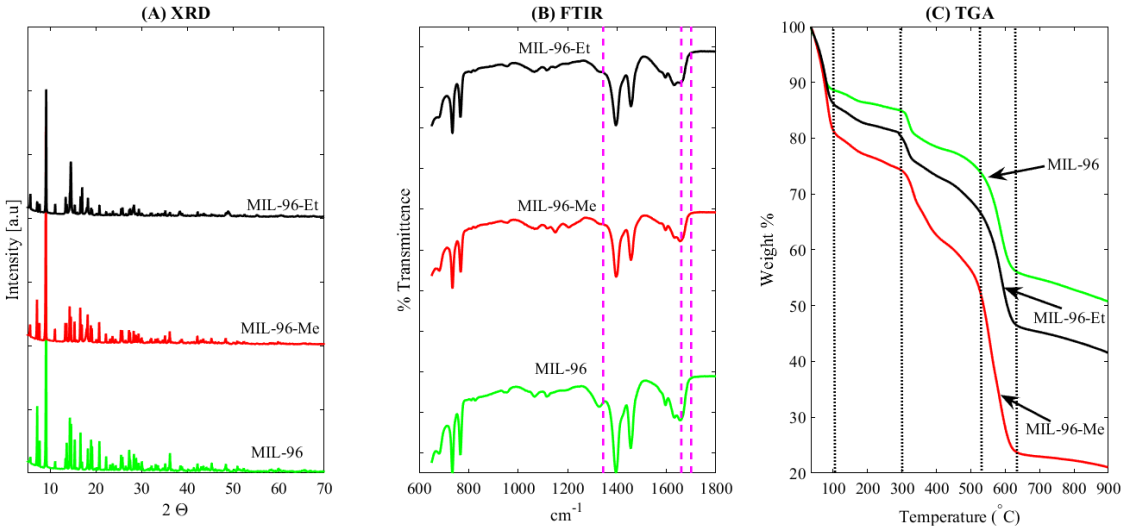

Figure 7-1. Characterization of synthesized MIL-96 samples; (A) XRD, (B) FTIR and (C) TGA.

FTIR spectra of all MIL-96 samples have the similar profiles except the peak at 1344 cm^{-1} displaying in MIL-96 spectrum, related to COO^- group (Figure 7-1B). The

spectra of MIL-96-Me and MIL-96-Et show a much attenuated peak, which may be attributed to the affinity of methanol and ethanol molecules to interact with carboxylic group of non-coordinated deprotonated BTC. The band at 1660-1700 cm^{-1} belongs to free BTC molecules, indicating they were present in the pores and not completely removed after the activation process because they could be connected by hydrogen bonds via their three carboxylic groups. In contrast, no peak at 1700 cm^{-1} occurs for completely deprotonating of BTC (Loiseau et al., 2006), suggesting that the BTC fully incorporated in the main structure. In addition, bridging hydroxyl group is shown at 1632 cm^{-1} and coordinated carboxylic group demonstrated as asymmetrically at 1595 cm^{-1} and symmetrically at 1456 and 1395 cm^{-1}. A distinct peak at 1400 cm^{-1} was related to C—O bond of carboxylic acid.(Abid et al., 2012c)

The weight loss profiles of three MIL-96 samples are shown in Figure1C. Based on the weight loss, BTC molecules are coordinated to aluminium ions in different weights% in the MIL-96 samples. The percentages of the coordinated organic linkers are 33%, 19% and 16% in MIL-96-Me, MIL-96-Et and MIL-96, respectively. Also, the ratios of non-coordinated BTC molecules in the samples are 10%, 3% and 2% in MIL-96-Me, MIL-96-Et and MIL-96, respectively. Therefore, MIL-96-Me exposed prominently in its interaction with BTC molecules inside the pores and in the synthesis reaction. The activation process by methanol can enhance the removal of non-connected BTC but it may not succeed to exchange the whole mass of methanol-water-BTC molecules.

Another significant effect of mixed solvents was observed in morphological properties. A hexagonal shape of crystal was obtained but the length of the crystal was changed. Figure 7-2 shows that MIL-96 presents the longest crystals while MIL-96-Et gives the shortest size. However, the crystal diameter can be measured to be 2.5, 3.5, 4.5 μm for MIL-96, MIL-96-Me and MIL-96-Et, respectively. Consequently, the aspect ratio (length/diameter) of MIL-96 was reduced with the additive of methanol (Yasue, 1984) and ethanol.(Zhang et al., 2014a)

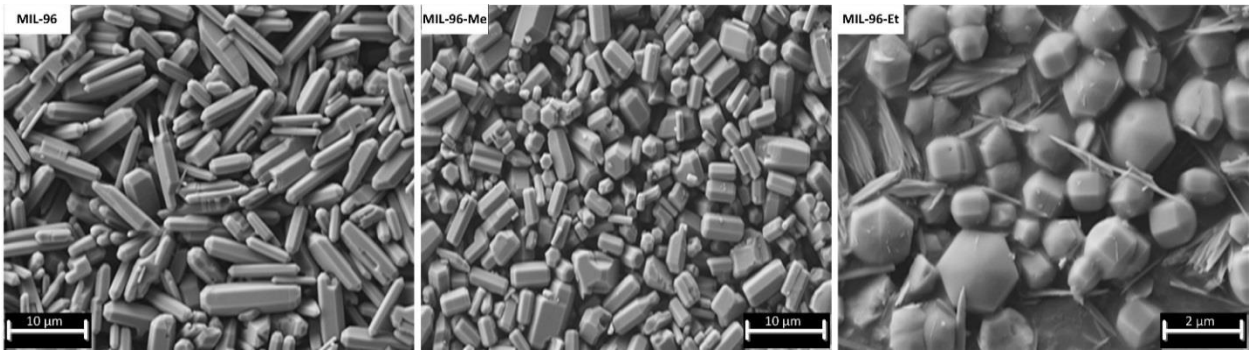

Figure 7-2 SEM images of MIL-96 samples.

N_2 adsorption/desorption isotherms are displayed in Figure 7-3A. All the isotherms present very long hysteresis loop of type H4, which depends upon the shape and size of pores (Thommes, Smarsly, Groenewolt, Ravikovitch, & Neimark, 2006). The hysteresis cycle in all the samples is closed at a relative pressure of 0.05 (Choi, Dincă, & Long, 2008). Figure3B shows microporous distributions of the samples. MIL-96-Me has the largest pore size at 0.82 nm with 55% of its pore volume, while MIL-96 shows the smallest pore size at 0.46 nm with 66.6% of the total pore volume. Moreover, mesopore size distribution using Barrett-Joyner-Halenda (BJH) method is shown in Figure 7-3C. A peak of pore size is at 2.4, 2.18 and 2.0 nm for MIL-96, MIL-96-Et, and MIL-96-Me respectively.

The textural properties of three samples are given in Table 7-1. The specific surface area (S_{BET}) was 695 m^2/g for MIL-96-Me, 687 m^2/g for MIL-96 and 665 m^2/g for MIL-96-Et. It is seen that the textural properties can be retained despite of the morphological change of MIL-96 samples with different solvents. Such morphological changes may be helpful in some other applications such as membrane applications (Knebel et al., 2016).

Table 7-1 Textural properties of MIL-96 samples.

Adsorbents	BET surface area (m^2/g)	Pore volume cm^3/g	Average pore size (nm)	Average mesopore size (nm)
MIL-96	687	0.26	0.46	2.40
MIL-96-Et	665	0.27	0.51	2.18
MIL-96-Me	695	0.33	0.82	2.0

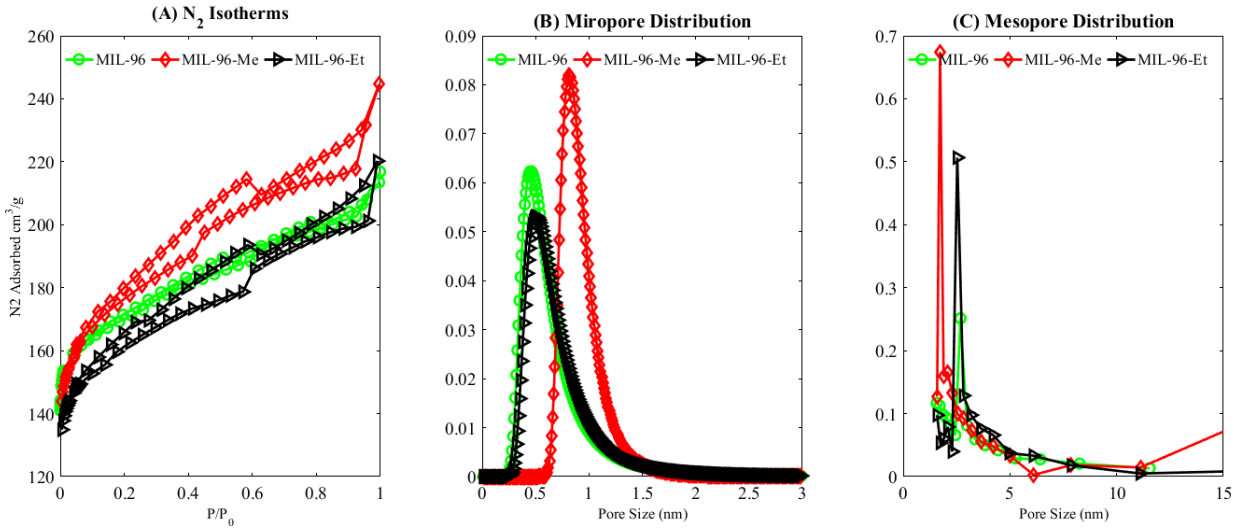

Figure 7-3 N_2 adsorption-desorption isotherms and pore size distributions; (A) N_2 adsorption-desorption isotherms, (B) Micropore size distribution and (c) Mesopore size distribution.

7.3.2 Adsorption of CO2 and N_2 and their selectitvity analysis

Figure 7-4A shows adsorption of CO_2 and N_2 on three MIL-96 samples. MIL-96-Et and MIL-96-Me presented a higher CO_2 adsorption capacity compared to MIL-96 at 25 °C. At 1 atm, CO_2 adsorption capacities were 115 and 110 cc/g on MIL-96-Et and MIL-96-Me, respectively, while the adsorption capacity is 96 cc/g on MIL-96. The adsorption capacities of MIL-96 samples are significantly higher than those of MIL-

96 previously published by Loiseau et al. (Loiseau et al., 2006), Mishra et al. (Mishra, Uppara, Mandal, & Gumma, 2014) and other researchers.(Liu, Thallapally, McGrail, Brown, & Liu, 2012)

For N_2 adsorption (Figure 7-4B), three MIL-96 samples show significantly lower adsorption compared to CO_2 adsorption. In general, the adsorption of MIL-96, MIL-96-Me and MIL-96-Et shows an order of MIL-96-Et > MIL-96 > MIL-96-Me. Figure 7-4C displays the separation factor of the three MIL-96 samples. It seems that MIL-96-Et demonstrates the lowest selectivity due high adsorption of both nitrogen and CO_2. MIL-196-Me and MIL-96 have a comparable separating factor for CO_2 and N_2. At 1 atm, MIL-196-Me exhibits a higher separating factor than MIL-96.

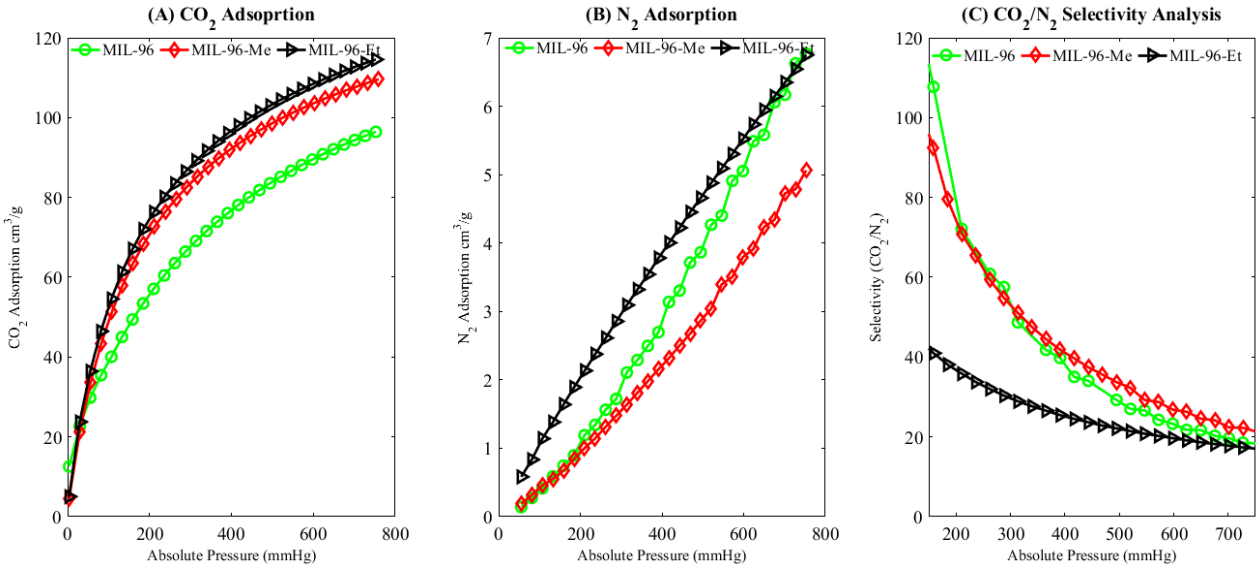

Figure 7-4 Adsorption of CO_2 and N_2 on MIL-96 samples and separation factors at varying pressures. The measurement temperature is 25 °C.

7.3.3 Adsorption of p-HBA

After CO_2 and N_2 adsorption tests, those MIL-96 samples were heat-treated for desorption and then further tested for liquid-phase adsorption to remove p-HBA. Figure 7-5 illustrates the dynamic adsorption of p-HBA on three MIL-96 at varying time. There is no big difference in achieving equilibrium for all the three MIL-96 samples and the equilibrium was established in almost 15 min, suggesting much less

resistance of p-HBA molecules in transport from bulk solution to the surface and pores of MOF samples.(Azhar et al., 2016; Thomas & Kelley, 2010) The similar dynamic adsorption is probably due to the similar textural structure of the materials. The fast equilibrium makes these materials very useful in large-scale practical applications.

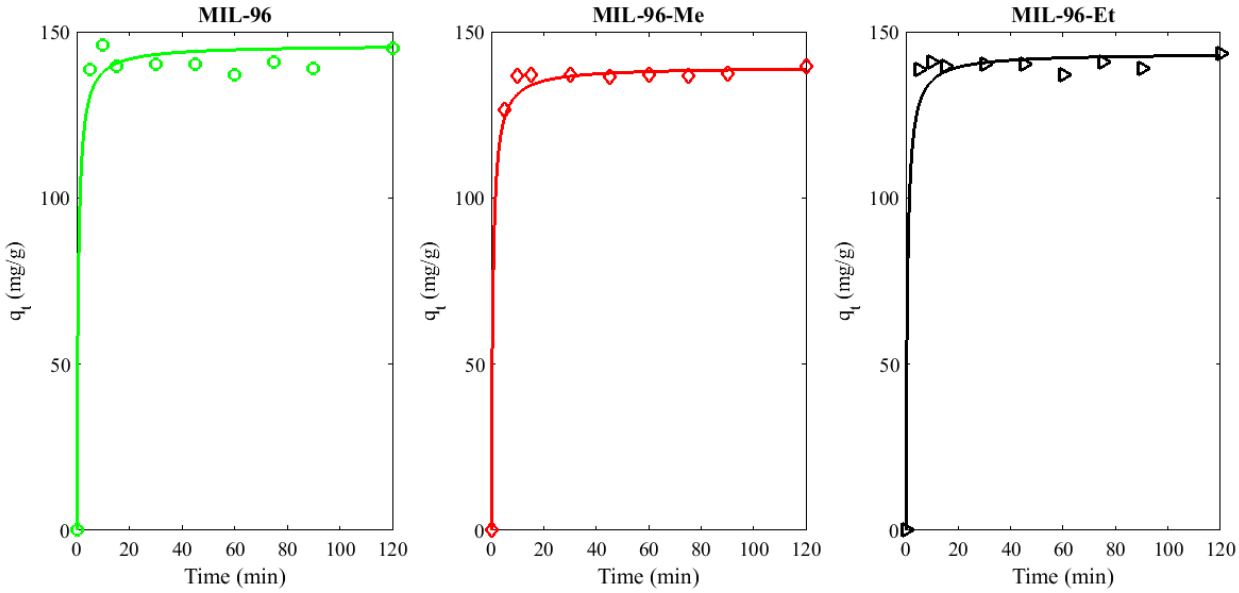

Figure 7-5 Effect of time on p-HBA adsorption on MIL-96 samples at 25 °C, initial concentration of p-HBA is 30 mg/L

It was revealed that adsorption takes place inside the pores of MIL-96s, evidencing from the changes in textural properties of used samples. Figure 7-6 shows N_2 adsorption-desorption isotherms of the p-HBA used samples. BET surface areas of used samples are just 35, 12 and 32 m^2/g for MIL-96, MIL-Me and MIL-96-Et, far less than the surface area of fresh samples. So, the lower surface area of used samples indicates pore filling mechanism of MIL-96 samples.

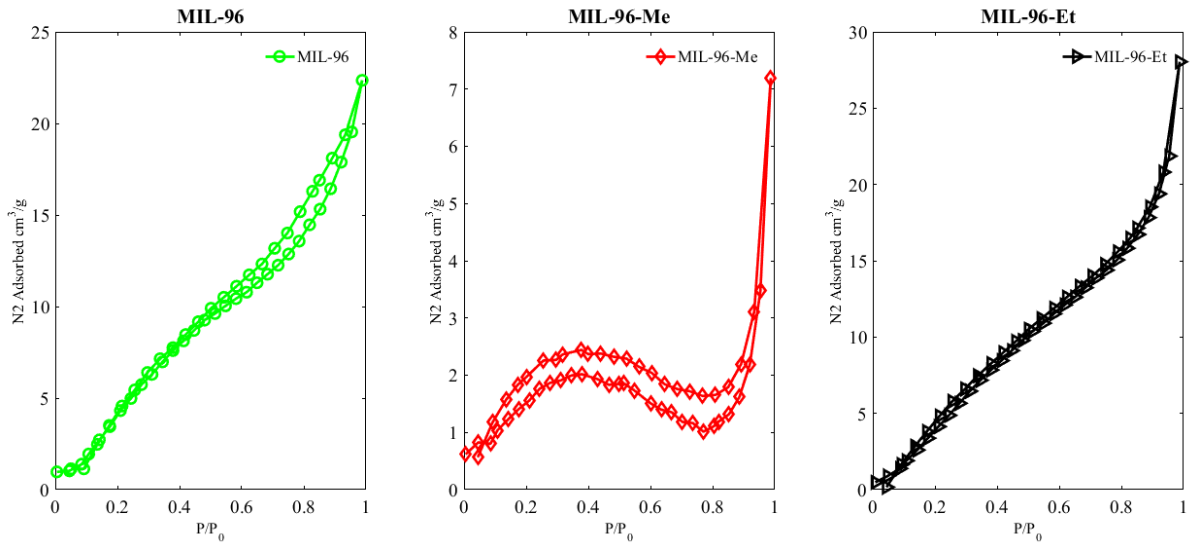

Figure 7-6 N_2 adsorption-desorption isotherms of MIL-96 samples after p-HBA adsorption.

The dimensions (1.85 × 0.52 × 0.63 nm) of p-HBA molecules are comparable or even less than the size of pores in MIL-96 MOFs, which facilitate the incorporation of these adsorbate molecules inside the pores (Heath, Singh, & Ebisuzaki, 1992; Hsieh, Su, Chen, Liou, & Lu, 2005; Nsangou, Dhaouadi, Jaidane, & Ben Lakhdar, 2008).

However, the crystalline structure of used samples remain intact as XRD patterns of used samples are similar to those of fresh MIL-96 (Figure 7-7). XRD of p-HBA adsorbed samples indicate that crystalline MIL-96 (all three samples) are stable in aqueous media. To further investigate any degradation of MOFs, ICP-OES was used to investigate Al^{3+} leaching into water. The highest leaching of Al was observed for MIL-96-Me while it was the lowest for MIL-96-Et at pH 4.5 (Table 7.3). Guest solvent molecules into the structure of MIL-96-Me can contribute in weakening the structural strength. On the contrary, this behaviour was far less common for MIL-96-Et.

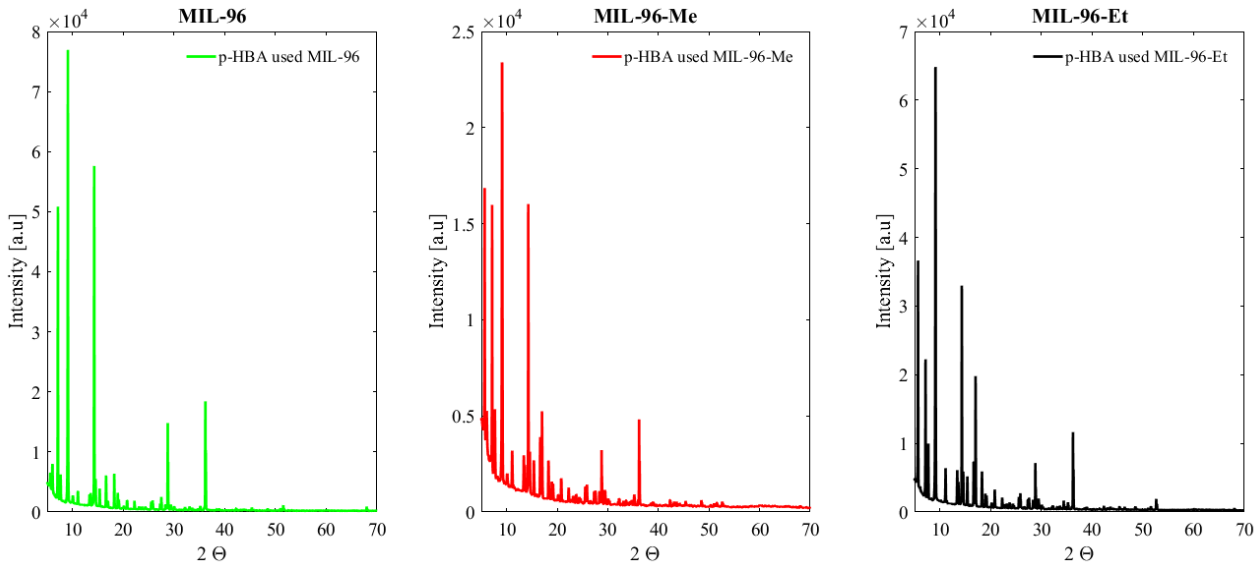

Figure 7-7 XRD pattern of MIL-96 samples after p-HBA adsorption

The adsorption isotherms of p-HBA are presented in Figure 7-8. The adsorption capacity increases with increased equilibrium concentration (C_e) of p-HBA. High adsorption of p-HBA is a result of increased number of molecules of p-HBA readily available for adsorption. It was interesting to observe that adsorption capacity was very high, i.e. 400 - 500 mg/g p-HBA at 25 °C for all three samples. Two adsorption isotherm models, Freundlich and Langmuir (Freundlich, 1906b; Langmuir, 1918), were fitted to the data (Langmuir model data not shown). It is clear from curve fitting that the data are best fitted by Freundlich model (Figure 7-9) and the parametric values are given in Table 7-2.

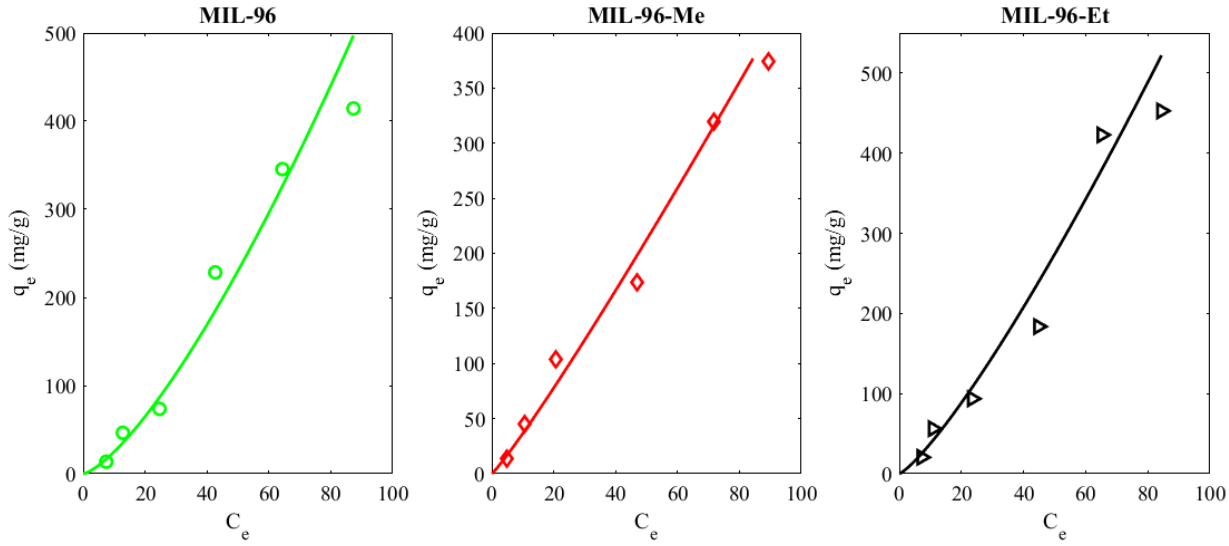

Figure 7-8 Adsorption of p-HBA on MIL-96 samples scattered points indicate experimental values and solid lines show calculated values from Freundlich isotherm at 25 °C

There is a marginal decrease in adsorption capacity of MIL-96 compared to MIL-96-Me. MIL-96-Et has the highest adsorption capacity. The decreased adsorption on MIL-96-Me could be due to lower surface area and the presence of guest molecules as shown in FTIR spectra (Figure 7-1B).

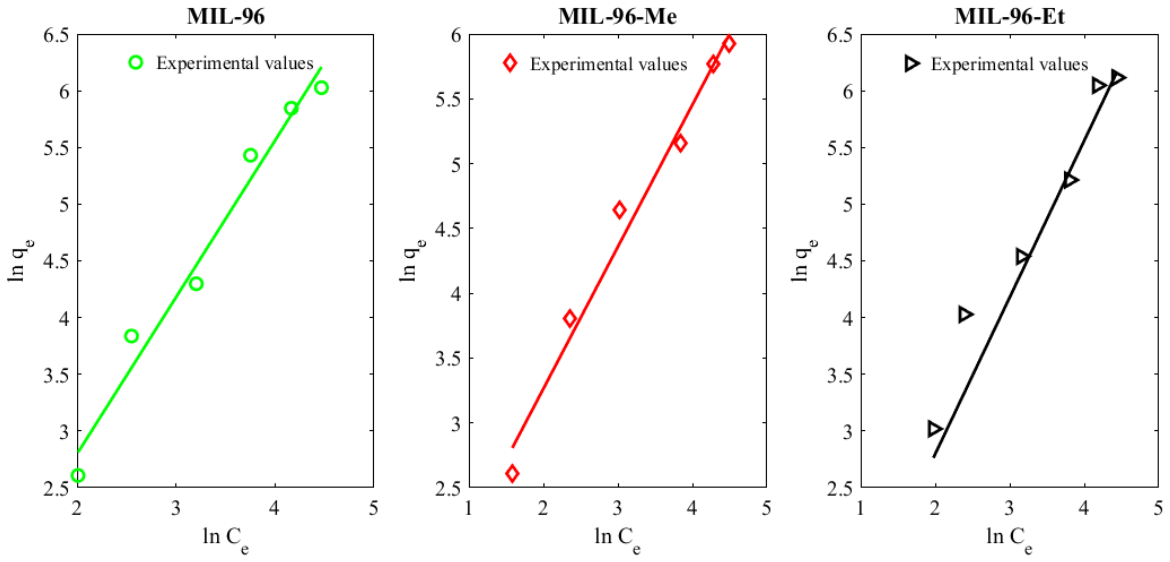

Figure 7-9 Freundlich isotherm of p-HBA adsorption on MIL-96.

Table 7-2 Experimental and calculated values of adsorption capacity with Freundlich isotherm.

MOFs	$q_{e,\ exp}$ (mg/g)	$q_{e,cal}$ (mg/g)	n	K_F	R^2
MIL-96	414	497	0.72	1.03	0.947
MIL-96-Me	375	401	0.91	2.92	0.982
MIL-96-Et	453	521	0.81	2.20	0.969

7.3.4 Effect of pH on p-HBA adsorption and removal mechanism

Adsorption mechanism can be explained with the help of characteristics of adsorbate, adsorbent and their interaction in the solution. Generally, electrostatic attraction, hydrogen bonding, hydrophobic interaction and π-π interactions have been reported.(Azhar et al., 2017a; Azhar et al., 2016; Chun et al., 2014). Effect of initial pH was studied to propose plausible adsorption mechanism of p-HBA adsorption in pH 2.5 – 10.5 range (Figure 7-10). It can be seen that adsorption capacity decreases with increasing pH. An important factor in governing adsorption process is surface charge of the adsorbent at a specific pH of solution.(Azhar et al., 2017a) For MIL-96, Zeta potential decreases with increasing pH from 2.5 – 10.5 and the point of zero charge (pH_{pzc}) is pH 9.3 ± 0.2 (Figure 7-11).

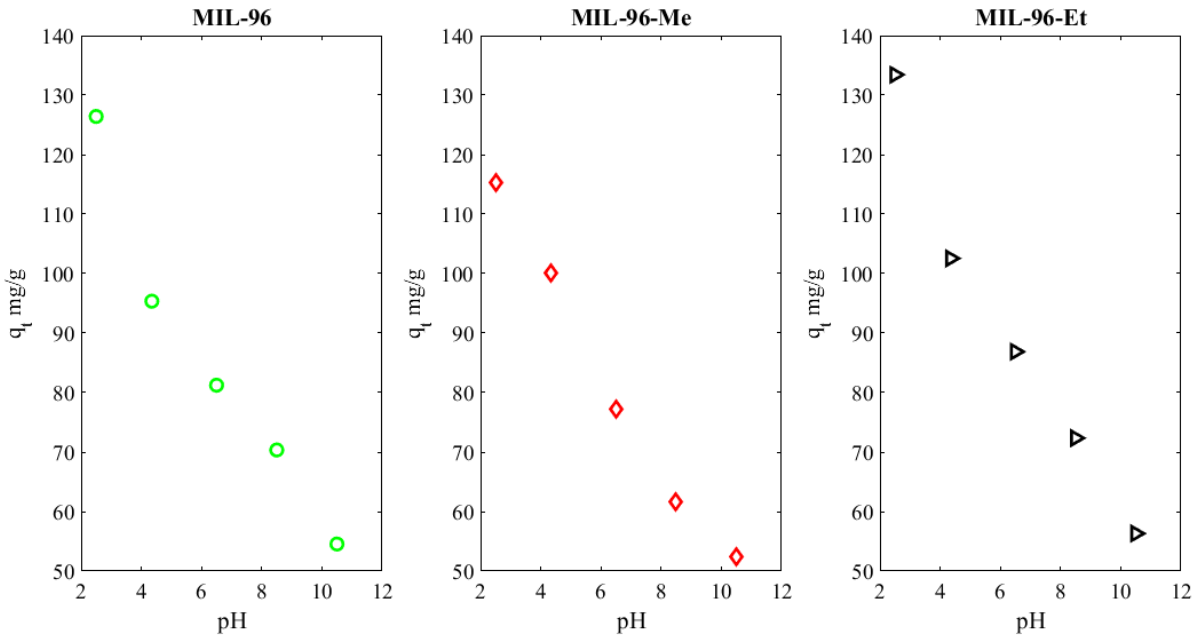

Figure 7-10 Effect of initial pH of p-HBA solution on adsorption, C0 = 25 mg/L, adsorbent dosage = 0.1 g/L and operating temperature =25 °C

At higher pH, p-HBA might become anionic by losing proton from carboxylic group (pKa_{COOH}, pKa_{OH} at 4.5 and 9.1, respectively). Generally, deprotonation of COOH takes place for p-HBA (Schroder et al., 2012) at higher pH levels while MIL-96 presents less positive surface charge, resulting in reduced electrostatic attraction between MIL-96 and p-HBA.

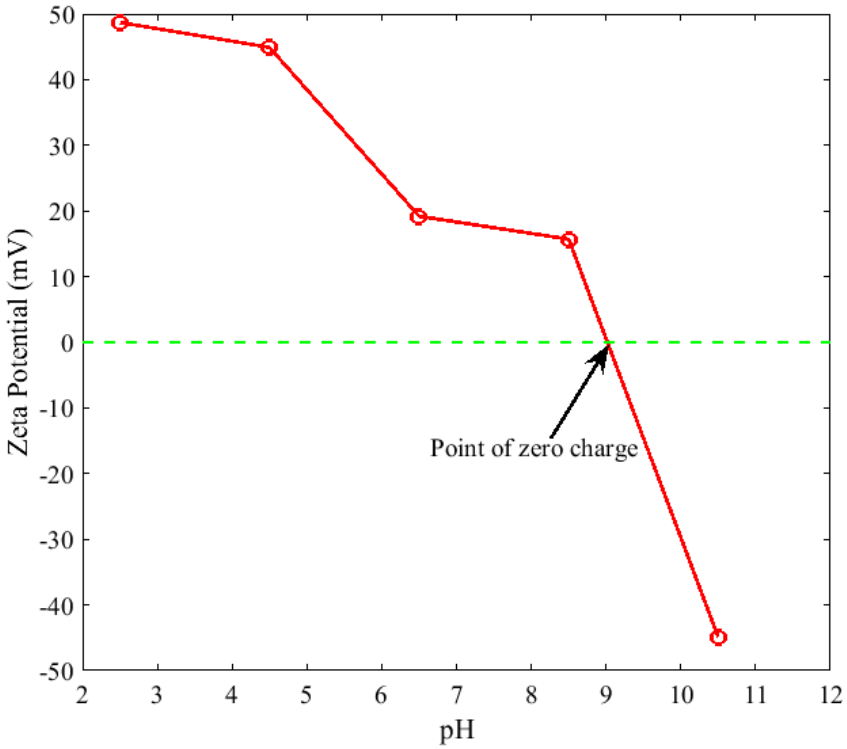

Figure 7-11 Effect of initial pH on zeta potential of MIL-96.

In adsorption experiments, initial pH of p-HBA solution was 4.35 ± 0.2, and a dynamic equilibrium between deprotonated and molecular forms of p-HBA occurs (Figure 7-12A). This equilibrium can be shifted to either side by supplying excess H^+ (HCl) or OH^- (NaOH) ions into solution. With addition of HCl to reduce solution pH to 2.5, excess of H^+ ions and more p-HBA molecules in the solution are generated. The positive surface charge of MIL-96 at this pH will not play an important role in the higher p-HBA adsorption, but increased hydrophobicity of p-HBA in its molecular form will play be the key for enhanced adsorption (Figure 7-12B). On the contrary, addition of NaOH to adjust pH to 6.5 and up to pH 10.5 will provide more HO^- and Na^+ ions to make more p-HBA^- and p-HBA-Na (Figure 7-12C), resulting in a decreased adsorption capacity on negatively charged MIL-96 at much high pH.

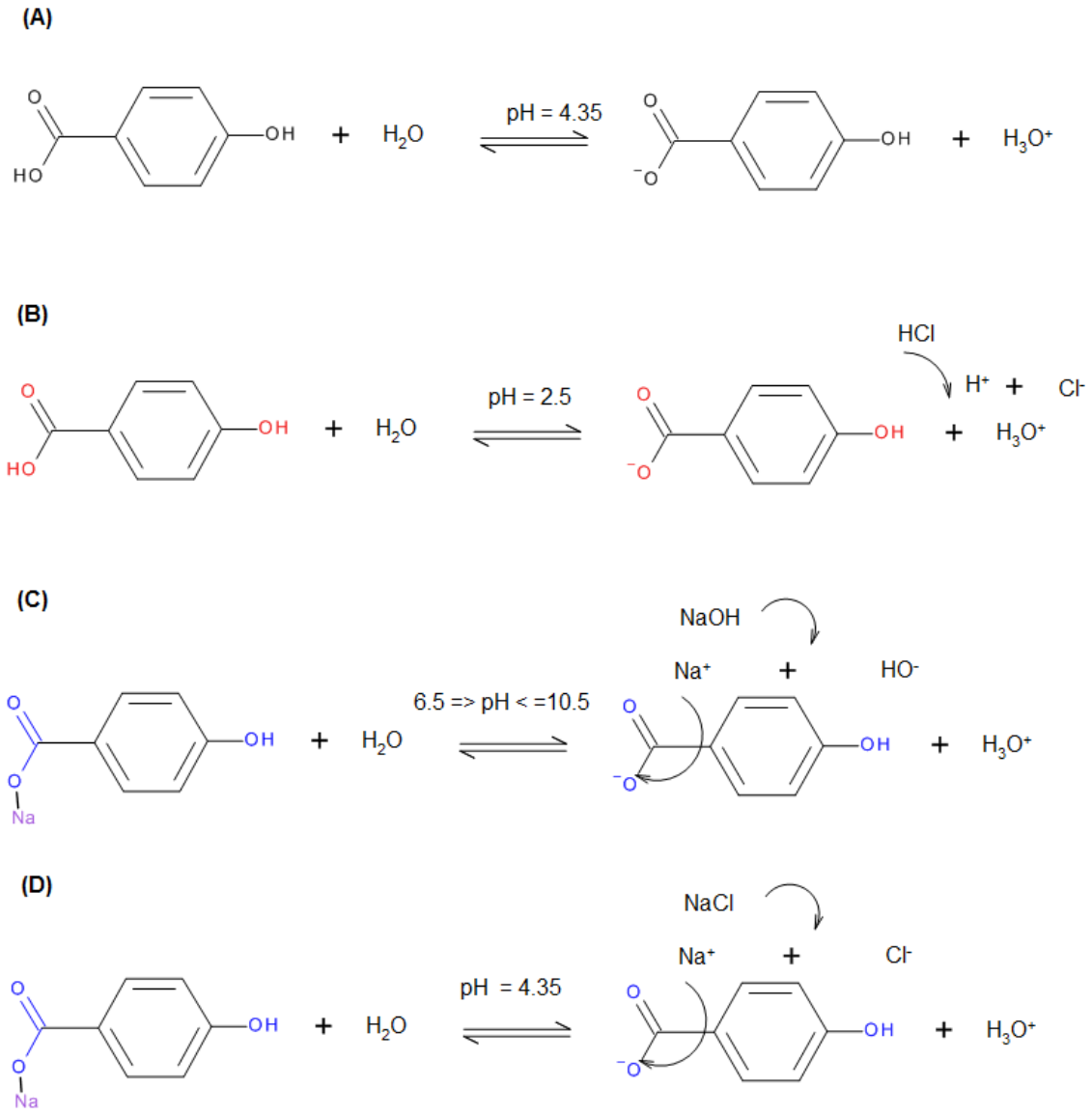

Figure 7-12 Schematic representation of p-HBA transformation due to external ions.

This phenomenon was further verified by addition of 0.1 M NaCl in p-HBA at initial pH 4.35 (Figure 7-12D.) It was observed that the adsorption capacity was reduced from 100 mg/g to 68 mg/g on MIL-96, suggesting the p-HBA-Na formation to lower the adsorption capacity. Another contribution to the decreased adsorption capacity at higher pH might be the competitive adsorption of ^{-}OH with adsorbate molecules on active adsorption sites.(Chen et al., 2016b)

In addition, both hydrogens from COOH and OH in p-HBA molecules may also take part in formation of hydrogen bonds with structural OH of MIL-96, which has been

reported in p-HBA interaction with hydroxide rich adsorbates(Heath et al., 1992) and MOFs adsorbents.(Ahmed & Jhung, 2017; Song & Jhung, 2017)

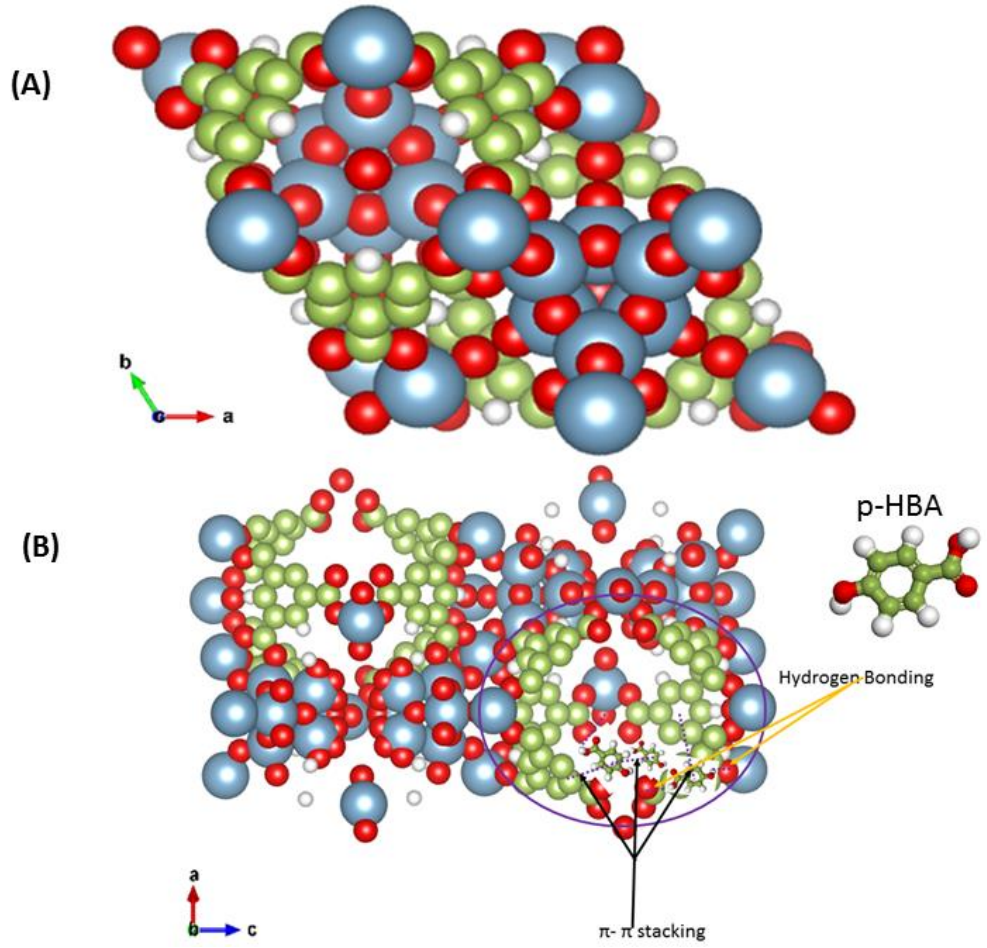

Figure 7-13 Structure of MIL-96 (A) and plausible adsorption mechanism for adsorption of p-HBA on MIL-96 samples (B); colours; light cyan: aluminium, light green: carbon, red: oxygen and white: hydrogen

Mainly, MIL-96 consists of two moieties, i.e. inorganic and organic, which are arranged to form a 3D structure. In the 3D structure of MIL-96 (Figure 7-13), isolated trinuclear μ_3-oxo-bridged aluminium clusters and 2D infinite chains of $AlO_4(OH)_2$ octahedra are connected to a 18 membered ring to form a hexagonal network, $Al_{12}O(OH)_{18}(H_2O)_3(Al_2(OH)_4)[btc]_6.24H_2O$ with a compact packing of cavities(Loiseau et al., 2006). There are two types of cavities in MIL-96. One is delimited by two trinuclear aluminium units along c axis connected to 18-membered ring (a,b) plane via 6 btc ligands to create a cavity of approximately 0.88 nm based

on ionic radius of oxygen, i.e. 0.135 nm (estimated pore volume 0.417 nm^3) and also having one water molecule. The other cavity is delimited by three turmeric μ_3-oxo-bridged aluminium clusters connected to two triangular units composed of aluminium octahedra via six btc species having a volume of 0.636 nm^3. Both cavities can have guest molecules upon adsorption and the coverage of cavities by the guest adsorbate with benzene rich btc can give rise to π-π stacking of p-HBA molecules.

Therefore, pH_{pzc} of MIL-96 and the effect of pH tests suggests that electrostatic interactions between p-HBA and MIL-96 will play a major role in p-HBA adsorption on MIL-96. In addition, chemical structures of p-HBA and MIL-96 also imply that hydrophobicity, hydrogen bonding and π-π stacking will also be involved in the adsorption.

Moreover, in checking the stability of MIL-96 at varying pH conditions, ICP-OES tests were further conducted for these MOFs after adsorption of p-HBA at different pHs (Table 7-3).

Table 7-3 Effect of pH on Al^{+3} leaching in p-HBA adsorption tests.

Samples		**Initial pH**				
		2.5	**4.5**	**6.5**	**8.5**	**10.5**
MIL-96	Al^{+3} leaching (mg/L)	1.14	0.852	0.643	0.495	0.943
MIL-96-Me		9.19	2.491	1.351	2.48	5.532
MIL-96-Et		0.601	0.511	0.291	0.266	2.286

The highest leaching of Al^{3+} (10 mg/L) occurred in a strong acidic solution at pH 2.5 and the least (0.3 mg/L) is near neutral pH 6.5. The Al^{3+} leaching was below threshold limits of Al^{3+} discharge into wastewater (100 mg/L) in Australia(2017), making it a promising material for large applications. Moreover, MIL-96-Me had higher discharge of Al^{+3} in solution, probably due to high amount of unreacted BTC molecules in its synthesis, giving rise to loosely attach Al^{+3} ions in the structure. Still, it was observed that BET surface area was decreased significantly after p-HBA adsorption.

7.3.5 Generated metal/metal oxide/C composite for catalytic degradation of contaminants

In order to further explore the reuse of MIL-96 samples after liquid adsorption, the used samples were carbonized to get Al-Al_2O_3/C composites which were further tested for catalytic dye degradation, particularly, methyl orange which is an anionic dye. XRD and SEM results of Al_2O_3/C composites are given in Figure 7-14 and 7-15, respectively. It can be seen from Figure 7-14 that most of XRD peaks are disappeared after carbonization at 750 °C while SEM images show the similar morphology to parent MIL-96. Moreover, higher magnification SEM (Figure 7-15) shows thinner crystal suggesting regular transformation of MOF into Al_2O_3/C composite. Such a transformation can help in tailoring core-shell structures from MOFs (Liu, Dai, Liu, Liu, & Liu, 2015a). Moreover, XPS spectra (Figure 7-16) were obtained to confirm Al-Al_2O_3/C composite. It can be seen clearly that distinct peaks of carbon, oxygen and Al are present in the survey spectra. There are two distinct peaks of Al, i.e. Al 2p and Al 2s in Figure 7-16. Some of Al can be present in a metallic form with a peak at 71.4 eV, however, the high intensity peak at 116.0 eV suggests conversion of Al_4OH_3 nodes into Al and Al_2O_3 composited with C of BTC linkers (Davies, Roberts, & Shukla, 1991; Turner & Single, 1990). The bonds can be broken in the presence of air, however, in N_2 the BTC linker converts to carbon. Peak fitting suggests that C 1s can be further deconvoluted into C=O and C-C from BTC linkers (Indrawirawan, Sun, Duan, & Wang, 2015b). From O 1s and Al 2p, it can be verified that the used MIL-96 sample was successfully transformed to Al-Al_2O_3/C composite. Since, Al_2O_3 has been successfully used as a catalyst support, which can help incorporation of other transition metals for catalytic reactions (Wang et al., 2017). It will be interesting to study effect of different phases of alumina on catalytic performance. This is an ongoing work and results will be presented in our future studies.

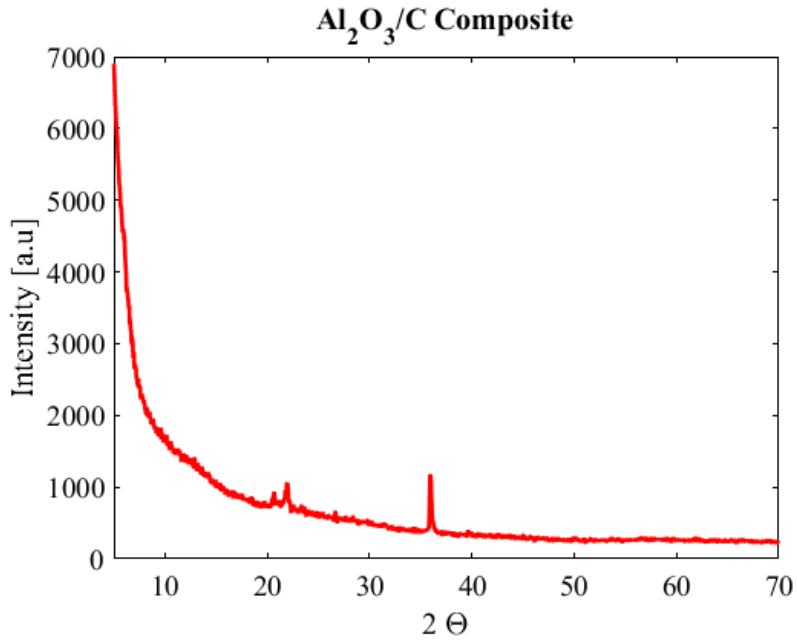

Figure 7-14 XRD profiles of Al2O3/C composite from MIL-96 after p-HBA adsorption.

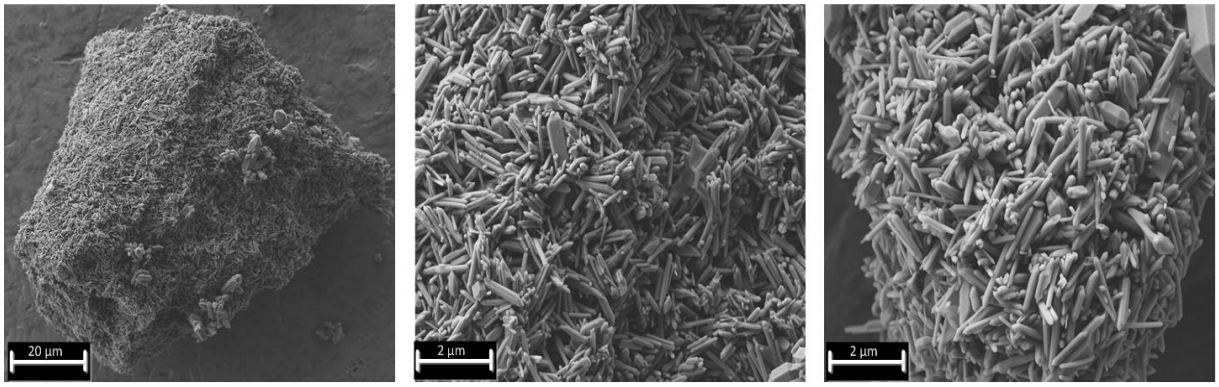

Figure 7-15 Low and high magnification SEM images of Al2O3/C composite derived from MIL-96 after p-HBA adsorption.

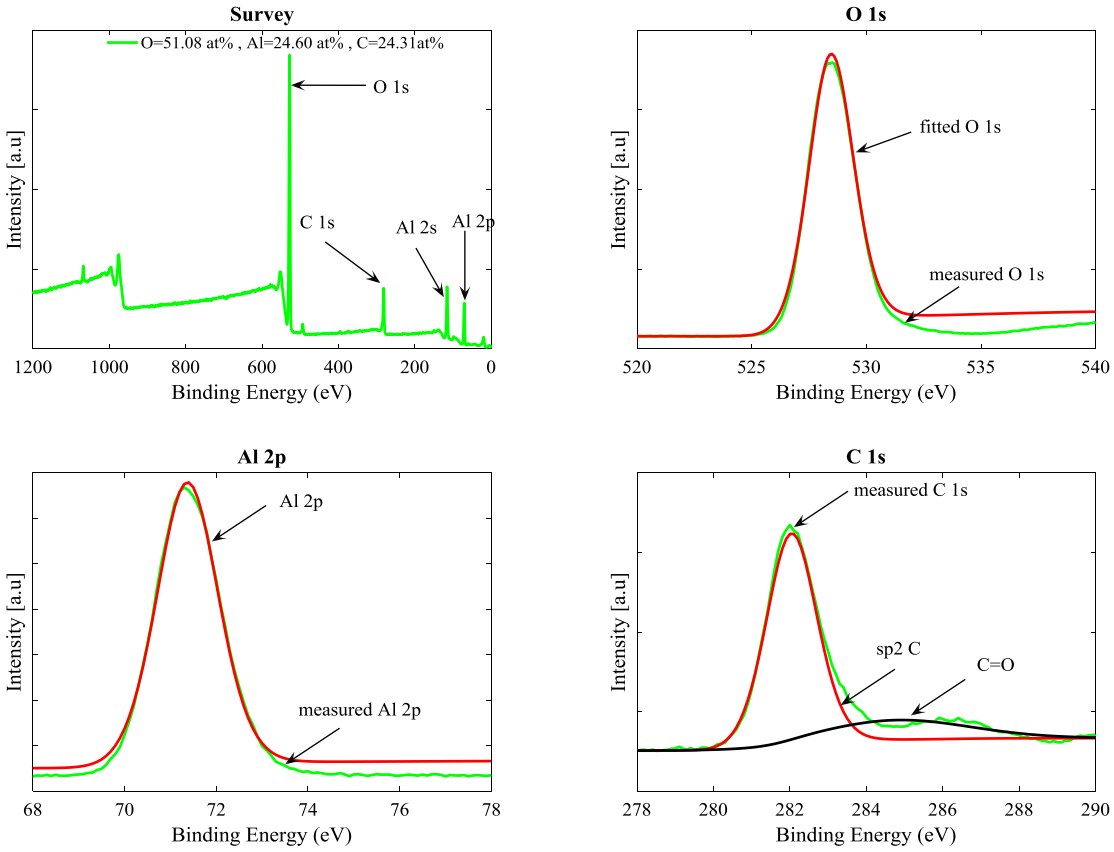

Figure 7-16 XPS spectra of p-HBA used carbonized MIL-96.

In the catalytic test, there was no adsorption of MO on Al-Al_2O_3/C, however, it was very interesting to report that MIL-96 derived Al-Al_2O_3/C composites could easily activate PMS to degrade MO in just 15 min (Figure 7-17). Further, very small amount of MO was degraded by PMS only (Liang et al., 2017; Yao et al., 2016; Zhang, Zhao, & Lian, 2014b). This signifies large scale application of these robust MOFs in various applications starting from gas phase adsorption for CO_2 mitigation and storage, for removal of personal care products and degradation of dyes. A detailed study on investigation of dyes degradation with Al_2O_3/C and other MOFs derived metal-oxide/C composites will be reported in future study.

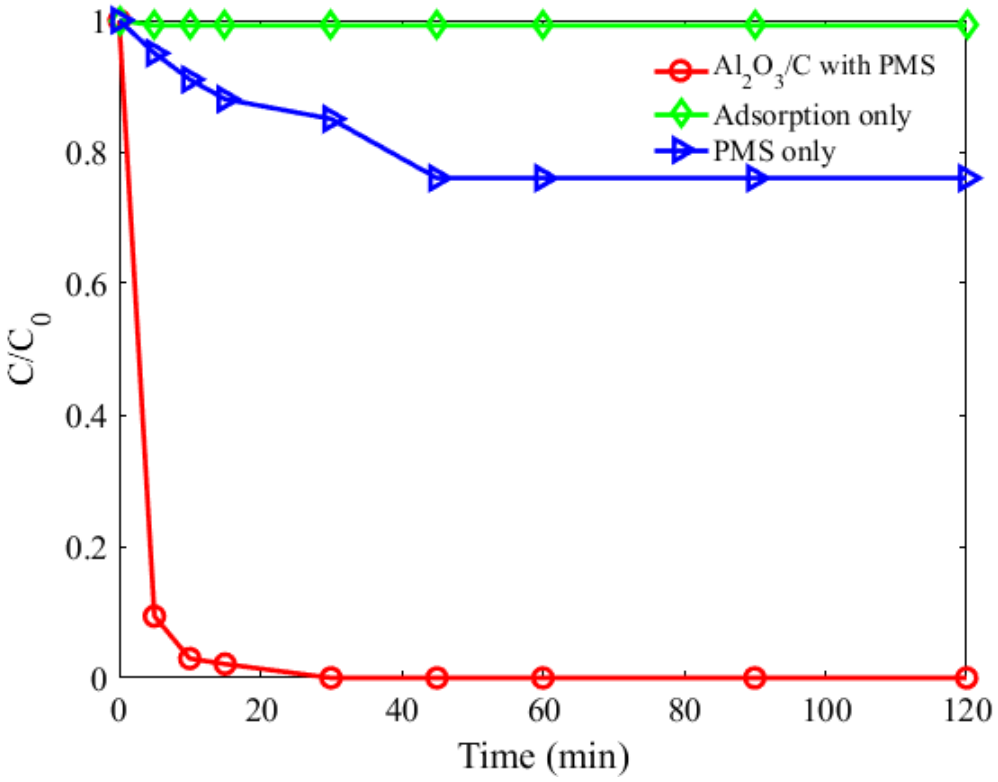

Figure 7-17 Adsorption and catalytic degradation of MO on MIL-96 derived Al2O3/C composite, C0 = 20 mg/L, PMS =0.81 mM and Al2O3/C = 0.05 g/L at 25 °C

7.4 Conclusion

MIL-96 samples were synthesized using ethanol and methanol as modulators and tested for a proof of concept in a cascade application in gas adsorption and separation, liquid pollutant removal and catalytic degradation. It was found that modulation can reduce the particle size and improve CO_2 adsorption. There were no changes in terms of textural properties in CO_2 used samples and the materials could be regenerated by simple heating to remove adsorbed gas for liquid phase adsorption of p-HBA. Maximum adsorption of p-HBA was reported as high as 521 mg/g on MIL-96-Et. A plausible adsorption mechanism of p-HBA was proposed based on pore-filling, functional groups of MIL-96 and solution chemistry of p-HBA. Furthermore, the used samples after liquid phase adsorption were carbonized to yield a Al_2O_3/C composite for further testing in catalytic degradation of MO. Complete

degradation of MO was achieved in just 15 min with PMS, demonstrating excellent performance of the composite in catalysis. The recycling use of MOF-96 in gas-phase adsorption, liquid-phase adsorption and then catalysis provides an effective strategy for cascade application of a material for transformation and application without being disposal of an expensive hybrid as a solid waste after each use.

Chapter 8 Facile synthesis of mesoporous carbon nanospheres for wastewater treatment; A pathway towards sustainable processes

8.1 Introduction

Water contaminants have been on the rise due to rapid urbanization and industrialization in the modern world. Conventional contaminants range from dyes, metal ions, to other aromatic compounds (Che & Liu, 2014; Holland, Luck, & Max Finlayson, 2015; Huston, Chan, Chapman, Gardner, & Shaw, 2012; Pal, He, Jekel, Reinhard, & Gin, 2014). Recently, some of chemicals as a potential threat to marine life are declared as contaminants of emerging concerns (Petrie, Barden, & Kasprzyk-Hordern, 2015). A few examples of these chemicals are antibiotics, pharmaceuticals and personal care products. Being one of the largest industries in the world, personal care products are posing serious threats to water bodies and acting as a source of parabens, a major constituent of cosmetics, cigarettes, food products and toys. Para-hydroxybenzoic acid (p-HBA) is a main building block of parabens and found in wastewater due to its persistent nature (Wang & Kannan, 2016). Various studies have been reported on removal of p-HBA through adsorption and/or catalytic degradation (Wang et al., 2016c; Wu & Fang, 2003). Adsorption using carbon based materials is a facile technique for the removal of water contaminants without posing serious threats of metal leaching into water bodies. High adsorption capacity and complete removal of water contaminants are major criteria to select adsorbents for a large scale application (Azhar et al., 2016).

Carbon based materials have attracted attention of researchers owing to benign nature of the process, since they do not pose any risk of secondary pollutants into water bodies by leaching of metal ions from metallic adsorbents/catalysts. Other benefits of metal free processes include low cost operation and easy regeneration of materials. Hence, carbon based materials are becoming one of the most efficient materials of waste mitigation in wastewater treatment processes (Duan, Indrawirawan, Sun, & Wang, 2015a; Duan et al., 2017a; Indrawirawan et al., 2015b; Sun, Zhou, Wang, Suvorova, & Wang, 2014b).

Recently, mesoporous carbons have gained popularity due to diversity of applications in imperative fields of modern life such as energy storage, hydrogen

storage, and wastewater treatment processes (Dutta, Bhaumik, & Wu, 2014; Kowalczyk et al., 2017; Ma, Liu, & Yuan, 2013; Otero et al., 2014; Tsai & Doong, 2015). In today's time, a focal point of research on carbon materials is the tuning of textural properties with ordered mesopores for customized applications such as adsorption, drug delivery and fuel cells. Without a doubt, microporous amorphous activated carbons have resulted in useful applications such as adsorption both in liquid and gas phases in the past and even in modern era (Goglio, Foy, & Demazeau, 2008; Jin, Tanaka, Egashira, & Nishiyama, 2010; Liu et al., 2014b; Mitome et al., 2013; Wang & Kaskel, 2012). However, in case of ordered mesoporous carbons (OMCs), the incorporation of nitrogen, sulphur species and/or transition metals into frameworks of OMCs could alter the characteristics of carbon and improve their performance in some capacitive, adsorptive, and catalytic applications (Dong, Zhang, Pan, & Qiu, 2014; Indrawirawan et al., 2015b; Liu et al., 2017; Tian, Zhang, Sun, Tadé, & Wang, 2017; Wang et al., 2014b).

Traditionally, porous carbons were prepared by hard template assisted processes where silica was used as a structure directing agent. However, removal of the hard template through toxic reagents such as hydrogen fluoride not only is dangerous but also involves various steps to achieve final product (Perazzolo et al., 2015; Tian, Duan, Shen, Xie, & Guo, 2017; Tian & Snyder, 2014). Therefore, soft templating processes using poly(ethylene oxide)–poly(propylene oxide)–poly(ethylene oxide) triblock copolymer ($EO_{106}PO_{70}EO_{106}$; Pluronic F127) under acidic conditions were introduced to achieve mesoporous carbons in a benign way compared to hard template methods (Jin, Mitome, Egashira, & Nishiyama, 2011; Liang & Dai, 2006; Wang et al., 2014c).

Phase separation and evaporation induced self-assembly (EISA) are two common methods used for preparation of high surface area carbons (Duan et al., 2017b; Górka, Fenning, & Jaroniec, 2009; Wang et al., 2011). The limitation of phase separation is poor control of textural properties in terms of pore volume and pore size distribution. In comparison, EISA results in tuneable synthesis of carbons with narrow pore size distribution and large pore volumes. Phenol-formaldehyde (PF), resorcinol-formaldehyde (RF) and phloroglucinol-formaldehyde (PhF) schemes are usual methods to synthesize mesoporous carbons (Górka et al., 2009; Wang et al., 2014c). Incorporation of heteroatom/s in carbon skeleton enhances functionalities of

carbon materials, which is very useful for energy storage and catalysis. However, the introduction of heteroatoms deteriorates surface area and regularity of pore size distribution (PSD). Moreover, long synthesis time due to solvent evaporation is also a limiting factor in EISA. Another debatable factor is whether formation mesoporous contents from cross linkage is due to slow evaporation of solvents and/or induced by thermal curing/theropolymerizating step (Dong et al., 2014; Liu et al., 2014b; Lopez-Salas et al., 2014; Song, Zhang, & Liu, 2015; Zhu et al., 2015). Schuster et al. reported that mesoporous structure is induced in thermopolymerization contrary to evaporation (Schuster et al., 2012).

There are various studies on individual topics such as adsorption and catalytic degradation of water contaminants, however, few studies are devoted to explore effectiveness of carbon nanomaterials in exploring multiple applications by introducing guest (adsorbate) molecules to induce active sites for catalytic degradation and/or other applications. In the present study, micro/mesoporous carbons were prepared by EISA at elevated temperatures for simultaneous solvent evaporation and mesopore formation through curing. This can reduce the time to form polymeric resin for carbonization and enhance efficiency of synthesis process. Two different temperatures (80 and 120 °C) were selected to prepare mesoporous carbons. Both evaporation temperatures resulted in very high surface area (800 m^2/g). Further, mesoporous carbons successfully removed organic by adsorption for p-HBA and organic dyes while regenerated adsorbent was used in catalytic degradation of phenol. Moreover, the used catalyst was further tested in adsorption of p-HBA, showing a high adsorption capacity. This provides details on adsorptive and catalytic properties of carbon nanospheres in multiple applications without generating secondary pollutants and/or solid waste.

8.2 Experimental

8.2.1 Synthesis of Carbon Nanospheres

Resorcinol, formaldehyde, ethanol, hydrochloric acid (HCl) and Pluronic F127 ($EO_{106}PO_{70}EO_{106}$) were sourced from Sigma-Aldrich, Australia and used without

further purification. Ultrapure water was prepared by a water purifying system (Agilan Technology) in our laboratory with 15 mΩ resistance.

A soft template assisted approach was adopted to synthesize high surface area carbons. In a typical synthesis, resorcinol was used as a carbon precursor, F127 as a template, HCl as a catalyst and formaldehyde as a polymerizing agent. Specifically, in each run, 1.1 g of resorcinol was dissolved in 4.5 mL of absolute ethanol while 1.1 g of F127 was dissolved in 11% HCl by vigorous stirring for 20 min. Later, two solutions were mixed together and stirred for another 15 min followed by introducing 1 mL formaldehyde slowly into the reaction mixture. The reaction was allowed to proceed in a closed container to avoid rapid reaction in the air for hard resin formation. The reaction mixture was then transferred to a large petri dish for solvent evaporation curing at 80 and 120 °C.

Finally, carbonization was carried out under N_2 environment at a heating rate of 1 °C and soaked at 400 °C for 1 h to remove the template and later at 2 °C/min to 800 °C for 2 h. The obtained carbon samples were crushed and stored for characterization and testing in wastewater treatment processes.

8.2.2 Characterizations

All the prepared samples were characterized for textural properties using N_2 adsorption-desorption isotherm at -196 °C using a Micromeritics BET Tristar plus. Prior to N_2 isotherms, the samples were degassed at 220 °C for 24 h to remove any trapped solvent molecules from the pores. X-ray diffraction (XRD) was used to figure out different phases on Bruker D8 Advanced XRD. Morphology of prepared samples was studied on a scanning electron microscope (Zeiss Neon 40 EsB CrossBeam). The samples were prepared as suspension in ethanol and spread on alumina stubs where the solvent was evaporated prior to imaging. Thermogravimetric analysis of all samples was carried out on a TGA/DSC1 STAR^e system from Mettler Toledo. A fixed weight of carbon samples was placed in a 150 µL alumina pan and heated from 35 – 800 °C under an air flow (70 mL/min). Moreover, Fourier transform infrared (FTIR) spectroscopy was carried out on a Perkin Elmer's Spectrum 100-FT-IR spectrometer. X-ray photoelectron spectroscopy

(XPS) was adopted to determine phases of carbon. Dynamic light scattering (DLS) measurements were performed using a Malvern Zetasizer Nano ZS instrument for particle size and zeta potential measurements. In a typical measurement, a dilute suspension (20 mg/L) of carbon samples was prepared in ultrapure water and analyzed for particle size. A 0.1 M NaOH and HCl solution was used to adjust pH (2.5-11.5) of the carbon nanospheres suspensions for zeta potential measurements.

8.2.3 Adsorption and catalytic degradation tests

Stock solutions (1000 ppm) of phenol, p-HBA, MO and RhB were prepared by dissolving them in ultrapure water and the test solutions were prepared by dilution of the stock solution.

The concentrations of MO and RhB were measured using a spectrophotometer (Thermo SpectronicGenesys 20, Thermo Scientific^{TM}, USA) at 464 and 554 nm, respectively. After certain time interval, dye samples were withdrawn and centrifuged to obtain a clear solution for measurement on the spectrometer. Adsorbent was filtered after experiment and dried at 180 °C without washing overnight for degradation reaction.

In case of catalytic degradation, all experiments were carried out at 25 °C using fixed amount of catalyst and PMS for 2 h for degradation of phenol. The initial concentration of phenol was kept at 20 mg/L in all experiments while the amount of catalyst was 0.4 g/L. Phenol concentration was analyzed at fixed time intervals on a Thermal UltiMate™ 3000 RSLCnano System through a C18 column using an UV detector (λ= 270 nm). The mobile phase consists of 30% acetonitrile and 70% deionized water with a flow rate of 1 mL/min. Catalyst was regenerated after washing with water and dried at 180 °C for adsorption of p-HBA. The column (C18) was used for p-HBA analysis, however, 30 mM acetic acid at 60% and methanol at 40% solution was used as a mobile phase.

Table 8-1 Textural and functional properties of carbon nanospheres

Material	Solvent evaporation/curing temperature (°C)	Surface area (m^2/g)	Total pore volume cm^3/g	Average pore size (nm)	High resolution C 1s XPS spectra				
					Sp^2 C=C	C-O-C/C-OH	O=C-O	C=O	Pi-pi shake up
PC-T1	80	826	0.65	4.6	67.0	13.7	5.4	8.97	3.92
PC-T2	120	800	0.60	4.5	61.0	15.1	10.0	8.69	4.80

8.3 Results and Discussion

8.3.1 Characterization of Carbon Nanospheres

The textural properties of prepared materials were studied by nitrogen adsorption-desorption isotherms (Sing, 2001). It can be seen that PC-T1 (Figure 8-1A) and PC-T2 (Figure 8-1C) showed type IV isotherm with significant hysteresis between adsorption-desorption. This observation reveals that simultaneous temperature induced evaporation and curing didn't deteriorate mesoporosity in prepared samples. The surface area was calculated using a multipoint BET method with P/P_0 ranging from 0.01 – 0.3 of adsorption isotherm and total pore volume was calculated at P/P_0 = 0.99. It has been reported previously that increased reaction temperature results in a decreased surface area at the maximum temperature of 55 °C (Górka et al., 2009). In other investigations, evaporation was usually carried out at room temperature for an extended period of time with subsequent thermal curing, since there is different opinions in mesopores creation by the self-assembly during evaporation process or thermopolymerization (Liang & Dai, 2006; Libbrecht et al., 2015; Schuster et al., 2012; Wang et al., 2014c). In the present study, two different elevated temperatures i.e. 80 and 120 °C were studied for simultaneous solvent evaporation and thermopolymerization for synthesis of mesoporous carbon. In the both cases, high surface area was observed (~ 800 m^2/g) without losing surface area and mesoporosity even at the different evaporation and curing temperatures. This also gives a wide degree of freedom to select evaporation temperature to speed up

synthesis process with high mesoporous carbons for specific applications. Usually, it is preferred to synthesize mesoporous materials for large molecules adsorption and also further processing of them with other materials for specific applications such as decoration of carbon structure with more active metallic species for catalysis (Libbrecht, Verberckmoes, Thybaut, Van Der Voort, & De Clercq, 2017; Liu et al., 2017; Shen et al., 2017). The pore size of PC-T1 was 4.6 nm (average pore size) calculated using the BJH method (Webb & Orr, 1997). It can also be seen from Figure 8-1B and 8-1D that a dome shape is observed between 4-6 nm for both PC-T1 and PC-T2. Total pore volumes are 0.65 and 0.60 cm^3/g for PC-T1 and PC-T2, respectively, shown in Table 8-1.

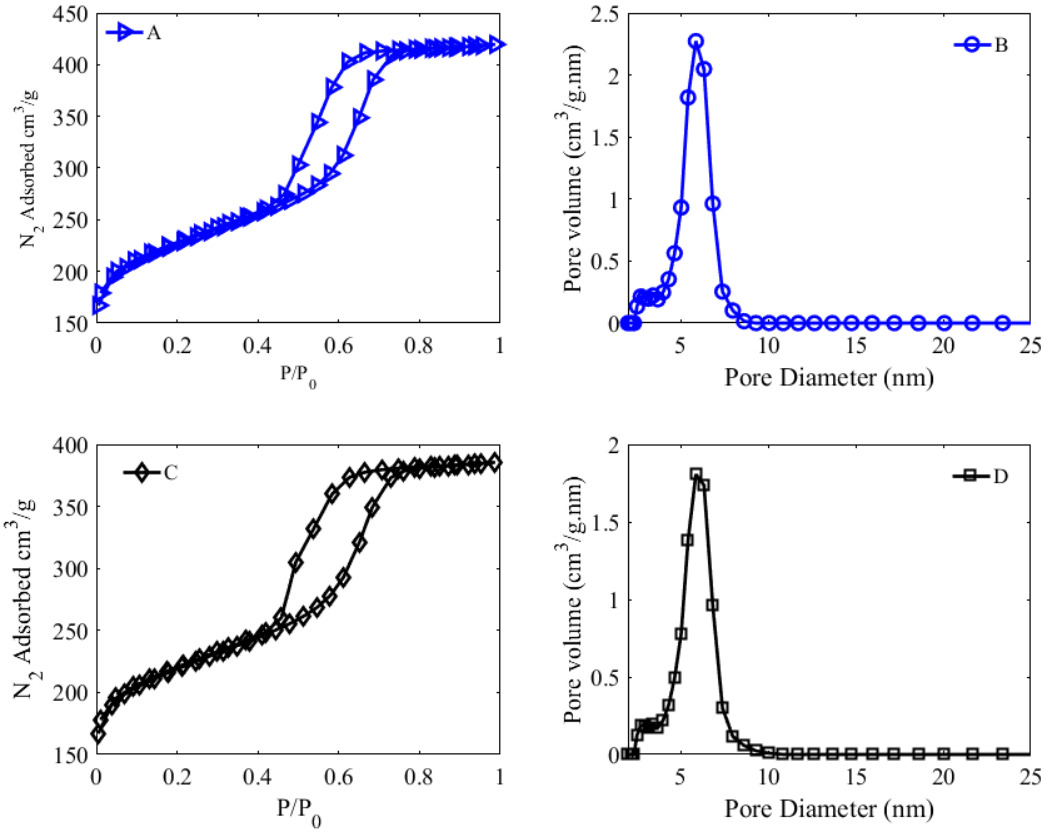

Figure 8-1 N_2 adsorption-desorption isotherms of PC-T1 and PC-T2 at -196 °C for textural properties.

Moreover, the functional groups were checked with the FTIR. There are weak bands at 1547, 1708, 1977 and 2124 cm^{-1} in both samples (Figure 8-2) (Indrawirawan et al., 2015b). The small humps in FTIR spectra at 1550 cm^{-1} indicate C=C, while the band at 1708 cm^{-1} shows C=O vibration of carboxyl/ketonic groups and the band at 1977 cm^{-1} indicates C-O-H (Indrawirawan et al., 2015b; Su et al., 2009). Figure 8-3

shows XRD of powder carbon samples. There is a broad peak between 23-26°, 2Ɵ range, signifying the conversion of resin into graphitic carbon and also at 2Ɵ range 43-46 (Elaigwu, Kyriakou, Prior, & Greenway, 2014; Zhao et al., 2012).

XPS is a powerful technique for surface characterization of nanomaterials. Figure 8-4 shows XPS spectra of the prepared carbon nanospheres. There are two main peaks in survey spectra i.e. carbon and oxygen. Carbon is present at about 92% and there is a marginal difference in carbon contents in PC-T1 and PC-T2, showing carbonaceous content doesn't depend on evaporation and/or curing temperature. Further, high resolution spectra of carbon are also presented in Figure 8-4, which indicate difference in chemical phases of carbon. The highest percentage of carbon is found to be sp^2 while there are small amounts of sp^3 and the presence of functional groups such as C-O-C and C=O is indicated. Availability of these functional groups help in degradation and adsorption processes (Fujimoto, Yamada, Koinuma, & Sato, 2016; Indrawirawan et al., 2015b; Smith, Scudiero, Espinal, McEwen, & Garcia-Perez, 2016). Detailed bonding of carbon from high resolution XPS spectra is given in Table 8-1. It is clear that the highest percentage of carbon is in the form of graphitic C=C at 67.9 and 61.0% in PC-T1 and PC-T2, respectively. This reinforces observations of FTIR and XRD. Figure 8.5 shows thermodynamic stability in TGA analysis. It can be seen that both the samples are stable up to 500 ℃ while degradation of carbon skeleton starts after 550 ℃ and the maximum weight loss is observed at this temperature.

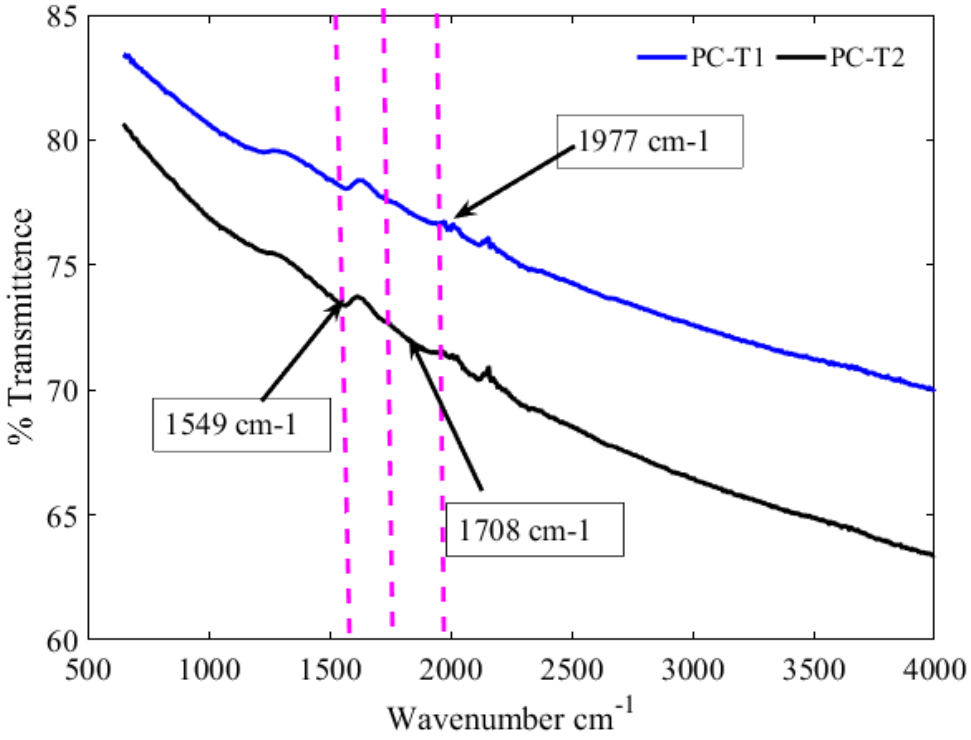

Figure 8-2 FTIR spectra of prepared carbon nanospheres.

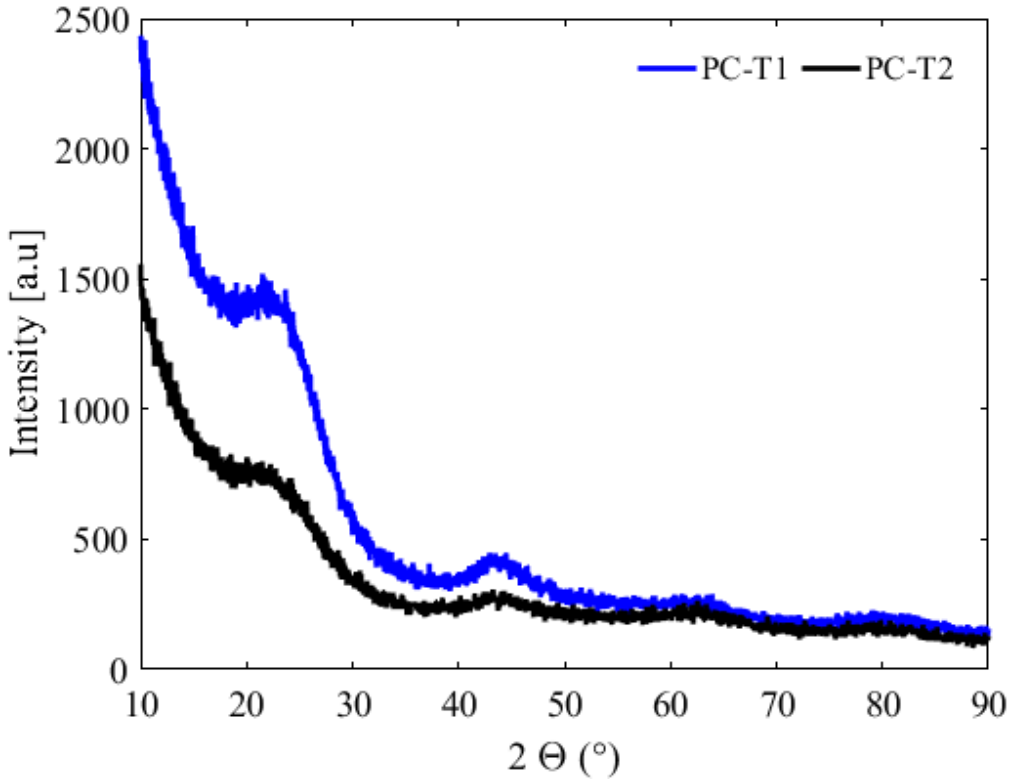

Figure 8-3 Powder XRD profiles of carbon nanospheres.

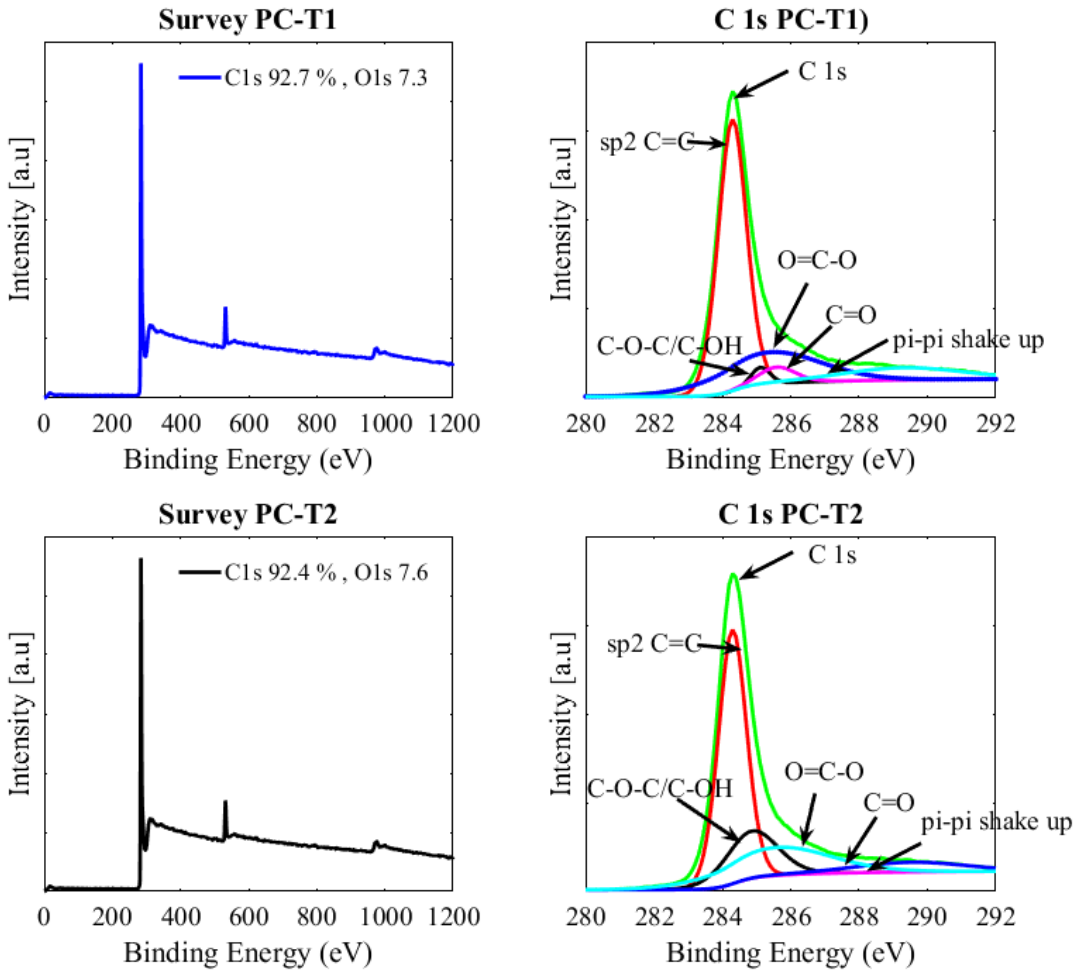

Figure 8-4 Survey and high resolution XPS spectra of PC-T1 and PC-T2.

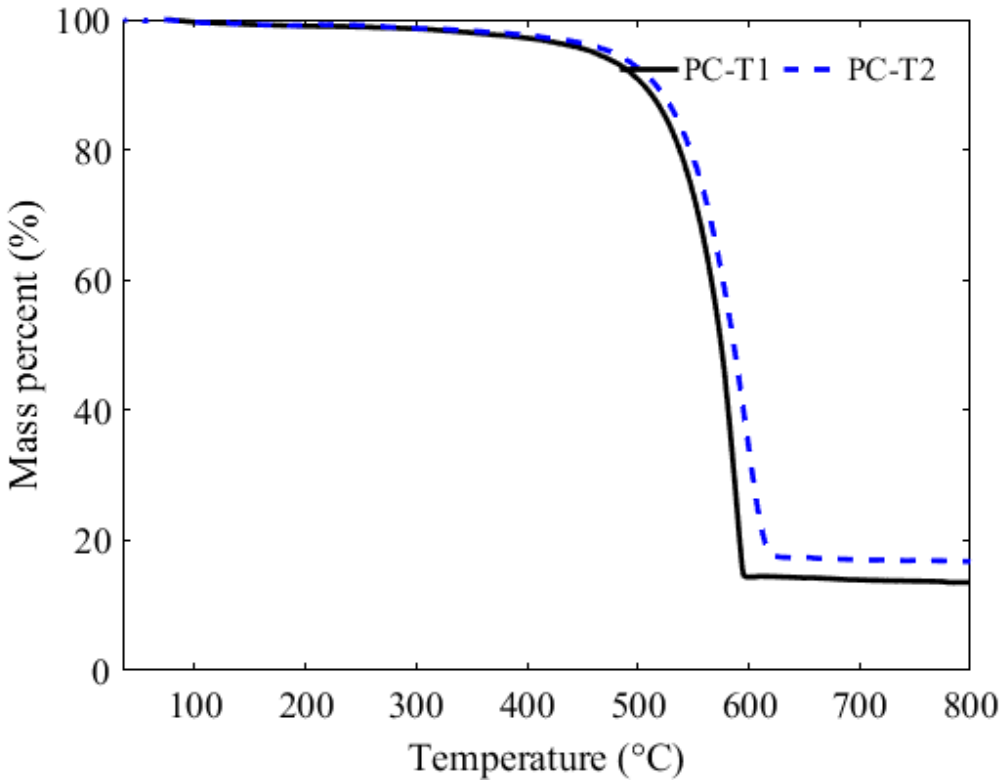

Figure 8-5 Thermal stability study of carbon nanospheres through TGA.

Morphology of prepared samples was studied with SEM analysis. Generally, carbon samples are found in spherical shapes (Zhang, Qiao, & Dai, 2015a), with particle size of 200-500 nm. A small quantity of particles are larger than 500 nm (Cheng et al., 2013). TEM shows well-ordered layers of mesoporous carbon nanospheres resulted from template removal in carbonization process (Duan et al., 2017a; Li & Xue, 2012; Su et al., 2009). Furthermore, particle size distribution was determined using dynamic lighting scattering (DLS) technique. It can be seen from Figure 8-6 (inset) that the most prominent particle range is 200-500 nm, which is consistent with SEM observations. The pH of point of zero charge (pH_{pzc}) of PC-T1 was measured to be 2.5 ± 0.2 (Figure8-7). These measurements provide useful information in adsorption and catalytic processes (Azhar et al., 2017b; Duan et al., 2017a).

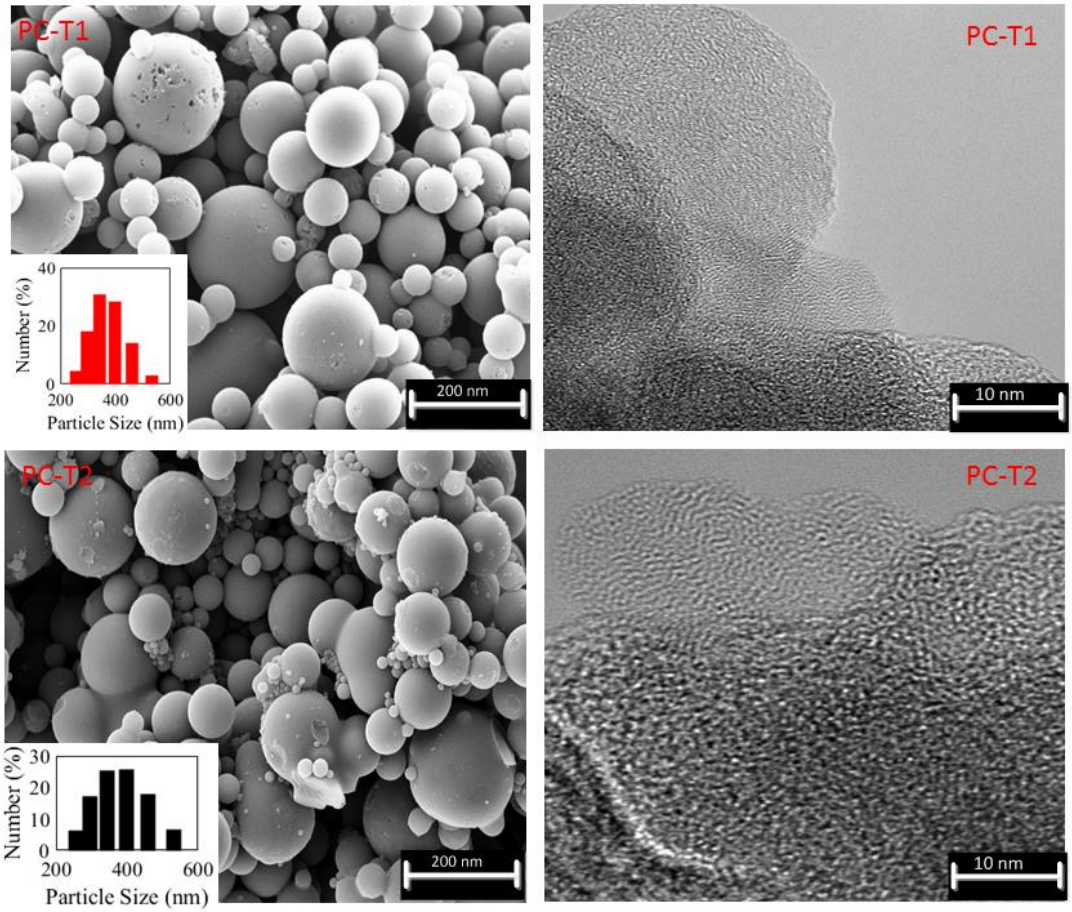

Figure 8-6 SEM, TEM and particle size distributions of PC-T1 and PC-T2.

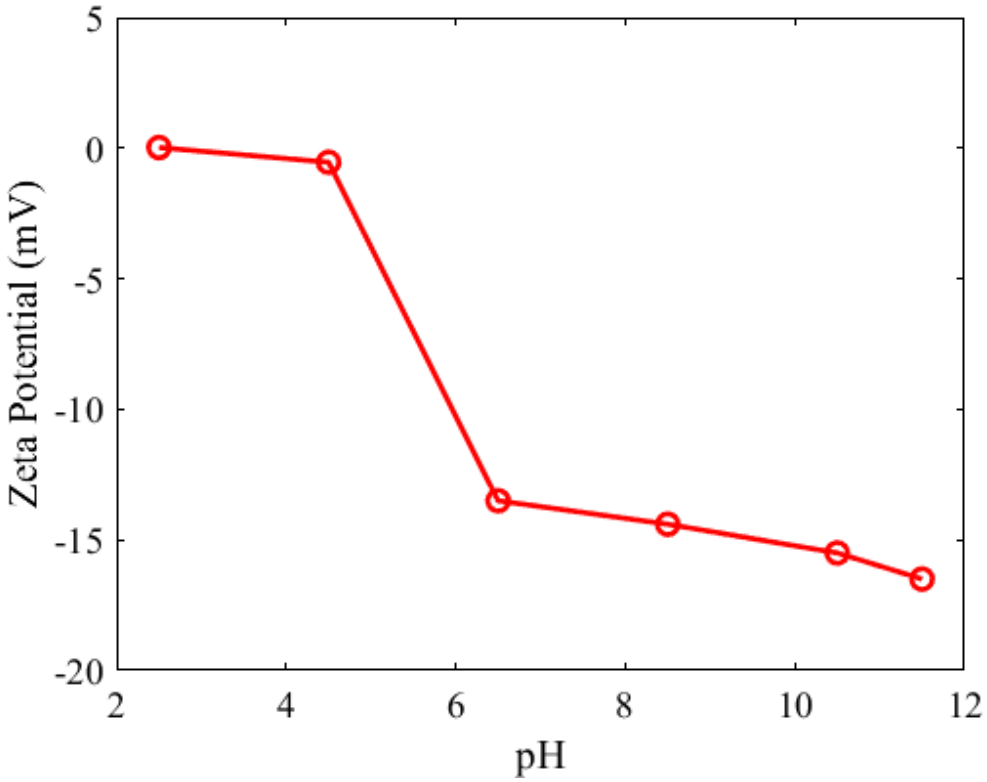

Figure 8-7 Effect of pH on zeta potential for PC-T1

8.3.2 Adsorption Kinetics of p-HBA, MO and RhB

In case of contaminants, rhodamine B (RhB) was taken as representative materials while methyl orange as anionic waste materials. Moreover, p-HBA was studied in detail after catalytic degradation of phenol as a representative of personal care product as a neutral species. Schematic representation of these water contaminants is given in Figure 8-8. Generally, adsorption of organic species was high on all tested materials in adsorption. There was not a significant difference between the performance of PC-T1 and PC-T2 in adsorption (kinetics and adsorption capacity), therefore, performance of just PC-T1 was studied in detail in adsorption and catalytic degradation of water contaminants. It can be seen from Figure 8-9 that three types of organic waste materials (RhB, MO and p-HBA) could be easily removed by PC-T1 up to 99% in 24 h for RhB and 96% for MO. However, it took just 3 h in 90% removal of all RhB, MO and p-HBA in case of PC-T1 due to maintaining mesoporous contents and pore volume. Interestingly, the dimensions of MO, RhB and p-HBA are 1.31 × 0.55 × 0.18, 1.59 × 1.18 × 0.56 and 1.85 × 0.52 × 0.63 nm,

respectively, which are smaller than the pore size of carbon nanospheres. Molecular structure of phenol, MO, RhB and p-HBA are shown in Figure 8-8 (Zhuang, Wan, Feng, Shen, & Zhao, 2009).

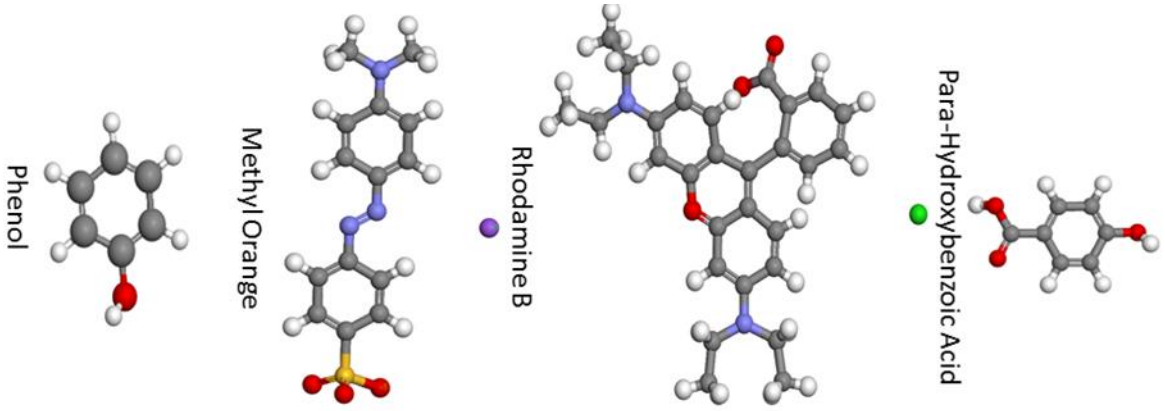

Figure 8-8 Schematic representations of water contaminants.

Adsorption kinetics of p-HBA, MO and RhB was studied at 25 °C without any adjustment in pH of respective solutions. In case of MO and RhB more than 90% removal was possible in 4 h when initial concentration was as high as 20 ppm. However, adsorption experiment was continued as long as 24 h to fully explore possibility of any adsorption to procced even for such a long period of time. Since, the size of p-HBA molecule is far less compared to MO and RhB, which makes the adsorption process very fast and 100% removal was achieved in 4 h. Moreover, single benzene ring in p-HBA molecules does not experience much resistance to form any linkage owing to π-π interactions. Usually, adsorption encounters slow kinetics, which might hinder effectiveness on commercial scale. It can be seen from Figure 8-9 that almost 75% p-HBA removal was achieved in less than 60 minutes on PC-T1. Such fast adsorption can be useful in treatment of storm water and other waste treatment facilities. Since, PC-T1 possess high surface area, regular pores structure and large pore volume, these textural properties contribute in such a significant fast removal of water contaminants. It seems adsorption of p-HBA follows intraparticle diffusion model and penetration of p-HBA doesn't find significant resistance to diffuse into pores. The only resistance is due to motion of p-HBA molecules from bulk solution to surface of PC-T1 where these enter inside the pores. Similarly, PC-T1 adsorbed dyes such as MB, MO to large extent despite of their large molecular size. However, adsorption was slower in dyes compared to p-HBA.

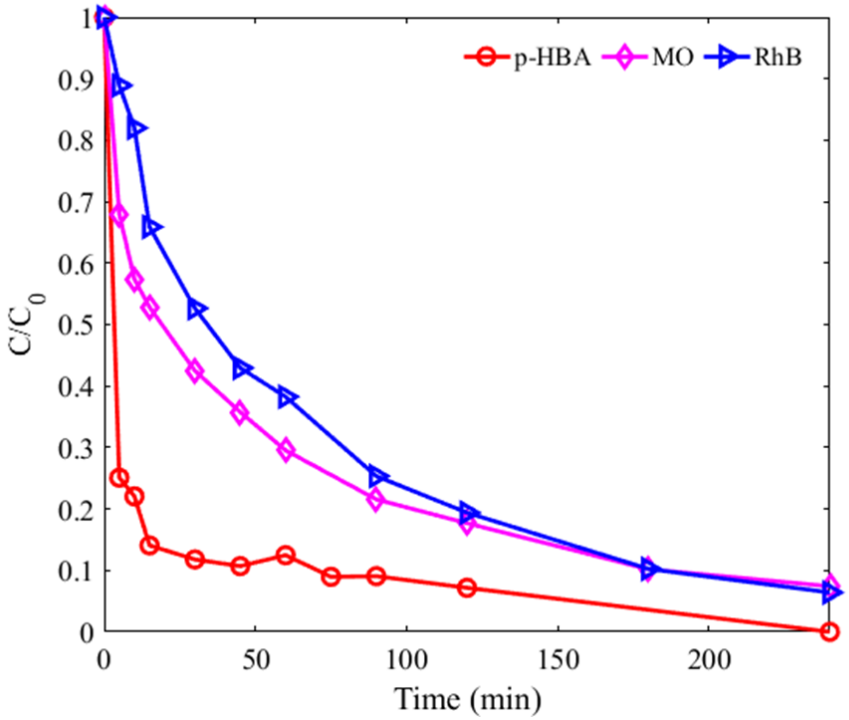

Figure 8-9 Adsorptive removal of p-HBA, MO and RhB on carbon nanospheres, m[PC-T1] = 0.4 g/L.

8.4 Reuse of adsorbent in catalytic degradation of phenol

The catalytic degradation of phenol was studied on used PC-T1. It can be clearly seen from Figure 8-10 that there is not a significant removal of phenol by PMS only. Without any PMS, more than 50% removal of phenol was achieved by adsorption. Since, toxicity of phenol is very high and complete removal is imperative to eliminate its risks to aquatic life. Therefore, catalytic degradation is a preferred process in phenol removal. As expected, degradation of phenol was 100% by PC-T1 as a catalyst with PMS. In the degradation process, a very fast process of adsorption and degradation takes places on PC-T1 with PMS in the first 15 min and then gradual degradation of phenol continues until complete removal is achieved in almost 60 min. In addition, it is interesting to observe that fast removal of phenol was achieved in a wide pH range (2- 11). This shows robustness of the catalyst in a vast range of pH (Figure 8-11). The pH_{PZC} for PC-T1 is 2.5, suggesting negatively charged surface of the catalyst at pH higher than 3 while phenol can only be

deprotonated at pH > 9.5, so that's why pH 11.0 was also selected to figure out effect of anionic phenol and high negative surface charge of PC-T1.

In this case, surface functional groups such as ketonic group can help in transfer of electrons to generate free radicals. Activation of PMS in metal free catalysis usually due to generation of free radicals by electron transfer through graphitic structure of carbon. Another possibility of electron transfer is through functional groups and/or heteratoms available in carbon structures. Moreover, at pH => 2.5, surface charge of carbon nanospheres is negative which can help transfer of electron, however, at pH 2.0 positive charge can hinder fast transfer of electrons, which show slightly slower degradation of phenol (Figure 8-11). Moreover, a pronounced difference is only seen at pH 11.0 where complete degradation took place in 10 minutes. Enhanced negative zeta potential of carbon samples and deprotonation of phenol result in fast activation of sulphate radicals, which help in fast degradation of phenol. There is not a significant difference in kinetics at pH i.e. 5.4 and pH 9.0.

Generation of free radicals was studied using methanol as a sulphate and hydroxyl trapping reagent in a large quantity i.e. 6.5 M, as it can trap both sulphate and hydroxyl radicals at the same time. It can be seen from Figure 8-12 that degradation of phenol was slowed down, however, complete degradation of phenol was possible. This is consistent with our recent study, where activation of persulfate (PS) was possible due to both radical and non-radical pathways on CMK-3 and CMK-8. Since, there is no significant effect of methanol on degradation, which confirms non-radical path due to electron rich pi electrons on the edges and due to availability of electrons on ketonic groups. This may result in continuous charge from surface of carbon lattice and ketonic groups and oxidation of phenol (Wang, Ao, Sun, Duan, & Wang, 2016b). Moreover, adsorption of MO, RhB and p-HBA provide additional heteroatoms i.e. N, S and O, which can further enhance performance of PC-T1 in degradation of phenol. This technique of immobilizing water contaminants into carbon structure reduces cost of incorporating heteroatoms in carbons and increases efficiency of wastewater treatment processes. Details on the effect of individual guest molecules on performance of carbon nanospheres in advanced oxidation processes will be presented in future study. Although, complete degradation was possible even with a very high concentration of methanol but still the rate of phenol degradation was slower, which suggests there is some contribution from sulphate

and hydroxyl radicals (Duan et al., 2017a; Indrawirawan et al., 2015b). Following is plausible degradation pathway for phenol parallel to non-radical reaction.

$$HSO_5^- + e^- \rightarrow HO^\bullet + SO_4^{2-} \quad (1)$$

$$HSO_5^- + e^- \rightarrow SO_4^{-\bullet} + OH^- \quad (2)$$

$$HSO_5^- + e^- \rightarrow SO_5^{-\bullet} + H^+ \quad (3)$$

$$HO^\bullet + SO_4^{2-} \rightarrow SO_4^{-\bullet} + OH^- \quad (4)$$

$$SO_4^{-\bullet} + OH^- \rightarrow SO_4^{2-} + HO^\bullet \quad (5)$$

$$Phenol + SO_4^{-\bullet}(HO^\bullet)\cdot \rightarrow several\text{K } steps \rightarrow CO_2 + H_2O + SO_4^{2-} \quad (6)$$

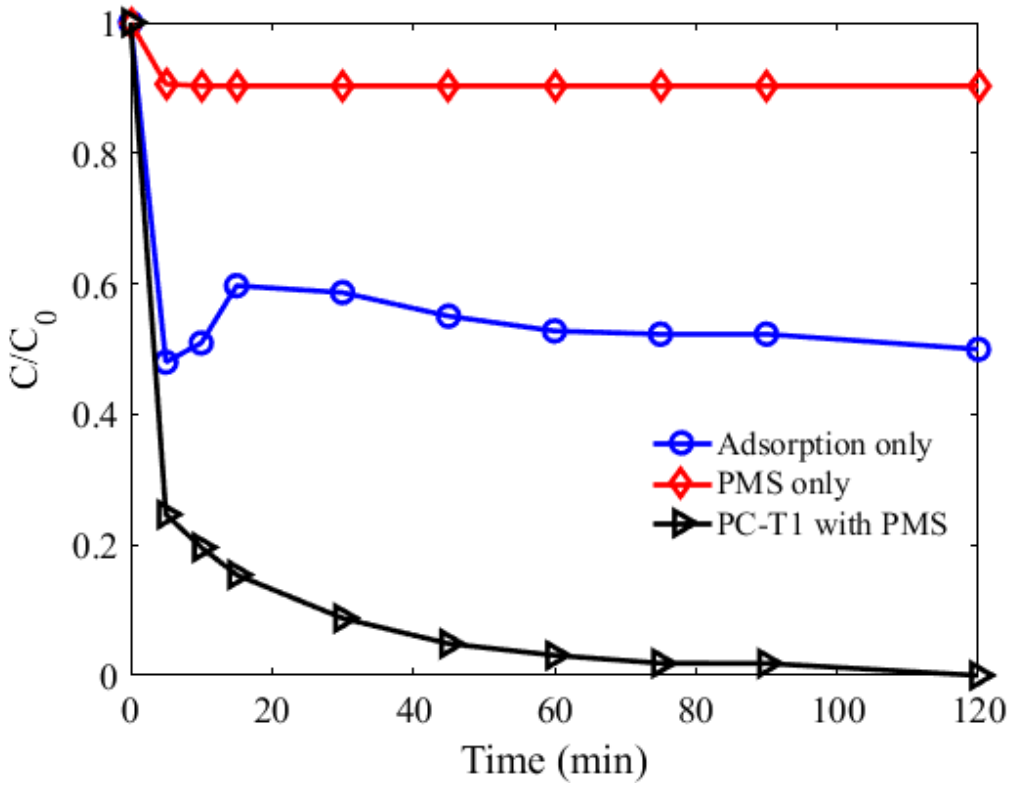

Figure 8-10 Removal of phenol by adsorption and catalytic degradation on carbon nanospheres, phenol= 20 ppm, m[PC-T1]= 0.4 g/L, PMS= 1.62 mM.

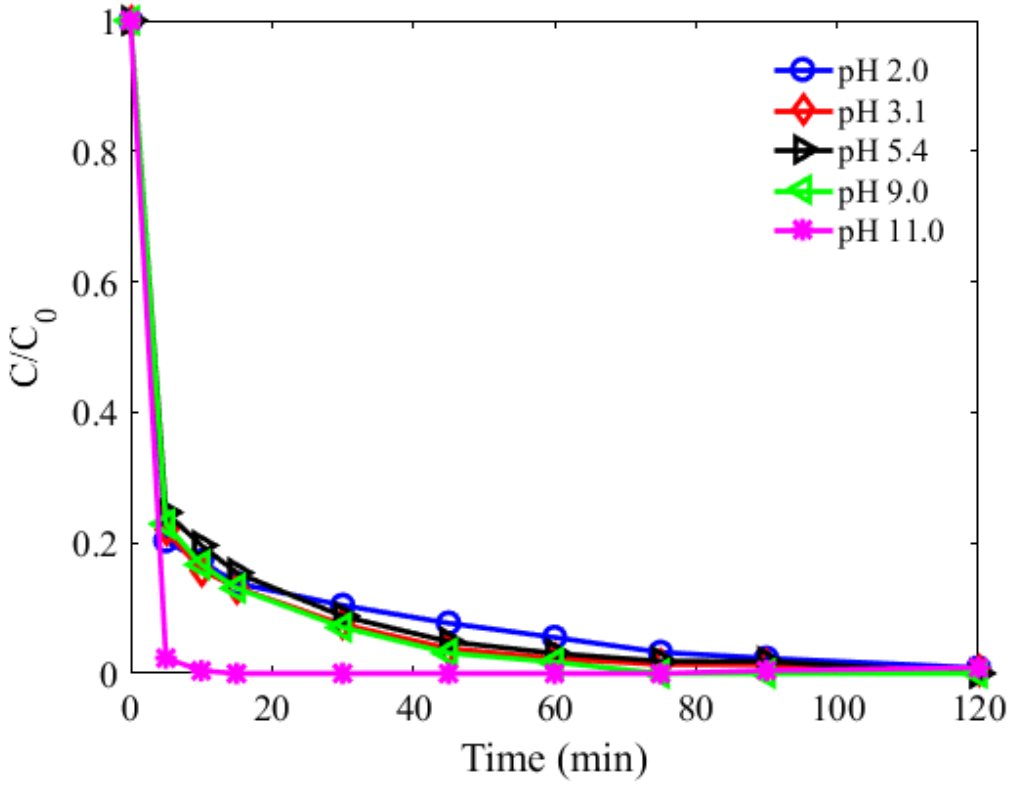

Figure 8-11 Effect of initial pH of phenol solution on degradation, m[cat]=0.4 g/L, PMS= 1.62 mM at 25 °C.

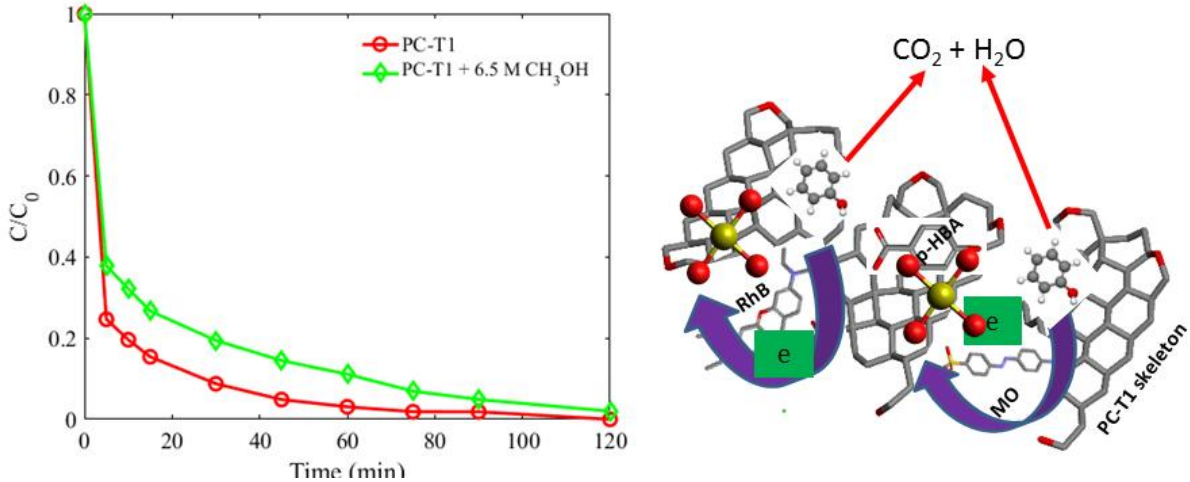

Figure 8-12 Plausible mechanism for degradation of phenol on carbon nanospheres.

8.5 2nd regeneration of carbon nanospheres for adsorption of p-HBA

Adsorption of p-HBA was studied in detail after washing and drying the catalyst after phenol degradation experiments. Langmuir and Freundlich isotherms (Freundlich, 1906b; Langmuir, 1918) were employed to know adsorption parameters such as maximum adsorption capacity, feasibility of adsorption process and physical and/or chemical nature of removal process of p-HBA. In each experiment, fixed initial concentration [C_i] of p-HBA was used and different amount of PC-T1 was used to achieve equilibrium concentration [C_e]. The range of mass of adsorbent was selected from 0.1- 0.5 g/L and C_i was kept at 20 ppm in all isothermal experiments at 25 °C. The amount of p-HBA adsorbed was calculated by the following equation

$$q_e = (C_i - C_e) * V / m_{ads} \quad (6)$$

where m_{ads} = mass of adsorbent in grams, V= volume of p-HBA solution in litres.

Another effective way of studying adsorption process is the removal efficiency of the process which indicate possibility of commercial scale application of any process including adsorption. In all instances, removal efficiency is reported in terms of percentage removal of p-HBA. It is interesting to report that high removal efficiency is achieved in all adsorption experiment i.e. 75-99 % within 120 minutes. Moreover, adsorption data was better fitted with Langmuir model compared to Freundlich model and the maximum adsorption capacity was calculated as 170 mg/g using Langmuir isotherm. It can be clearly seen from Figure 8-13 (A) that isothermal data is fitted with Langmuir model with R^2 = 0.9965, moreover, experimental and calculated values by Langmuir isotherms are shown in Figure 8-13 (B). The data was also analysed with Freundlich isotherm, however, Freundlich model is not as good as Langmuir model, shown (Figure 8-13, C & D) because of poor fitting i.e. R^2 value 0.8832 (Azhar et al., 2016). The details on adsorption mechanism are given in the next section.

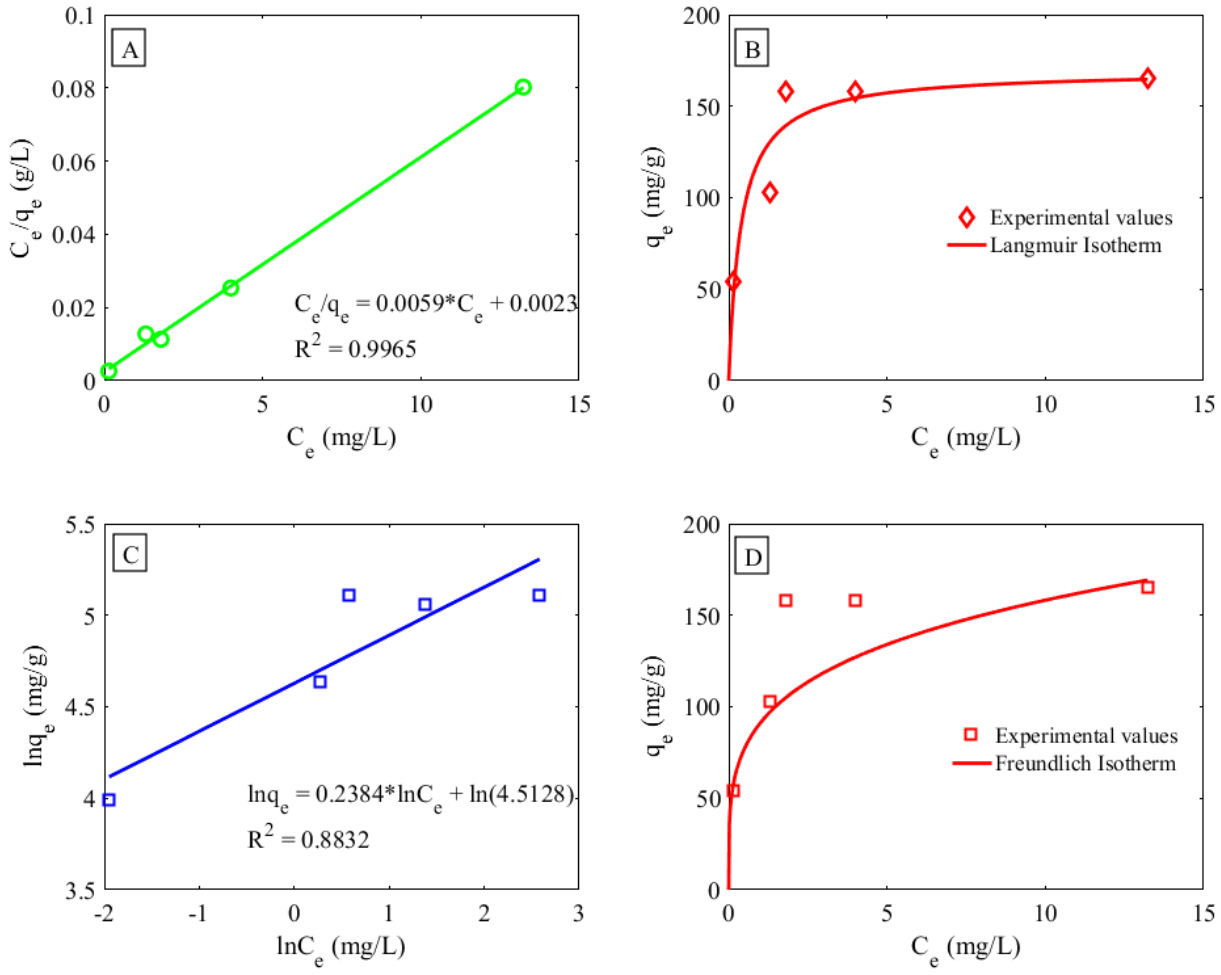

Figure 8-13 Adsorption isotherms for p-HBA on PC-T1 at 25 °C; A = Langmuir model fitting, B = experimental and calculated adsorption capacity from Langmuir model, C = Freundlich model fitting and D = experimental and calculated adsorption capacity from Freundlich model.

8.6 Effect of pH on p-HBA adsorption

Surface charge of an adsorbent at a particular pH and existence of adsorbate in solution as cationic, anionic and/or neutral molecules play significant roles in adsorption process. Zeta potential measurements can help identify the charge on surface of adsorbent to explain plausible adsorption mechanism in combination with other characterization techniques such as FTIR, XPS and textural properties (Yagub et al., 2014). Zeta potential of the adsorbent and solution chemistry of adsorbate have been selected to illustrate adsorption mechanism, since it has been explained in above sections that the average pore size of PC-T1 is higher than that of p-HBA

molecules. Adsorption of p-HBA is favourable in molecular form without any adjustment in initial pH of solution (pH= 4.35) shown in Fig. 15C. Since, pH_{pzc} is 2.8 and the zeta potential decreases with increasing pH, resulting higher electrostatic repulsion between PC-T1 surface and anionic p-HBA (Azhar et al., 2016). Beyond that point, electrostatic repulsion exists at higher levels resulting in least adsorption capacity. Apart from the electrostatic forces, ionic nature of p-HBA molecules needs special attention, due to availability of reactive species on them i.e. COOH and OH. Due to these reactive polar functional groups on p-HBA, the effect of pH was studied to check the stability and transformation of p-HBA molecules by adjusting pH. The pH of p-HBA solution was 4.35 ± 0.3 and pK_{COOH} and pK_{OH} values of p-HBA are 4.5 and 9.1, respectively. Addition of HCl results in enhanced H^+ ions in solution, which transforms more p-HBA into molecular form (Fig. 15A). Although, surface of PC-T1 becomes positive charged at pH 2.5, still higher adsorption takes place at this due to molecular form of p-HBA (Azhar et al., 2018). It can also be seen from Fig. 8-14 that adsorption is high at pH 4.35 when p-HBA exits in a molecular form (Fig. 8-15C), however, the adsorption decreases with an increase in pH, which may be attributed to electrostatic repulsion. With increasing pH, abundance of Na^+ ions are attracted by negatively charged p-HBA resulting in salt formation similar to esterification reactions of carboxylic acids (Fig. 8-15B). In addition to electrostatic repulsion, there might be chemical transformation of p-HBA into salt of p-HBA. This gives rise to a reverse Kolbe–Schmitt more persistent to be removed compared to pristine p-HBA molecules (Kosugi et al., 2003). At pH ≥ 9.5, there are two possibilities for Na^{+1} ions to attack i.e. O^{-1} due to deprotonation of OH or COO^- because of removal of proton from COOH. However, it seems that a more prominent reaction was on phenoxide site (Kosugi et al., 2003). The addition of minerals can decrease the performance of adsorbent due to competitive adsorption between adsorbate and added ions into solution. Previously, effect of Sodium and calcium ions has been studied which shows negative effect on adsorption capacity (Huo & Yan, 2012; Lin et al., 2014). Added ions can also change solutioin chemistry by reacting with adsorbate molecules transforming them into different molecules. To further testify effect of Na^{+1} ions, different amount of NaCl was added to p-HBA solution at pH 4.35 (Fig. 8-15D). It can be clearly seen that addition of Na^{+1} results in decreased adsorption capacity even without apparent change in pH to some extent (Lin et al., 2014). The adsorption capacity was decreased from 190 mg/g to 135

mg/g by the addition of 0.1 M NaCl at pH 4.35. Moreover, at higher pH, the decrease in adsorption capacity was very prominent due to dissociation of COOH into COO- which act as active sites for Na^{+1} ions (Azhar et al., 2018).

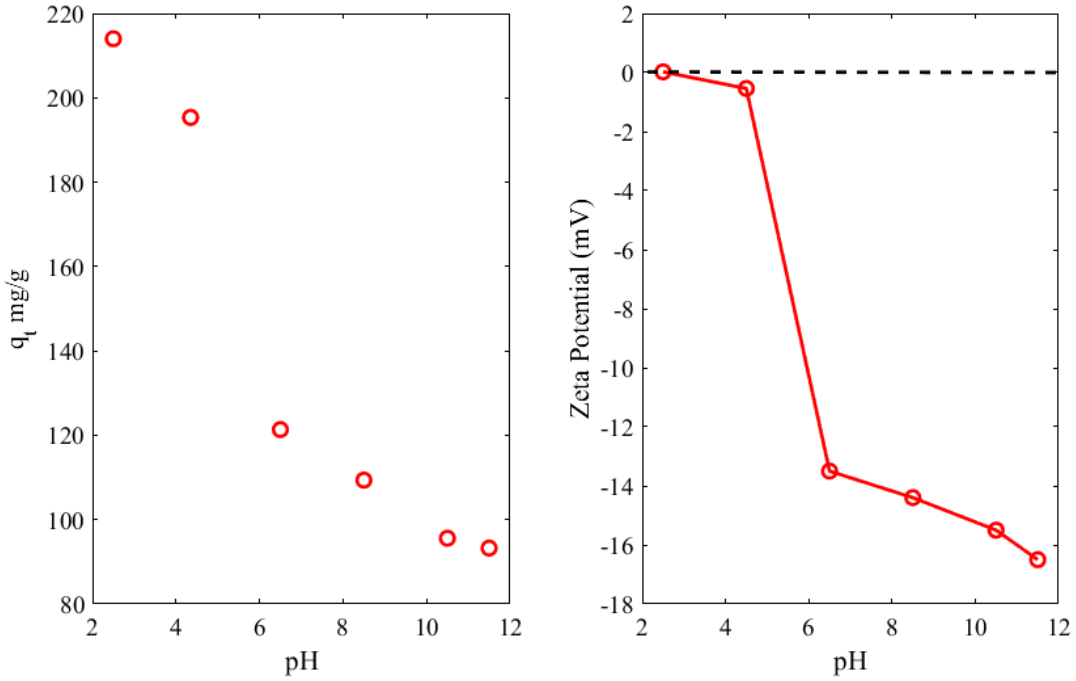

Figure 8-14 Effect of initial pH on adsorption of p-HBA on PC-T1.

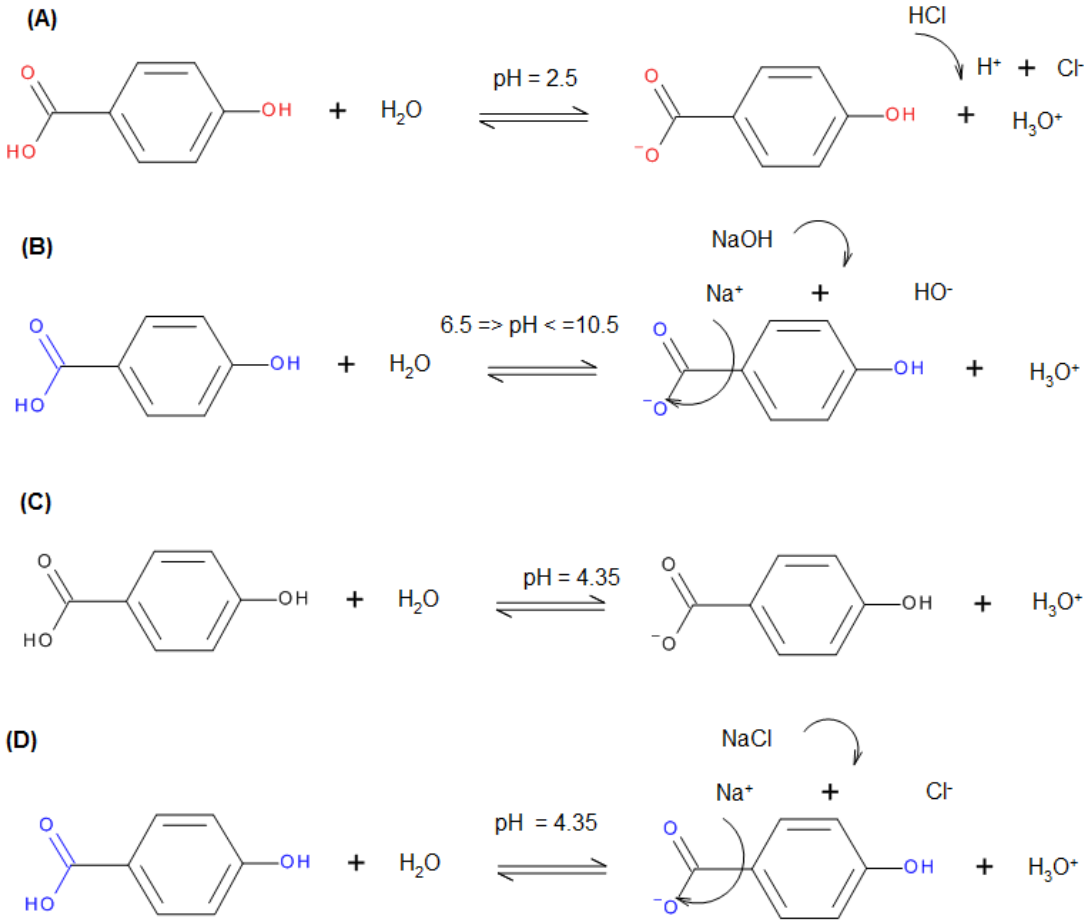

Figure 8-15 Effect of pH and transition in p-HBA solution chemistry with added ions

8.7 Conclusions

In this study, mesoporous carbon nanospheres have been synthesized using evaporative temperature induced self-assembly of RF resin with F127 as a soft template. High surface area, large pore volume and uniform pore size distribution was obtained for the prepared carbon materials. Moreover, the prepared carbons were used in an integrated manner as an adsorbent and catalyst in wastewater treatment processes for removal of conventional and emerging contaminates to make the process cost effective. The as-synthesised carbon nanospheres were used for adsorption of p-HBA, MO and RhB. Rapid removal of MO, RhB and p-HBA was achieved with PC-T1 with more than 95% removal efficiency. Fast catalytic degradation of phenol was also achieved over a wide range of solution pH. Furthermore, the used catalyst was again employed in adsorption of p-HBA. The adsorption data was fitted with Langmuir and Freundlich and best fitting was

obtained with Langmuir model with adsorption capacity of 172 mg/g at 25 °C. Zeta potential and pH measurements showed hydrogen bonding and pi-pi interactions are main factors in efficient adsorption p-HBA on PC-T1. This study highlights a sustainable approach to utilize metal free adsorbent/catalyst in wastewater treatment processes. These results will be helpful in exploring the role of guest adsorbate molecules by introducing heteroatoms in carbon backbone in useful applications such as advanced oxidation processes, energy storage and beyond.

Chapter 9 Conclusions and Recommendations

9.1 Conclusions

This thesis covers synthesis of nanomaterials and their integration in WWTPs. Various synthesis techniques were adopted to prepare MOFs and characterize their structure and properties using FTIR, XRD, SEM, TGA, BET and other surface analysis techniques to check successful synthesis of MOFs. Specifically, HKUST-1, UiO-66, ZIF-67, Bio-MOF-11, MIL-96 were synthesized according to either previously developed methods or with novel facile methods. Subsequently, different water contaminants namely sulfachloropyradazine (antibiotic), methylene blue, methyl orange (dyes), para-hydroxybenzoic acid (personal care product) and phenol (phenolics) were targeted to treat from synthetic wastewater. Adsorption and advanced oxidation processes were used to treat wastewater.

In case of adsorption, high adsorption capacity, fast kinetics with good reusability for a multiple use was reported for HKUST-1, UiO-66, and MIL-96. On the other hand, Bio-MOF-11 was used in catalytic degradation of SCP and p-HBA individually and combined (p-HBA & SCP) in single degradation process. Again, excellent reusability of the catalyst was reported with simply water washing and drying of Bio-MOF-11. Later, both adsorption and AOPs were used in sequence with MIL-96 for CO_2 and p-HBA adsorption. Moreover, used MIL-96 samples were carbonized to obtain metal/metal-oxide/carbon composites and further used in PMS activation to degrade MO from wastewater. This study reinforces the concept of elimination of solid waste generation and protection of the environment from secondary pollutants. Furthermore, mesoporous carbon nanospheres were synthesized using resorcinol-formaldehyde (RF) strategy by temperature induced solvent evaporation technique which resulted in fast synthesis of carbon nanospheres. The resulted carbon nanospheres were used in cyclic applications i.e. adsorption-degradation-adsorption. This study opens up new horizons in exploring effect of adsorbate guest molecules in useful applications such as catalytic degradation, energy storage and electronic devices. Moreover, such processes will make it cost effective to introduce active sites in adsorbents in practical applications.

9.2 Recommendations

1- Abundance of literature suggests chromium- and cadmium-based MOFs have been tested in WWTPs, however, less studies are available on hazard associated with synthesis of these MOFs and risk of introducing secondary pollutants in water bodies. Careful studies are needed in proposing MOFs for WWTPs at a larger scale.
2- A holistic approach should be adopted while developing new materials in environmental applications such as adsorption and/or catalytic processes in environmental remediation.
3- Cyclic stability of MOFs requires testing in terms of structural deformation and metal leaching into water bodies.
4- Since most of water stable MOFs are less active in catalytic degradation processes therefore development of binary MOFs with more catalytically active metals are proposed for future studies despite of decreased surface area in binary MOFs.
5- Corrugated core-shell MOFs with less stable in core and highly stable MOF shell can lead to highly efficient materials for specific applications.

9.3 Summary of new and significant findings

1- HKUST-1, a well-established MOF, was used in adsorption of SCP for the first time with a higher adsorption capacity.
2- Binary (HKUST-1 and UiO-66) MOFs were synthesized for MB removal with superior performance compared to pristine MOFs. This study opened new horizons to explore new methods to enhance performance of MOFs in WWTPs and beyond.
3- There are less studies which explore non-conventional factors in adsorption, therefore, structure features of UiO-66 were explored in adsorption process based on pi-pi and hydrophobic interactions.
4- Complex synthesis procedures are one of the most hindering factor in synthesis of robust MOFs such as Bio-MOFs. To overcome this issue, a

facile method was introduced for synthesis of Bio-MOF-11. Moreover, efficient activation of PMS was observed in degradation of p-HBA and SCP, which is the first study in AOPs for p-HBA and SCP.

5- Availability of Lewis basic sites in adenine was tested in activation of PMS with promising result in degradation of SCP and p-HBA. This will help in exploring organic-organic self-assembly for AOPs.
6- MIL-96 was synthesized by a solvent modulated technique with various morphologies. Moreover, synthesized MOFs were used in gas phase adsorption, and the used MOFs were re-activated by heat treatment for adsorption of p-HBA. Furthermore, the used MIL-96 was carbonized into a Al_2O_3/C composite, which successfully activated PMS for degradation of MO. This study reinforces the importance of functionalized nanomaterials in multiple applications in a sustainable way without generating solid waste.
7- Carbon nanospheres were synthesized by a modified solvent evaporation method at elevated temperatures to form RF resin. Moreover, integrated approach is used in combining adsorption and catalytic degradation of water contaminants owing to excellent textural and functional characteristics of carbon nanospheres. Particularly, adsorption of dyes, or other heteroatomic organic guest molecules can have a positive effect in catalytic properties of carbon materials.

9.4 Outlook for future work based on new knowledge gaps

1- Adsorption of metal ions is less studied in terms of MOFs application in WWTPs, which requires attention of research community.
2- In the current project, batch process was used in WWTPs, other processes such as, tube flow reactors and membrane reactors are proposed for future work.
3- Post synthetic strategies such as surface coating either electrochemically or by nonelectro processes are encouraged to functionalize MOFs surface for targeted applications.
4- Mathematical modelling of adsorption process in MOFs requires special attention according to adsorbate-adsorbent interactions.

5- There are lot of studies on structural deformation of MOFs under the influence of guest molecules, however, there is no study to synthesize MOFs using organic linkers (less soluble in water) as a starting material to construct MOFs in removing metals from wastewater.

References

2017. Water Corporation. ***Trade Waste, Acceptance criteria for trade waste – Information sheet 6***, https://www.watercorporation.com.au/-/media/files/business/trade-waste/applying-to-discharge/acceptance-criteria.pdf.

Abbasi, A. R., Rizvandi, M., Azadbakht, A., & Rostamnia, S. 2016. Controlled uptake and release of imatinib from ultrasound nanoparticles Cu3(BTC)2 metal-organic framework in comparison with bulk structure. ***J Colloid Interface Sci***, 471: 112-117.

Abid, H. r. 2012. ***Capture of carbon dioxide in metal organic frameworks***. Curtin University, Australia

Abid, H. R., Ang, H. M., & Wang, S. 2012a. Effects of ammonium hydroxide on the structure and gas adsorption of nanosized Zr-MOFs (UiO-66). ***Nanoscale***, 4(10): 3089-3094.

Abid, H. R., Pham, G. H., Ang, H.-M., Tade, M. O., & Wang, S. 2012b. Adsorption of CH4 and CO2 on Zr-metal organic frameworks. ***Journal of Colloid and Interface Science***, 366(1): 120-124.

Abid, H. R., Rada, Z. H., Shang, J., & Wang, S. 2016. Synthesis, characterization, and CO2 adsorption of three metal-organic frameworks (MOFs): MIL-53, MIL-96, and amino-MIL-53. ***Polyhedron***, 120: 103-111.

Abid, H. R., Tian, H., Ang, H.-M., Tade, M. O., Buckley, C. E., & Wang, S. 2012c. Nanosize Zr-metal organic framework (UiO-66) for hydrogen and carbon dioxide storage. ***Chemical Engineering Journal***, 187: 415-420.

Adeyemo, A. A., Adeoye, I. O., & Bello, O. S. 2012. Metal organic frameworks as adsorbents for dye adsorption: overview, prospects and future challenges. ***Toxicological & Environmental Chemistry***, 94(10): 1846-1863.

Ahmad, N., Younus, H. A., Chughtai, A. H., & Verpoort, F. 2015. Metal-organic molecular cages: applications of biochemical implications. ***Chem Soc Rev***, 44(1): 9-25.

Ahmaruzzaman, M. 2008. Adsorption of phenolic compounds on low-cost adsorbents: A review. ***Advances in Colloid and Interface Science***, 143(1–2): 48-67.

Ahmed, I., & Jhung, S. H. 2014. Composites of metal–organic frameworks: Preparation and application in adsorption. ***Materials Today***, 17(3): 136-146.

Ahmed, I., & Jhung, S. H. 2017. Applications of metal-organic frameworks in adsorption/separation processes via hydrogen bonding interactions. ***Chemical Engineering Journal***, 310: 197-215.

Ahmed, I., Khan, N. A., Hasan, Z., & Jhung, S. H. 2013. Adsorptive denitrogenation of model fuels with porous metal-organic framework (MOF) MIL-101 impregnated with phosphotungstic acid: effect of acid site inclusion. ***J Hazard Mater***, 250-251: 37-44.

Ahmed, M. B., Zhou, J. L., Ngo, H. H., & Guo, W. 2015a. Adsorptive removal of antibiotics from water and wastewater: Progress and challenges. ***Science of the Total Environment***, 532: 112-126.

Ahmed, M. B., Zhou, J. L., Ngo, H. H., & Guo, W. 2015b. Adsorptive removal of antibiotics from water and wastewater: Progress and challenges. ***Sci Total Environ***, 532: 112-126.

Al-Zoubi, H., Ibrahim, K. A., & Abu-Sbeih, K. A. 2015. Removal of heavy metals from wastewater by economical polymeric collectors using dissolved air flotation process. ***Journal of Water Process Engineering***, 8: 19-27.

Almáši, M., Zeleňák, V., Kuchár, J., Bourrelly, S., & Llewellyn, P. L. 2016. New members of MOF-76 family containing Ho(III) and Tm(III) ions: Characterization, stability and gas adsorption properties. ***Colloids and Surfaces A: Physicochemical and Engineering Aspects***, 496: 114-124.

An, J., Farha, O. K., Hupp, J. T., Pohl, E., Yeh, J. I., & Rosi, N. L. 2012. Metal-adeninate vertices for the construction of an exceptionally porous metal-organic framework. ***Nat Commun***, 3: 604.

An, J., Geib, S. J., & Rosi, N. L. 2010. High and Selective CO2 Uptake in a Cobalt Adeninate Metal−Organic Framework Exhibiting Pyrimidine- and Amino-Decorated Pores. ***Journal of the American Chemical Society***, 132(1): 38-39.

Andrew Lin, K.-Y., & Hsieh, Y.-T. 2015. Copper-based metal organic framework (MOF), HKUST-1, as an efficient adsorbent to remove p-nitrophenol from water. ***Journal of the Taiwan Institute of Chemical Engineers***, 50: 223-228.

Andrew Lin, K.-Y., & Lee, W.-D. 2016. Self-assembled magnetic graphene supported ZIF-67 as a recoverable and efficient adsorbent for benzotriazole. ***Chemical Engineering Journal***, 284: 1017-1027.

Arshadi, M., Mousavinia, F., Amiri, M. J., & Faraji, A. R. 2016. Adsorption of methyl orange and salicylic acid on a nano-transition metal composite: Kinetics, thermodynamic and electrochemical studies. ***J Colloid Interface Sci***, 483: 118-131.

Asfaram, A., Ghaedi, M., Azqhandi, M. H. A., Goudarzi, A., & Dastkhoon, M. 2016a. Statistical experimental design, least squares-support vector machine (LS-SVM) and artificial neural network (ANN) methods for modeling the facilitated adsorption of methylene blue dye. ***RSC Adv.***, 6(46): 40502-40516.

Asfaram, A., Ghaedi, M., Goudarzi, A., & Rajabi, M. 2015. Response surface methodology approach for optimization of simultaneous dye and metal ion ultrasound-assisted adsorption onto Mn doped Fe3O4-NPs loaded on AC: kinetic and isothermal studies. ***Dalton Trans***, 44(33): 14707-14723.

Asfaram, A., Ghaedi, M., Hajati, S., & Goudarzi, A. 2015. Ternary dye adsorption onto MnO2nanoparticle-loaded activated carbon: derivative spectrophotometry and modeling. ***RSC Adv.***, 5(88): 72300-72320.

Asfaram, A., Ghaedi, M., Hajati, S., Goudarzi, A., & Dil, E. A. 2017. Screening and optimization of highly effective ultrasound-assisted simultaneous adsorption of cationic dyes onto Mn-doped Fe3O4-nanoparticle-loaded activated carbon. ***Ultrason Sonochem***, 34: 1-12.

Asfaram, A., Ghaedi, M., Yousefi, F., & Dastkhoon, M. 2016b. Experimental design and modeling of ultrasound assisted simultaneous adsorption of cationic dyes onto ZnS: Mn-NPs-AC from binary mixture. ***Ultrason Sonochem***, 33: 77-89.

Azhar, M. R., Abid, H. R., Periasamy, V., Sun, H., Tade, M. O., & Wang, S. 2017a. Adsorptive removal of antibiotic sulfonamide by UiO-66 and ZIF-67 for wastewater treatment. ***J Colloid Interface Sci***, 500: 88-95.

Azhar, M. R., Abid, H. R., Sun, H., Periasamy, V., Tade, M. O., & Wang, S. 2016. Excellent performance of copper based metal organic framework in adsorptive removal of toxic sulfonamide antibiotics from wastewater. ***J Colloid Interface Sci***, 478: 344-352.

Azhar, M. R., Abid, H. R., Sun, H., Periasamy, V., Tade, M. O., & Wang, S. 2017b. One-pot synthesis of binary metal organic frameworks (HKUST-1 and UiO-

66) for enhanced adsorptive removal of water contaminants. ***J Colloid Interface Sci***, 490: 685-694.

Azhar, M. R., Abid, H. R., Tade, M. O., Periasamy, V., Sun, H., & Wang, S. 2018. Cascade applications of robust MIL-96 metal organic frameworks in environmental remediation: Proof of concept. ***Chemical Engineering Journal***.

Bai, Z. Y., Yang, Q., & Wang, J. L. 2015. Fe3O4/multi-walled carbon nanotubes as an efficient catalyst for catalytic ozonation of p-hydroxybenzoic acid. ***International Journal of Environmental Science and Technology***, 13(2): 483-492.

Bakhtiari, N., & Azizian, S. 2015. Adsorption of copper ion from aqueous solution by nanoporous MOF-5: A kinetic and equilibrium study. ***Journal of Molecular Liquids***, 206: 114-118.

Banu, A.-M., Friedrich, D., Brandani, S., & Düren, T. 2013. A Multiscale Study of MOFs as Adsorbents in H2PSA Purification. ***Industrial & Engineering Chemistry Research***, 52(29): 9946-9957.

Bao, Z., Chang, G., Xing, H., Krishna, R., Ren, Q., & Chen, B. 2016. Potential of microporous metal–organic frameworks for separation of hydrocarbon mixtures. ***Energy Environ. Sci.***, 9(12): 3612-3641.

Basdogan, Y., & Keskin, S. 2015. Simulation and modelling of MOFs for hydrogen storage. ***CrystEngComm***, 17(2): 261-275.

Belpaire, C., Reyns, T., Geeraerts, C., & Van Loco, J. 2015. Toxic textile dyes accumulate in wild European eel Anguilla anguilla. ***Chemosphere***, 138: 784-791.

Biswas, S., & Van Der Voort, P. 2013. A General Strategy for the Synthesis of Functionalised UiO-66 Frameworks: Characterisation, Stability and CO2Adsorption Properties. ***European Journal of Inorganic Chemistry***, 2013(12): 2154-2160.

Blasioli, S., Martucci, A., Paul, G., Gigli, L., Cossi, M., Johnston, C. T., Marchese, L., & Braschi, I. 2014a. Removal of sulfamethoxazole sulfonamide antibiotic from water by high silica zeolites: a study of the involved host-guest interactions by a combined structural, spectroscopic, and computational approach. ***J Colloid Interface Sci***, 419: 148-159.

Blasioli, S., Martucci, A., Paul, G., Gigli, L., Cossi, M., Johnston, C. T., Marchese, L., & Braschi, I. 2014b. Removal of sulfamethoxazole sulfonamide antibiotic from water by high silica zeolites: a study of the involved host-guest interactions by a combined structural, spectroscopic, and computational approach. ***Journal of Colloid and Interface Science***, 419: 148-159.

Brain, R. A., Ramirez, A. J., Fulton, B. A., Chambliss, C. K., & Brooks, B. W. 2008. Herbicidal Effects of Sulfamethoxazole in Lemna gibba: Using p-Aminobenzoic Acid As a Biomarker of Effect. ***Environmental Science & Technology***, 42(23): 8965-8970.

Braschi, I., Blasioli, S., Buscaroli, E., Montecchio, D., & Martucci, A. 2015. Physicochemical regeneration of high silica zeolite Y used to clean-up water polluted with sulfonamide antibiotics. ***Journal of Environmental Sciences***: In Press.

Braschi, I., Blasioli, S., Gigli, L., Gessa, C. E., Alberti, A., & Martucci, A. 2010a. Removal of sulfonamide antibiotics from water: Evidence of adsorption into an organophilic zeolite Y by its structural modifications. ***Journal of Hazardous Materials***, 178(1-3): 218-225.

Braschi, I., Blasioli, S., Gigli, L., Gessa, C. E., Alberti, A., & Martucci, A. 2010b. Removal of sulfonamide antibiotics from water: Evidence of adsorption into an organophilic zeolite Y by its structural modifications. ***J Hazard Mater***, 178(1-3): 218-225.

Braschi, I., Gatti, G., Paul, G., Gessa, C. E., Cossi, M., & Marchese, L. 2010c. Sulfonamide antibiotics embedded in high silica zeolite Y: a combined experimental and theoretical study of host-guest and guest-guest interactions. ***Langmuir***, 26(12): 9524-9532.

Braschi, I., Paul, G., Gatti, G., Cossi, M., & Marchese, L. 2013. Embedding monomers and dimers of sulfonamide antibiotics into high silica zeolite Y: an experimental and computational study of the tautomeric forms involved. ***RSC Advances***, 3(20): 7427.

Britt, D., Lee, C., Uribe-Romo, F. J., Furukawa, H., & Yaghi, O. M. 2010. Ring-Opening Reactions within Porous Metal−Organic Frameworks. ***Inorganic Chemistry***, 49(14): 6387-6389.

Bu, Q., Wang, B., Huang, J., Deng, S., & Yu, G. 2013. Pharmaceuticals and personal care products in the aquatic environment in China: A review. ***Journal of Hazardous Materials***, 262(0): 189-211.

Burkhardt, M., Stamm, C., Waul, C., Singer, H., & Muller, S. 2005. Surface runoff and transport of sulfonamide antibiotics and tracers on manured grassland. ***Journal of Environmental Quality***, 34(4): 1363-1371.

Burtch, N. C., Jasuja, H., & Walton, K. S. 2014. Water stability and adsorption in metal-organic frameworks. ***Chem Rev***, 114(20): 10575-10612.

C. Adams, M. A., Y.Wang, K. Loftin and M. Meyer 2002. Removal of Antibiotics from Surface and Distilled Water in Conventional Water Treatment Processes. ***Journal of Environmental Engineering***, 128(3): 253-260.

Canivet, J., Fateeva, A., Guo, Y., Coasne, B., & Farrusseng, D. 2014. Water adsorption in MOFs: fundamentals and applications. ***Chem Soc Rev***, 43(16): 5594-5617.

Carmona, E., Andreu, V., & Pico, Y. 2014a. Occurrence of acidic pharmaceuticals and personal care products in Turia River Basin: from waste to drinking water. ***Sci Total Environ***, 484: 53-63.

Carmona, E., Andreu, V., & Pico, Y. 2014b. Occurrence of acidic pharmaceuticals and personal care products in Turia River Basin: from waste to drinking water. ***Science of the Total Environment***, 484: 53-63.

Carrales-Alvarado, D. H., Ocampo-Perez, R., Leyva-Ramos, R., & Rivera-Utrilla, J. 2014. Removal of the antibiotic metronidazole by adsorption on various carbon materials from aqueous phase. ***Journal of Colloid and Interface Science***, 436: 276-285.

Cavka, J. H., Jakobsen, S., Olsbye, U., Guillou, N., Lamberti, C., Bordiga, S., & Lillerud, K. P. 2008. A New Zirconium Inorganic Building Brick Forming Metal Organic Frameworks with Exceptional Stability. ***Journal of the American Chemical Society***, 130(42): 13850-13851.

Chan, Y. J., Chong, M. F., Law, C. L., & Hassell, D. G. 2009. A review on anaerobic–aerobic treatment of industrial and municipal wastewater. ***Chemical Engineering Journal***, 155(1-2): 1-18.

Chang, I.-S., Clech, P. L., Jefferson, B., & Judd, S. 2002. Membrane Fouling in Membrane Bioreactors for Wastewater Treatment. ***Journal of Environmental Engineering***, 128(11): 1018-1029.

Che, H., & Liu, S. 2014. Contaminant Detection Using Multiple Conventional Water Quality Sensors in an Early Warning System. ***Procedia Engineering***, 89: 479-487.

Chen, A., Li, Y., Yu, Y., Li, Y., Xia, K., Wang, Y., Li, S., & Zhang, L. 2016a. Synthesis of hollow mesoporous carbon spheres via "dissolution-capture" method for effective phenol adsorption. ***Carbon***, 103: 157-162.

Chen, B., Liu, Y., Chen, S., Zhao, X., Yue, W., & Pan, X. 2016b. Nitrogen-rich core/shell magnetic nanostructures for selective adsorption and separation of anionic dyes from aqueous solution. ***Environ. Sci.: Nano***, 3(3): 670-681.

Chen, C., Zhang, M., Guan, Q., & Li, W. 2012. Kinetic and thermodynamic studies on the adsorption of xylenol orange onto MIL-101(Cr). ***Chemical Engineering Journal***, 183: 60-67.

Chen, J., Zhang, H., Liu, P., Li, Y., Li, G., An, T., & Zhao, H. 2015a. Thiourea sole doping reagent approach for controllable N, S co-doping of pre-synthesized large-sized carbon nanospheres as electrocatalyst for oxygen reduction reaction. ***Carbon***, 92: 339-347.

Chen, K., & Zhou, J. L. 2014. Occurrence and behavior of antibiotics in water and sediments from the Huangpu River, Shanghai, China. ***Chemosphere***, 95: 604-612.

Chen, Q., He, Q., Lv, M., Xu, Y., Yang, H., Liu, X., & Wei, F. 2015b. Selective adsorption of cationic dyes by UiO-66-NH2. ***Applied Surface Science***, 327: 77-85.

Chen, X. Y., Hoang, V.-T., Rodrigue, D., & Kaliaguine, S. 2013. Optimization of continuous phase in amino-functionalized metal–organic framework (MIL-53) based co-polyimide mixed matrix membranes for CO2/CH4 separation. ***RSC Advances***, 3(46): 24266.

Chen, Z., Luo, J., Chen, X., Hang, X., Shen, F., & Wan, Y. 2016c. Fully recycling dairy wastewater by an integrated isoelectric precipitation–nanofiltration–anaerobic fermentation process. ***Chemical Engineering Journal***, 283: 476-485.

Cheng, Y., Li, T., Fang, C., Zhang, M., Liu, X., Yu, R., & Hu, J. 2013. Soft-templated synthesis of mesoporous carbon nanospheres and hollow carbon nanofibers. ***Applied Surface Science***, 282: 862-869.

Cherfi, A., Achour, M., Cherfi, M., Otmani, S., & Morsli, A. 2015. Health risk assessment of heavy metals through consumption of vegetables irrigated with reclaimed urban wastewater in Algeria. ***Process Safety and Environmental Protection***, 98: 245-252.

Cho, Y.-S., Lee, B.-U., & Oh, K.-H. 2008. Simultaneous degradation of nitroaromatic compounds TNT, RDX, atrazine, and simazine byPseudomonas putidaHK-6 in bench-scale bioreactors. ***Journal of Chemical Technology & Biotechnology***, 83(9): 1211-1217.

Choi, H. J., Dincă, M., & Long, J. R. 2008. Broadly Hysteretic H2 Adsorption in the Microporous Metal−Organic Framework Co(1,4-benzenedipyrazolate). ***Journal of the American Chemical Society***, 130(25): 7848-7850.

Choi, K. M., Park, J. H., & Kang, J. K. 2015. Nanocrystalline MOFs Embedded in the Crystals of Other MOFs and Their Multifunctional Performance for Molecular Encapsulation and Energy-Carrier Storage. ***Chemistry of Materials***, 27(14): 5088-5093.

Chughtai, A. H., Ahmad, N., Younus, H. A., Laypkov, A., & Verpoort, F. 2015. Metal-organic frameworks: versatile heterogeneous catalysts for efficient catalytic organic transformations. ***Chemical Society Reviews***.

Chui, S. S.-Y., Lo, S. M.-F., Charmant, J. P. H., Orpen, A. G., & Williams, I. D. 1999a. A Chemically Functionalizable Nanoporous Material [Cu3(TMA)2(H2O)3]n. ***Science***, 283(5405): 1148-1150.

Chui, S. S. Y., Lo, S. M. F., Charmant, J. P. H., Orpen, A. G., & Williams, I. D. 1999b. A Chemically Functionalizable Nanoporous Material [Cu3(TMA)2(H2O)3]n. ***Science***, 283(5405): 1148.

Chun, J., Kang, S., Park, N., Park, E. J., Jin, X., Kim, K. D., Seo, H. O., Lee, S. M., Kim, H. J., Kwon, W. H., Park, Y. K., Kim, J. M., Kim, Y. D., & Son, S. U. 2014. Metal-organic framework@microporous organic network: hydrophobic adsorbents with a crystalline inner porosity. ***J Am Chem Soc***, 136(19): 6786-6789.

Clough, A., Zheng, S.-T., Zhao, X., Lin, Q., Feng, P., & Bu, X. 2014. New Lithium Ion Clusters for Construction of Porous MOFs. ***Crystal Growth & Design***, 14(3): 897-900.

Colombo, V., Galli, S., Choi, H. J., Han, G. D., Maspero, A., Palmisano, G., Masciocchi, N., & Long, J. R. 2011. High thermal and chemical stability in pyrazolate-bridged metal–organic frameworks with exposed metal sites. ***Chemical Science***, 2(7): 1311.

Cruz, d. l., Fournier, M. L., García, F., Molina, A., Chavarría, G., Alfaro, M., Ramírez, F., & Rodrigues, C. 2014. Hazard prioritization and risk characterization of antibiotics in an irrigated Costa Rican region used for intensive crop, livestock and aquaculture farming. ***Journal of Environmental Biology*** 35: 85-98.

Cychosz, K. A., & Matzger, A. J. 2010. Water stability of microporous coordination polymers and the adsorption of pharmaceuticals from water. ***Langmuir***, 26(22): 17198-17202.

Daughton, C. G., & Ternes, T. A. 1999. Pharmaceuticals and personal care products in the environment: Agents of subtle change? ***Environmental Health Perspectives***, 107(SUPPL. 6): 907-938.

Davies, P. R., Roberts, M. W., & Shukla, N. 1991. The reactive chemisorption of formic acid at A1(111) surfaces and the influence of surface oxidation and coadsorption with water: a combined XPS and HREELS investigation. ***Journal of Physics: Condensed Matter***, 3(S): S237.

Dawood, S., & Sen, T. K. 2012. Removal of anionic dye Congo red from aqueous solution by raw pine and acid-treated pine cone powder as adsorbent: equilibrium, thermodynamic, kinetics, mechanism and process design. ***Water Res***, 46(6): 1933-1946.

Deleu, W. P. R., Stassen, I., Jonckheere, D., Ameloot, R., & De Vos, D. E. 2016. Waste PET (bottles) as a resource or substrate for MOF synthesis. ***Journal of Materials Chemistry A***, 4(24): 9519-9525.

Dil, E. A., Ghaedi, M., Ghaedi, A., Asfaram, A., Jamshidi, M., & Purkait, M. K. 2016. Application of artificial neural network and response surface methodology for the removal of crystal violet by zinc oxide nanorods loaded on activate carbon: kinetics and equilibrium study. ***Journal of the Taiwan Institute of Chemical Engineers***, 59: 210-220.

Dirany, A., Sires, I., Oturan, N., Ozcan, A., & Oturan, M. A. 2012a. Electrochemical treatment of the antibiotic sulfachloropyridazine: kinetics, reaction pathways, and toxicity evolution. ***Environ Sci Technol***, 46(7): 4074-4082.

Dirany, A., Sires, I., Oturan, N., Ozcan, A., & Oturan, M. A. 2012b. Electrochemical treatment of the antibiotic sulfachloropyridazine: kinetics, reaction pathways, and toxicity evolution. ***Environmental Science & Technology***, 46(7): 4074-4082.

Djukić, A., Jovanović, U., Tuvić, T., Andrić, V., Grbović Novaković, J., Ivanović, N., & Matović, L. 2013. The potential of ball-milled Serbian natural clay for removal of heavy metal contaminants from wastewaters: Simultaneous sorption of Ni, Cr, Cd and Pb ions. ***Ceramics International***, 39(6): 7173-7178.

Dodge, L. E., Kelley, K. E., Williams, P. L., Williams, M. A., Hernandez-Diaz, S., Missmer, S. A., & Hauser, R. 2015. Medications as a source of paraben exposure. ***Reprod Toxicol***, 52: 93-100.

Dong, G., Zhang, Y., Pan, Q., & Qiu, J. 2014. A fantastic graphitic carbon nitride (g-C3N4) material: Electronic structure, photocatalytic and photoelectronic properties. ***Journal of Photochemistry and Photobiology C: Photochemistry Reviews***, 20: 33-50.

Du, J. J., Yuan, Y. P., Sun, J. X., Peng, F. M., Jiang, X., Qiu, L. G., Xie, A. J., Shen, Y. H., & Zhu, J. F. 2011. New photocatalysts based on MIL-53 metal-organic frameworks for the decolorization of methylene blue dye. ***J Hazard Mater***, 190(1-3): 945-951.

Du, Z., Deng, S., Chen, Y., Wang, B., Huang, J., Wang, Y., & Yu, G. 2015. Removal of perfluorinated carboxylates from washing wastewater of perfluorooctanesulfonyl fluoride using activated carbons and resins. ***J Hazard Mater***, 286: 136-143.

Duan, X., Indrawirawan, S., Sun, H., & Wang, S. 2015a. Effects of nitrogen-, boron-, and phosphorus-doping or codoping on metal-free graphene catalysis. ***Catalysis Today***, 249: 184-191.

Duan, X., Su, C., Zhou, L., Sun, H., Suvorova, A., Odedairo, T., Zhu, Z., Shao, Z., & Wang, S. 2016. Surface controlled generation of reactive radicals from persulfate by carbocatalysis on nanodiamonds. ***Applied Catalysis B: Environmental***, 194: 7-15.

Duan, X., Sun, H., Kang, J., Wang, Y., Indrawirawan, S., & Wang, S. 2015b. Insights into Heterogeneous Catalysis of Persulfate Activation on Dimensional-Structured Nanocarbons. ***ACS Catalysis***, 5(8): 4629-4636.

Duan, X., Sun, H., Tade, M., & Wang, S. 2017a. Metal-free activation of persulfate by cubic mesoporous carbons for catalytic oxidation via radical and nonradical processes. ***Catalysis Today***.

Duan, Y., Pan, F., Liu, Q., Zhou, Y., Liang, A., & Zhang, J. 2017b. Salt-Induced Phase Separation to Synthesize Ordered Mesoporous Carbon by pH-Controlled Self-Assembly. ***The Journal of Physical Chemistry C***, 121(2): 1243-1248.

Dutta, S., Bhaumik, A., & Wu, K. C. W. 2014. Hierarchically porous carbon derived from polymers and biomass: effect of interconnected pores on energy applications. ***Energy & Environmental Science***, 7(11): 3574-3592.

e Silva, F. A., Sintra, T., Ventura, S. P. M., & Coutinho, J. A. P. 2014. Recovery of paracetamol from pharmaceutical wastes. ***Separation and Purification Technology***, 122: 315-322.

El-Sherif, I. Y., Tolani, S., Ofosu, K., Mohamed, O. A., & Wanekaya, A. K. 2013. Polymeric nanofibers for the removal of Cr(III) from tannery waste water. ***J Environ Manage***, 129: 410-413.

Elaigwu, S. E., Kyriakou, G., Prior, T. J., & Greenway, G. M. 2014. Microwave-assisted hydrothermal synthesis of carbon monolith via a soft-template method using resorcinol and formaldehyde as carbon precursor and pluronic F127 as template. ***Materials Letters***, 123: 198-201.

Erucar, I., & Keskin, S. 2016. Efficient Storage of Drug and Cosmetic Molecules in Biocompatible Metal Organic Frameworks: A Molecular Simulation Study. ***Industrial & Engineering Chemistry Research***, 55(7): 1929-1939.

Estrada, J. M., Kraakman, N. J., Lebrero, R., & Munoz, R. 2015. Integral approaches to wastewater treatment plant upgrading for odor prevention: Activated Sludge and Oxidized Ammonium Recycling. ***Bioresour Technol***, 196: 685-693.

Evans, J. D., Sumby, C. J., & Doonan, C. J. 2014. Post-synthetic metalation of metal-organic frameworks. ***Chemical Society Reviews***, 43(16): 5933-5951.

Evans, W. A., Davies, P. J., & McRae, C. 2016. The occurrence of methyl, ethyl, propyl, and butyl parabens in the urban rivers and stormwaters of Sydney, Australia. ***Environ. Sci.: Water Res. Technol.***, 2(4): 733-742.

Fabianska, A., Bialk-Bielinska, A., Stepnowski, P., Stolte, S., & Siedlecka, E. M. 2014. Electrochemical degradation of sulfonamides at BDD electrode: kinetics, reaction pathway and eco-toxicity evaluation. ***J Hazard Mater***, 280: 579-587.

Fakhri, A., & Behrouz, S. 2015. Comparison studies of adsorption properties of MgO nanoparticles and ZnO–MgO nanocomposites for linezolid antibiotic removal from aqueous solution using response surface methodology. ***Process Safety and Environmental Protection***, 94: 37-43.

Ferey, G. 2008. Hybrid porous solids: past, present, future. ***Chemical Society Reviews***, 37(1): 191-214.

Finizio, A., Azimonti, G., & Villa, S. 2011. Occurrence of pesticides in surface water bodies: a critical analysis of the Italian national pesticide survey programs. ***Journal of Environmental Monitoring***, 13(1): 49-57.

Fiol, N., & Villaescusa, I. 2008. Determination of sorbent point zero charge: usefulness in sorption studies. ***Environmental Chemistry Letters***, 7(1): 79-84.

Freundlich, H. 1906a. Adsorption in solution. ***International Journal of Research in Physical Chemistry and Chemical Physics***, 57: 384-470.

Freundlich, H. M. F. 1906b. Over the adsorption in solution. ***J. Phys. Chem***, 57(385): e470.

Fujimoto, A., Yamada, Y., Koinuma, M., & Sato, S. 2016. Origins of sp(3)C peaks in C1s X-ray Photoelectron Spectra of Carbon Materials. ***Anal Chem***, 88(12): 6110-6114.

Fukahori, S., Fujiwara, T., Ito, R., & Funamizu, N. 2011. pH-Dependent adsorption of sulfa drugs on high silica zeolite: Modeling and kinetic study. ***Desalination***, 275(1–3): 237-242.

Furukawa, H., Gandara, F., Zhang, Y. B., Jiang, J., Queen, W. L., Hudson, M. R., & Yaghi, O. M. 2014. Water adsorption in porous metal-organic frameworks and related materials. ***J Am Chem Soc***, 136(11): 4369-4381.

Gandara, F., Furukawa, H., Lee, S., & Yaghi, O. M. 2014a. High methane storage capacity in aluminum metal-organic frameworks. ***J Am Chem Soc***, 136(14): 5271-5274.

Gandara, F., Furukawa, H., Lee, S., & Yaghi, O. M. 2014b. High methane storage capacity in aluminum metal-organic frameworks. ***Journal of American Chemical Society***, 136(14): 5271-5274.

Gao, J., Miao, J., Li, P. Z., Teng, W. Y., Yang, L., Zhao, Y., Liu, B., & Zhang, Q. 2014. A p-type Ti(IV)-based metal-organic framework with visible-light photo-response. ***Chem Commun (Camb)***, 50(29): 3786-3788.

García-Galán, M. J., Díaz-Cruz, M. S., & Barceló, D. 2012. Occurrence and Fate of Sulfonamide Antibiotics in Surface Waters: Climatic Effects on Their Presence in the Mediterranean Region and Aquatic Ecosystem Vulnerability. 21: 167-192.

Garcia, X., & Pargament, D. 2015. Reusing wastewater to cope with water scarcity: Economic, social and environmental considerations for decision-making. ***Resources, Conservation and Recycling***, 101: 154-166.

Getman, R. B., Bae, Y. S., Wilmer, C. E., & Snurr, R. Q. 2012. Review and analysis of molecular simulations of methane, hydrogen, and acetylene storage in metal-organic frameworks. ***Chem Rev***, 112(2): 703-723.

Ghanbari, F., & Moradi, M. 2017. Application of peroxymonosulfate and its activation methods for degradation of environmental organic pollutants: Review. ***Chemical Engineering Journal***, 310: 41-62.

Ghosh, P., Colon, Y. J., & Snurr, R. Q. 2014. Water adsorption in UiO-66: the importance of defects. ***Chem Commun (Camb)***, 50(77): 11329-11331.

Goglio, G., Foy, D., & Demazeau, G. 2008. State of Art and recent trends in bulk carbon nitrides synthesis. ***Materials Science and Engineering: R: Reports***, 58(6): 195-227.

Gomes, C. S., Piccin, J. S., & Gutterres, M. 2016. Optimizing adsorption parameters in tannery-dye-containing effluent treatment with leather shaving waste. ***Process Safety and Environmental Protection***, 99: 98-106.

Gong, Y., Zhao, X., Cai, Z., O'Reilly, S. E., Hao, X., & Zhao, D. 2014. A review of oil, dispersed oil and sediment interactions in the aquatic environment: Influence on the fate, transport and remediation of oil spills. ***Marine Pollution Bulletin***, 79(1–2): 16-33.

Górka, J., Fenning, C., & Jaroniec, M. 2009. Influence of temperature, carbon precursor/copolymer ratio and acid concentration on adsorption and structural properties of mesoporous carbons prepared by soft-templating. ***Colloids and Surfaces A: Physicochemical and Engineering Aspects***, 352(1-3): 113-117.

Gotthardt, M. A., Schoch, R., Wolf, S., Bauer, M., & Kleist, W. 2015. Synthesis and characterization of bimetallic metal-organic framework Cu-Ru-BTC with HKUST-1 structure. ***Dalton Trans***, 44(5): 2052-2056.

Grant Glover, T., Peterson, G. W., Schindler, B. J., Britt, D., & Yaghi, O. 2011. MOF-74 building unit has a direct impact on toxic gas adsorption. ***Chemical Engineering Science***, 66(2): 163-170.

Gul-E-Noor, F., Jee, B., Mendt, M., Himsl, D., Pöppl, A., Hartmann, M., Haase, J., Krautscheid, H., & Bertmer, M. 2012. Formation of Mixed Metal Cu3–xZnx(btc)2Frameworks with Different Zinc Contents: Incorporation of Zn2+into the Metal–Organic Framework Structure as Studied by Solid-State NMR. ***The Journal of Physical Chemistry C***, 116(39): 20866-20873.

Guo, X., Xing, T., Lou, Y., & Chen, J. 2016. Controlling ZIF-67 crystals formation through various cobalt sources in aqueous solution. ***Journal of Solid State Chemistry***, 235: 107-112.

Gupta, V. K., & Suhas. 2009. Application of low-cost adsorbents for dye removal – A review. ***Journal of Environmental Management***, 90(8): 2313-2342.

Haines, A. 2003. Climate Change 2001: The Scientific Basis. Contribution of Working Group 1 to the Third Assessment report of the Intergovernmental Panel on Climate Change.: JT Houghton, Y Ding, DJ Griggs, M Noguer, PJ van der Winden, X Dai. Cambridge: Cambridge University Press, 2001, pp. 881, £34.95 (HB) ISBN: 0-21-01495-6; £90.00 (HB) ISBN: 0-521-80767-0. ***International Journal of Epidemiology***, 32(2): 321.

Hameed, B. H. 2009. Spent tea leaves: A new non-conventional and low-cost adsorbent for removal of basic dye from aqueous solutions. ***Journal of Hazardous Materials***, 161(2–3): 753-759.

Hamoudi, S., Saad, R., & Belkacemi, K. 2007. Adsorptive Removal of Phosphate and Nitrate Anions from Aqueous Solutions Using Ammonium-Functionalized Mesoporous Silica. ***Industrial & Engineering Chemistry Research***, 46(25): 8806-8812.

Han, W., Yue, Q., Wu, S., Zhao, Y., Gao, B., Li, Q., & Wang, Y. 2013. Application and advantages of novel clay ceramic particles (CCPs) in an up-flow anaerobic bio-filter (UAF) for wastewater treatment. ***Bioresour Technol***, 137: 171-178.

Haque, E., Jun, J. W., & Jhung, S. H. 2011. Adsorptive removal of methyl orange and methylene blue from aqueous solution with a metal-organic framework material, iron terephthalate (MOF-235). ***J Hazard Mater***, 185(1): 507-511.

Haque, E., Lee, J. E., Jang, I. T., Hwang, Y. K., Chang, J. S., Jegal, J., & Jhung, S. H. 2010a. Adsorptive removal of methyl orange from aqueous solution with metal-organic frameworks, porous chromium-benzenedicarboxylates. ***Journal of Hazardous Materials***, 181: 535-542.

Haque, E., Lee, J. E., Jang, I. T., Hwang, Y. K., Chang, J. S., Jegal, J., & Jhung, S. H. 2010b. Adsorptive removal of methyl orange from aqueous solution with metal-organic frameworks, porous chromium-benzenedicarboxylates. ***J Hazard Mater***.

Haque, E., Lo, V., Minett, A. I., Harris, A. T., & Church, T. L. 2014a. Dichotomous adsorption behaviour of dyes on an amino-functionalised metal–organic framework, amino-MIL-101(Al). ***Journal of Materials Chemistry A***, 2(1): 193.

Haque, E., Lo, V., Minett, A. I., Harris, A. T., & Church, T. L. 2014b. Dichotomous adsorption behaviour of dyes on an amino-functionalised metal–organic framework, amino-MIL-101(Al). ***Journal of Materials Chemistry A***, 2(1): 193-203.

Hartmann, M., Kullmann, S., & Keller, H. 2010. Wastewater treatment with heterogeneous Fenton-type catalysts based on porous materials. ***Journal of Materials Chemistry***, 20(41): 9002-9017.

Hasan, Z., Choi, E.-J., & Jhung, S. H. 2013. Adsorption of naproxen and clofibric acid over a metal–organic framework MIL-101 functionalized with acidic and basic groups. ***Chemical Engineering Journal***, 219: 537-544.

Hasan, Z., Jeon, J., & Jhung, S. H. 2012. Adsorptive removal of naproxen and clofibric acid from water using metal-organic frameworks. ***J Hazard Mater***, 209-210: 151-157.

Hasan, Z., & Jhung, S. H. 2014. Removal of hazardous organics from water using metal-organic frameworks (MOFs): Plausible mechanisms for selective adsorptions. ***J Hazard Mater***, 283C: 329-339.

Hasan, Z., Tong, M., Jung, B. K., Ahmed, I., Zhong, C., & Jhung, S. H. 2014. Adsorption of Pyridine over Amino-Functionalized Metal–Organic Frameworks: Attraction via Hydrogen Bonding versus Base–Base Repulsion. ***The Journal of Physical Chemistry C***, 118(36): 21049-21056.

Hayat, H., Mahmood, Q., Pervez, A., Bhatti, Z. A., & Baig, S. A. 2015. Comparative decolorization of dyes in textile wastewater using biological and chemical treatment. ***Separation and Purification Technology***, 154: 149-153.

Heath, E. A., Singh, P., & Ebisuzaki, Y. 1992. Structure of p-hydroxybenzoic acid and p-hydroxybenzoic acid-acetone complex (2/1). ***Acta Crystallographica***, C48: 1960-1965.

Hernandez-Ramirez, O., & Holmes, S. M. 2008. Novel and modified materials for wastewater treatment applications. ***Journal of Materials Chemistry***, 18(24): 2751.

Herrero, P., Borrull, F., Pocurull, E., & Marcé, R. M. 2014. An overview of analytical methods and occurrence of benzotriazoles, benzothiazoles and benzenesulfonamides in the environment. ***Trends in Analytical Chemistry***, 62: 46-55.

Ho, Y. S., & McKay, G. 1999a. Pseudo-second order model for sorption processes. ***Process Biochemistry***, 34(5): 451-465.

Ho, Y. S., & McKay, G. 1999b. The sorption of lead(II) ions on peat. ***Water Research***, 33(2): 578-584.

Holland, J. E., Luck, G. W., & Max Finlayson, C. 2015. Threats to food production and water quality in the Murray–Darling Basin of Australia. ***Ecosystem Services***, 12: 55-70.

Horcajada, P., Gref, R., Baati, T., Allan, P. K., Maurin, G., Couvreur, P., Ferey, G., Morris, R. E., & Serre, C. 2012. Metal-organic frameworks in biomedicine. ***Chem Rev***, 112(2): 1232-1268.

Horcajada, P., Surble, S., Serre, C., Hong, D. Y., Seo, Y. K., Chang, J. S., Greneche, J. M., Margiolaki, I., & Ferey, G. 2007. Synthesis and catalytic properties of MIL-100(Fe), an iron(III) carboxylate with large pores. ***Chem Commun (Camb)***(27): 2820-2822.

Hsieh, T.-J., Su, C.-C., Chen, C.-Y., Liou, C.-H., & Lu, L.-H. 2005. Using experimental studies and theoretical calculations to analyze the molecular mechanism of coumarin, p-hydroxybenzoic acid, and cinnamic acid. ***Journal of Molecular Structure***, 741(1-3): 193-199.

http://www.medicinescomplete.com/mc/clarke/current/index.htm.

Huang, X., Li, X., Pan, B., Li, H., Zhang, Y., & Xie, B. 2015. Self-enhanced ozonation of benzoic acid at acidic pHs. ***Water Res***, 73: 9-16.

Huerta, B., Rodriguez-Mozaz, S., Nannou, C., Nakis, L., Ruhi, A., Acuna, V., Sabater, S., & Barcelo, D. 2015. Determination of a broad spectrum of pharmaceuticals and endocrine disruptors in biofilm from a waste water treatment plant-impacted river. ***Science of the Total Environment***, 540: 241-249.

Huo, S.-H., & Yan, X.-P. 2012. Metal–organic framework MIL-100(Fe) for the adsorption of malachite green from aqueous solution. ***Journal of Materials Chemistry***, 22(15): 7449.

Huston, R., Chan, Y. C., Chapman, H., Gardner, T., & Shaw, G. 2012. Source apportionment of heavy metals and ionic contaminants in rainwater tanks in a subtropical urban area in Australia. ***Water Res***, 46(4): 1121-1132.

Ihsan Hamawand. 2015. Review of wastewater treatment chemicals and organic chemistry alternatives for abattoir effluent. ***Australian Meat Processor Corporation***.

Indrawirawan, S., Sun, H., Duan, X., & Wang, S. 2015a. Low temperature combustion synthesis of nitrogen-doped graphene for metal-free catalytic oxidation. ***J. Mater. Chem. A***, 3(7): 3432-3440.

Indrawirawan, S., Sun, H., Duan, X., & Wang, S. 2015b. Nanocarbons in different structural dimensions (0–3D) for phenol adsorption and metal-free catalytic oxidation. ***Applied Catalysis B: Environmental***, 179: 352-362.

Ishihama, Y., Nakamura, M., Miwa, T., Kajima, T., & Asakawa, N. 2002a. A rapid measurement for pKa determination of drugs using pressure assited capillary electrophoresis with photodiode array detection in drug discovery ***Journal of pharmaceutical sciences***, 91: 933-942.

Ishihama, Y., Nakamura, M., Miwa, T., Kajima, T., & Asakawa, N. 2002b. A Rapid Method for pKa Determination of Drugs Using Pressure-Assisted Capillary Electrophoresis with Photodiode Array Detection in Drug Discovery. ***Journal of Pharmaceutical Sciences***, 91(4): 933-942.

Janiak, C., & Vieth, J. K. 2010. MOFs, MILs and more: concepts, properties and applications for porous coordination networks (PCNs). ***New Journal of Chemistry***, 34(11): 2366.

Jankovský, O., Šimek, P., Klímová, K., Sedmidubský, D., Pumera, M., & Sofer, Z. 2015. Highly selective removal of Ga3+ ions from Al3+/Ga3+ mixtures using graphite oxide. ***Carbon***, 89: 121-129.

Jasuja, H., Jiao, Y., Burtch, N. C., Huang, Y. G., & Walton, K. S. 2014. Synthesis of Cobalt, Nickel, Copper, and Zinc-based Water Stable Pillared Metal-Organic Frameworks. ***Langmuir***.

Jasuja, H., & Walton, K. S. 2013. Effect of catenation and basicity of pillared ligands on the water stability of MOFs. ***Dalton Trans***, 42(43): 15421-15426.

Jeremias, F., Lozan, V., Henninger, S. K., & Janiak, C. 2013. Programming MOFs for water sorption: amino-functionalized MIL-125 and UiO-66 for heat transformation and heat storage applications. ***Dalton Trans***, 42(45): 15967-15973.

Ji, L., Chen, W., Zheng, S., Xu, Z., & Zhu, D. 2009. Adsorption of sulfonamide antibiotics to multiwalled carbon nanotubes. ***Langmuir***, 25(19): 11608-11613.

Jia, Y., Jin, Q., Li, Y., Sun, Y., Huo, J., & Zhao, X. 2015. Investigation of the adsorption behaviour of different types of dyes on MIL-100(Fe) and their removal from natural water. ***Analytical Methods***, 7(4): 1463-1470.

Jian, M., Wang, H., Liu, R., Qu, J., Wang, H., & Zhang, X. 2016. Self-assembled one-dimensional MnO2@zeolitic imidazolate framework-8 nanostructures for highly efficient arsenite removal. ***Environ. Sci.: Nano***, 3(5): 1186-1194.

Jiang, J., Gandara, F., Zhang, Y. B., Na, K., Yaghi, O. M., & Klemperer, W. G. 2014. Superacidity in sulfated metal-organic framework-808. ***J Am Chem Soc***, 136(37): 12844-12847.

Jiang, S., Zhang, H., & Yan, Y. 2015. Catalytic wet peroxide oxidation of phenol wastewater over a novel Cu–ZSM-5 membrane catalyst. ***Catalysis Communications***, 71: 28-31.

Jin, J., Mitome, T., Egashira, Y., & Nishiyama, N. 2011. Phase control of ordered mesoporous carbon synthesized by a soft-templating method. ***Colloids and Surfaces A: Physicochemical and Engineering Aspects***, 384(1-3): 58-61.

Jin, J., Tanaka, S., Egashira, Y., & Nishiyama, N. 2010. KOH activation of ordered mesoporous carbons prepared by a soft-templating method and their enhanced electrochemical properties. ***Carbon***, 48(7): 1985-1989.

Jonckheere, D., Coutino-Gonzalez, E., Baekelant, W., Bueken, B., Reinsch, H., Stassen, I., Fenwick, O., Richard, F., Samorì, P., Ameloot, R., Hofkens, J., Roeffaers, M. B. J., & De Vos, D. E. 2016. Silver-induced reconstruction of an adeninate-based metal–organic framework for encapsulation of luminescent adenine-stabilized silver clusters. ***J. Mater. Chem. C***, 4(19): 4259-4268.

Juan-Alcaniz, J., Gielisse, R., Lago, A. B., Ramos-Fernandez, E. V., Serra-Crespo, P., Devic, T., Guillou, N., Serre, C., Kapteijn, F., & Gascon, J. 2013. Towards acid MOFs - catalytic performance of sulfonic acid functionalized architectures. ***Catalysis Science & Technology***, 3(9): 2311-2318.

Jun, J. W., Tong, M., Jung, B. K., Hasan, Z., Zhong, C., & Jhung, S. H. 2015. Effect of central metal ions of analogous metal-organic frameworks on adsorption of organoarsenic compounds from water: plausible mechanism of adsorption and water purification. ***Chemistry***, 21(1): 347-354.

Jung, B. K., Hasan, Z., & Jhung, S. H. 2013. Adsorptive removal of 2,4-dichlorophenoxyacetic acid (2,4-D) from water with a metal–organic framework. ***Chemical Engineering Journal***, 234: 99-105.

Jung, B. K., Jun, J. W., Hasan, Z., & Jhung, S. H. 2015. Adsorptive removal of p-arsanilic acid from water using mesoporous zeolitic imidazolate framework-8. ***Chemical Engineering Journal***, 267: 9-15.

Kajenthira, A., Siddiqi, A., & Anadon, L. D. 2012. A new case for promoting wastewater reuse in Saudi Arabia: bringing energy into the water equation. ***J Environ Manage***, 102: 184-192.

Kandiah, M., Usseglio, S., Svelle, S., Olsbye, U., Lillerud, K. P., & Tilset, M. 2010. Post-synthetic modification of the metal-organic framework compound UiO-66. ***Journal of Materials Chemistry***, 20(44): 9848-9851.

Kang, J., Duan, X., Zhou, L., Sun, H., Tadé, M. O., & Wang, S. 2016. Carbocatalytic activation of persulfate for removal of antibiotics in water solutions. ***Chemical Engineering Journal***, 288: 399-405.

Kang, L., Sun, S.-X., Kong, L.-B., Lang, J.-W., & Luo, Y.-C. 2014. Investigating metal-organic framework as a new pseudo-capacitive material for supercapacitors. ***Chinese Chemical Letters***, 25(6): 957-961.

Ke, F., Qiu, L. G., Yuan, Y. P., Peng, F. M., Jiang, X., Xie, A. J., Shen, Y. H., & Zhu, J. F. 2011a. Thiol-functionalization of metal-organic framework by a facile coordination-based postsynthetic strategy and enhanced removal of Hg2+ from water. ***J Hazard Mater***, 196: 36-43.

Ke, F., Qiu, L. G., Yuan, Y. P., Peng, F. M., Jiang, X., Xie, A. J., Shen, Y. H., & Zhu, J. F. 2011b. Thiol-functionalization of metal-organic framework by a facile coordination-based postsynthetic strategy and enhanced removal of Hg2+ from water. ***Journal of Hazardous Matererials***, 196: 36-43.

Kebir, M., Boudjemaa, A., & Bachari, K. 2015. Enhancement photo-catalytic degradation of benzoic acid using the heterosystem NiCo2O4/ZnO. ***Materials Science in Semiconductor Processing***, 39: 300-307.

Khan, N. A., Jung, B. K., Hasan, Z., & Jhung, S. H. 2015. Adsorption and removal of phthalic acid and diethyl phthalate from water with zeolitic imidazolate and metal-organic frameworks. ***J Hazard Mater***, 282: 194-200.

Khin, M. M., Nair, A. S., Babu, V. J., Murugan, R., & Ramakrishna, S. 2012. A review on nanomaterials for environmental remediation. ***Energy & Environmental Science***, 5(8): 8075-8109.

Kim, S.-N., Kim, J., Kim, H.-Y., Cho, H.-Y., & Ahn, W.-S. 2013. Adsorption/catalytic properties of MIL-125 and NH2-MIL-125. ***Catalysis Today***, 204: 85-93.

Kim, Y., & Huh, S. 2016. Pore engineering of metal–organic frameworks: introduction of chemically accessible Lewis basic sites inside MOF channels. ***CrystEngComm***, 18(20): 3524-3550.

Knebel, A., Friebe, S., Bigall, N. C., Benzaqui, M., Serre, C., & Caro, J. 2016. Comparative Study of MIL-96(Al) as Continuous Metal-Organic Frameworks Layer and Mixed-Matrix Membrane. ***ACS Appl Mater Interfaces***, 8(11): 7536-7544.

Koh, H. S., Rana, M. K., Wong-Foy, A. G., & Siegel, D. J. 2015. Predicting Methane Storage in Open-Metal-Site Metal–Organic Frameworks. ***The Journal of Physical Chemistry C***, 119(24): 13451-13458.

Kosugi, Y., Imaoka, Y., Gotoh, F., Rahim, M. A., Matsui, Y., & Sakanishi, K. 2003. Carboxylations of alkali metal phenoxides with carbon dioxide. ***Organic & Biomolecular Chemistry***, 1(5): 817-821.

Kowalczyk, P., Gauden, P. A., Furmaniak, S., Terzyk, A. P., Wiśniewski, M., Ilnicka, A., Łukaszewicz, J., Burian, A., Włoch, J., & Neimark, A. V. 2017. Morphologically disordered pore model for characterization of micro-mesoporous carbons. ***Carbon***, 111: 358-370.

Koyuncu, I., Arikan, O. A., Wiesner, M. R., & Rice, C. 2008. Removal of hormones and antibiotics by nanofiltration membranes. ***Journal of Membrane Science***, 309(1-2): 94-101.

Kozlova, E. A., Panchenko, V. N., Hasan, Z., Khan, N. A., Timofeeva, M. N., & Jhung, S. H. 2016. Photoreactivity of metal-organic frameworks in the decolorization of methylene blue in aqueous solution. ***Catalysis Today***, 266: 136-143.

Kurokawa, J., Ohara, T., Morikawa, T., Hanayama, S., Janssens-Maenhout, G., Fukui, T., Kawashima, K., & Akimoto, H. 2013. Emissions of air pollutants and greenhouse gases over Asian regions during 2000–2008: Regional Emission inventory in ASia (REAS) version 2. ***Atmos. Chem. Phys.***, 13(21): 11019-11058.

Lai, H. T., Hou, J. H., Su, C. I., & Chen, C. L. 2009. Effects of chloramphenicol, florfenicol, and thiamphenicol on growth of algae Chlorella pyrenoidosa, Isochrysis galbana, and Tetraselmis chui. ***Ecotoxicology and Environmental Safety***, 72(2): 329-334.

Lakatos, G., Veres, Z., Kundrát, J., & Mészáros, I. 2014. The management and development of constructed wetlands for treatment of petrochemical waste waters in Hungary: 35 years of experience. ***Ecohydrology & Hydrobiology***, 14(1): 83-88.

Langmuir, I. 1918. THE ADSORPTION OF GASES ON PLANE SURFACES OF GLASS, MICA AND PLATINUM. ***Journal of the American Chemical Society***, 40(9): 1361-1403.

Lässig, D., Lincke, J., Moellmer, J., Reichenbach, C., Moeller, A., Gläser, R., Kalies, G., Cychosz, K. A., Thommes, M., Staudt, R., & Krautscheid, H. 2011. A Microporous Copper Metal–Organic Framework with High H2 and CO2 Adsorption Capacity at Ambient Pressure. ***Angewandte Chemie International Edition***, 50(44): 10344-10348.

Lee, J. S., & Jhung, S. H. 2010. Vapor-phase adsorption of alkylaromatics on aluminum-trimesate MIL-96: An unusual increase of adsorption capacity with temperature. ***Microporous and Mesoporous Materials***, 129(1-2): 274-277.

Lemos, A. O., Oliveira, N. C., & Lemos, C. T. 2011. In vitro micronuclei tests to evaluate the genotoxicity of surface water under the influence of tanneries. ***Toxicol In Vitro***, 25(4): 761-766.

Leng, F., Wang, W., Zhao, X. J., Hu, X. L., & Li, Y. F. 2014. Adsorption interaction between a metal–organic framework of chromium–benzenedicarboxylates and uranine in aqueous solution. ***Colloids and Surfaces A: Physicochemical and Engineering Aspects***, 441: 164-169.

Li, H., & Hill, M. R. 2017. Low-Energy CO2 Release from Metal-Organic Frameworks Triggered by External Stimuli. ***Acc Chem Res***, 50(4): 778-786.

Li, H., Ma, H., Wang, X., Gao, J., Chen, C., Shi, S., Qu, M., Feng, N., & Xu, J. 2014. Efficient oxidation of ethylbenzene catalyzed by cobalt zeolitic imidazolate framework ZIF-67 and NHPI. ***Journal of Energy Chemistry***, 23(6): 742-746.

Li, J., Huang, Y., Ye, R., Yuan, G.-L., Wu, H.-Z., Han, P., & Fu, S. 2015a. Source identification and health risk assessment of Persistent Organic Pollutants (POPs) in the topsoils of typical petrochemical industrial area in Beijing, China. ***Journal of Geochemical Exploration***, 158: 177-185.

Li, L., Liu, X. L., Geng, H. Y., Hu, B., Song, G. W., & Xu, Z. S. 2013a. A MOF/graphite oxide hybrid (MOF: HKUST-1) material for the adsorption of methylene blue from aqueous solution. ***Journal of Materials Chemistry A***, 1(35): 10292.

Li, M., & Xue, J. 2012. Ordered mesoporous carbon nanoparticles with well-controlled morphologies from sphere to rod via a soft-template route. ***J Colloid Interface Sci***, 377(1): 169-175.

Li, N., Xu, J., Feng, R., Hu, T. L., & Bu, X. H. 2016a. Governing metal-organic frameworks towards high stability. ***Chem Commun (Camb)***, 52(55): 8501-8513.

Li, T., Chen, D.-L., Sullivan, J. E., Kozlowski, M. T., Johnson, J. K., & Rosi, N. L. 2013b. Systematic modulation and enhancement of CO2 : N2 selectivity and water stability in an isoreticular series of bio-MOF-11 analogues. ***Chemical Science***, 4(4): 1746.

Li, T., Sullivan, J. E., & Rosi, N. L. 2013c. Design and preparation of a core-shell metal-organic framework for selective CO2 capture. ***J Am Chem Soc***, 135(27): 9984-9987.

Li, T., Yang, Z., Zhang, X., Zhu, N., & Niu, X. 2015b. Perchlorate removal from aqueous solution with a novel cationic metal–organic frameworks based on amino sulfonic acid ligand linking with Cu-4,4′-bipyridyl chains. ***Chemical Engineering Journal***, 281: 1008-1016.

Li, Y., Qiu, W., Qin, F., Fang, H., Hadjiev, V. G., Litvinov, D., & Bao, J. 2016b. Identification of Cobalt Oxides with Raman Scattering and Fourier

Transform Infrared Spectroscopy. ***The Journal of Physical Chemistry C***, 120(8): 4511-4516.

Li, Y., Wee, L. H., Volodin, A., Martens, J. A., & Vankelecom, I. F. J. 2015c. Polymer supported ZIF-8 membranes prepared via an interfacial synthesis method. ***Chemical Communications***, 51(5): 918-920.

Li, Z.-Q., Yang, J.-C., Sui, K.-W., & Yin, N. 2015d. Facile synthesis of metal-organic framework MOF-808 for arsenic removal. ***Materials Letters***: MLBLUED1501427.

Liang, C., & Dai, S. 2006. Synthesis of Mesoporous Carbon Materials via Enhanced Hydrogen-Bonding Interaction. ***Journal of the American Chemical Society***, 128(16): 5316-5317.

Liang, P., Zhang, C., Duan, X., Sun, H., Liu, S., Tade, M. O., & Wang, S. 2017. An insight into metal organic framework derived N-doped graphene for the oxidative degradation of persistent contaminants: formation mechanism and generation of singlet oxygen from peroxymonosulfate. ***Environ. Sci.: Nano***, 4(2): 315-324.

Libbrecht, W., Deruyck, F., Poelman, H., Verberckmoes, A., Thybaut, J., De Clercq, J., & Van Der Voort, P. 2015. Optimization of soft templated mesoporous carbon synthesis using Definitive Screening Design. ***Chemical Engineering Journal***, 259: 126-134.

Libbrecht, W., Verberckmoes, A., Thybaut, J. W., Van Der Voort, P., & De Clercq, J. 2017. Soft templated mesoporous carbons: Tuning the porosity for the adsorption of large organic pollutants. ***Carbon***, 116: 528-546.

Lin, A. Y., & Tsai, Y. T. 2009. Occurrence of pharmaceuticals in Taiwan's surface waters: impact of waste streams from hospitals and pharmaceutical production facilities. ***Sci Total Environ***, 407(12): 3793-3802.

Lin, K.-Y. A., & Chang, H.-A. 2015a. Zeolitic Imidazole Framework-67 (ZIF-67) as a heterogeneous catalyst to activate peroxymonosulfate for degradation of Rhodamine B in water. ***Journal of the Taiwan Institute of Chemical Engineers***, 53: 40-45.

Lin, K.-Y. A., Chen, S.-Y., & Jochems, A. P. 2015. Zirconium-based metal organic frameworks: Highly selective adsorbents for removal of phosphate from water and urine. ***Materials Chemistry and Physics***, 160: 168-176.

Lin, K. Y., & Chang, H. A. 2015b. Ultra-high adsorption capacity of zeolitic imidazole framework-67 (ZIF-67) for removal of malachite green from water. ***Chemosphere***, 139: 624-631.

Lin, K. Y., & Chen, B. C. 2016. Efficient elimination of caffeine from water using Oxone activated by a magnetic and recyclable cobalt/carbon nanocomposite derived from ZIF-67. ***Dalton Trans***, 45(8): 3541-3551.

Lin, S., Song, Z., Che, G., Ren, A., Li, P., Liu, C., & Zhang, J. 2014. Adsorption behavior of metal–organic frameworks for methylene blue from aqueous solution. ***Microporous and Mesoporous Materials***, 193: 27-34.

Ling, S., & Slater, B. 2016. Dynamic acidity in defective UiO-66. ***Chemical Science***.

Liu, B., Li, Y., Oh, S. C., Fang, Y., & Xi, H. 2016. Fabrication of a hierarchically structured HKUST-1 by a mixed-ligand approach. ***RSC Adv.***, 6(66): 61006-61012.

Liu, B., Yang, F., Zou, Y., & Peng, Y. 2014a. Adsorption of Phenol andp-Nitrophenol from Aqueous Solutions on Metal–Organic Frameworks: Effect

of Hydrogen Bonding. ***Journal of Chemical & Engineering Data***, 59(5): 1476-1482.

Liu, C., Wang, J., Li, J., Luo, R., Sun, X., Shen, J., Han, W., & Wang, L. 2017. Fe/N decorated mulberry-like hollow mesoporous carbon fibers as efficient electrocatalysts for oxygen reduction reaction. ***Carbon***, 114: 706-716.

Liu, D., Dai, F., Liu, H., Liu, Y., & Liu, C. 2015a. An investigation of the transformation of Al-based metal-organic frameworks to mesoporous Al2O3 with core-shell and nanoporous structure. ***Materials Letters***, 139: 7-11.

Liu, D., Liu, Y., Dai, F., Zhao, J., Yang, K., & Liu, C. 2015b. Size- and morphology-controllable synthesis of MIL-96 (Al) by hydrolysis and coordination modulation of dual aluminium source and ligand systems. ***Dalton Transactions***, 44(37): 16421-16429.

Liu, J., Thallapally, P. K., McGrail, B. P., Brown, D. R., & Liu, J. 2012. Progress in adsorption-based CO2 capture by metal-organic frameworks. ***Chemical Society Reviews***, 41(6): 2308-2322.

Liu, R.-L., Ji, W.-J., He, T., Zhang, Z.-Q., Zhang, J., & Dang, F.-Q. 2014b. Fabrication of nitrogen-doped hierarchically porous carbons through a hybrid dual-template route for CO2 capture and haemoperfusion. ***Carbon***, 76: 84-95.

Liu, Y., Chen, J., Chen, M., Zhang, B., Wu, D., & Cheng, Q. 2015c. Adsorption characteristics and mechanism of sewage sludge-derived adsorbent for removing sulfonated methyl phenol resin in wastewater. ***RSC Advances***, 5(93): 76160-76169.

Loiseau, T., Lecroq, L., Volkringer, C., Marrot, J., Férey, G., Haouas, M., Taulelle, F., Bourrelly, S., Llewellyn, P. L., & Latroche, M. 2006. MIL-96, a Porous Aluminum Trimesate 3D Structure Constructed from a Hexagonal Network of 18-Membered Rings and μ3-Oxo-Centered Trinuclear Units. ***Journal of the American Chemical Society***, 128(31): 10223-10230.

Lopez-Salas, N., del Monte, F., Tamayo, A., Fierro, J. L., De Lacey, A. L., Ferrer, M. L., & Gutierrez, M. C. 2014. Sulfur-doped carbons prepared from eutectic mixtures containing hydroxymethylthiophene as metal-free oxygen reduction catalysts. ***ChemSusChem***, 7(12): 3347-3355.

Ma, T. Y., Liu, L., & Yuan, Z. Y. 2013. Direct synthesis of ordered mesoporous carbons. ***Chem Soc Rev***, 42(9): 3977-4003.

Marques, L. F., Correa, C. C., Ribeiro, S. J. L., dos Santos, M. V., Dutra, J. D. L., Freire, R. O., & Machado, F. C. 2015. Synthesis, structural characterization, luminescent properties and theoretical study of three novel lanthanide metal-organic frameworks of Ho(III), Gd(III) and Eu(III) with 2,5-thiophenedicarboxylate anion. ***Journal of Solid State Chemistry***, 227: 68-78.

Marshall, R. J., Hobday, C. L., Murphie, C. F., Griffin, S. L., Morrison, C. A., Moggach, S. A., & Forgan, R. S. 2016. Amino acids as highly efficient modulators for single crystals of zirconium and hafnium metal–organic frameworks. ***J. Mater. Chem. A***, 4(18): 6955-6963.

Martin, R. L., & Haranczyk, M. 2013. Optimization-Based Design of Metal-Organic Framework Materials. ***J Chem Theory Comput***, 9(6): 2816-2825.

Martucci, A., Cremonini, M. A., Blasioli, S., Gigli, L., Gatti, G., Marchese, L., & Braschi, I. 2013. Adsorption and reaction of sulfachloropyridazine sulfonamide antibiotic on a high silica mordenite: A structural and spectroscopic combined study. ***Microporous and Mesoporous Materials***, 170: 274-286.

McGuire, C. V., & Forgan, R. S. 2015. The surface chemistry of metal-organic frameworks. ***Chemical Communications***, 51(25): 5199-5217.

Mehrjouei, M., Müller, S., & Möller, D. 2014. Treatment of pyrolysis wastewater using heterogeneous advanced oxidation processes. ***Environmental Progress & Sustainable Energy***, 33(1): 178-183.

Michael, I., Rizzo, L., McArdell, C. S., Manaia, C. M., Merlin, C., Schwartz, T., Dagot, C., & Fatta-Kassinos, D. 2013. Urban wastewater treatment plants as hotspots for the release of antibiotics in the environment: a review. ***Water Research***, 47(3): 957-995.

Miller, S. E., Teplensky, M. H., Moghadam, P. Z., & Fairen-Jimenez, D. 2016. Metal-organic frameworks as biosensors for luminescence-based detection and imaging. ***Interface Focus***, 6(4): 20160027.

Millward, A. R., & Yaghi, O. M. 2005. Metal−Organic Frameworks with Exceptionally High Capacity for Storage of Carbon Dioxide at Room Temperature. ***Journal of the American Chemical Society***, 127(51): 17998-17999.

Mishra, P., Uppara, H. P., Mandal, B., & Gumma, S. 2014. Adsorption and Separation of Carbon Dioxide Using MIL-53(Al) Metal-Organic Framework. ***Industrial & Engineering Chemistry Research***, 53(51): 19747-19753.

Mitome, T., Uchida, Y., Egashira, Y., Hayashi, K., Nishiura, A., & Nishiyama, N. 2013. Adsorption of indole on KOH-activated mesoporous carbon. ***Colloids and Surfaces A: Physicochemical and Engineering Aspects***, 424: 89-95.

Münch, A. S., & Mertens, F. O. R. L. 2012. HKUST-1 as an open metal site gas chromatographic stationary phase—capillary preparation, separation of small hydrocarbons and electron donating compounds, determination of thermodynamic data. ***Journal of Materials Chemistry***, 22(20): 10228-10234.

Nichela, D. A., Donadelli, J. A., Caram, B. F., Haddou, M., Rodriguez Nieto, F. J., Oliveros, E., & García Einschlag, F. S. 2015. Iron cycling during the autocatalytic decomposition of benzoic acid derivatives by Fenton-like and photo-Fenton techniques. ***Applied Catalysis B: Environmental***, 170-171: 312-321.

Nielsen, L., & Bandosz, T. J. 2016. Analysis of sulfamethoxazole and trimethoprim adsorption on sewage sludge and fish waste derived adsorbents. ***Microporous and Mesoporous Materials***, 220: 58-72.

Ning, X. A., Liang, J. Y., Li, R. J., Hong, Z., Wang, Y. J., Chang, K. L., Zhang, Y. P., & Yang, Z. Y. 2015. Aromatic amine contents, component distributions and risk assessment in sludge from 10 textile-dyeing plants. ***Chemosphere***, 134: 367-373.

Ning, Y., Wang, L., Yang, G. P., Wu, Y., Bai, N., Zhang, W., & Wang, Y. Y. 2016. Four new lanthanide-organic frameworks: selective luminescent sensing and magnetic properties. ***Dalton Trans***, 45(32): 12800-12806.

Nsangou, M., Dhaouadi, Z., Jaidane, N., & Ben Lakhdar, Z. 2008. DFT study of the structure of hydroxybenzoic acids and their reactions with OH and radicals. ***Journal of Molecular Structure: THEOCHEM***, 850(1-3): 135-143.

Odoh, S. O., Cramer, C. J., Truhlar, D. G., & Gagliardi, L. 2015. Quantum-Chemical Characterization of the Properties and Reactivities of Metal-Organic Frameworks. ***Chem Rev***, 115(12): 6051-6111.

Oh, W.-D., Dong, Z., & Lim, T.-T. 2016. Generation of sulfate radical through heterogeneous catalysis for organic contaminants removal: Current

development, challenges and prospects. ***Applied Catalysis B: Environmental***, 194: 169-201.

Öhrström, L. 2015. Let's Talk about MOFs—Topology and Terminology of Metal-Organic Frameworks and Why We Need Them. ***Crystals***, 5(1): 154-162.

Oliveira, T. S., Murphy, M., Mendola, N., Wong, V., Carlson, D., & Waring, L. 2015a. Characterization of Pharmaceuticals and Personal Care products in hospital effluent and waste water influent/effluent by direct-injection LC-MS-MS. ***Sci Total Environ***, 518-519: 459-478.

Oliveira, T. S., Murphy, M., Mendola, N., Wong, V., Carlson, D., & Waring, L. 2015b. Characterization of Pharmaceuticals and Personal Care products in hospital effluent and waste water influent/effluent by direct-injection LC-MS-MS. ***Science of the Total Environment***, 518-519: 459-478.

Olsson, G. 2012. ICA and me--a subjective review. ***Water Research***, 46(6): 1585-1624.

Ostace, G. S., Baeza, J. A., Guerrero, J., Guisasola, A., Cristea, V. M., Agachi, P. Ş., & Lafuente, J. 2013. Development and economic assessment of different WWTP control strategies for optimal simultaneous removal of carbon, nitrogen and phosphorus. ***Computers & Chemical Engineering***, 53: 164-177.

Otero, R., Esquivel, D., Ulibarri, M. A., Romero-Salguero, F. J., Van Der Voort, P., & Fernández, J. M. 2014. Mesoporous phenolic resin and mesoporous carbon for the removal of S-Metolachlor and Bentazon herbicides. ***Chemical Engineering Journal***, 251: 92-101.

Pal, A., He, Y., Jekel, M., Reinhard, M., & Gin, K. Y. 2014. Emerging contaminants of public health significance as water quality indicator compounds in the urban water cycle. ***Environ Int***, 71: 46-62.

Park, E. Y., Hasan, Z., Khan, N. A., & Jhung, S. H. 2013. Adsorptive Removal of Bisphenol-A from Water with a Metal-Organic Framework, a Porous Chromium-Benzenedicarboxylate. ***Journal of Nanoscience and Nanotechnology***, 13(4): 2789-2794.

Pei, J., Yao, H., Wang, H., Shan, D., Jiang, Y., Ma, L., & Yu, X. 2015. Effect of ultrasonic and ozone pre-treatments on pharmaceutical waste activated sludge's solubilisation, reduction, anaerobic biodegradability and acute biological toxicity. ***Bioresour Technol***, 192: 418-423.

Pejman, A., Nabi Bidhendi, G., Ardestani, M., Saeedi, M., & Baghvand, A. 2015. A new index for assessing heavy metals contamination in sediments: A case study. ***Ecological Indicators***, 58: 365-373.

Perazzolo, V., Durante, C., Pilot, R., Paduano, A., Zheng, J., Rizzi, G. A., Martucci, A., Granozzi, G., & Gennaro, A. 2015. Nitrogen and sulfur doped mesoporous carbon as metal-free electrocatalysts for the in situ production of hydrogen peroxide. ***Carbon***, 95: 949-963.

Perlovich, G. L., Ryzhakov, A. M., Strakhova, N. N., Kazachenko, V. P., Schaper, K.-J., & Raevsky, O. A. 2011. Thermodynamic aspects of solubility, solvation and partitioning processes of some sulfonamides. ***The Journal of Chemical Thermodynamics***, 43(5): 683-689.

Peterson, G. W., Rossin, J. A., DeCoste, J. B., Killops, K. L., Browe, M., Valdes, E., & Jones, P. 2013. Zirconium Hydroxide–Metal–Organic Framework Composites for Toxic Chemical Removal. ***Industrial & Engineering Chemistry Research***, 52(15): 5462-5469.

Petit, C., & Bandosz, T. J. 2010. Enhanced Adsorption of Ammonia on Metal-Organic Framework/Graphite Oxide Composites: Analysis of Surface Interactions. ***Advanced Functional Materials***, 20(1): 111-118.

Petrie, B., Barden, R., & Kasprzyk-Hordern, B. 2015. A review on emerging contaminants in wastewaters and the environment: current knowledge, understudied areas and recommendations for future monitoring. ***Water Res***, 72: 3-27.

Phan, A., Czaja, A. U., Gandara, F., Knobler, C. B., & Yaghi, O. M. 2011. Metal-organic frameworks of vanadium as catalysts for conversion of methane to acetic acid. ***Inorg Chem***, 50(16): 7388-7390.

Pouya, E. S., Abolghasemi, H., Esmaieli, M., Fatoorehchi, H., Hashemi, S. J., & Salehpour, A. 2015. Batch adsorptive removal of benzoic acid from aqueous solution onto modified natural vermiculite: Kinetic, isotherm and thermodynamic studies. ***Journal of Industrial and Engineering Chemistry***, 31: 199-215.

Prieto, M. A., Prieto, I., Vazquez, J. A., & Ferreira, I. C. 2015. An environmental management industrial solution for the treatment and reuse of mussel wastewaters. ***Sci Total Environ***, 538: 117-128.

Pugazhendhi, D., Pope, G. S., & Darbre, P. D. 2005. Oestrogenic activity of p-hydroxybenzoic acid (common metabolite of paraben esters) and methylparaben in human breast cancer cell lines. ***J Appl Toxicol***, 25(4): 301-309.

Qadir, N. u., Said, S. A. M., & Bahaidarah, H. M. 2015. Structural stability of metal organic frameworks in aqueous media – Controlling factors and methods to improve hydrostability and hydrothermal cyclic stability. ***Microporous and Mesoporous Materials***, 201: 61-90.

Qi, Y., Luo, F., Che, Y., & Zheng, J. 2008. Hydrothermal Synthesis of Metal−Organic Frameworks Based on Aromatic Polycarboxylate and Flexible Bis(imidazole) Ligands. ***Crystal Growth & Design***, 8(2): 606-611.

Qian, J., Sun, F., & Qin, L. 2012. Hydrothermal synthesis of zeolitic imidazolate framework-67 (ZIF-67) nanocrystals. ***Materials Letters***, 82: 220-223.

Qin, F.-X., Jia, S.-Y., Liu, Y., Li, H.-Y., & Wu, S.-H. 2014. Adsorptive removal of bisphenol A from aqueous solution using metal-organic frameworks. ***Desalination and Water Treatment***, 54(1): 93-102.

Rada, Z. H., Abid, H. R., Shang, J., He, Y., Webley, P., Liu, S., Sun, H., & Wang, S. 2015. Effects of amino functionality on uptake of CO2, CH4 and selectivity of CO2/CH4 on titanium based MOFs. ***Fuel***, 160: 318-327.

Radi, S., Tighadouini, S., El Massaoudi, M., Bacquet, M., Degoutin, S., Revel, B., & Mabkhot, Y. N. 2015. Thermodynamics and Kinetics of Heavy Metals Adsorption on Silica Particles Chemically Modified by Conjugated β-Ketoenol Furan. ***Journal of Chemical & Engineering Data***: 150908095443004.

Rahman, Z., & Singh, V. P. 2014. Cr(VI) reduction by Enterobacter sp. DU17 isolated from the tannery waste dump site and characterization of the bacterium and the Cr(VI) reductase. ***International Biodeterioration & Biodegradation***, 91: 97-103.

Rao, D., Lu, R., Xiao, C., Kan, E., & Deng, K. 2011. Lithium-doped MOF impregnated with lithium-coated fullerenes: A hydrogen storage route for high gravimetric and volumetric uptakes at ambient temperatures. ***Chemical Communications***, 47(27): 7698-7700.

Rehman, M. S., Rashid, N., Ashfaq, M., Saif, A., Ahmad, N., & Han, J. I. 2015. Global risk of pharmaceutical contamination from highly populated developing countries. ***Chemosphere***, 138: 1045-1055.

Richardson, S. D., & Ternes, T. A. 2014. Water analysis: emerging contaminants and current issues. ***Anal Chem***, 86(6): 2813-2848.

Rivas, F. J., Beltrán, F. J., Frades, J., & Buxeda, P. 2001. Oxidation of p-hydroxybenzoic acid by Fenton's reagent. ***Water Research***, 35(2): 387-396.

Rodger, C. A. 1997. Spectroscopic methods in organic chemistry, fifth edition. ***Concepts in Magnetic Resonance***, 9(5): 355-356.

Rossner, A., Snyder, S. A., & Knappe, D. R. 2009. Removal of emerging contaminants of concern by alternative adsorbents. ***Water Res***, 43(15): 3787-3796.

Rostamnia, S., Alamgholiloo, H., & Liu, X. 2016. Pd-grafted open metal site copper-benzene-1,4-dicarboxylate metal organic frameworks (Cu-BDC MOF's) as promising interfacial catalysts for sustainable Suzuki coupling. ***J Colloid Interface Sci***, 469: 310-317.

Saidi, W. A. 2015. Trends in the Adsorption and Growth Morphology of Metals on the MoS2(001) Surface. ***Crystal Growth & Design***, 15(7): 3190-3200.

Saleh, T. A., & Gupta, V. K. 2014. Processing methods, characteristics and adsorption behavior of tire derived carbons: a review. ***Adv Colloid Interface Sci***, 211: 93-101.

Saputra, E., Muhammad, S., Sun, H., Ang, H.-M., Tadé, M. O., & Wang, S. 2013a. Manganese oxides at different oxidation states for heterogeneous activation of peroxymonosulfate for phenol degradation in aqueous solutions. ***Applied Catalysis B: Environmental***, 142-143: 729-735.

Saputra, E., Muhammad, S., Sun, H., Ang, H. M., Tade, M. O., & Wang, S. 2013b. A comparative study of spinel structured Mn3O4, Co3O4 and Fe3O4 nanoparticles in catalytic oxidation of phenolic contaminants in aqueous solutions. ***J Colloid Interface Sci***, 407: 467-473.

Saputra, E., Muhammad, S., Sun, H., Ang, H. M., Tade, M. O., & Wang, S. 2013c. Different crystallographic one-dimensional MnO2 nanomaterials and their superior performance in catalytic phenol degradation. ***Environ Sci Technol***, 47(11): 5882-5887.

Schroder, D., Budesinsky, M., & Roithova, J. 2012. Deprotonation of p-hydroxybenzoic acid: does electrospray ionization sample solution or gas-phase structures? ***J Am Chem Soc***, 134(38): 15897-15905.

Schuster, J., Kohn, R., Doblinger, M., Keilbach, A., Amenitsch, H., & Bein, T. 2012. In situ SAXS study on a new mechanism for mesostructure formation of ordered mesoporous carbons: thermally induced self-assembly. ***J Am Chem Soc***, 134(27): 11136-11145.

Seckler, D., Barker, R., & Amarasinghe, U. 1999. Water Scarcity in the Twenty-first Century. ***International Journal of Water Resources Development***, 15(1-2): 29-42.

Seo, Y. S., Khan, N. A., & Jhung, S. H. 2015. Adsorptive removal of methylchlorophenoxypropionic acid from water with a metal-organic framework. ***Chemical Engineering Journal***, 270: 22-27.

Seoane, B., Dikhtiarenko, A., Mayoral, A., Tellez, C., Coronas, J., Kapteijn, F., & Gascon, J. 2015. Metal organic framework synthesis in the presence of surfactants: towards hierarchical MOFs? ***CrystEngComm***, 17(7): 1693-1700.

Shao, Y., Wang, X., Kang, Y., Shu, Y., Sun, Q., & Li, L. 2014. Application of Mn/MCM-41 as an adsorbent to remove methyl blue from aqueous solution. ***J Colloid Interface Sci***, 429: 25-33.

Shearer, G. C., Chavan, S., Ethiraj, J., Vitillo, J. G., Svelle, S., Olsbye, U., Lamberti, C., Bordiga, S., & Lillerud, K. P. 2014. Tuned to Perfection: Ironing Out the Defects in Metal–Organic Framework UiO-66. ***Chemistry of Materials***, 26(14): 4068-4071.

Sheet, I., Kabbani, A., & Holail, H. 2014. Removal of Heavy Metals Using Nanostructured Graphite Oxide, Silica Nanoparticles and Silica/ Graphite Oxide Composite. ***Energy Procedia***, 50: 130-138.

Shen, G., Mei, B., Wu, H., Wei, H., Fang, X., & Xu, Y. 2017. Microwave Electromagnetic and Absorption Properties of N-Doped Ordered Mesoporous Carbon Decorated with Ferrite Nanoparticles. ***The Journal of Physical Chemistry C***, 121(7): 3846-3853.

Shen, T., Luo, J., Zhang, S., & Luo, X. 2015. Hierarchically mesostructured MIL-101 metal–organic frameworks with different mineralizing agents for adsorptive removal of methyl orange and methylene blue from aqueous solution. ***Journal of Environmental Chemical Engineering***, 3(2): 1372-1383.

Shukla, P., Sun, H., Wang, S., Ang, H. M., & Tadé, M. O. 2011a. Co-SBA-15 for heterogeneous oxidation of phenol with sulfate radical for wastewater treatment. ***Catalysis Today***, 175(1): 380-385.

Shukla, P., Sun, H., Wang, S., Ang, H. M., & Tadé, M. O. 2011b. Nanosized Co3O4/SiO2 for heterogeneous oxidation of phenolic contaminants in waste water. ***Separation and Purification Technology***, 77(2): 230-236.

Shukla, P., Wang, S., Singh, K., Ang, H. M., & Tadé, M. O. 2010. Cobalt exchanged zeolites for heterogeneous catalytic oxidation of phenol in the presence of peroxymonosulphate. ***Applied Catalysis B: Environmental***, 99(1-2): 163-169.

Shukla, P. R., Wang, S., Sun, H., Ang, H. M., & Tadé, M. 2010. Activated carbon supported cobalt catalysts for advanced oxidation of organic contaminants in aqueous solution. ***Applied Catalysis B: Environmental***, 100(3-4): 529-534.

Sim, W. J., Kim, H. Y., Choi, S. D., Kwon, J. H., & Oh, J. E. 2013a. Evaluation of pharmaceuticals and personal care products with emphasis on anthelmintics in human sanitary waste, sewage, hospital wastewater, livestock wastewater and receiving water. ***Journal of Hazardous Materials***, 248-249: 219-227.

Sim, W. J., Kim, H. Y., Choi, S. D., Kwon, J. H., & Oh, J. E. 2013b. Evaluation of pharmaceuticals and personal care products with emphasis on anthelmintics in human sanitary waste, sewage, hospital wastewater, livestock wastewater and receiving water. ***J Hazard Mater***, 248-249: 219-227.

Sindoro, M., Jee, A. Y., & Granick, S. 2013. Shape-selected colloidal MOF crystals for aqueous use. ***Chem Commun (Camb)***, 49(83): 9576-9578.

Sing, K. 2001. The use of nitrogen adsorption for the characterisation of porous materials. ***Colloids and Surfaces A: Physicochemical and Engineering Aspects***, 187: 3-9.

Smith, M., Scudiero, L., Espinal, J., McEwen, J.-S., & Garcia-Perez, M. 2016. Improving the deconvolution and interpretation of XPS spectra from chars by ab initio calculations. ***Carbon***, 110: 155-171.

Smith, S. C., & Rodrigues, D. F. 2015. Carbon-based nanomaterials for removal of chemical and biological contaminants from water: A review of mechanisms and applications. ***Carbon***, 91: 122-143.

Song, J., Zhang, Y., & Liu, Y. 2015. The influence of formaldehyde/phenol molar ratio on microstructure of B-OMCs. ***RSC Adv.***, 5(27): 20734-20740.

Song, J. Y., & Jhung, S. H. 2017. Adsorption of pharmaceuticals and personal care products over metal-organic frameworks functionalized with hydroxyl groups: Quantitative analyses of H-bonding in adsorption. ***Chemical Engineering Journal***, 322: 366-374.

Song, X., Oh, M., & Lah, M. S. 2013. Hybrid bimetallic metal-organic frameworks: modulation of the framework stability and ultralarge CO2 uptake capacity. ***Inorg Chem***, 52(19): 10869-10876.

Soni, M. G., Carabin, I. G., & Burdock, G. A. 2005. Safety assessment of esters of p-hydroxybenzoic acid (parabens). ***Food Chem Toxicol***, 43(7): 985-1015.

Stoller, M., Pulido, J. M. O., Di Palma, L., & Ferez, A. M. 2015. Membrane process enhancement of 2-phase and 3-phase olive mill wastewater treatment plants by photocatalysis with magnetic-core titanium dioxide nanoparticles. ***Journal of Industrial and Engineering Chemistry***, 30: 147-152.

Su, D. S., Delgado, J. J., Liu, X., Wang, D., Schlogl, R., Wang, L., Zhang, Z., Shan, Z., & Xiao, F. S. 2009. Highly ordered mesoporous carbon as catalyst for oxidative dehydrogenation of ethylbenzene to styrene. ***Chem Asian J***, 4(7): 1108-1113.

Subramanian, V., Pangarkar, V. G., & Beenackers, A. A. C. M. 2000. Photocatalytic degradation of para-hydroxybenzoic acid: Relationship between substrate adsorption and photocatalytic degradation. ***Clean Products and Processes***, 2(3): 149-156.

Sun, H.-Y., Liu, C.-B., Cong, Y., Yu, M.-H., Bai, H.-Y., & Che, G.-B. 2013. New photocatalyst for the degradation of organic dyes based on [Co2(1,4-BDC)(NCP)2]n·4nH2O. ***Inorganic Chemistry Communications***, 35: 130-134.

Sun, H., Liu, S., Liu, S., & Wang, S. 2014a. A comparative study of reduced graphene oxide modified TiO2, ZnO and Ta2O5 in visible light photocatalytic/photochemical oxidation of methylene blue. ***Applied Catalysis B: Environmental***, 146: 162-168.

Sun, H., Zhou, G., Wang, Y., Suvorova, A., & Wang, S. 2014b. A new metal-free carbon hybrid for enhanced photocatalysis. ***ACS Appl Mater Interfaces***, 6(19): 16745-16754.

Tan, F., Liu, M., Li, K., Wang, Y., Wang, J., Guo, X., Zhang, G., & Song, C. 2015. Facile synthesis of size-controlled MIL-100(Fe) with excellent adsorption capacity for methylene blue. ***Chemical Engineering Journal***, 281: 360-367.

Tang, W. W., Zeng, G. M., Gong, J. L., Liang, J., Xu, P., Zhang, C., & Huang, B. B. 2014. Impact of humic/fulvic acid on the removal of heavy metals from aqueous solutions using nanomaterials: a review. ***Sci Total Environ***, 468-469: 1014-1027.

Tao, C. W., Hsu, B. M., Ji, W. T., Hsu, T. K., Kao, P. M., Hsu, C. P., Shen, S. M., Shen, T. Y., Wan, T. J., & Huang, Y. L. 2014a. Evaluation of five antibiotic resistance genes in wastewater treatment systems of swine farms by real-time PCR. ***Science of the Total Environment***, 496: 116-121.

Tao, C. W., Hsu, B. M., Ji, W. T., Hsu, T. K., Kao, P. M., Hsu, C. P., Shen, S. M., Shen, T. Y., Wan, T. J., & Huang, Y. L. 2014b. Evaluation of five antibiotic

resistance genes in wastewater treatment systems of swine farms by real-time PCR. ***Sci Total Environ***, 496: 116-121.

Tavares, R. S., Martins, F. C., Oliveira, P. J., Ramalho-Santos, J., & Peixoto, F. P. 2009. Parabens in male infertility-is there a mitochondrial connection? ***Reprod Toxicol***, 27(1): 1-7.

Thomas, J. E., & Kelley, M. J. 2010. A study of competitive adsorption of organic molecules onto mineral oxides using DRIFTS. ***J Colloid Interface Sci***, 342(2): 474-478.

Thomas, L. t. L., Gebbink, W. A., & Tolls, J. 2006. The effect of pH and ionic strength on the sorption of sulfachloropyridazine, tylosin, and oxytetracycline to soil. ***Environmental Toxicology and Chemistry***, 25(4): 904-911.

Thommes, M., Smarsly, B., Groenewolt, M., Ravikovitch, P. I., & Neimark, A. V. 2006. Adsorption Hysteresis of Nitrogen and Argon in Pore Networks and Characterization of Novel Micro- and Mesoporous Silicas. ***Langmuir***, 22(2): 756-764.

Tian, W., Zhang, H., Duan, X., Sun, H., Tade, M. O., Ang, H. M., & Wang, S. 2016. Nitrogen- and Sulfur-Codoped Hierarchically Porous Carbon for Adsorptive and Oxidative Removal of Pharmaceutical Contaminants. ***ACS Appl Mater Interfaces***, 8(11): 7184-7193.

Tian, W., Zhang, H., Sun, H., Tadé, M. O., & Wang, S. 2017. Template-free synthesis of N-doped carbon with pillared-layered pores as bifunctional materials for supercapacitor and environmental applications. ***Carbon***, 118: 98-105.

Tian, Z., Duan, S., Shen, Y., Xie, M., & Guo, X. 2017. SiO 2 @MgO nanoparticles templated mesoporous carbon with rich electro-active oxygenic functionalities and enhanced supercapacitive performances. ***Applied Surface Science***, 407: 463-469.

Tian, Z., & Snyder, M. A. 2014. Hard templating of symmetric and asymmetric carbon thin films with three-dimensionally ordered mesoporosity. ***Langmuir***, 30(32): 9828-9837.

Titirici, M. M., White, R. J., Brun, N., Budarin, V. L., Su, D. S., del Monte, F., Clark, J. H., & MacLachlan, M. J. 2015. Sustainable carbon materials. ***Chem Soc Rev***, 44(1): 250-290.

Tong, M., Liu, D., Yang, Q., Devautour-Vinot, S., Maurin, G., & Zhong, C. 2013. Influence of framework metal ions on the dye capture behavior of MIL-100 (Fe, Cr) MOF type solids. ***Journal of Materials Chemistry A***, 1(30): 8534.

Tonucci, M. C., Gurgel, L. V. A., & Aquino, S. F. d. 2015. Activated carbons from agricultural byproducts (pine tree and coconut shell), coal, and carbon nanotubes as adsorbents for removal of sulfamethoxazole from spiked aqueous solutions: Kinetic and thermodynamic studies. ***Industrial Crops and Products***, 74: 111-121.

Tsai, Y.-C., & Doong, R.-a. 2015. Activation of hierarchically ordered mesoporous carbons for enhanced capacitive deionization application. ***Synthetic Metals***, 205: 48-57.

Turner, N. H., & Single, A. M. 1990. Determination of peak positions and areas from wide-scan XPS spectra. ***Surface and Interface Analysis***, 15(3): 215-222.

Valenzano, L., Civalleri, B., Chavan, S., Bordiga, S., Nilsen, M. H., Jakobsen, S., Lillerud, K. P., & Lamberti, C. 2011. Disclosing the Complex Structure of

UiO-66 Metal Organic Framework: A Synergic Combination of Experiment and Theory. ***Chemistry of Materials***, 23(7): 1700-1718.

Vhahangwele, M., & Mugera, G. W. 2015. The potential of ball-milled South African bentonite clay for attenuation of heavy metals from acidic wastewaters: Simultaneous sorption of Co2+, Cu2+, Ni2+, Pb2+, and Zn2+ ions. ***Journal of Environmental Chemical Engineering***.

Vyas, N., Turner, A., & Sewell, G. 2014. Platinum-based anticancer drugs in waste waters of a major UK hospital and predicted concentrations in recipient surface waters. ***Sci Total Environ***, 493: 324-329.

Walcarius, A., & Mercier, L. 2010. Mesoporous organosilica adsorbents: nanoengineered materials for removal of organic and inorganic pollutants. ***Journal of Materials Chemistry***, 20(22): 4478-4511.

Wang, C.-C., Li, J.-R., Lv, X.-L., Zhang, Y.-Q., & Guo, G. 2014a. Photocatalytic organic pollutants degradation in metal–organic frameworks. ***Energy & Environmental Science***, 7(9): 2831.

Wang, C., Liu, X., Chen, J. P., & Li, K. 2015a. Superior removal of arsenic from water with zirconium metal-organic framework UiO-66. ***Scientific Reports***, 5: 16613.

Wang, F., Dong, C., Wang, C., Yu, Z., Guo, S., Wang, Z., Zhao, Y., & Li, G. 2015b. Fluorescence detection of aromatic amines and photocatalytic degradation of rhodamine B under UV light irradiation by luminescent metal–organic frameworks. ***New J. Chem.***, 39(6): 4437-4444.

Wang, F., Guo, H., Chai, Y., Li, Y., & Liu, C. 2013a. The controlled regulation of morphology and size of HKUST-1 by "coordination modulation method". ***Microporous and Mesoporous Materials***, 173: 181-188.

Wang, G. H., Hilgert, J., Richter, F. H., Wang, F., Bongard, H. J., Spliethoff, B., Weidenthaler, C., & Schuth, F. 2014b. Platinum-cobalt bimetallic nanoparticles in hollow carbon nanospheres for hydrogenolysis of 5-hydroxymethylfurfural. ***Nat Mater***, 13(3): 293-300.

Wang, H.-N., Liu, F.-H., Wang, X.-L., Shao, K.-Z., & Su, Z.-M. 2013b. Three neutral metal–organic frameworks with micro- and meso-pores for adsorption and separation of dyes. ***Journal of Materials Chemistry A***, 1(42): 13060.

Wang, J., & Kaskel, S. 2012. KOH activation of carbon-based materials for energy storage. ***Journal of Materials Chemistry***, 22(45): 23710.

Wang, J., Xue, C., Lv, Y., Zhang, F., Tu, B., & Zhao, D. 2011. Kilogram-scale synthesis of ordered mesoporous carbons and their electrochemical performance. ***Carbon***, 49(13): 4580-4588.

Wang, L., Feng, X., Ren, L., Piao, Q., Zhong, J., Wang, Y., Li, H., Chen, Y., & Wang, B. 2015c. Flexible Solid-State Supercapacitor Based on a Metal-Organic Framework Interwoven by Electrochemically-Deposited PANI. ***J Am Chem Soc***, 137(15): 4920-4923.

Wang, L., Han, Y., Feng, X., Zhou, J., Qi, P., & Wang, B. 2015d. Metal–organic frameworks for energy storage: Batteries and supercapacitors. ***Coordination Chemistry Reviews***.

Wang, L., Han, Y., Feng, X., Zhou, J., Qi, P., & Wang, B. 2015e. Metal–organic frameworks for energy storage: Batteries and supercapacitors. ***Coordination Chemistry Reviews***, 307: 361-381.

Wang, L., Han, Y., Feng, X., Zhou, J., Qi, P., & Wang, B. 2016a. Metal–organic frameworks for energy storage: Batteries and supercapacitors. ***Coordination Chemistry Reviews***, 307: 361-381.

Wang, Q., Shao, Y., Gao, N., Chu, W., Chen, J., Lu, X., Zhu, Y., & An, N. 2017. Activation of peroxymonosulfate by Al 2 O 3 -based CoFe 2 O 4 for the degradation of sulfachloropyridazine sodium: Kinetics and mechanism. ***Separation and Purification Technology***, 189: 176-185.

Wang, Q., Zhang, W., Mu, Y., Zhong, L., Meng, Y., & Sun, Y. 2014c. Synthesis of ordered mesoporous carbons with tunable pore size by varying carbon precursors via soft-template method. ***Microporous and Mesoporous Materials***, 197: 109-115.

Wang, S., Ng, C. W., Wang, W., Li, Q., & Hao, Z. 2012. Synergistic and competitive adsorption of organic dyes on multiwalled carbon nanotubes. ***Chemical Engineering Journal***, 197: 34-40.

Wang, W., & Kannan, K. 2016. Fate of Parabens and Their Metabolites in Two Wastewater Treatment Plants in New York State, United States. ***Environ Sci Technol***, 50(3): 1174-1181.

Wang, X.-X., Li, Z.-X., Yu, B., Van Hecke, K., & Cui, G.-H. 2015f. Synthesis and characterizations of a bis(triazole)-based 3D crystalline copper(II) MOF with high adsorption capacity for congo red dye. ***Inorganic Chemistry Communications***, 54: 9-11.

Wang, Y., Ao, Z., Sun, H., Duan, X., & Wang, S. 2016b. Activation of peroxymonosulfate by carbonaceous oxygen groups: experimental and density functional theory calculations. ***Applied Catalysis B: Environmental***, 198: 295-302.

Wang, Y., Indrawirawan, S., Duan, X., Sun, H., Ang, H. M., Tadé, M. O., & Wang, S. 2015g. New insights into heterogeneous generation and evolution processes of sulfate radicals for phenol degradation over one-dimensional α-MnO2 nanostructures. ***Chemical Engineering Journal***, 266: 12-20.

Wang, Y., Xie, Y., Sun, H., Xiao, J., Cao, H., & Wang, S. 2016c. Efficient Catalytic Ozonation over Reduced Graphene Oxide for p-Hydroxylbenzoic Acid (PHBA) Destruction: Active Site and Mechanism. ***ACS Appl Mater Interfaces***, 8(15): 9710-9720.

Webb, P. A., & Orr, C. 1997. ***Analytical methods in fine particle technology***: Micromeritics Instrument Corp.

Wu, D., & Fang, Y. 2003. The adsorption behavior of p-hydroxybenzoic acid on a silver-coated filter paper by surface enhanced Raman scattering. ***Journal of Colloid and Interface Science***, 265(2): 234-238.

Wu, Z., Zhong, H., Yuan, X., Wang, H., Wang, L., Chen, X., Zeng, G., & Wu, Y. 2014. Adsorptive removal of methylene blue by rhamnolipid-functionalized graphene oxide from wastewater. ***Water Res***, 67: 330-344.

Xia, W., Zhu, J., Guo, W., An, L., Xia, D., & Zou, R. 2014. Well-defined carbon polyhedrons prepared from nano metal–organic frameworks for oxygen reduction. ***Journal of Materials Chemistry A***, 2(30): 11606.

Xiao, J.-D., Qiu, L.-G., Jiang, X., Zhu, Y.-J., Ye, S., & Jiang, X. 2013a. Magnetic porous carbons with high adsorption capacity synthesized by a microwave-enhanced high temperature ionothermal method from a Fe-based metal-organic framework. ***Carbon***, 59: 372-382.

Xiao, S.-L., Liu, Y.-G., Qin, L., & Cui, G.-H. 2013b. A hexanuclear CuII-based coordination framework with non-interpenetrated α-Po topology displaying catalytic activity. ***Inorganic Chemistry Communications***, 36: 220-223.

Xie, L., Liu, D., Huang, H., Yang, Q., & Zhong, C. 2014. Efficient capture of nitrobenzene from waste water using metal–organic frameworks. ***Chemical Engineering Journal***, 246: 142-149.

Xu, W.-J., Xue, Q.-J., Liang, P., Zhang, L.-Y., Huang, Y.-F., & Feng, Y. 2014. A Series of Transition-metal Coordination Complexes Assembled from 3-Nitrophthalic Acid and Thiabendazole: Synthesis, Structure and Properties. ***Bulletin of the Korean Chemical Society***, 35(1): 218-224.

Yaghi, O. M., Li, G., & Li, H. 1995. Selective binding and removal of guests in a microporous metal-organic framework. ***Nature***, 378(6558): 703-706.

Yaghi, O. M., & Li, H. 1995. Hydrothermal Synthesis of a Metal-Organic Framework Containing Large Rectangular Channels. ***Journal of the American Chemical Society***, 117(41): 10401-10402.

Yagub, M. T., Sen, T. K., Afroze, S., & Ang, H. M. 2014. Dye and its removal from aqueous solution by adsorption: a review. ***Adv Colloid Interface Sci***, 209: 172-184.

Yan, A. X., Yao, S., Li, Y. G., Zhang, Z. M., Lu, Y., Chen, W. L., & Wang, E. B. 2014. Incorporating polyoxometalates into a porous MOF greatly improves its selective adsorption of cationic dyes. ***Chemistry***, 20(23): 6927-6933.

Yang, E.-C., Zhao, H.-K., Ding, B., Wang, X.-G., & Zhao, X.-J. 2007. Four Novel Three-Dimensional Triazole-Based Zinc(II) Metal−Organic Frameworks Controlled by the Spacers of Dicarboxylate Ligands: Hydrothermal Synthesis, Crystal Structure, and Luminescence Properties. ***Crystal Growth & Design***, 7(10): 2009-2015.

Yang, J.-M., Liu, Q., & Sun, W.-Y. 2014. Shape and size control and gas adsorption of Ni(II)-doped MOF-5 nano/microcrystals. ***Microporous and Mesoporous Materials***, 190: 26-31.

Yang, Q., Chen, G., Zhang, J., & Li, H. 2015. Adsorption of sulfamethazine by multi-walled carbon nanotubes: effects of aqueous solution chemistry. ***RSC Advances***, 5(32): 25541-25549.

Yang, X., & Clark, A. E. 2014. Preferential Solvation of Metastable Phases Relevant to Topological Control Within the Synthesis of Metal–Organic Frameworks. ***Inorganic Chemistry***, 53(17): 8930-8940.

Yang, Y., Shukla, P., Wang, S., Rudolph, V., Chen, X.-M., & Zhu, Z. 2013. Significant improvement of surface area and CO2 adsorption of Cu–BTC via solvent exchange activation. ***RSC Advances***, 3(38): 17065-17072.

Yao, Y., Chen, H., Lian, C., Wei, F., Zhang, D., Wu, G., Chen, B., & Wang, S. 2016. Fe, Co, Ni nanocrystals encapsulated in nitrogen-doped carbon nanotubes as Fenton-like catalysts for organic pollutant removal. ***J Hazard Mater***, 314: 129-139.

Yasue, T., Tsuchida, Y. and Arai, Y. 1984. Crystal shape and precepitation conditions of. Ca(OH)2. ***Gypsum and Lime***, 189(83).

Yee, K. K., Reimer, N., Liu, J., Cheng, S. Y., Yiu, S. M., Weber, J., Stock, N., & Xu, Z. 2013. Effective mercury sorption by thiol-laced metal-organic frameworks: in strong acid and the vapor phase. ***J Am Chem Soc***, 135(21): 7795-7798.

Yi, F. Y., Li, J. P., Wu, D., & Sun, Z. M. 2015. A Series of Multifunctional Metal-Organic Frameworks Showing Excellent Luminescent Sensing, Sensitization, and Adsorbent Abilities. ***Chemistry***, 21(32): 11475-11482.

Yilmaz, G., & Keskin, S. 2014. Molecular modeling of MOF and ZIF-filled MMMs for CO2/N2 separations. ***Journal of Membrane Science***, 454: 407-417.

Yuan, B., Wu, X., Chen, Y., Huang, J., Luo, H., & Deng, S. 2013. Adsorption of CO2, CH4, and N2 on Ordered Mesoporous Carbon: Approach for Greenhouse Gases Capture and Biogas Upgrading. ***Environmental Science & Technology***, 47(10): 5474-5480.

Yurtsever, A., Sahinkaya, E., Aktas, O., Ucar, D., Cinar, O., & Wang, Z. 2015. Performances of anaerobic and aerobic membrane bioreactors for the treatment of synthetic textile wastewater. ***Bioresour Technol***, 192: 564-573.

Zessel, K., Mohring, S., Hamscher, G., Kietzmann, M., & Stahl, J. 2014. Biocompatibility and antibacterial activity of photolytic products of sulfonamides. ***Chemosphere***, 100: 167-174.

Zhang, K.-L., Jing, C.-Y., Deng, Y., Zhang, L., Meng, Q.-H., Zhu, P.-Z., & Ng, S. W. 2014a. Synthesis and characterization of a pair of temperature and cosolvent-dependent Zn(II)-organic frameworks containing a novel discrete single-walled Zn(II)-organic coordination polymer nanotube. ***Journal of Coordination Chemistry***, 67(9): 1596-1612.

Zhang, L., Zhao, L., & Lian, J. 2014b. Nanostructured Mn3O4–reduced graphene oxide hybrid and its applications for efficient catalytic decomposition of Orange II and high lithium storage capacity. ***RSC Adv.***, 4(79): 41838-41847.

Zhang, P., Qiao, Z. A., & Dai, S. 2015a. Recent advances in carbon nanospheres: synthetic routes and applications. ***Chem Commun (Camb)***, 51(45): 9246-9256.

Zhang, Q., Yu, J., Cai, J., Song, R., Cui, Y., Yang, Y., Chen, B., & Qian, G. 2014c. A porous metal-organic framework with -COOH groups for highly efficient pollutant removal. ***Chemical Communications***, 50(92): 14455-14458.

Zhang, Q., Yu, J., Cai, J., Song, R., Cui, Y., Yang, Y., Chen, B., & Qian, G. 2014d. A porous metal-organic framework with -COOH groups for highly efficient pollutant removal. ***Chem Commun (Camb)***, 50(92): 14455-14458.

Zhang, X., Gao, Y., Liu, H., & Liu, Z. 2015b. Fabrication of porous metal–organic frameworks via a mixed-ligand strategy for highly selective and efficient dye adsorption in aqueous solution. ***CrystEngComm***, 17(31): 6037-6043.

Zhang, Y. B., Furukawa, H., Ko, N., Nie, W., Park, H. J., Okajima, S., Cordova, K. E., Deng, H., Kim, J., & Yaghi, O. M. 2015c. Introduction of functionality, selection of topology, and enhancement of gas adsorption in multivariate metal-organic framework-177. ***Journal of American Chemical Society***, 137(7): 2641-2650.

Zhang, Y. B., Furukawa, H., Ko, N., Nie, W., Park, H. J., Okajima, S., Cordova, K. E., Deng, H., Kim, J., & Yaghi, O. M. 2015d. Introduction of functionality, selection of topology, and enhancement of gas adsorption in multivariate metal-organic framework-177. ***J Am Chem Soc***, 137(7): 2641-2650.

Zhang, Z., Wang, J. J., Tang, C., & DeLaune, R. D. 2015e. Heavy metals and metalloids content and enrichment in Gulf Coast sediments in the vicinity of an oil refinery. ***Journal of Geochemical Exploration***.

Zhao, F., Repo, E., Yin, D., Meng, Y., Jafari, S., & Sillanpaa, M. 2015a. EDTA-Cross-Linked beta-Cyclodextrin: An Environmentally Friendly Bifunctional Adsorbent for Simultaneous Adsorption of Metals and Cationic Dyes. ***Environ Sci Technol***, 49(17): 10570-10580.

Zhao, J., Wang, Y., Zhou, J., Qi, P., Li, S., Zhang, K., Feng, X., Wang, B., & Hu, C. 2016. A copper(ii)-based MOF film for highly efficient visible-light-driven hydrogen production. ***Journal of Materials Chemistry A***, 4(19): 7174-7177.

Zhao, N., Wu, S., He, C., Shi, C., Liu, E., Du, X., & Li, J. 2012. Hierarchical porous carbon with graphitic structure synthesized by a water soluble template method. ***Materials Letters***, 87: 77-79.

Zhao, Y., Qi, W., Chen, G., Ji, M., & Zhang, Z. 2015b. Behavior of Cr(VI) removal from wastewater by adsorption onto HCl activated Akadama clay. ***Journal of the Taiwan Institute of Chemical Engineers***, 50: 190-197.

Zhou, Q., Gao, Q., Luo, W., Yan, C., Ji, Z., & Duan, P. 2015. One-step synthesis of amino-functionalized attapulgite clay nanoparticles adsorbent by hydrothermal carbonization of chitosan for removal of methylene blue from wastewater. ***Colloids and Surfaces A: Physicochemical and Engineering Aspects***, 470: 248-257.

Zhu, B.-J., Yu, X.-Y., Jia, Y., Peng, F.-M., Sun, B., Zhang, M.-Y., Luo, T., Liu, J.-H., & Huang, X.-J. 2012. Iron and 1,3,5-Benzenetricarboxylic Metal–Organic Coordination Polymers Prepared by Solvothermal Method and Their Application in Efficient As(V) Removal from Aqueous Solutions. ***The Journal of Physical Chemistry C***, 116(15): 8601-8607.

Zhu, W., Yang, X.-Y., Li, Y.-H., Li, J.-P., Wu, D., Gao, Y., & Yi, F.-Y. 2014. A novel porous molybdophosphate-based FeII,III-MOF showing selective dye degradation as a recyclable photocatalyst. ***Inorganic Chemistry Communications***, 49: 159-162.

Zhu, Y.-P., Liu, Y., Liu, Y.-P., Ren, T.-Z., Chen, T., & Yuan, Z.-Y. 2015. Direct Synthesis of Phosphorus-Doped Mesoporous Carbon Materials for Efficient Electrocatalytic Oxygen Reduction. ***ChemCatChem***, 7(18): 2903-2909.

Zhuang, X., Wan, Y., Feng, C., Shen, Y., & Zhao, D. 2009. Highly Efficient Adsorption of Bulky Dye Molecules in Wastewater on Ordered Mesoporous Carbons. ***Chemistry of Materials***, 21(4): 706-716.

Appendix A

Copyright Clearance Center RightsLink®

Home | Create Account | Help

Title: Excellent performance of copper based metal organic framework in adsorptive removal of toxic sulfonamide antibiotics from wastewater

Author: Muhammad Rizwan Azhar,Hussein Rasool Abid,Hongqi Sun,Vijay Periasamy,Moses O. Tadé,Shaobin Wang

Publication: Journal of Colloid and Interface Science

Publisher: Elsevier

Date: 15 September 2016

LOGIN

If you're a copyright.com user, you can login to RightsLink using your copyright.com credentials.

Already a RightsLink user or want to learn more?

Please note that, as the author of this Elsevier article, you retain the right to include it in a thesis or dissertation, provided it is not published commercially. Permission is not required, but please ensure that you reference the journal as the original source. For more information on this and on your other retained rights, please visit: https://www.elsevier.com/about/our-business/policies/copyright#Author-rights

BACK | CLOSE WINDOW